Faculty of Medicine
and Health Sciences
School of Life Sciences

University of
Nottingham
UK | CHINA | MALAYSIA

Investigation of the role of L-type Ca^{2+} channels in the mobilisation of lipophilic compounds from white adipocytes: a possible aetiology of metabolic disorders

By

Akaniro-Ejim, Nneoma Emmanuela

B.Sc. (Biochemistry & Microbiology), M.Sc. (Pharmacology & Biotechnology)

Thesis submitted to the University of Nottingham in fulfilment of the requirements for the Degree of Doctor of Philosophy in Biomedical Sciences (Physiology & Pharmacology)

October 2022

Abstract

Voltage gated calcium channels (Ca_Vs) are transmembrane proteins which allow the entry of calcium ions into cells in response to membrane depolarisation. They are readily expressed in excitable cells where their molecular and functional expression are well characterised, however they are less characterised in unexcitable cells such as white fat adipocytes (WFAs). The physiological role of WFAs has been recognised to transcend its central role as the main energy storage of the body. The need for intracellular calcium in physiological processes mediated by the adipose tissue has been recognised. Furthermore, the aetiology of metabolic disorders such as type 2 diabetes and obesity involves derangements in physiological processes of WFAs such as lipolysis, as well as exposure to highly lipophilic obesogenic and diabetogenic compounds, which can be released into the general circulation during lipolysis. This study thus aimed to characterise Ca_V channels in WFAs and determine the contribution of intracellular calcium in adipocyte lipolysis and release of fat stored compounds.

Molecular expression and proteomic analysis were respectively determined by western blotting and tandem mass spectrometry. Epifluorescent microscopy using the calcium specific dye, Fluo 4 for intracellular calcium imaging was used to study functional expression. Fluorescent measurement of nile red release and free fatty acid analysis were employed to monitor lipophilic compound release from the fat cell as well as lipolysis under calcitropic conditions.

A $Ca_V1.2$ α_1 subunit of ~290 kDa, a splice isoform of the canonical $Ca_V1.2$ α_1 subunit, was differentially expressed in the plasma membrane of rat visceral and sub-cutaneous WFAs and 3T3-L1 adipocytes. This large protein was absent in undifferentiated 3T3-L1 cells, instead a protein of ~210 kDa, similar to that found in the control rat brain tissue, was detected. Also, the Cav3.1 α_1 subunit of ~265 kDa was detected only in undifferentiated 3T3-L1 adipocytes. Proteomic analysis also revealed the presence of α_2/δ_1 subunits of $Ca_V1.2$ in the primary adipocytes. Calcium imaging confirmed that the detected proteins were indeed functional and were of the L-type, based on the pharmacology of their response to L-type antagonists. Intracellular calcium influx in CD1 male mice visceral WFAs was insensitive to regulation by conditions previously shown to modulate the adipocyte membrane potential. However, hormonal stimulation by recombinant human

growth hormone and the full-length parathyroid hormone (1-84) led to increases in calcium influx in these cells. Nile red fluorescent measurements and free fatty acid analysis showed that conditions previously shown to unequivocally increase intracellular calcium had no effect on release of fat stored lipophiles and on lipolysis. This study has confirmed the molecular identity of WFA Ca_V channels as $Ca_V1.2$ and increased our understanding of how these channels are modulated in the fat cell. Knowledge of the role of these channels in the release of fat stored lipophiles is however still lacking.

Dedication

…To the memory of my father, Sir Barr. Gregory Eberechukwu Akaniro, and the birth of my daughter, Zimchikachim Zoe Ejim

Acknowledgements

To my primary supervisor, Dr. Paul Andrew Smith, who gave me an opportunity to bring my dreams to reality; what I could only once dream of, today I have the capacity, capability, confidence and competence to do! I thank you for your patience, continuous encouragement and kind support throughout these years. Thank you for your close involvement with my training and skill development and for your mentorship.

To my secondary supervisor, Dr. Sue Chan, who challenged me and taught me how to ask the right questions; your rigour and thoroughness in research has helped me develop a necessity to critically appraise my work and aim for excellence.

To all those who made this thesis a reality, Dr. Michael Garle, Dr. Maxine Fowler, Julie, Paul Millns, Sally Cordon, Helen and all the technical staff of BSU, Laura Rich, Wafa, Syaheedah, Dr. Olena Fedorenko, Yan Meng, Dr. Steve Woodhams, Dr. Ian Kerr, Prof Robert Layfield, Jala Alahmed and others too numerous to mention; your kind help, technical advice, stimulating discussions and shared resources are very much appreciated.

To my oak-tree, Mrs C. N. - Nwa Chinemere 1, who flew thousands of miles to nurse our little one so I could focus and complete my thesis; na uwa m ozo, I ga abu nne m (in my next world, you would still be my mother).

To my life partner and best friend, Ifechukwu m, who juggled the responsibility of provider, whilst studying full-time; words cannot describe my admiration for your discipline and call to duty. Na uwa m ozo, I ga abu di m (in my next world, you would still be my husband).

To my siblings, Chichi, George, Ogo, Peepee, the sense of community you bring to my life is amazing. Your constant encouragement, love, and prayers have borne good fruits – I PhinisheD.

To my soul-sisters, Mama Ejima and Mama Reward, who have stood by me through thick and thin, I bless the day our paths crossed.

To Schlumberger Foundation, who gave me a life-time opportunity by granting me a fully funded doctoral fellowship, because of you I have received world class education and made connections to continue advocacy for STEM education for girls.

To the University of Nottingham, I walked through you. I have grown in you. You have given me wings to fly. Thank you.

Publications, conferences and posters

PUBLICATIONS

- **Akaniro-Ejim, N.E.** and Smith, P.A., 2021. Intracellular Ca2+ in Mouse White Fat Adipocytes: Effects of Extracellular Anions, Growth Hormone, and Their Interaction with Ca2+ Influx. *Bioelectricity*, *3*(4), pp.282-291.
- **Nneoma E. Akaniro-Ejim** and Paul A. Smith. 2021. Modulation of L-type Ca^{2+} channels interferes with intracellular Ca^{2+} mobilisation in mouse white fat adipocytes. - The Physiological Society. In *Proc Physiol Soc*, 48: PC031.
- Yan Meng, Olena A Fedorenko, **Nneoma Akaniro-Ejim**, Maria Toledo-Rodriguez, and Paul A Smith. 2021. Adipose depot dependency of chloride channels expression in murine white fat. - The Physiological Society. In *Proc Physiol Soc*, 48: PC055.
- Fedorenko, O.A., Pulbutr, P., Banke, E., **Akaniro-Ejim, N.E.**, Bentley, D.C., Olofsson, C.S., Chan, S. and Smith, P.A., 2020. CaV1. 2 and CaV1. 3 voltage-gated L-type Ca2+ channels in rat white fat adipocytes. *Journal of Endocrinology*, *244*(2), pp.369-381.
- Smith P & **Akaniro-Ejim N.** 2019. Anion species confounds measurement of intracellular Ca2+ in murine white fat adipocytes. - The Physiological Society. In *Proc Physiol Soc*, 43: PC087.
- Olena A. Fedorenko, Maria Toledo-Rodriguez, **Nneoma Akaniro-Ejim** & Paul A. Smith. (2019, July). Age, gender and species dependency of expression of voltage-gated calcium channels in murine white fat adipose depots. - The Physiological Society. In *Proc Physiol Soc*, 43: PC186.
- **Akaniro-Ejim N. E.**, Chan S. L. F. & Smith P. A. 2018. The plasma membrane of Rat sub-cutaneous white adipocytes expresses a long $Ca_v1.2$ channel isoform. The Physiological Society. In *Proc Physiol Soc*, 41: PCB220.

ORAL PRESENTATIONS

- Voltage-gated calcium influx in white fat adipocytes: influence of calcium exchangers and hormonal regulation. Oral presentation at the School of Life Sciences Postgraduate Research Symposium, University of Nottingham, Nottingham - United Kingdom, July, 2020.
- Proteomic Analysis of White Fat Adipocytes: Detection of Voltage-Gated Calcium Channels. Oral presentation at the 2019 Cold Spring Habor Laboratory Proteomics Course, New York – USA, August 14, 2019.
- Characterisation and functional regulation of L-type calcium channels in white fat adipocytes. Oral presentation at the Calcium Channel Network Meeting, Penang - Malaysia, April 4, 2019.

POSTER PRESENTATIONS

- **Nneoma E. Akaniro-Ejim**, Robert Layfield, Sue L. F. Chan, Paul A. Smith. (2019, September). *Proteomic Analysis of White Fat Adipocytes and Functional Role of Detected Voltage-Gated Calcium Channels.* Poster session presented at The 40th British Mass Spectrometry Society Annual Meeting, Royal Northern College of Music Manchester, United Kingdom.
- **Akaniro-Ejim N. E.**, Chan S. L. F. & Smith P. A. (2019, June). *Can Ca^{2+} channels in white fat cells be potential therapeutic targets for metabolic disorders?* Poster session presented at School of Life Sciences Postgraduate Research Symposium, University of Nottingham, United Kingdom.
- **Akaniro-Ejim N. E.**, Chan S. L. F. & Smith P. A. (2019, May). *Molecular and Functional Expression of Voltage-Gated Calcium Channels in White Fat Cells.* Poster session presented at Royal Society of Biology's Postgraduate Poster Symposium, De Montfort University, United Kingdom.
- **Akaniro-Ejim N. E.**, Chan S. L. F. & Smith P. A. (2018, September). *Characterisation of voltage-gated Ca^{2+} channels in white adipocytes and their role in the release of lipophilic compounds: a possible aetiology of metabolic disorders.* Poster session presented at EMDoc conference: Impact and exchange – making connections beyond the academy, Bishop Grosseteste University, United Kingdom.
- **Akaniro-Ejim N. E.**, Chan S. L. F. & Smith P. A. (2017, November). *The role of L-type voltage-gated Ca^{2+} channel in the mobilisation of lipophilic compounds from white adipocytes.* Poster session presented at Schlumberger Foundation Faculty for the Future Fellows & Alumnae Forum, Cambridge, United Kingdom.

List of abbreviations

$[Ca^{+}]_o$	Extracellular calcium concentration
$[Ca^{2+}]_i$	Intracellular calcium concentration
$[K^{+}]_o$	Extracellular potassium concentration
$[Na^{+}]_o$	Extracellular sodium concentration
ADP	Adenosine diphosphate
AMPK	AMP-activated protein kinase
AR	Adrenergic receptor
AT	Adipose tissue
ATGL	Adipose triglyceride lipase
ATP	Adenosine triphosphate
Bay-K8644	1,4-Dihydro-2,6-dimethyl-5-nitro-4-[2-(trifluoromethyl)phenyl]-3-pyridinecarboxylic acid, methyl ester
BM	Basal medium
BMI	Body mass index
BSA	Bovine serum albumin
C.F.	Cytoplasmic fraction
C.I.	Confidence interval
C/EBPα	CCAAT enhancer binding protein α
Ca^{2+}	Calcium ion
$CaCl_2$	Calcium chloride
CAMKII	Calmodulin-dependent protein kinase II
cAMP	Cyclic adenosine monophosphate
$Ca_V1.x$	L-type calcium channel where subtype is unknown
CDI	Calcium dependent inactivation
cDNA	Complementary DNA
CGI-58	Comparative gene identification-58
Cl^{-}	Chloride ions
CRACs	Calcium release activated channels
C-terminal	Carboxyl terminal
DAG	Diacyl glycerol

DCPIB	4-(2-butyl-6,7-dichlor-2-cyclopentylindan-1-on-5-yl) oxobutyric acid
DFM	Differentiation medium
DMEM	Dulbecco's Modified Eagle's Medium
DMSO	Dimethyl sulfoxide
DNA	Deoxynucleic acid
DPBS	Dulbecco's Phosphate Buffered Saline
eCa^{2+}	Extracellular calcium
EDTA	Ethylenediamine tetraacetic acid
EGTA	Ethylene glycol-bis(β-aminoethyl ether)-N,N,N',N'-tetraacetic acid
Eq.	Equivalent
ER	Endoplasmic reticulum
ERK	Extracellular signal regulated kinase
FAS	Fatty acid synthase
FBS	Fetal bovine serum
FFA	Free fatty acid
Fluo 4 AM	N-[4-[6-[(Acetyloxy)methoxy]-2,7-difluoro-3-oxo-3H-xanthen-9-yl]-2-[2-[2-[bis[2-[(acetyloxy)methoxy]-2-oxoethyl]amino]-5-methylphenoxy]ethoxy]phenyl]-N-[2-[(acetyloxy)methoxy]-2-oxoethyl]glycine (acetyloxy)methyl ester
GHR	Growth hormone receptor
GLUT-4	Glucose transporter
G_s	Stimulatory GTP-binding protein
GTP	Guanosine triphosphate
H^+	Hydrogen ion
HCO_3^-	Bicarbonate
HEPES	4-(2-hydroxyethyl)-1-piperazineethanesulfonic acid
HFD	High-fat diet
HICC	Hypertonicity induced cation channels
HSL	Hormone sensitive lipase
IBMX	3-isobutyl-1-methylxanthine
IC_{50}	Concentration at which half maximal inhibition occurs

I_{Ca}	Calcium current
$I_{clswell}$	Swelling activated chloride current
IP_3	Inositol 1,4,5 trisphosphate
IP_3R	Inositol 1,4,5-triphosphate receptor
K^+	Potassium ion
KB-R7943	2-[2-[4-(4-Nitrobenzyloxy)phenyl]ethyl]isothiourea mesylate
KCC	K^+-Cl^+ cotransporter
KCl	Potassium chloride
MAG	Monoacyl glycerol
MAPK	Mitogen activated protein kinase
Memb.	Plasma membrane fraction
$MgCl_2$	Magnesium chloride
Na^+	Sodium ion
NaCl	Sodium chloride
NaOH	Sodium hydroxide
NCKX	Potassium-dependent Na^+/Ca^{2+} exchanger
NCS	Newborn calf serum
NCX	Na^+/Ca^{2+} exchanger
NMDG	N-Methyl-D-glucamine
NR	Nile red
p38-MAPK	p38-mitogen activated protein kinase
PBS	Phosphate Buffered Saline
PCB	Polychlorinated biphenyl
PCV	Packed cell volume
PDE	Phosphodiesterase
PIP_2	Phosphatidyl inositol 4,5-bisphosphate
PKA	Protein kinase A
PKB/Akt	Protein kinase B
PKC	Protein kinase C
PLC	Phospholipase C
PLIN	Perilipin

PMCA	Plasma membrane Ca^{2+}-ATPase
PMCCs	Plasma membrane calcium channels
POP	Persistent organic pollutants
PPARγ	Proliferator-activated receptor γ
PTH	Parathyroid hormone
rhGH	Recombinant human growth hormone
RMP	Resting membrane potential
RVI	Regulatory volume increase
RYR	Ryanodine receptor
S.D.	Standard deviation
S.E.M.	Standard error of the mean
SC	Subcutaneous
SCD	Stearoyl CoA desaturase
SDS-PAGE	Sodium dodecyl-sulfate polyacrylamide gel electrophoresis
STIM	Stromal interacting molecule 1
TAG	Triacylglycerides
TBST	Tris buffered saline Tween 20
TNF	α Tumour necrosis factor α
Tris	2-Amino-2-(hydroxymethyl)propane-1,3-diol
TRP	transient receptor potential
VDA	Voltage dependent activation
VDI	Voltage dependent inactivation
VGCC	Voltage gated calcium channel
VIS	Visceral
V_m	Plasma membrane potential
VRAC	Volume regulatory anion channels
WFA	White fat adipocyte
Δ	Change

Table of Contents

List of Figures

List of Tables

CHAPTER ONE

General introduction

1.1 An overview of calcium as a signalling molecule

Intracellular calcium is a ubiquitous signalling molecule that controls numerous and diverse cellular processes such as fertilization, proliferation, early development, muscle contraction, hormone secretion and exocytosis, energy metabolism, transcription, chemotaxis and synaptic plasticity during learning and memory (Berridge, 1997, Berridge et al., 2000, Berridge et al., 2003). Cells usually have a resting intracellular calcium concentration ($[Ca^{2+}]_i$) of around 100 nM, which is maintained against an extracellular concentration in the millimolar range (2.5 mM). Activation of the cell occurs when the $[Ca^{2+}]_i$ increases by several 100 fold, up to 10,000-fold (≥ 1 mM) (Berridge et al., 2000, Berridge, 2014, Squire et al., 2009, Dolphin, 2016). However, prolonged high calcium concentration can be cytotoxic to cells (Berridge, 1997). The signalling functions of Ca^{2+} are controlled by a variety of means, one of which is availability of Ca^{2+} as brief Ca^{2+} sparks. The availability of Ca^{2+} to cells can be from release from internal endoplasmic or sarcoplasmic stores, particularly mediated via the inositol 1,4,5-triphosphate receptor (IP3R) and ryanodine receptor (RYR) families (Berridge et al., 2000), or entry from outside through a variety of plasma membrane channels such as voltage-gated (or voltage-operated) channels, ligand-gated (or receptor-operated) channels and store-operated channels (Berridge, 1997). These plasma membrane calcium channels (PMCCs) are defined by the mechanisms controlling their gating (opening and closing). The gating of voltage-operated channels is based on membrane potential changes, receptor-operated channels depend on

binding of ligands to their receptors, while store-operated channels are controlled by Ca^{2+} levels in the endoplasmic reticulum (ER) (Squire et al., 2009).

1.1.1 Calcium signalling pathways

The functional significance of calcium signalling pathways which allow transient increases in intracellular calcium is the need to maintain a tight control on calcium homeostasis through passive (calcium binding proteins) and active (calcium pumps) buffers. This is due to toxicity to cells resulting from prolonged elevation of intracellular calcium (Berridge and Dupont, 1994). Calcium signals can be localised or occur as a global event, and it can be transient or oscillatory depending on the nature of the stimuli and the cell type (Bootman et al., 2002). Calcium signalling pathways thought to be involved in the regulation of obesity are the inositol 1,4,5-triphosphate-calcium pathway, the p38-mitogen activated protein kinase (p38-MAPK) pathway and calcium-calmodulin pathway (Song et al., 2019).

1.1.2 Calcium mobilization in adipocytes

The main function of Ca^{2+}-mobilising signals (such as inositol-1,4,5-trisphosphate, cyclic ADP ribose, electrical activity resulting in Ca^{2+} entry via voltage-gated calcium (Ca_V) channels) is to increase the sensitivity of inositol 1,4,5-triphosphate receptor and ryanodine receptor to the stimulatory actions of Ca^{2+}, leading to further release of Ca^{2+} (Berridge et al., 2000, Turovsky et al., 2012). Generation of a Ca^{2+} signal is usually translated by various Ca^{2+} sensitive processes into a functional response, through various pathways in different cell types (Berridge et al., 2000, Turovsky et al., 2012). In excitable tissues like skeletal muscle, depolarisation of the α_{1s} L-type Ca_V channel, which is linked to the cytosolic head of RYR1, causes a conformational change of the receptor, leading to Ca^{2+} release from the sarcoplasmic reticulum. On the other hand, cardiac cells gate a small

amount of trigger Ca^{2+} through the α_{1c} L-type Ca_v channel, stimulating Ca^{2+}-induced Ca^{2+} release via the RYR2 from the sarcoplasmic reticulum (Berridge et al., 2000). In non-excitable cells like adipocytes, agonists such as acetyl-choline trigger calcium release through involvement of ADP-ribosyl cyclase and interaction with RYR in these cells, while fetal bovine serum mobilized Ca^{2+} release occurs through the activity of phospholipase C (Turovsky et al., 2012). Thus, different agonists can engage distinct calcium signalling pathways and generate calcium transients with distinct temporal patterns. The main routes of calcium mobilisation in white adipocytes include entry through store-operated calcium channels (El Hachmane et al., 2018), Ca_V channels (Pershadsingh et al., 1989) and the reverse mode of sodium calcium exchangers (Bentley et al., 2014).

Store-operated calcium entry is a calcium signalling mechanism which is activated in conditions of low intracellular calcium due to IP3R-mediated calcium release from the ER and the depletion of intracellular calcium stores, coupled with the rapid Ca^{2+} efflux by plasma membrane calcium ATPase (Clapham, 2007). Store operated calcium entry occurs through calcium release activated channels (CRACs) which are formed by the tethering of stromal interacting molecule 1 (STIM1) (which senses and relates ER [Ca^{2+}]) to ORA1 on the plasma membrane (Wang et al., 2010, Lunz et al., 2019). CRACs are activated only in response to emptying of the endoplasmic stores and are insensitive to cytoplasmic calcium levels, unlike other calcium channels such as transient receptor potential (TRP) channels. Other mediators of intracellular calcium signalling include the cation-permeable two-pore channels found on endolysosomal membranes and acidic calcium stores which also serve as mobilizable stores of Ca^{2+} (Patel, 2018, Patel and Kilpatrick, 2018).

Voltage-gated calcium entry is a calcium signalling mechanism which is activated in response to changes to transmembrane voltage across a cell and mediated by channels known as voltage gated calcium (Ca_V) channels. The movement of charged residues in Ca_V channels result in opening of the channel pore and influx of calcium down a steep concentration gradient into the cell (Catterall, 2011, Dolphin, 2016).

1.1.3 Calcium exchangers and pumps

Cytosolic calcium concentration is usually restored to its resting level as soon as Ca^{2+} has completed its signalling functions. This is achieved through plasma membrane Ca^{2+}-ATPase pumps (PMCA) and Na^+/Ca^{2+} exchangers (sodium calcium exchangers - NCX and potassium-dependent sodium calcium exchangers - NCKX), which pump Ca^{2+} out from the cell and the sarco-endoplasmic reticulum ATPase pumps which pump Ca^{2+} into the internal stores (Berridge et al., 2000, Clapham, 2007). PMCA is the main Ca^{2+} ejector in the plasma membrane of non-excitable cells, while NCX plays a dominant role in excitable tissues, where it mediates removal of one Ca^{2+} by importing three Na^+ ions into the cell (Squire et al., 2009), or cotransports one K^+ with one Ca^{2+} out of the cell in exchange for four Na^+ into the cell for NCKX (Clapham, 2007). However, depending on the thermodynamic values of Ca^{2+} and Na^+ and on the membrane potential, the direction of the Na^+/Ca^{2+} (-K^+) exchanger-mediated transport of Na^+ and Ca^{2+} can be reversed – that is, Ca^{2+} may enter cells in exchange for extruded Na^+ (Squire et al., 2009, Clapham, 2007).

1.2 Voltage-gated calcium channels

Voltage-gated calcium (Ca_V) channels are a super-family of ion channels that allow cells to couple changes in plasma membrane potential, predominantly in the form

of electrical activity to increase in intracellular calcium and changes in signalling (Catterall, 2011, Powell et al., 2014). Ca_V channels are regulated by change in voltage across the plasma membrane of the cell and are usually opened upon membrane depolarization and closed in hyperpolarized conditions (Berridge, 2014, Dolphin, 2016). Ca_V channels activate and mediate calcium influx into cells in response to membrane depolarisation and regulate intracellular processes such as contraction, secretion, neurotransmission, and gene expression in many different cell types (Ertel et al., 2000, Catterall, 2011, Dolphin, 2016).

1.2.1 Nomenclature and classification

Signal transduction in different cell types require voltage-gated calcium currents of different physiological, pharmacological and regulatory properties, which are mediated by different molecular sub-types of Ca_v channels. Calcium currents and their mediating Ca_V channels may thus be defined by their physiological and pharmacological properties (Catterall, 2011). Ca_V channels may either be high-voltage activated if they are activated and mediate calcium influx at high (>−40 mV) membrane potential (V_m) values or low-voltage activated if they are activated and mediate calcium influx at more negative (~-70 to - 60 mV) membrane potential values (Table 1.1) (Powell et al., 2014). They are classified based on their α_1 subunit into three families, namely:

- $Ca_V1.x$ family of L-type channels, which are found in the skeletal muscle, heart, neurons, endocrine cells and the retina. They are considered as the best characterized Ca_V channels (Lipscombe et al., 2004). L-type calcium currents typically require a strong depolarization for activation, are long-lasting, and are blocked by the organic L-type calcium channel antagonists, including dihydropyridines (eg nimodipine, nifedipine), phenylalkylamines (eg verapamil) and benzothiazepines (eg diltiazem). They are the main

calcium currents recorded in muscle and endocrine cells, where they initiate contraction and secretion respectively (Ertel et al., 2000, Catterall, 2011).

- $Ca_V2.x$ family of P/Q-types, N-type and R-type channels, which are found mainly in the nervous system where they initiate synaptic transmission at fast synapses (Ertel et al., 2000, Berridge, 2014). The $Ca_V2.x$ family of calcium channels, like the L-type channels, also require a strong depolarisation for activation, but are not sensitive to antagonism by organic L-type channel blockers. They are however susceptible to inhibition by specific polypeptide toxins from cone snail and spider venoms (Ertel et al., 2000).
- $Ca_V3.x$ family of T-type channels, which are widely expressed throughout the body including the heart, central and peripheral nervous systems, kidney, smooth muscle, reproductive organs and endocrine organs (Powell et al., 2014). They are well-known for their transient Ca^{2+} currents, are activated by weak depolarisation and are resistant to antagonism by both organic L-type channel blockers, as well as cone snail and spider polypeptide toxins (Ertel et al., 2000). They function mainly in repetitive firing of action potentials in rhythmically firing cells (such as the sino-atrial node of the heart and the thalamic neurons), in stimulus-secretion coupling in adrenal glomerulosa cells, sperm acrosome reaction and in cell proliferation (Table 1.1) (Catterall, 2011, Berridge, 2014).

Table 1.1: Nomenclature, Classification and Properties of Voltage Gated Calcium Channels

Ca_v channel	Subunit and gene		Pharmacology	Conductance (pS)	Activation threshold (mV)
Ca_V1 family					
$Ca_V1.1$ L-type	α_{1S} subunit	*CACNA1S*	Dihydropyridine	11-25	~ −30
$Ca_V1.2$ L-type	α_{1C} subunit	*CACNA1C*	Dihydropyridine	11-25	~ −30
$Ca_V1.3$ L-type	α_{1D} subunit	*CACNA1D*	Dihydropyridine	11-25	~ −30
$Ca_V1.4$ L-type	α_{1F} subunit	*CACNA1F*	Dihydropyridine	11-25	~ −30
Ca_V2 family					
$Ca_V2.1$ P/Q-type	α_{1A} subunit	*CACNA1A*	ω-Agatoxin	10-20	~ −30
$Ca_V2.2$ N-type	α_{1B} subunit	*CACNA1B*	ω-conotoxin	16	~ −30
$Ca_V2.3$ R-type	α_{1E} subunit	*CACNA1E*	SNX-482	12	~ −30
Ca_V3 family					
$Ca_V3.1$ T-type	α_{1G} subunit	*CACNA1G*	Kurotoxin	7	~ −60 to −70
$Ca_V3.2$ T-type	α_{1H} subunit	*CACNA1H*	Kurotoxin, Mibefradil	5	~ −60 to −70
$Ca_V3.3$ T-type	α_{1I} subunit	*CACNA1I*		11	~ −60 to −70

Abbreviations: Ca_V channels, Voltage gated calcium channels; SNX-482, a synthetic version of a peptide toxin from the tarantula *Hysterocrates gigas*. Adapted from: Catterall (2011) and Berridge (2014).

The high voltage activated (HVA) channels include the L-type channels ($Ca_V1.1$, $Ca_V1.2$, $Ca_V1.4$), the P/Q-type ($Ca_V2.1$), N-type ($Ca_V2.2$) and R-type channels ($Ca_V2.3$), while the low voltage activated (LVA) channels include the T-type channels ($Ca_V3.1$, $Ca_V3.2$, $Ca_V3.3$) (Powell et al., 2014). Although $Ca_V1.3$ channels are a member of the $Ca_V1.x$ (L-type) gene family, they are characterized by low-voltage activating calcium currents, a feature which is equally shared by $Ca_V3.x$ (T-type) channels (Lipscombe et al., 2004, Bentley et al., 2014). The classification of $Ca_V1.3$ as HVA channels is based on their great sequence homology to $Ca_V1.2$, however the unique biophysical characteristics of $Ca_V1.3$ channels allow them to support sustained calcium entry at more negative membrane potential values than other $Ca_V1.x$ channels (Dolphin, 2009). Past literature contain reports of low-voltage activated neuronal L-type calcium channels (Lipscombe et al., 2004). The properties of these $Ca_V1.3$ channels, including its low activation thresholds, are in

stark contrast to prevailing criteria used to describe L-type calcium channels (Lipscombe et al., 2004).

1.2.2 Structure and subunit composition

The Ca_v channels are multimeric complexes consisting of distinct subunits, which are encoded by several genes (Ertel et al., 2000, Berridge, 2014). The five-subunit complex of HVA calcium channels consists of a membrane spanning and central pore-forming alpha1 (α_1) subunit of 190-250 kDa , a disulphide-linked glycoprotein dimer of alpha2 (α_2) and delta (δ) subunits ($\alpha_2\delta$) of 170 kDa, an intracellular beta (β) subunit of 55kDa and a transmembrane glycoprotein gamma (γ) subunit of 33 kDa (Catterall, 2011) (Figure 1.1).

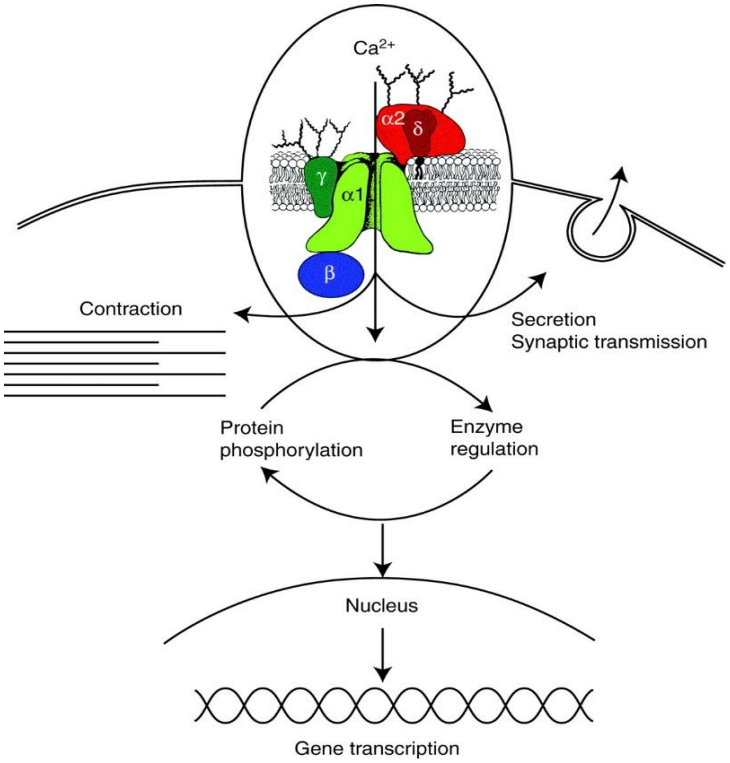

Figure 1.1: The five subunit complex of voltage-gated calcium channels and physiological functions of intracellular calcium.

Adapted from: Catterall (2011).

The $\alpha_2\delta$, β and γ subunits mainly serve as the regulatory subunits of the channel. The main function of the $\alpha_2\delta$ subunit is to increase Ca^{2+} channel current, by promoting the trafficking and retention of the pore-forming α_1 subunit at the plasma membrane (Buraei and Yang, 2010). The α_1 subunit of 190-250 kDa, which consists of the conduction pore, the gating apparatus and the voltage sensor, is the largest subunit of the channel (Ertel et al., 2000, Squire et al., 2009). The α_1 subunit confers specific functional and pharmacological properties to the channel (Daroff and Aminoff, 2014), and is the main site for channel regulation by second messengers, drugs and toxins (Ertel et al., 2000). The diverse types of Ca^{2+} currents arise primarily from the existence of multiple forms of α_1 subunits.

Ten different mammalian α_1 subunits encoded by ten distinct genes have been characterized by complementary DNA (cDNA) cloning and functional expression in mammalian cells or *Xenopus oocytes* (Table 1.1) (Ertel et al., 2000, Catterall, 2011). Four distinct genes have each been identified to encode the $\alpha_2\delta$ ($\alpha_2\delta_{1-4}$) and β subunits (β_{1-4}). Each of these genes are subject to alternative splicing, leading to splice variants or additional isoforms (Catterall, 2000). Each $\alpha_2\delta$ protein is encoded by a single mRNA, cleaved post-translation and linked by disulphide bonds (Buraei and Yang, 2010). The ten known isoforms of α_1 subunit (divided into three subfamilies – Ca_V1, Ca_V2, and Ca_V3), four known isoforms of $\alpha_2\delta$ subunit ($\alpha_2\delta_{1-4}$), and four known isoforms of β subunit (β_{1-4}), are each encoded by a unique gene and all possess splice variants or splice isoforms (Buraei and Yang, 2010, Heck et al., 2021). The α_1 subunit comprises 24 transmembrane segments, organised into four domains (DI – DIV), and each domain contains six transmembrane segments (S1 – S6) (Figure 1.2).

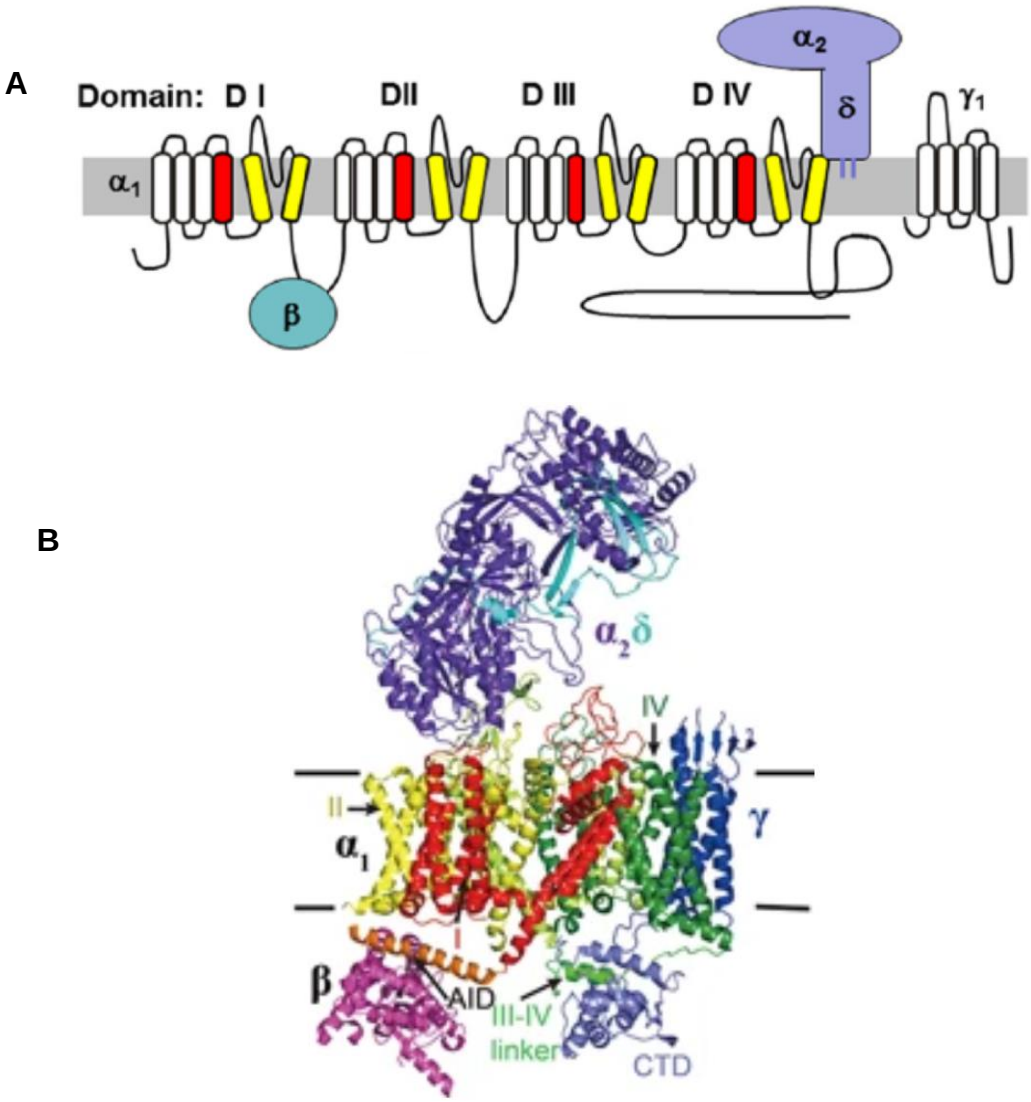

Figure 1.2: The topology of voltage-gated calcium channels showing the 24 transmembrane segments of the α_1 subunit.

(A) Diagram of α_1 subunit topology and calcium channel subunit structure, also showing $\alpha_2\delta$ (purple) and β (blue). Υ_1 is only present in skeletal muscle calcium channel complexes. S4 voltage sensors in each α_1 domain are represented by red transmembrane segments. Yellow denotes S5 and S6 pore transmembrane segments in each domain. **(B)** Structure model of the hetero-tetrameric human $Ca_V1.1$. Cryo-electron microscopy enabled the determination of the structure of $Ca_V1.1$ at 3.6 Å resolution, displaying a closed pore and the voltage sensing domains in the activated up-state. The different subunits are differentially coloured, so are the four repeats, the AID, the III-IV linker and the proximal C-terminal domain (CTD) of the α1-subunit.

Adapted from: Wu et al. (2016), Yang (2016), Dolphin (2018)

The existence of multiple α_1 subunits gives rise to the pharmacological and electrophysiological diversity of Ca_V channels. The association of the α_1 subunit with various combinations of the $\alpha_2\delta$ subunit and β subunit increases the molecular diversity and function of Ca_V channels (Heck et al., 2021). In addition, the existence of multiple $\alpha_2\delta$ and β subunits further increases the diversity of the structure and function of Ca_V channels. For instance, different β subunit isoforms have different shifts on the voltage dependence of channel gating. Hence association of the α_1 subunit with different $\alpha_2\delta$ and β subunits can have a remarkable effect on the channel function (Catterall, 2000).

1.2.3 Activation/inactivation mechanism

As with other families of voltage-gated ion channels, Ca_V channels are defined by their sensitivity to channel activation following membrane depolarisation (Satin, 2014). Voltage dependent activation (VDA) of Ca_V channels is mediated by membrane depolarization that shifts the four S4 segments (the voltage sensor) of DI through DIV within the membrane and opens the channel gate at the inner side of the membrane (Bezanilla, 2000). The S4 segments of domains I - IV of the α_{1C} subunit contain eight positively charged lysine or arginine residues which are electrostatically drawn to the cytosol at a negative V_m. During depolarisation, the four S4 segments displace towards the extracellular space due to the relative motion of the S4 charges towards the extracellular space. This displacement of S4 segments causes allosteric rearrangement of the channel subunits, resulting in an increase in channel conductance (Satin, 2014). In addition to the voltage sensor, the external pore and the ion selectivity filter of Ca_V1 channels, the inner pore of Ca_V1 channels and the activation gate, all contribute as molecular determinants of VDA (Hofmann et al., 2014).

The molecular determinants of voltage dependent inactivation (VDI) include the cytosolic ends of the S6 segments, the DI - DII linker, considered to be the inactivation gate, and the NH_2 and COOH termini of $Ca_V1.x$ (Hofmann et al., 2014). Furthermore, VDA and VDI are accelerated and delayed by $Ca_V\alpha_2\delta$ and $Ca_V\beta$, respectively. The $Ca_V\beta$ subunit interacts at the $Ca_V1.2$ α1 subunit through a conserved 18-amino acid section present in the DI - DII intracellular loop named α1 interacting domain (AID) (Hofmann et al., 2014). Binding of the $Ca_V\beta$ subunit to AID induces a conformational change in the DIS6 and the DI - DII linker that modifies VDA and VDI. The DI-DII linker is suggested to be the particle that occludes the channel pore during inactivation under voltage dependent inactivation and calcium dependent inactivation conditions (Buraei and Yang, 2010).

Calcium dependent inactivation (CDI) is a negative feedback mechanism by which an increase in intracellular calcium promotes channel inactivation to prevent calcium overload of the cell (Lacinová and Hofmann, 2001). CDI of $Ca_V1.x$ channels require the presence of an isoleucine-glutamine (IQ) - motif on the carboxy-terminal sequence of the α1c subunit. Calmodulin (CaM) is constitutively tethered to a region on the carboxy-terminus of the α1c subunit, different from the IQ-motif. Binding of calcium to CaM allows interaction of CaM to the IQ-motif which rapidly mediates inactivation of the channel (Lacinová and Hofmann, 2001, Pitt and Marx, 2014). CaM tethered to the IQ motif in the C-terminus of the α1c subunit serves as the Ca^{2+} sensor for CDI of the channel (Pitt and Marx, 2014). The contribution of CaM to CDI of $Ca_V1.x$ channels is also thought to involve its interaction with the amino-terminal of the α1c subunit, however the mechanistic details are still unclear (Pitt and Marx, 2014).

1.2.4 Basic Physiology of L-type Voltage Gated Calcium Channels

The L-type calcium currents are distinguishable from Ca_V2 channel currents mainly by their unique pharmacology, their sensitivity to dihydropyridine agonists and antagonists and insensitivity to ω-agatoxin and ω-conotoxin which inhibit P/Q calcium currents and N-type calcium currents respectively (Table 1.2) (Lipscombe et al., 2004). The L-type calcium currents are so called because they have a large single channel conductance and due to their slow voltage dependent inactivation, are long-lasting when Ba^{2+} is the current carrier and there is little Ca^{2+} dependent inactivation of the channel (Catterall, 2011). Besides their importance in excitation-contraction coupling in cardiac, smooth, and skeletal muscles, L-type calcium currents initiate hormone release from endocrine cells and are equally important in regulation of gene expression, integration of synaptic input and initiation of neurotransmitter release in sensory neuronal cells (Table 1.2) (Catterall, 2011).

Table 1.2: Tissue Distribution and Physiological Functions of Voltage Gated Calcium Channels

Ca_V channel	*Splice variant	Tissue distribution	Principal physiological functions	Inherited diseases
Ca_V1 family				
$Ca_V1.1$ L-type		Skeletal muscle	Excitation-contraction coupling in skeletal muscle, regulation of transcription	Hypokalemic periodic paralysis
$Ca_V1.2$ L-type	$Ca_V1.2a$	Heart	Excitation-contraction coupling in cardiac and smooth muscle, endocrine secretion, neuronal Ca^{2+} transients in cell bodies and dendrites, regulation of enzyme activity, regulation of transcription	Timothy syndrome: cardiac arrhythmia with developmental abnormalities and autism spectrum disorders
	$Ca_V1.2b$	Smooth muscle		
	$Ca_V1.2c$	Brain, heart, pituitary, adrenal		
$Ca_V1.3$ L-type		Brain, pancreas, kidney, ovary, cochlea	Endocrine secretion, cardiac pacemaking, neuronal Ca^{2+} transients in cell bodies and dendrites, auditory transduction	
$Ca_V1.4$ L-type		Retina	Visual transduction	Stationary night blindness
Ca_V2 family				
$Ca_V2.1$ P/Q-type	$Ca_V2.1a$	Brain, cochlea, pituitary	Neurotransmitter release, dendritic Ca^{2+} transients	Familial hemiplegic migraine, cerebellar ataxia
	$Ca_V2.1b$	Brain, cochlea, pituitary		
$Ca_V2.2$ N-type	$Ca_V2.2a$	Brain, nervous system	Neurotransmitter release, dendritic Ca^{2+} transients	
	$Ca_V2.2b$	Brain, nervous system		
$Ca_V2.3$ R-type	$Ca_V2.3a$	Brain, cochlea, retina, heart, pituitary	Neurotransmitter release, dendritic Ca^{2+} transients	
	$Ca_V2.3b$	Brain, cochlea, retina		
Ca_V3 family				
$Ca_V3.1$ T-type	$Ca_V3.1a$	Brain, nervous system	Pacemaking and repetitive firing	
$Ca_V3.2$ T-type	$Ca_V3.2a$	Brain, heart, liver, kidney, zona glomerulosa	Pacemaking and repetitive firing	Absence seizures
$Ca_V3.3$ T-type	$Ca_V3.3a$	Brain		

*****The cloned Ca_V channels and most widely studied alternate splice forms.

Adapted from: Ertel et al. (2000), Catterall (2011) and Berridge (2014).

1.3 White fat adipocytes and their physiological roles

Adipose tissue (AT) has historically been considered a simple energy storage tissue; however, its physiological functions have been appreciably reassessed over the last decade (Lafontan, 2011), and evidence for other metabolic and endocrine functions of AT has accumulated (Casteilla et al., 2008, Yanev and Chaldakov, 2012, La Merrill et al., 2013). The adipose tissue is anatomically, a type of loose connective tissue comprised of lipid-filled cells called adipocytes (fat cells), surrounded by a matrix of collagen fibres, blood vessels, fibroblasts and immune cells (Ahima and Flier, 2000). Adipocytes are now known to produce a vast number of bioactive peptides, referred to as adipokines, which exert autocrine/paracrine (local) and endocrine (systemic) actions (Ahima and Flier, 2000, Trayhurn and Beattie, 2001, Kershaw and Flier, 2004). Major adipocyte secretory proteins include: leptin, adiponectin, resistin, metallothionein, tumor necrosis factor α, angiotensinogen, adipsin, acylation-stimulating protein, retinol-binding protein, interleukin 6, plasminogen activator inhibitor-1 and tissue factor (Ahima and Flier, 2000, Trayhurn and Beattie, 2001, Ahima, 2006). Adipokines do not only regulate nutrient intake, metabolism and energy expenditure, but also insulin sensitivity, angiogenesis, immune function, brain and bone development and other physiological functions (Table 1.3) (Müllerová and Kopecký, 2007).

Table 1.3: Physiological functions of adipocyte-specific derived factors and pathophysiological consequence of their deficiency.

Adipocyte-specific derived protein	Function	Pathophysiological consequence of change in adipocyte protein production	References
Leptin	• Regulation of appetite and energy balance; acts in the brain to inhibit feeding and adiposity. • Regulation of immune function; potent mediator of immune suppression during fasting through direct regulation of T lymphocytes and cytokine production. • Regulation of neuroendocrine functions.	Total deficiency or insensitivity to leptin causes hyperphagia, decreased energy expenditure, morbid obesity, diabetes, a variety of neuroendocrine abnormalities and autonomic and immune dysfunction.	Friedman and Halaas (1998) Lord et al. (1998) Ahima and Flier (2000)
Adiponectin	• Modulates endothelial adhesion molecules and inhibit inflammatory responses. • Directly sensitizes the body to insulin by stimulating AMP-activated protein kinase (AMPK) phosphorylation and activation to regulate energy metabolism.	Decreased expression correlates with increased body mass index, glycemia, circulating insulin levels, as well as with risk to develop obesity, type 2 diabetes and cardiovascular diseases	Trayhurn and Beattie (2001) Wang et al. (2008) Feijóo-Bandín et al. (2016)
Perilipin	• Prevents lipolysis in basal conditions, favouring the lipid storage	Reduced adipose tissue mass and constitutively high levels of basal lipolysis	Arimura et al. (2004) Carmen and Víctor (2006)
Resistin	• Induces insulin resistance, linking diabetes to obesity	Lack of expression of resistin gene is associated with lower fasting glucose levels, better glucose tolerance and insulin sensitivity, while over-expression is linked with insulin resistance and dyslipidemia	Trayhurn and Beattie (2001) Wang et al. (2008) Feijóo-Bandín et al. (2016)
Metallothionein	• A metal-binding and stress-response protein with possible antioxidant role	-	Trayhurn and Beattie (2001)
Fasting-induced adipose factor	• Responsible for metabolic adaptation to fasting.	-	Trayhurn and Beattie (2001)
Angiotensinogen	• The sole precursor to angiotensin II, which promotes adipocyte growth and differentiation, both directly by promoting lipogenesis and	Increased expression associated with obesity and obesity complications such as hypertension.	Faloia et al. (2000) Kershaw and Flier (2004)

	indirectly by stimulating prostaglandin synthesis.		
Tumour necrosis factor α (TNF α)	• Reduces perilipin expression in adipocytes, resulting in enhanced lipolysis. • Regulates key components of lipid metabolism; prevents obesity through inhibition of lipogenesis, increased lipolysis and facilitation of adipocyte death by apoptosis. • Mediator of insulin resistance in obesity.	Increased expression correlates with its proinflammatory characteristics; reduction of insulin sensitivity in muscle, liver, and AT.	Sethi and Hotamisligil (1999) Carmen and Víctor (2006) Proença et al. (2014)
Interleukin 6	• Acts as a lipolytic agent in the adipose tissue.	Increased expression associated with subclinical inflammatory states that result in insulin resistance.	Trujillo and Scherer (2006) Proença et al. (2014)
Acylation-stimulating protein	• Involved in postprandial clearance of triacylglyerols by stimulating the uptake and esterification of fatty acids in white adipocytes.	Increased expression positively correlates with adiposity, insulin resistance, dyslipidaemia, and cardiovascular disease.	Trayhurn and Beattie (2001) Kershaw and Flier (2004)
Plasminogen activator inhibitor-1 and tissue factor	• A member of serine protease inhibitor family and the primary inhibitor of fibrinolysis, is involved in angiogenesis and atherogenesis.	Increased expression correlates with BMI and incidence of cardiovascular disease.	Trayhurn and Beattie (2001) Kershaw and Flier (2004)

1.3.1 Adipose tissue types and depots

There are two main types of adipose tissue based on morphological and functional differences: white adipose tissue and brown adipose tissue (Vasconcelos et al., 2016). White adipose tissue is more commonly associated with lipid and energy storage and acts as an active endocrine organ, releasing free fatty acid from the breakdown of triglyceride stores as well as adipokines for various physiological functions. Brown adipose tissue, on the other hand, is majorly made up of multilocular, mitochondria-rich adipocytes which express uncoupling protein 1, and is associated with thermogenesis and energy release due to uncoupling of oxidation and ATP production (Koivisto et al., 1993, Yanev and Chaldakov, 2012, Vasconcelos et al., 2016). In addition to classical white and brown adipocytes derived from white and brown adipose tissue respectively, beige adipocytes have also been identified and have characteristics of both white and brown adipocytes (Morrison and McGee, 2015).

White adipocytes are found in white adipose tissue depots, which are distributed in several locations of the body; such as the subcutaneous, inguinal, abdominal or visceral, epididymal, retroperitoneal and gonadal fat depots (Figure 1.3) (Rodríguez et al., 2015, Chusyd et al., 2016). It is essential in regulation of energy homeostasis (El Hachmane et al., 2018), as well as the endocrine functions of the adipose tissue.

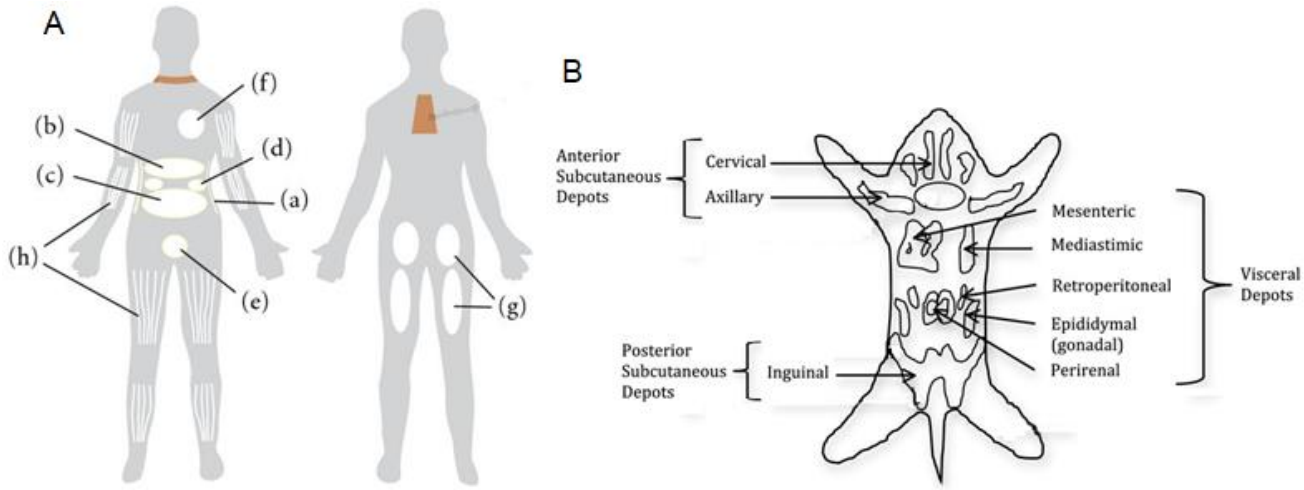

Figure 1.3: The main white adipose tissue depots in human and mouse.

(A) Distribution of white adipocyte fat depots in human. Subcutaneous adipose tissue depots: abdominal (a), gluteofemoral (g), and intramuscular white adipose tissue (h). Visceral adipose tissue depots: omental (b), mesenteric (c), retroperitoneal (d), gonadal (e), and pericardial (f). (B) Distribution of fat pads in the mouse. The fat is composed of two subcutaneous pads and several visceral pads. The main white adipose tissue (WAT) pads are the inguinal and epididymal fat pads.

Adapted from: Chusyd et al. (2016).

1.3.2 Role of intracellular calcium in adipocyte physiology

1.3.2.1 Insulin-stimulated glucose uptake

Cytosolic calcium is involved in the mechanism of insulin-mediated glucose uptake; including the translocation and fusion of GLUT-4 transporters with the plasma membrane (Whitehead et al., 2001, Lanner et al., 2006). Draznin et al. (1987) noted the requirement of an optimal range of extracellular calcium (1-2 mM) and intracellular calcium (140 - 370 nM) for insulin stimulated glucose uptake, below and above which sensitivity to insulin signal transduction is significantly diminished. Intracellular calcium has been shown to have both positive and negative effects on the action of insulin (Draznin et al., 1987, Worrall and Olefsky,

2002). It is required for proper insulin signal transduction, however high concentrations of intracellular calcium blunt sensitivity of insulin target cells to the actions of insulin (Worrall and Olefsky, 2002). This is shown by the requirement of free calcium for both basal and insulin-stimulated glucose uptake, as both processes were significantly reduced in the absence of extracellular calcium (Draznin et al., 1987). In addition, the occurrence of insulin resistance, obesity, type 2 diabetes mellitus, and hypertension have been associated with the presence of a high $[Ca^{2+}]_i$ and the attenuation of these metabolic states by calcium channel antagonists (Worrall and Olefsky, 2002).

The pathophysiologic mechanisms of insulin resistance is multifactorial and includes impairments at the level of the insulin receptor and post-receptor sites (Draznin, 1993). Of the various pathophysiologic mechanisms that contribute to an insulin resistant state, elevated $[Ca^{2+}]_i$ has been identified as a key factor. In patients with obesity, type 2 diabetes, hypertension and normal individual receiving insulin and glucose infusions, an association between elevated $[Ca^{2+}]_i$ and insulin resistance was observed in adipocytes isolated from these patients (Draznin, 1993). Adipocytes from obese and hyperinsulinemic subjects showed an increased $[Ca^{2+}]_i$, suggesting that intracellular calcium plays a key role in post-receptor modulation of the cellular response to insulin (Draznin et al., 1987). Rat adipocytes with high $[Ca^{2+}]_i$ (220 ± 15nM) showed a 10% decrease in autophosphorylation and tyrosine kinase activity of the insulin receptors, as well as a 30% reduction in insulin stimulated 2-deoxyglucose uptake compared with control cells ($[Ca^{2+}]_i$; 140 ± 18nM) (Draznin et al., 1989).

1.3.2.2 Adipogenesis (adipocyte development and maturation)

Adipogenesis involves commitment of mesenchymal stem cells to the adipocyte lineage (pre-adipocytes) and the terminal differentiation of pre-adipocytes into mature adipocytes (Zhang et al., 2018). The requirement for intracellular calcium in adipogenesis has been reported. Agouti protein promotes adipogenesis and obesity through an increase in transcription of fatty acid synthase (FAS) and SCD (stearoyl CoA desaturase); both key enzymes in fatty acid synthesis which require an undefined involvement of increase in intracellular calcium (Jones et al., 1996). Adipogenesis due to agouti protein was inhibited by nitrendipine, an L-type calcium channel antagonist (Jones et al., 1996), supporting a requirement for intracellular calcium in this process. In porcine bone marrow mesenchymal stem cells, high extracellular calcium concentration induced calcium influx via L-type voltage gated calcium channels ($Ca_V1.x$ channels) and led to intracellular calcium elevation and stimulation of adipogenesis (Zhang et al., 2018). The adipogenic differentiation potential of human umbilical cord blood-derived mesenchymal stem cells has also been determined to be dependent on its intracellular calcium levels (Bae et al., 2018). The increase in intracellular calcium activates various signalling pathways, leading to the transcription of genes involved in adipocyte proliferation and differentiation (Goudarzi et al., 2018, Zhai et al., 2020). Increased expression of transcriptional genes; including CCAAT (cytosine-cytosine-adenosine-adenosine-thymidine box motif) enhancer binding protein α (C/EBPα) and peroxisome proliferator-activated receptor γ (PPARγ) promote development of the adipogenic phenotype, which is marked by the formation of lipid droplets in the cytoplasm (Goudarzi et al., 2018, Zhai et al., 2020). The lipid droplets increase in size and overtime coalesce into a single, large lipid droplet in white adipocytes.

1.3.2.3 Lipogenesis

De novo lipogenesis is one of two processes by which adipocytes accumulate lipids, with the second process being the uptake of dietary lipids, liberated from circulating triacylglycerides (TAGs) by lipoprotein lipase (Bolsoni-Lopes and Alonso-Vale, 2015, Richard et al., 2020). De novo lipogenesis occurs within adipocytes and involves production of TAGs from free fatty acids synthesized from acetyl coenzyme A and esterified to a glycerol backbone (Richard et al., 2020). High intracellular calcium levels stimulate the expression and activity of fatty acid synthase, a key enzyme in de novo lipogenesis (Zemel, 1998, Zemel and Sun, 2008, Goudarzi et al., 2018). With increased fatty acid synthase activity and lipogenesis, there is increased adiposity and total fat pad mass and a concomitant decrease in adipocyte lipolysis (Shi et al., 2001, Zemel, 2002, Goudarzi et al., 2018).

1.3.2.4 Lipolysis

Several studies in the past have suggested a key role of calcium in the lipolytic process. The involvement of both intracellularly released calcium and a requirement for extracellular calcium has been strongly supported. The response of adipocyte lipolysis to intracellular calcium fluctuations is thought to be two fold – lipolytic in conditions of high extracellular calcium and anti-lipolytic in conditions of low extracellular calcium. This idea is supported by the work of Ziegler et al. (1980), and suggests a bell-shaped response of adipocyte lipolysis to elevated extracellular calcium. Data to support the antilipolytic effects of intracellular calcium include the 40% and 50% decrease in 100μM forskolin induced lipolysis in human adipocytes following by 25mM and 40mM KCl stimulated increases in $[Ca^{2+}]_i$ (Xue et al., 2001, Xue et al., 1998).

1.4 Lipolysis Pathways

Lipolysis is the process through which triglyceride stores in white adipocytes are hydrolysed to glycerol and free fatty acids, to serve as oxidative fuels for tissues such as the liver, kidney, skeletal muscle and myocardium during periods of negative energy balance (Carmen and Víctor, 2006). Basal lipolysis in adipocytes is regulated by physical activity, location of the fat depot, species, genetic variance, sex and age, whereas stimulated lipolysis is controlled by these and other factors (Figure 1.2) (Frühbeck et al., 2014). Both basal and catecholamine stimulated lipolysis occur during periods of negative energy balance, contributing to the release of non-esterified fatty acids (Frühbeck et al., 2014).

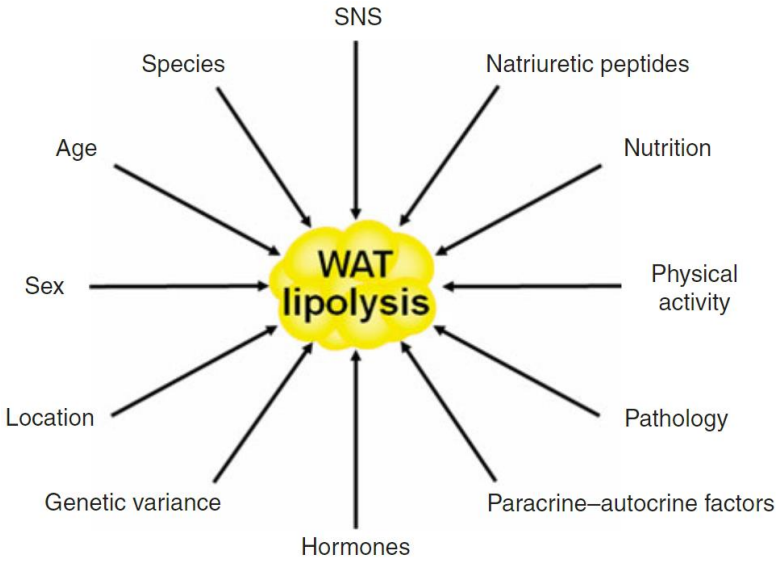

Figure 1.4: Main factors influencing basal and stimulated lipolysis in adipocytes.

SNS, somatic nervous system; WAT, white adipose tissue.

Adapted from: Frühbeck et al. (2014).

Human adipocytes express alpha (α-) and beta (β-) adrenoceptors involved in the regulation of lipolysis (Table 1.4) (Flechtner-Mors et al., 2002). There are several lipolytic pathways based on the specific receptor activated and the activating ligand/stimulus. Lipolysis in white fat adipocytes is based on the predominance of

specific receptors on the plasma membrane of the adipocyte, their relative density and expression (Frühbeck et al., 2014).

Table 1.4: Effector Mechanism and Function of Adrenoceptors in White Adipocyte Lipolysis

Receptor Subtype	Mechanism	Function
Beta $_{1/2/3}$	Stimulation of adenylyl cyclase and cyclic AMP through Gs protein	Increase lipolysis rate
Alpha $_{2}$	Inhibition of adenylate cyclase and cyclic AMP through Gi protein	Decrease lipolysis rate
Alpha $_{1}$	Increased Ca^{2+}, protein kinase C and phosphoinositide hydrolysis through Gq protein	Increase lipolysis rate

Adapted from: Arner (1992)

1.4.1 Major lipolysis pathway

The major lipolytic pathway is the adenylyl cyclase / cyclic adenosine monophosphate (cAMP) / protein kinase A (PKA) / hormone sensitive lipase (HSL) pathway (Gs/AC/cAMP/PKA/HSL pathway). This pathway is dependent on stimulatory GTP-binding protein (Gs) coupled β-adrenoceptor stimulation by hormones, peptides and neurotransmitters (such as the catecholamine, adrenaline) for its activation (Carmen and Víctor, 2006, Chaves et al., 2011, Gerhardt et al., 1999). Activation of cAMP-dependent PKA following stimulation of adenylyl cyclase from receptor activation and subsequent increase in intracellular cAMP, leads to phosphorylation of serine residues on HSL and perilipin A (a protein which coats the lipid droplet of adipocytes). Phosphorylated perilipins lose their ability to inhibit the translocation of HSL from the cytosol to the adipocyte lipid droplet. Adipose tissue triglyceride lipase (ATGL) which is specific for triglycerides first hydrolyses triacyl glycerol (TAG) to diacyl glycerol (DAG), followed by hydrolysis of DAG to monoacyl glycerol (MAG) by HSL and finally hydrolysis of MAG by monoglyceride lipase and release of glycerol and free fatty acids (Figure 1.5) (Carmen and Víctor, 2006, Chaves et al., 2011).

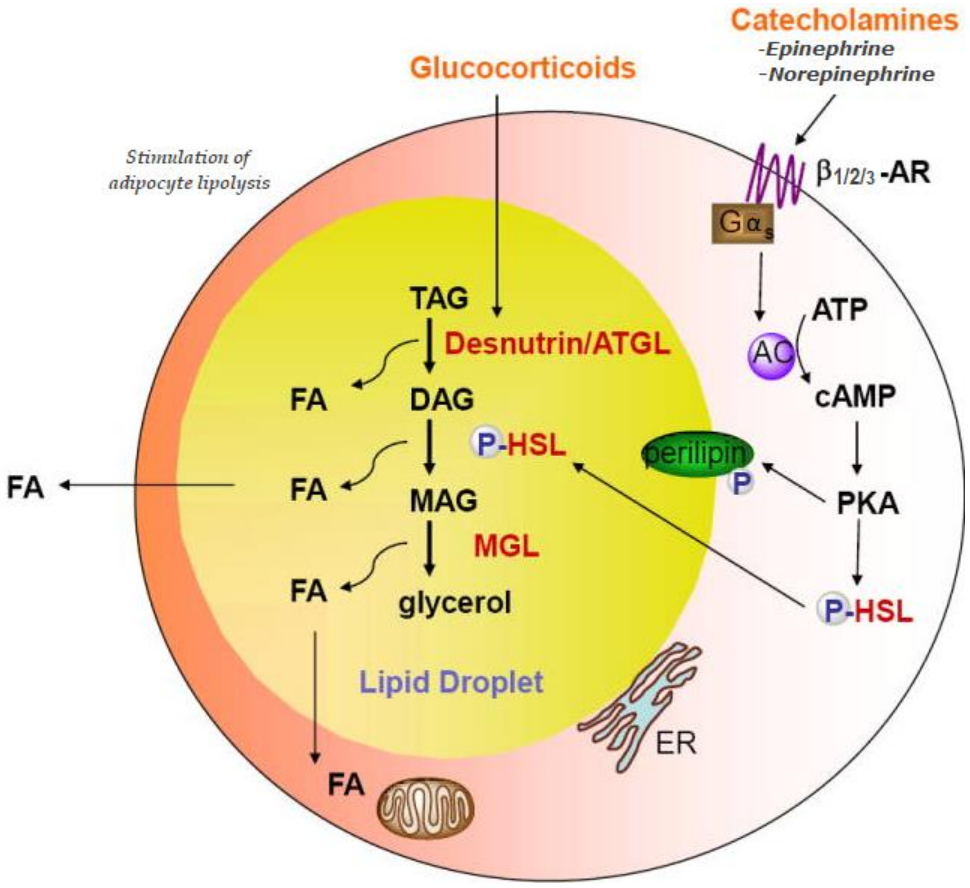

Figure 1.5 Major pathway (Gαs/ac/cAMP/PKA/HSL pathway) involved in the control of white adipocyte lipolysis.

Signal transduction pathways for catecholamines via beta adrenergic receptors (β1/2/3 –AR). During fasting, catecholamines, by binding to Gαs-coupled β-adrenergic receptors, activate adenylyl cyclase (AC) to increase cAMP and activate protein kinase A (PKA). PKA phosphorylates hormone-sensitive lipase (HSL), resulting in translocation of HSL from the cytosol to the lipid droplet. PKA also phosphorylates the lipid droplet associated protein perilipin. Perilipin phosphorylation leads to the physical alteration of the droplet surface that facilitates the action of HSL and initiation of lipolysis. Additionally, during fasting, glucocorticoids increase the expression of desnutrin/Adipose triglyceride lipase (ATGL). ATGL exhibits high substrate specificity for triacylglycerol (TAG) and catalyses the initial step in triglyceride hydrolysis to diacylglycerol (DAG); it is not regulated as HSL. HSL hydrolyzes DAG to monoacylglycerol (MAG), which is subsequently hydrolyzed by MAG lipase to generate glycerol and three fatty acids (FAs). The FAs generated during lipolysis can be released into the circulation for use by other organs or oxidized within adipocytes.

Adapted from: Lafontan et al. (2005), Ahmadian et al. (2010), Dolphin (2018).

1.4.2 Minor lipolysis pathway

The Gαs/cAMP/PKA/HSL pathway, mediated through β-adrenergic receptor (β1/2/3 –AR) coupling to Gs protein, has been extensively described. A less

understood and less described pathway of hormonal control of lipolysis is that mediated by a protein kinase C (PKC) / HSL / mitogen activated protein kinase (MAPK) - extracellular signal regulated kinase (ERK) pathway (Gαq/PKC/HSL/ERK pathway), through the alpha 1 adrenergic receptor (α1-AR) coupled to the Gαq protein (Carmen and Víctor, 2006, Chaves et al., 2011, Gerhardt et al., 1999). The Gαq/PKC/HSL/ERK lipolytic pathway, though similar to the β-adrenoceptor stimulated PKA pathway, is based on the phosphorylation of the serine 600 residue in HSL for its activation (Carmen and Víctor, 2006). Stimulation of the adipocyte plasma membrane receptor, α1–AR, by an agonist leads to hydrolysis of the Gαq subunit and a concomitant rise in phospholipase C (PLC). PLC cleaves phosphatidyl inositol 4,5-bisphosphate (PIP_2) into inositol 1,4,5 trisphosphate (IP_3) and diacylglyerol (DAG). IP_3 stimulates the release of Ca^{2+} from intracellular stores, while DAG causes the activation and translocation of protein kinase C (PKC) to the adipocyte plasma membrane. Additionally, influx of Ca^{2+} through Ca_V channels on the adipocyte plasma membrane further contributes to an increase in $[Ca^{2+}]_i$, which in turn stimulates activation of PKC. Both intracellular Ca^{2+} and PKC cause an increase in extracellular signal regulated kinase 1/2 (ERK1/2). Intracellular Ca^{2+} is thought to induce ERK1/2 activation through calcium/calmodulin-dependent protein kinase II (CAMKII) (Carmen and Víctor, 2006, Chaves et al., 2011). Activated ERK1/2 phosphorylates serine residues on HSL, leading to its activation and subsequent hydrolysis of triglycerides and release of non-esterified fatty acids (Figure 1.6).

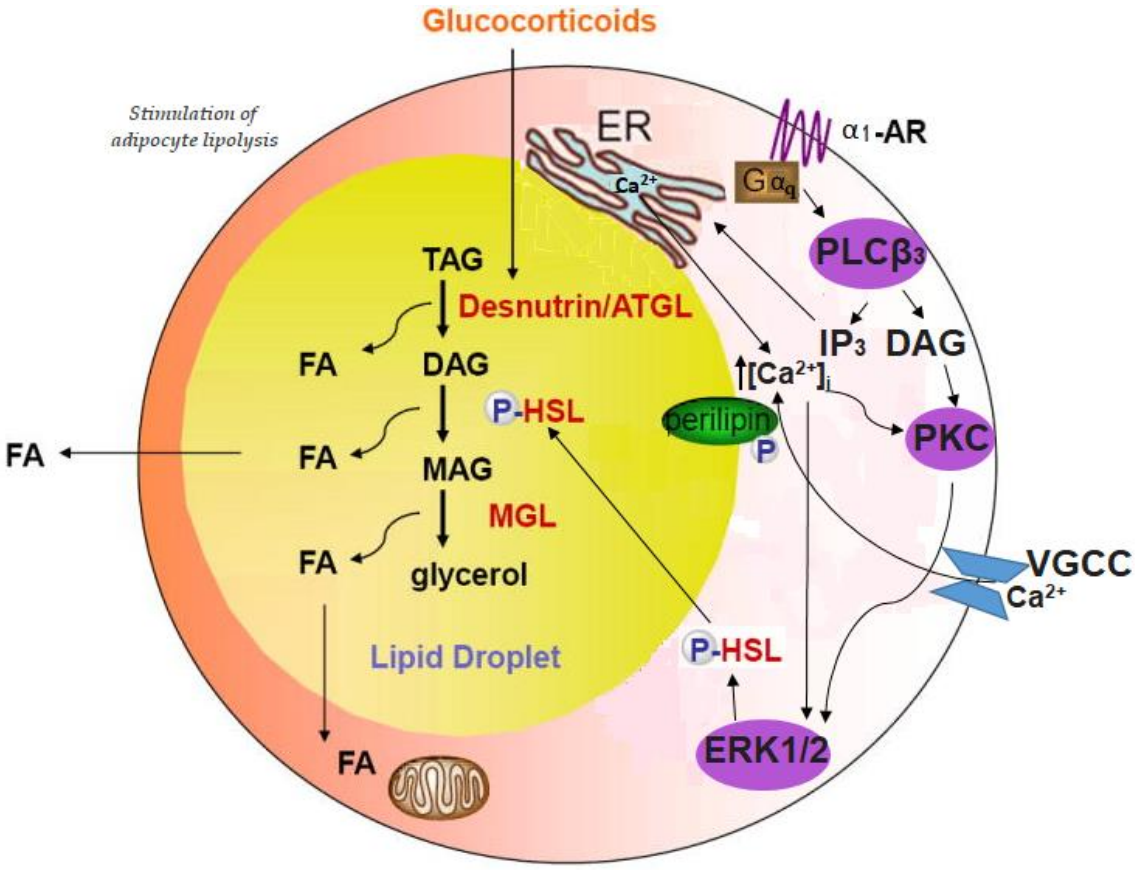

Figure 1.6: The Gαq/PKC/HSL/ERK lipolytic pathway.

Lipolysis through this pathway is thought to involve the entry of calcium through Ca_V channels, as well as protein kinase C (PKC) mediated activation of extracellular signal regulated kinase 1/2 (ERK1/2). ERK1/2 initiates downstream signalling through phosphorylation of lipases.

1.4.3 Link between the major and minor lipolysis pathways

The β3 adrenergic receptor is also thought to be associated with the MAPK/ERK 1/2 pathway through inhibitory GTP-binding protein (Gi/o) coupling, as it is poorly coupled to adenylyl cyclase (Gerhardt et al., 1999), and may initiate lipolysis in white adipocytes through this signalling pathway. Gerhardt et al. (1999) has shown activation of β3-AR, independent from adenylyl cyclase activation, and the resulting Gi/o mediated activation of ERK1/2 showed a different pharmacological profile to Gs mediated activation of cAMP. The MAPK / ERK1/2 pathway is known to be involved in the control of proliferation and differentiation of adipocytes

(Gerhardt et al., 1999). GPCRs may thus directly or indirectly modulate white adipocyte lipolysis through modulation of this signalling pathway.

1.5 Adipocytes as a store for lipophiles: persistent organic pollutants

White adipose tissue (WAT) is the most abundant tissue of fat mass, and may account for more than half of body weight in severe obesity (Casteilla et al., 2008). The mature white adipocyte is primarily composed of a single large lipid droplet that is ~100 μm in diameter in mice (Martinez-Santibañez et al., 2014). Nuclear and other sub-cellular components are localized within a thin cytoplasmic layer that lines the lipid droplet (Fruhbeck et al., 2001, Chaves et al., 2011, Martinez-Santibañez et al., 2014). Adipocytes synthesize and accumulate massive amounts of triglycerides, which are stored within the intracellular lipid droplet (Louis et al., 2014). *In vivo*, the lipid droplet of adipocytes can fill from 90 - 99 percent of the cell volume (Carmen and Víctor, 2006, Chaves et al., 2011, Louis et al., 2014), making the adipose tissue capable of providing a virtually limitless storage site for triglycerides (Ahima and Flier, 2000, Fruhbeck et al., 2001). To accommodate the lipids, adipocytes are capable of changing their diameter 20-fold and their volumes by several thousand fold (Fruhbeck et al., 2001). The core of the lipid droplet though filled with neutral lipids for the major part, are able to localise other lipophilic/hydrophobic compounds and as such acts as an internal storage site for lipid-soluble compounds in the body (Louis et al., 2014).

Many fat-soluble xenobiotic chemicals such as persistent lipophilic environmental pollutants tend to accumulate in the body's fatty tissues. WAT has thus been recognised as the main body site for distribution of lipophilic compounds (Yanev and Chaldakov, 2012). Importantly, chemicals such as persistent organic

pollutants (POPs) are stored in lipid-rich compartments and have the potential for long-term disruption of metabolic and endocrine processes. Although accumulation and storage of persistent organic pollutants in adipocytes may initially be protective by keeping toxic chemicals away from target organs, it eventually leads to a chronic low-grade internal exposure of humans to these toxicants (Figure 1.7) (Kim et al., 2011, Kim et al., 2012, La Merrill et al., 2013, Louis et al., 2014). The toxicological functions of white adipose tissue are three-fold: as a storage site for hydrophobic environmental pollutants, particularly POPs; as a chronic low-grade internal source of POPs to other vital tissues; as a target site for xenobiotic chemicals which disrupt metabolic and endocrine functions of the adipose tissue (La Merrill et al., 2013). Storage of POPs in the adipose tissue is thought to be primarily in white fat (Bourez et al., 2012), owing to the diffusion limited characteristics of these highly lipophilic chemicals (La Merrill et al., 2013).

1.5.1 Obesogenic and diabetogenic potential of POPs

There are three general categories of POPs: pesticides (including insecticides, herbicides, and fungicides), industrial chemicals, and unintentionally produced by-products of certain chemical and combustion processes (Burleson and Dougherty, 2012). Some of the well-known POPs include dioxins, polychlorinated biphenyls (PCBs) and polybrominated diphenyl ethers (PBDEs) (Haffner and Schecter, 2014). Due to the resistance of POPs to chemical and metabolic degradation, they become more concentrated as they move up through food webs. Biomagnification can lead to concentrations of POPs in humans several orders of magnitude higher than in the general environment (Kim and Lee, 2014, Lee et al., 2014). Also, bioaccumulation of POPs in adipose tissue becomes a source of chronic internal exposure because they are continuously released to the circulation and vital

organs with lipid content (Figure 1.7) (La Merrill et al., 2013, Haffner and Schecter, 2014, Lee et al., 2014).

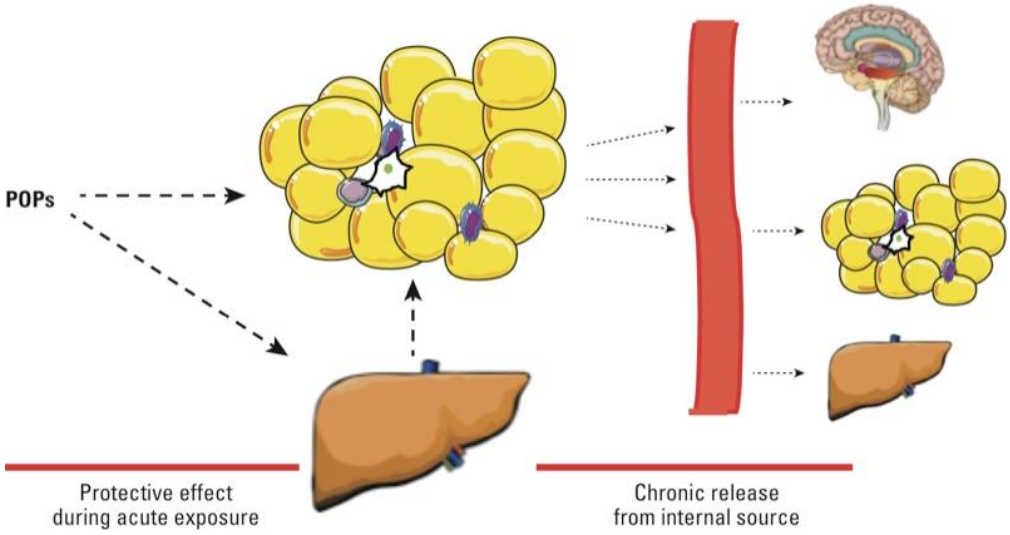

Figure 1.7: Dual role of AT in the regulation of POP kinetics.

Upon exposure to POPs, these lipophilic pollutants are stored in liver and AT (left); this prevents the action of these pollutants in other sensitive tissues and may be protective to a certain extent. POPs released from their storage site in AT constitute a source of low-level internal exposure (right).

Adapted from: La Merrill et al. (2013), Dolphin (2018).

The metabolic and toxic effects of exposure to POPs abound in the literature. These compounds have been termed environmental "obesogens" due to their ability to disrupt the normal endocrine function of adipocytes, resulting in obesity (Pestana et al., 2014). Coplanar PCBs have been demonstrated to impair glucose homeostasis in mice and have been associated with the activation of inflammatory cytokines in the adipose tissue and the development of insulin resistance (Baker et al., 2013a, Baker et al., 2013b). Similarly, 2,3,7,8-tetrachloro-dibenzo-p-dioxin (TCDD) has been associated with low-grade inflammation *in vitro* and *in vivo* (Kim et al., 2012). Polychlorinated Biphenyl-77 promoted the release of pro-inflammatory cytokines in 3T3-L1 adipocytes, and has been suggested to be

capable of contributing to obesity development and obesity-induced atherosclerosis (Arsenescu et al., 2008).

Serum levels of organochlorine pesticides in the general (non-diabetic) population are associated with humoral markers of insulin resistance. This association is stronger in overweight individuals with the highest serum pesticide concentration and absent in those with the lowest concentration (Lee et al., 2007). Exposure to the herbicide atrazine can cause mitochondrial dysfunction and promote obesity and insulin resistance (Lim et al., 2009), and even more detrimental effects are observed when animals are fed a high-fat diet (Lim et al., 2009, Ruzzin et al., 2010). Animal studies have shown that polychlorinated compounds, such as 2,3,7,8-tetrachlorodibenzo-p-dioxin and 1,2,3,4,7,8-hexachlorodibenzo-p-dioxin, may impair glucose metabolism and regulation by reducing glucose uptake in adipose tissue (Enan and Matsumura, 1994). Insulin resistance, visceral obesity and other type 2 diabetes-related abnormalities have been observed in adult rats exposed to chronic, low-dose POP mixtures (primarily consisting of dichlorodiphenyltrichloroethane (DDT), dichlorodiphenyldichloroethylene (DDE), and PCBs) (Ruzzin et al., 2010). Similar findings have been observed in Northern Europeans at 40 to 50+ years of age, suggesting a strong relevance of these experimental findings to humans (Lee et al., 2014). The retention and toxicity of POPs related to the risk of diabetes is thought to be higher in obese individuals (Lee et al., 2006a, Lee et al., 2006b, Vaclavik et al., 2006), suggesting a possible interaction between POPs and obesity on the risk of type 2 diabetes (Lee et al., 2006b). Obesity might however be only weakly associated with diabetes among people with very low serum concentrations of POPs, suggesting that the POPs stored in the adipose tissue may be a key in the pathogenesis of type 2 diabetes

rather than obesity itself (Lee et al., 2006a). A positive dose–response relationship has been observed between prevalence of type 2 diabetes and serum concentrations of several individual POPs, with 15–40-fold increase in the prevalence of type 2 diabetes among those with detectable concentrations of POPs (Lee et al., 2006b). Obesity could invariably lead to bioaccumulation of POPs in the adipose tissues, resulting in a higher risk of type 2 diabetes in such individuals.

POPs are mobilised from their storage site in the adipose tissue into the general circulation during the lipolytic process (Lee et al., 2017). Increased intracellular calcium through Ca_V channels in white adipocytes may further mobilise the release of toxic POPs during lipolysis (Westerink, 2014).

1.6 Study rationale

WAT, though considered to be electrically silent and non-excitable (Beigelman and Hollander, 1963, Bentley et al., 2014), requires an optimal cytosolic concentration of Ca^{2+} to perform its metabolic functions (Draznin et al., 1987, Smith et al., 2014). In addition to regulating key physiological functions of white adipocytes, intracellular calcium may potentiate the toxicological functions of white adipocytes. Lipophillic compounds and organic pollutants are mobilized from WAT on lipolysis (Louis et al., 2014). Since WAT constitutes a continual source of internal exposure to lipophilic compounds (which may induce obesogenic and diabetogenic effects) (La Merrill et al., 2013), and basal lipolysis is regulated by calcium current (I_{Ca}) (Smith et al., 2014), an increase in $Ca_V1.x$ activity could lead to further mobilisation of fat-stored POPs, leading to metabolic disorders.

Relatively little is known about Ca^{2+} signalling in WAT, particularly Ca^{2+} influx pathways in white adipocytes, despite its suggested importance in their function (Koivisto et al., 1993, Sukumar et al., 2012). Preliminary evidence for L-type Ca_v

channel expression and its molecular identity as $Ca_V1.x$ comes from calcium imaging data, RT-PCR and western blots (Bentley et al., 2014, Smith et al., 2014, Forostyak et al., 2016). This project was designed to further investigate the presence of L-type voltage gated Ca^{2+} channels in murine white adipocytes and 3T3-L1 adipocytes and determine their role in white adipocyte physiology, with particular reference to lipolysis and release of lipophilic compounds. Due to the difficulties in obtaining direct-functional evidence for the existence of Ca_V channels in white fat adipocytes by patch-clamp techniques, functional expression will be assessed by imaging techniques, based on intracellular calcium detection by the fluorophore Fluo 4AM (Bentley et al., 2014).

1.7 Aims and Objectives

The overall aim of this study is to corroborate data from previous studies in our laboratory which explored the functional existence of L-type voltage-gated Ca^{2+} channels in white adipocytes with molecular methods. Secondly, to further investigate the role of these channels in the mobilisation of lipophilic compounds from the fat cell. The specific objectives of this study are as follows:

- To characterise the molecular expression of $Ca_v1.x$ in differentiated 3T3-L1 cells (a widely acceptable model of *in vitro* adipogenesis) and murine primary adipocytes by molecular biology techniques, followed by proteomics analysis and cataloguing of identified $Ca_V1.x$ channels in the adipocytes.
- To explore the functional expression and regulation of $Ca_v1.x$ in white adipocytes by endogenous compounds such as growth hormone and parathyroid hormone, agents which have previously been shown to modulate $Ca_V1.x$ channel gating and $[Ca^{2+}]_i$.

- To explore the relationship between $Ca_v1.x$ channel activity and mobilization of fat soluble compounds.

CHAPTER TWO

Molecular expression of voltage-gated calcium channels in white fat adipocytes

2.1. Introduction

Obesity is defined by hyperplasia, due to an increase in pre-adipocyte proliferation and differentiation into mature adipocytes, as well as hypertrophy of adipocytes and the accompanying increase in fat mass (Oguri et al., 2010). The development of obesity is a pre-disposing factor for the development of other metabolic disorders; including diabetes mellitus, hyperlipidemia, hypertension and cardiovascular diseases. The role of intracellular calcium in cell proliferation and differentiation of other cell types has been well researched, however, calcium influx pathways in the adipose tissue, particularly WFAs and the role of intracellular calcium in adipose tissue physiology has remained largely uncharacterized.

2.1.1. Background literature on molecular expression of voltage-gated calcium channels in white fat adipocytes

Despite the ubiquitous expression of Ca_V channels in various tissues and their physiological relevance/role in cellular functioning, the molecular expression profile of these channels in the adipose tissue has remained largely unexplored. A number of studies have reported the observation of different Ca_V channel isoforms, particularly members of the $Ca_V1.x$ and $Ca_V3.x$ channel families in pre-adipocytes, as well as cultured primary adipocytes. Recent studies by Zhang et al. (2018) has identified the involvement of $Ca_V1.x$ in the adipogenesis of porcine bone marrow mesenchymal stem cells, by mediating intracellular calcium increase which was

sensitive to inhibition by the dihydropyridine antagonist, nifedipine. Similarly, Sun et al. (2012a) has noted the role of $Ca_V1.x$ channels in the adipogenesis of mice primary pre-adipocytes. $Ca_V3.1$ (T-type Ca_V channel) is thought to be predominantly expressed in pre-adipocytes (Zhai et al., 2020), where it plays a role in adipocyte proliferation. Its expression in mature adipocytes is diminished and inhibition of the channel using T-type channel antagonists, NNC55-0396 and TTA-A2, results in inhibition of adipocyte proliferation (Uebele et al., 2009).

2.1.2. Alternative splicing/splice variants of L-type voltage gated calcium channels

Alternative splicing is a post-transcriptional modification process in which multiple functional variants can be generated from a single gene (Liao and Soong, 2010, Hu et al., 2017). It leads to the generation of functionally diverse isoforms of the gene with modified biophysical, pharmacological and functional characteristics, through inclusion or exclusion of alternative exons in various combinations (Hu et al., 2017). For instance, the $\alpha_2\delta$ subunit of $Ca_V1.2$ has 4 isoforms; $\alpha_2\delta_{1\text{-}4}$. Of these, the $\alpha_2\delta_1$ isoform which is predominantly expressed in skeletal muscles, as well as in cardiac and smooth muscles, where it promotes cell surface expression of the $Ca_V1.2$ channel and increases the contractile ability of cerebral arteries (Bannister et al., 2012).

The human $Ca_V1.2$ gene contains extensive splice variants in the domain IV segment 3 and domain IV segment 3 – 4 linker regions. About 19 of the 55 known exons of the human $Ca_V1.2$ gene, *CACNA1C*, which encodes the transmembrane pore-forming α_1 subunit of the $Ca_V1.2$ channel undergo alternative splicing (Liao and Soong, 2010), however the full set of splice loci and variations, as well as their anatomical distribution could be well underestimated (Figure 2.1).

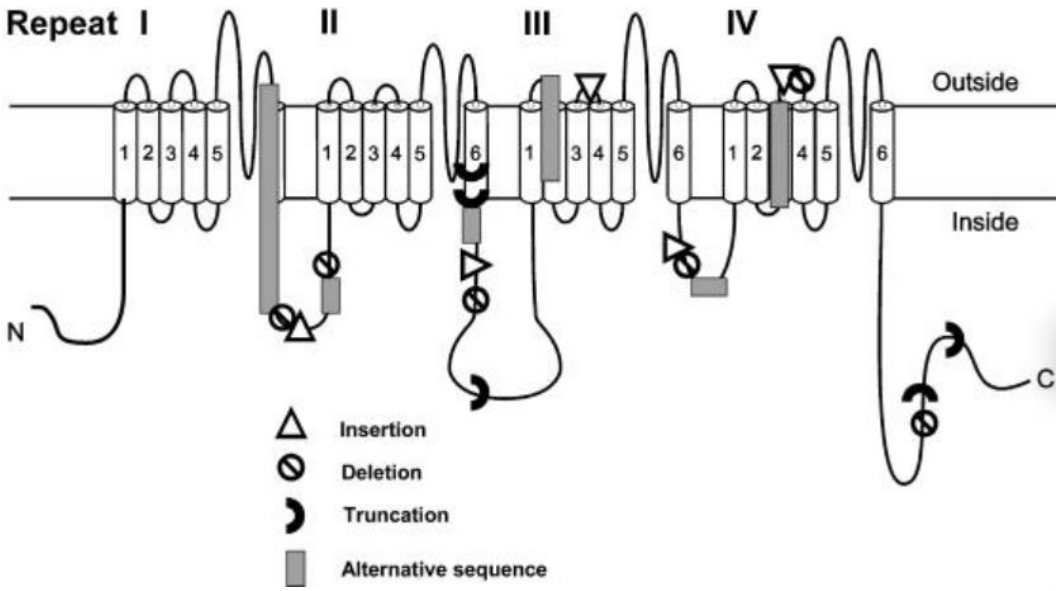

Figure 2.1: Alternative splicing regions in the α_1 subunit.

The diversity of the primary protein sequence is shown by the various symbols.

Adapted from: Jurkat - Rott and Lehmann - Horn (2004)

Tissue specificity of splice variants provides the fine-tuning of channel function in adaption to various cellular or tissue conditions or pathological conditions (Liao et al., 2015, Hu et al., 2017). This generates structural and functional diversity in the channel protein (Bannister et al., 2011). Alternative splicing of the $Ca_V1.2$ channels leads to functionally distinct $Ca_V1.2$ channel isoforms with altered channel properties such as changes to gating properties, altered sensitivity to channel blockade by calcium channel antagonists and regulation by protein kinases (Tang et al., 2004, Liao and Soong, 2010). For instance, exon 33, in addition to exon8/8a can determine the sensitivity of $Ca_V1.2$ channels to the 1,4-dihydropyridine calcium channel antagonist, nifedipine (Li et al., 2017). Also, cardiac and smooth muscle splice variants of the $Ca_V1.2$ channel exhibit different

sensitivities to the non-dihydropyridine calcium channel antagonist, diltiazem based on the levels of exons 1, 8 and 9 present (Zhang et al., 2010). Expression of $Ca_V1.2$ channel isoforms could be tissue/species specific, developmentally regulated or expressed under pathological conditions (Hu et al., 2017).

2.1.3. Post-translational modifications of L-type voltage gated calcium channels

Several cell signalling pathways act on Ca_V channels and regulate their cell surface expression. In addition, Ca_V channels undergo post-translational modifications which regulate their function and density in the plasma membrane (Huang and Zamponi, 2017). Ca_V channel isoforms are modulated and regulated post translationally through various mechanisms, including; phosphorylation, glycosylation, ubiquitination, proteolysis and direct GPCR binding (Huang and Zamponi, 2017). Ca_V channels can form physical interactions with GPCRs leading to their regulation. The first of such channel-receptor complexes observed was a macromolecular signalling complex of $Ca_V1.2$ L-type calcium channels with β-adrenergic receptors, as well as the presence of adenylyl cyclase, phosphatase 2A and protein kinase A (Huang and Zamponi, 2017). Although it is unknown if this channel-receptor interaction is mediated directly or through the action of scaffolding proteins, these channel-receptor complexes enhance signal specificity by improving the efficiency of receptor coupling with the channel. The main effector of GPCR interaction are kinases. Phosphorylation by protein kinases, including protein kinase A, protein kinase C and calmodulin-dependent protein kinases, is a key regulatory mechanism which all Ca_V channels undergo (Catterall, 2000, Dolphin, 2009).

In addition of GPCR modulation, post-translational modifications such as glycosylation of calcium channels provide longer term changes in channel function and cell surface expression. $Ca_V1.2$ channels contain a number of glycosylation sites, which are involved in regulation of channel gating properties and cell surface expression (Huang and Zamponi, 2017). N-linked glycosylation is a post translational modification in which glycan chains are linked or conjugated to extracellular facing asparagine residues within the consensus motifs N-X-S or N-S-T. Cell surface expression and voltage dependent gating of $Ca_V1.2$ channels is also enhanced by asparagine-linked glycosylation (Park et al., 2015). The Ca_V α2/δ subunit of HVA calcium channels additionally has about 16 potential glycosylation sites, with four of these being particularly important for proper functioning of the Ca_V channel (Huang and Zamponi, 2017). The functional importance of post-translational modification of Ca_V channels though not fully understood, has been demonstrated for $Ca_V3.2$ T-type calcium channels, in which administration of neuraminidase to mediate deglycosylation in diabetic mice allows analgesic response (Huang and Zamponi, 2017).

2.2. Study rationale

Intracellular Ca^{2+} sources in endocrine cells such as WFAs is through Ca_V channel Ca^{2+} influx and/or Ca^{2+} release from intracellular endoplasmic reticulum or sarcoplasmic reticulum stores (Komai, 2015). Pharmacological evidence suggests Ca^{2+} influx through $Ca_V1.x$ channel in WAT is necessary for lipolysis (Bleicher et al., 1966), lipogenesis (Avasthy et al., 1988), and insulin action (Draznin et al., 1987). Different facets of insulin action is dependent on extracellular and intracellular [Ca^{2+}] (Draznin et al., 1988). Sustained levels of increasing $[Ca^{2+}]_i$ contributes to metabolic disorders such as obesity (Draznin et al., 1988, Draznin

et al., 1987) and type 2 diabetes (Worrall and Olefsky, 2002), as elevated $[Ca^{2+}]_i$ levels have been associated with blunted sensitivity to insulin action and decreased utilisation of glucose (Zemel, 1998, Draznin, 1993). The involvement of $Ca_V1.x$ channels in the maintenance of resting $[Ca^{2+}]_i$ (Smith et al., 1993, Gaur et al., 1998) and regulation of lipolysis in adipocytes (Gaur et al., 1998) has also been suggested. Hence, determination of the molecular identity and Ca_V channel isoforms in WFAs is imperative, as we aim to further our understanding of the involvement of Ca_v channels in metabolic disease development.

2.2.1 Aim of study

The aim of the study is to determine the expression profile of Ca_v channels in WFAs. The specific objectives are as follows:

- To characterise the molecular expression of Ca_V channels in differentiated 3T3-L1 cells (a widely acceptable model of *in vitro* adipogenesis) and murine primary adipocytes by western blotting.
- To validate identified proteins using mass spectrometric analysis and cataloguing of Ca_V channels in the adipocyte plasma membrane.

2.3. Methodology

2.3.1 Sample / Tissue Preparation

2.3.1.1 Establishment of 3T3-L1 Pre-Adipocyte Cell Line

The 3T3-L1 pre-adipocyte cell line is the predominant cell line for the *in vitro* study of adipogenesis (Trujillo and Scherer, 2006). The 3T3-L1 cell line was originally derived by clonal expansion from disaggregated 17 – 19 day old Swiss 3T3 mouse embryos based on their ability to accumulate lipids (Ruiz-Ojeda et al., 2016). The cells exhibit a fibroblast-like morphology and under specific conditions, they can acquire an adipocyte-like phenotype. Differentiation of the fibroblastic 3T3-L1 pre-adipocytes to mature adipocytes involves exposure of the cells to a differentiation cocktail, comprised of insulin, a synthetic glucocorticoid such as dexamethasone and a phosphodiestase inhibitor such as 3-isobutyl-1-methyl xanthine (Zebisch et al., 2012, Morrison and McGee, 2015, Ruiz-Ojeda et al., 2016). The cells initially undergo cell cycle growth arrest, followed by transcription of proadipogenic genes and the differentiation of the 3T3-L1 fibroblasts into lipid laden adipocyte-like cells. These so-called 3T3-L1 adipocytes are a widely accepted *in vitro* cell model for white fat adipocyte as the gene expression profile and basal bioenergetics of 3T3-L1 adipocytes are typical of white adipocytes (Morrison and McGee, 2015).

Frozen 3T3-L1 pre-adipocytes (ATCC CRL 1658) (passage 8 – p8) in 1 ml of freezing media (10 % v/v dimethyl sulfoxide (DMSO) in Dulbecco's Modified Eagle's Medium (DMEM) supplemented with 10 % newborn calf serum (NCS), 2 mM L-glutamine, penicillin/streptomycin (100 units/ml)(100 µg/ml)) was obtained from Dr S. L. F. Chan and was gently thawed under running warm tap water. The 3T3-L1 pre-adipocytes were then transferred into a 25 cm^2 Nunclon flask which contained 6 ml of basal medium I (high glucose DMEM (Sigma D6546)

supplemented with 10 % NCS (Sigma N4637), 2 mM L-glutamine (Sigma G7513), penicillin/streptomycin (100 units/ml and 100 µg/ml respectively; Sigma PO781) and 25 mM HEPES (Sigma H0887; pH 7.4). The cultured cells were incubated for 1 hour at 37°C, in a humidified atmosphere of 5 % carbon dioxide.

The cells were then examined microscopically with a x10 objective lens in phase contrast mode to confirm attachment of the cells to the surface of the culture vessel. The culture media was discarded to remove the DMSO in the freezing media and replaced with 7 ml of fresh basal medium I, after which they were incubated at 37 °C in a humidified atmosphere of 5% carbon dioxide. The pre-adipocytes were maintained in culture by changing the media every 2-3 days, until they attained ~80 % confluence, after which the cells were passaged by detachment with 1 x trypsin/EDTA (Sigma T4174). Briefly, the media was discarded, and the cells washed with 5 ml of Dulbecco's Phosphate Buffered Saline (DPBS) (Sigma D8537) to remove any remnant serum. 1 ml of 1 x trypsin/EDTA was added, and the cells were incubated at 37 °C for 2 minutes to allow detachment of the cells from the surface of the culture vessel. The action of trypsin was inhibited by addition of 3 ml basal medium, and the resulting cell suspension was transferred to a T75 cm^2 flask containing 15 ml of basal medium I and re-incubated at 37 °C, in a humidified atmosphere of 5 % carbon dioxide. Subsequently, the cells were maintained at a 1:3 split ratio and following expansion, a small stock of early passage 3T3-L1 cells (p11) were frozen down and stored in liquid nitrogen. This was followed by further expansion of the cells and freezing of cells of a later passage (p16), from which subsequent experiments were conducted.

2.3.1.2 Differentiation of 3T3-L1 Pre-Adipocytes

Differentiation of 3T3-L1 pre-adipocytes to adipocytes was achieved using a hormonal cocktail that typically includes insulin, a glucocorticoid, a phosphodiesterase inhibitor, and often a PPARγ agonist (e.g. rosiglitazone (Zebisch et al., 2012)). A flask of 3T3-L1 cells (p10) in T75 cm^2 flask at 80 % confluence was trypsinized as previously described. The action of trypsin was inhibited by addition of 3 ml of basal medium I. 10 µl of the resulting cell suspension was mixed with 10 µl of trypan blue (BioRad 145-0013) and this was loaded onto a dual chamber counting slide (BioRad 145-0011) and the cells counted using the automated cell counter (BioRad TC20). The cells were then reseeded (onto 22 mm coverslips in 6 well plates for calcium imaging experiments or in T75 cm^2 flasks for western blotting experiments) at a density of 30,000 cells/ml of the culture medium. 3 ml of cell suspension was added to each well of a 6-well plate and followed by incubation at 37 °C, in a humidified atmosphere of 5 % carbon dioxide.

Differentiation of pre-adipocytes was carried out using the methods described by Zebisch et al. (2012). 48 hours post-confluent 3T3-L1 cells (day 0) at passage 11 were treated with differentiation medium I (DFM I), which consisted of basal medium II (basal medium I with 10% NCS substituted by 10 % fetal bovine serum (FBS) (Sigma F9665)) supplemented with differentiation cocktail: 1 µg/ml insulin (Sigma I5523), 0.5 mM 3-isobutyl-1-methylxanthine (IBMX) (Sigma I7018) and 0.25 µM dexamethasone (Sigma D1756). Negative control cells were maintained in BM II supplemented with equal volume of the vehicles used to dissolve the differentiation chemicals (1:9 v/v acetic acid/distilled water, DMSO and ethanol). Test cells were treated with DFM I (BM II supplemented with 1 ug/ml insulin, 0.5

mM IBMX, 0.25 µM dexamethasone), while positive control cells were treated with DFM I supplemented with 2 µM rosiglitazone (Sigma R2408). On Day 2 of differentiation, DFM I was replaced with DFM II (BM II supplemented with 1 µg/ml insulin) in both test cells and positive control cells, while media in negative control cells was replaced with BM II supplemented with equal volume of the vehicle used to dissolve insulin (1:9 v/v acetic acid/distilled water). On day 4, media in all cells (negative control cells, test cells and positive control cells) was replaced with fresh basal medium II and adipocytes were subsequently maintained in culture by changing the media every 2 days. To monitor differentiation, images of day 2, 4 and day 8 cells were obtained using a CMEX-18PRO digital microscope camera (Euromex) attached to a Nikon TMS Inverted Phase Contrast Microscope, using the x10 objective lens. Oil red O staining of day 9 3T3-L1 adipocytes was carried out to confirm differentiation. Further experiments were carried out using day 8 – day 15 3T3-L1 adipocytes, not later than passage 21.

2.3.1.3 Primary Adipocyte Isolation

Sub-cutaneous and visceral adipocytes were respectively prepared from inguinal and epididymal fat pads excised from male Wistar rats (body weight 260-360 g) and Sprague-Dawley rats (body weight ~280 g) fed ad libitum. Animals were killed by stunning, followed by cervical dislocation in accordance with UK Home Office guidelines. Primary white adipocytes were isolated from the respective fat pads using a modification of the method of Rodbell (1964). Fat pads were dissected and transferred into 10ml of Hanks solution, which contained 5.6 mM KCl, 138 mM NaCl, 4.2 mM $NaHCO_3$, 1.2 mM NaH_2PO4, 1.2 mM $MgCl_2$, 2.6 mM $CaCl_2$, 10 mM HEPES, pH 7.4, supplemented with 0.5 % w/v bovine serum albumin fraction V (Sigma A3059) and 5 mM glucose. The fat pad was washed thoroughly to remove

residual blood and any visible arteries (and the epididymis for epididymal fat pad) were carefully dissected out. The fat pad was then cut in ~5mm pieces into a glass scintillation vial which contained 10 ml of 0.5 mg/ml of collagenase type 2 (Sigma C6885). The tissue was minced for 2 minutes, and the resulting mixture transferred to a 25 ml Nalgene Erlenmeyer flask. A further 10 ml of Hanks solution was used to rinse the scintillation vial into the flask and the flask was capped and placed in a shaking Grant water bath (Griffin and George 896331) at 37 °C for ~ 50 minutes (at which time the digest turned milky and turbid, an indication of adipocyte liberation).

Following digestion, the digest was filtered, to remove undigested lumps of tissue, through a 350 µm nylon mesh into a 50 ml syringe, with its attached Luer lock closed. The suspension was left for 5 mins to allow the adipocytes to rise to the top of the syringe and form a visible white layer, at which time the infranatant was drained off. This characteristic of the adipocytes to float and form a visible white layer due to their high lipid content, aids in the isolation process, as cell debris and other contaminating cell types present within the adipose tissue explants (fibroblasts, macrophages, stromal cells, monocytes and pre-adipocytes (Vázquez-Vela et al., 2008, Bentley et al., 2014)) precipitate out. The adipocytes were re-suspended with another 20 ml of Hanks solution and the above procedure repeated twice. To obtain the adipocytes, the cells were re-suspended in 20 ml of Hanks solution and after draining off the lower solution, the cells were either collected into a 2 ml tube, spun down at 1,000 g for 10 mins to remove any excess Hanks solution and obtain packed cells. Cells for western blotting were labelled accordingly and stored at -80 °C until further analysis.

2.3.2 Western Blotting of 3T3-L1 Adipocytes and Rat Sub-Cutaneous and Visceral Adipocytes

2.3.2.1 Protein isolation

Cytosolic and solubilised membrane proteins were prepared from day 7 3T3-L1 adipocytes (p19) (in 6-well plates) and 3T3-L1 adipocytes (p20) (in T75 cm^2 flasks) as follows. Lysis solution was prepared by addition of 10 µl of protease inhibitor cocktail (Sigma P8340) per 1 ml of lysis buffer (containing 20 mM Tris, 1 mM EGTA, 320 mM sucrose, 0.1 % v/v Triton X-100, 1 mM sodium fluoride, 10 mM beta glycerophosphate, pH 7.6). For cells grown on 6-well plates, spent media was discarded and cells were rinsed with 1 ml of ice-cold DPBS. 100 µl of lysis solution was added to each well and the cells lysed using the rubber end of a 1 ml syringe plunger. The cell lysates were incubated on ice for ~10 mins before collection into 1.5 ml Eppendorf tubes (replicate wells were collected into the same tube). To ensure all the cells were collected, a further 100 µl of lysis solution was used to rinse each well. Cells grown in T75 cm^2 flasks were harvested by rinsing with 10 ml of ice-cold DPBS, followed by addition of 3 ml of lysis solution to the flask and scraping the cells with a cell scraper. The cells were collected into a 50 ml falcon tube and a further 2 ml of lysis solution used to rinse each flask, to ensure all the cells were collected. At this point, both well grown- and T75 flask grown cells were centrifuged at 300 g for 10 minutes at 4 °C and resuspension of the cell pellets in 400 – 500 µl of lysis solution. Cells were lysed by 3 cycles of 20 seconds freeze thaw cycles and 3 cycles of passage through a 19G needle. Each sample was centrifuged at 21,380 relative centrifugal force (rcf) for 15 minutes at 4 °C. The resulting supernatant was collected as cytosolic proteins. The resulting pellets were re-suspended in 400 µl of lysis solution and homogenised by pipetting up and down several times. A second centrifugation at 21,380 rcf for 15 minutes

at 4 °C was carried out and the supernatant collected as solubilized membrane proteins. Crude tissue homogenates were prepared from male Wistar rat brain and heart and used as positive control samples. Tissue homogenates were prepared by addition of 5 mg of the respective tissue to 300 µl of ice-cold lysis buffer and homogenized using an electric homogenizer. 100 µl of the cytosolic fraction, membrane fraction and tissue homogenate of the respective samples was separately collected into 1.5 ml Eppendorf tubes on ice, for determination of protein concentration by Lowry's assay and for the western blotting gel. All samples were labelled accordingly and stored at -80 °C until further analysis.

2.3.2.2 Optimisation of enriched plasma membrane protein isolation

To optimise the isolation of enriched crude plasma membrane proteins, two different methods were employed as follows:

Method 1: Membrane isolation buffer 1 was prepared by addition of 10 µl of protease inhibitor cocktail (Sigma P8340) per 1 ml of lysis buffer (containing 10 mM tris, 250 mM sucrose, 0.2 mM $CaCl_2$, pH 7.4). Cell pellets were obtained as described above. The re-suspended cells in lysis solution were lysed by 3 cycles of 30 second sonication at ~ 40 % power and cooling on ice for 30 seconds. This was followed by 3 cycles of passage through a 19G/23G needle and then 3 cycles through a 26G needle and centrifugation of the cell homogenate at 3,000 g for 15 minutes at 4 °C to pellet out any unbroken cells. A pre-weighed polyallomer tube was loaded to 60 % full with the resulting supernatant. Ultracentrifugation was performed at 100,000 g for 60 minutes at 4 °C using a Beckman Coulter Optima Ultracentrifuge. This was followed by resuspension of the resulting pellets in 230 µl of membrane isolation buffer 2 (10 mM tris, 250 mM sucrose, pH 7.4) and 12 cycles of passage through a 19G needle and another 12 cycles of passage through

a 26G needle. The thoroughly re-suspended pellets were collected as the crude plasma membrane proteins.

Method 2: This was based on a standard method for adipocyte plasma membrane protein purification by McKeel and Jarett (1970). Membrane isolation buffer was prepared by addition of 10 µl of protease inhibitor cocktail (Sigma P8340) per 1 ml of lysis buffer (containing 10 mM tris, 250 mM sucrose, 1 mM EDTA, pH 7.4). Cell pellets were obtained as described above. The re-suspended cells in lysis solution were lysed as described above, followed by centrifugation of the cell homogenate at 16,000 g for 15 minutes at 4 °C. A pre-weighed polyallomer tube was loaded to 60 % full with the resulting supernatant. Ultracentrifugation was performed at 160,000 g for 45 minutes at 4 °C using a Beckman Coulter Optima Ultracentrifuge. This was followed by resuspension of the resulting pellets in 700 µl of lysis solution and 12 cycles of passage through a 19G/23G needle and another 12 cycles of passage through a 26G needle in order to thoroughly re-suspend the cell pellets. Another centrifugation at 160,000 g for 45 minutes at 4 °C was carried out, after which the pellets were re-suspended in 300 µl of lysis solution and collected as microsomal proteins. For the crude plasma membrane proteins, pellets resulting from 16,000 g x 15 minutes centrifugation of the cell homogenate above was re-suspended in 400 µl of lysis solution and centrifuged at 1,000 g for 10 minutes and the pellets were again re-suspended in 230 µl of lysis solution and collected as the nuclei fraction. The supernatant was further centrifuged at 16,000 g for 20 minutes and the resulting pellets were re-suspended in 230 µl of lysis solution and collected as the crude plasma membrane fraction (Figure 2.2).

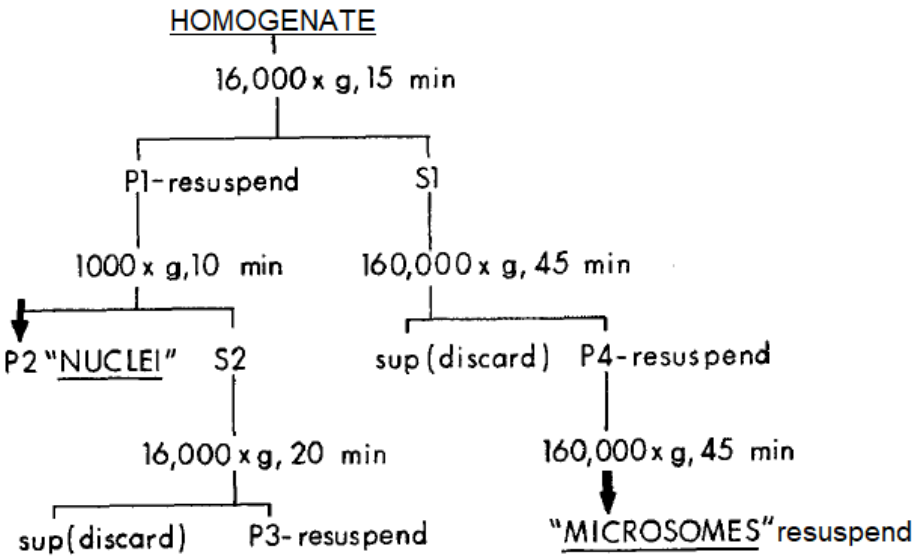

Figure 2.2: Schematic representation of the procedure for isolation of enriched crude plasma membrane proteins using method 2.

S = supernatant, P = pellet. Adapted from: McKeel and Jarett (1970).

2.3.2.3 Determination of protein sample concentration by lowry assay

To determine the protein concentration of all samples and thus the amount of protein to load on the PAGE gel, a Lowry assay was carried out as follows. A 1 mg/ml stock solution of bovine serum albumin (BSA) in distilled water was prepared and the following dilutions of BSA stock solution in distilled water were prepared for the BSA standard curve.

Table 2.1: Concentrations and dilutions of 1mg/ml BSA stock solution for protein assay standard curve.

Tube no.	Sample concentration (µg/µl)	BSA (µl)	DH_20 (µl)
0	0	0	200
1	0.05	10	190
2	0.10	20	180
3	0.15	30	170
4	0.20	40	160
5	0.25	50	150
6	0.30	60	140
7	0.35	70	130
8	0.40	80	120
9	0.45	90	110
10	0.50	100	100

Each concentration was made up in a separate 1.5 ml Eppendorf tube. A new standard curve was constructed for every sample set to be assayed for protein concentration. All standards and samples were assayed in triplicate wells of a 96-well plate.

In separate 1.5 ml Eppendorf tubes, 1:20 dilution in distilled water of rat brain and heart tissue lysates and 1:2 dilution in distilled water of cytosolic and membrane proteins from day 7 3T3-L1 adipocytes (p19) was prepared. 1 ml of Lowry AB solution, prepared by addition of 100 µl of 2 % NaK tartrate and 100 µl of 1% $CuSO_4$ to 20 ml of Lowry A solution (see appendix 2 for composition) was added to all samples, followed by a 10 minutes incubation at room temperature. Thereafter, 100 µl of a 1:1 solution of Folin & Ciocalteu's phenol reagent (Sigma, F9252) in distilled water was added to all samples, after which the samples were immediately vortexed and incubated for 45 minutes in the dark, at room temperature. The samples were then pipetted in triplicate in a 96-well plate at 200 µl/well and the average absorbance at 700 nm determined using the SpectraMax M2 (Molecular Devices) plate reader and the SoftMax Pro 7.0

software. The protein concentration of cytosolic and membrane fractions of the adipocytes were interpolated from the BSA standard curve by linear regression using GraphPad Prism, and utilized if R^2 were ≥ 0.90. Due to dilution of the initial samples for Lowry assay with distilled water, the adjusted protein concentration (in µg/µl) of the samples were determined as follows:

$$\text{Adjusted concentration (µg/µl)} = \text{Interpolated conc. (µg/µl) x dilution factor}$$

Considering that the samples will be further diluted 5 parts to 1 part of a 6x solubilisation buffer (5/6 dilution ratio), the actual protein concentration (in µg/µl) of the adipocyte samples were determined as follows:

$$\text{Actual concentration (µg/µl)} = \text{adjusted concentration (µg/µl) x } \frac{5}{6}$$

Following determination of the amount of protein per microliter of each sample, the volume of each sample to be loaded on the PAGE gel for a specified amount of protein was determined for each sample and experiment.

2.3.2.4 Sodium dodecyl sulphate polyacrylamide gel electrophoresis (SDS-PAGE)

SDS-PAGE was performed using 4 - 20% gradient precast minigels TGX (Biorad #456-1095). The samples were removed and thawed on ice. 20 µl of a 6 x solubilisation buffer (see appendix 1 for composition) was added to 100 µl of the samples separately. The samples were briefly vortexed, then denatured by heating at 95 °C for 5 minutes, after which the samples were again vortexed and spun at 13,000 rpm for 1 min. A 10 x electrophoresis buffer (see appendix 1 for composition) was diluted to 1 x with distilled water and poured into the electrophoresis tank. The gels were cut open and placed in electrophoresis chamber and 1.5 µl of 10 – 250 kDa Precision Plus pre-stained protein marker (Bio-Rad, cat no 161-0374) was loaded on the gel. A specified amount (10 – 30

µg) of protein samples was then loaded onto the gel and a voltage of 170 volts was applied to the samples for 30 minutes (subsequently increased to 40 minutes for better protein separation), after which electrophoresed proteins were blotted onto a nitrocellulose membrane.

Protein transfer onto the nitrocellulose membrane was carried out at 100 volts for 60 minutes in cold transfer buffer (see appendix 1 for composition), after which success of the transfer was always confirmed by staining the membrane with 1 x Ponceau S solution (Sigma, P7170). The appearance of red bands on the nitrocellulose membrane was indicative of successful protein transfer. The membranes were quickly washed with TBST (see appendix 1 for composition) to remove the Ponceau S staining and blocked by gentle rocking in 5% milk in TBST for 4 hours at room temperature. This was followed by overnight incubation at 4 °C with primary antibodies (anti $Ca_V1.2$ (ACC-003), anti $Ca_V1.3$ (ACC-005) and anti $Ca_V3.1$ (ACC-021) at a 1:500 dilution (Alomone labs), anti Na,K-ATPase at 1:20,000 (Abcam ab76020), anti β-actin (Sigma A1978) initially at a 1:30,000 dilution and subsequently increased to 1:5000 dilution for better band visualisation). Membranes were washed for 6 x 5 minutes with TBST and incubated for 1 hour (subsequently increased to 80 minutes) at room temperature with a 1:10,000 dilution of infra-red dye labelled secondary antibodies; IRDye 800 CW goat anti-rabbit IgG (Li-COR™ 926-32211) and IRDye 680 CW goat anti-mouse IgG (Li-COR™ 926-68070). All antibody dilutions were made in 5 % milk in TBST. After a second washing, for 6 x 5 minutes with TBST, membranes were rinsed in distilled water and imaged with the Li-COR Odyssey Imaging System. Western blots were quantified using Image Studio software.

2.3.2.5 Statistical analysis

Data were expressed as signal intensity of the protein sample normalized to β-actin expression in each sample. However, prior to normalisation of the target protein signal intensities to the corresponding β-actin control in the same sample, the lane normalisation factor for each β-actin lane was first determined. For each β-actin lane that was used to normalize the experimental intensity values, the highest signal detected for the housekeeping protein was first located. The value of this band was then used to normalize the rest of the housekeeping bands on the blot as follows:

$$\text{Lane normalisation factor} = \frac{\text{Observed signal of housekeeping protein for each lane}}{\text{Highest observed signal of housekeeping protein on the blot}}$$

To calculate the normalized signal of each experimental target band, the observed signal intensities of each experimental target band was then divided by the lane normalization factor as follows:

$$\text{Normalised experimental signal} = \frac{\text{Observed experimental signal}}{\text{Lane normalization factor}}$$

The statistical significance of the data was then determined using appropriate statistical tests as mentioned within the text.

2.3.3 Mass Spectrometric Analysis

100 µg of plasma membrane proteins, prepared using the optimized in-house plasma membrane isolation procedure described above, was first stained with Coomassie blue, subjected to in-gel tryptic digestion, followed by liquid chromatography tandem mass spectrometry (LC/MS-MS).

2.3.3.1 Sucrose density gradient ultracentrifugation for plasma membrane enrichment

Sucrose density gradient ultracentrifugation for plasma membrane enrichment was initially attempted, although I eventually utilized crude plasma membrane proteins, prepared using the optimized in-house plasma membrane isolation procedure for mass spectrometry analysis.

Briefly, 800 µl of 53 % sucrose solution was layered into a polyallomer tube, followed by an equal volume of 12 % sucrose solution. A clear band was formed at the interface of the two sucrose solutions. 200 µl of crude plasma membrane protein was carefully layered on top of the sucrose gradient and the sample was stirred using a needle, to break up any air between the sample and the 12 % sucrose solution. A control tube was set-up in a similar manner, with 200 µl of lysis solution in place of the protein sample. Ultracentrifugation of the samples was carried out at 30,000 revolutions per minute (rpm) for 90 minutes at room temperature. After centrifugation, a turbid band appeared between the two sucrose solutions, and this was gently collected using a syringe and placed into a 1.5 ml Eppendorf tube. 400 µl of lysis solution was added to the tube and the resulting mixture centrifuged at 16,000 g for 15 minutes. The supernatant was collected as cytosolic proteins and labeled accordingly. The pellets were re-suspended in 800 µl of lysis solution and centrifuged at 16,000 g for 15 minutes. The resulting pellets were re-suspended in 100 µl of lysis buffer II (containing 10 mM tris, 250 mM sucrose, pH 7.4) and collected as membrane proteins.

2.3.3.2 Coomassie blue staining

100 µg of plasma membrane proteins were loaded onto a precast minigel and electrophoresis performed at 170 V for 10 mins, 400 A at room temperature using

1x electrophoresis buffer (see appendix 1 for buffer composition). After electrophoresis, the gel was soaked in water for 5 mins to loosen the edges of the gel tray and the gel was transferred to a polystyrene plate. 80 ml of Coomassie blue stain (see appendix 1 for composition) was added to the plate, with gentle shaking for 1hour. The stained gel was then rinsed with 3 times with water, after which 140 ml of destaining solution (see appendix 1 for composition) was added to the plate and the gel destained overnight. The Coomassie stained band for each sample lane (which was just above the dye front) was excised and the gel pieces were separately added to ddH_20 in Eppendorf tubes and sent for further processing and LC MS/MS analysis.

2.3.3.3 De-Staining of gel slices

Each gel piece was cut into 1-2 mm cubes and separately placed in a 0.5 ml Eppendorf tube. 100 µl of 50% acetonitrile / 100 mM ammonium bicarbonate solution was added to the tube and incubated at 37 °C for 10 mins. The resulting liquid was discarded, and the above step repeated until the gel pieces were completely clear. The gel pieces were then washed several times with HPLC water, and the resulting liquid discarded. 100 µl of 100 % acetonitrile at 37 °C was added to the tubes until the gel pieces appeared white and very shrunken. The acetonitrile was discarded, and the gel pieces left for ~ 10 mins at 37 °C, to ensure that the acetonitrile was totally evaporated.

2.3.3.4 Reduction and Alkylation

About 50 µl of 10 mM dithiothreitol (DTT) in 100 mM NH_4HCO_3 was added to each tube and the reduction reaction allowed to proceed for 1 hour at 37 °C. Afterwards, the DTT solution was removed and 50 µl of 55 mM iodoacetamide in 100 mM NH_4HCO_3 was added to the tubes. The alkylation reaction was allowed to proceed

for 45 mins at room temperature in the dark, after which the resulting liquid was discarded. 100 µl of 100 mM NH_4HCO_3 was then added for 10 mins at 37 °C, after which the resulting liquid was replaced by 100 µl of 100 mM NH_4HCO_3 in 50 % acetonitrile, for 10 min at 37 °C. The resulting liquid was again discarded, followed by addition of 100 µl of 100 % acetonitrile to dry gel pieces. The liquid was then removed when the gel was totally dry (white) and the gel pieces were left for another 10 min at 37 °C to ensure that the acetonitrile had completely evaporated prior to trypsin digestion.

2.3.3.5 Digestion

Tryptic digestion of the proteins was carried out using the (Promega) Sequencing Grade Modified Trypsin (Promega V5111). First, 20 µg of trypsin was resuspended in 40µl of trypsin resuspension solution and further diluted to 4 ml with 50 mM ammonium bicarbonate, to a final concentration of 5 ng/ml. ~60 µl of the trypsin mixture was then added to cover the gel pieces in each tube and the proteins digested over night at 37 °C. The resulting supernatants were made up to 0.1 % formic acid before loading on to LC MS/MS. Mass spectrometric analysis was performed at the Cambridge Centre for Proteomics.

2.3.3.6 Database Searching

Tandem mass spectra from LC MS/MS were extracted. Charge state deconvolution and deisotoping were not performed. All MS/MS samples were analyzed using Mascot (Matrix Science, London, UK; version 2.6.2). Mascot was set up to search the cRAP_20190401.fasta; CCP_Rattus_norvegicus_20181203 database (unknown version, 31681 entries) assuming the digestion enzyme trypsin. Mascot was searched with a fragment ion mass tolerance of 0.100 Da and a parent ion tolerance of 20 PPM. Carbamidomethyl of cysteine was specified in Mascot as a

fixed modification. Deamidated structures of asparagine and glutamine, oxidation of methionine and phosphorylation of serine, threonine and tyrosine were specified in Mascot as variable modifications.

2.3.3.7 Criteria For Protein Identification

Scaffold (version Scaffold_4.8.8, Proteome Software Inc., Portland, OR) was used to validate MS/MS based peptide and protein identifications. Peptide identifications were accepted if they could be established at greater than 95.0% probability by the Peptide Prophet algorithm (Keller et al., 2002), with Scaffold delta-mass correction. Protein identifications were accepted if they could be established at greater than 95.0% probability and contained at least 2 identified peptides. Protein probabilities were assigned by the Protein Prophet algorithm (Nesvizhskii et al., 2003). Proteins that contained similar peptides and could not be differentiated based on MS/MS analysis alone were grouped to satisfy the principles of parsimony. Proteins sharing significant peptide evidence were grouped into clusters.

2.3.4 Immunoprecipitation

2.3.4.1 Direct method

Preparation of the bead-antibody-protein complex

Dynabeads™ Protein A (Invitrogen by Thermo Fisher Scientific 10001D) was homogenised by placing on a roller mixer for 5 mins. 50 µl of the Dynabeads was placed in a 1.5 ml Eppendorf tube and placed on a magnet rack. The supernatant was removed, and the beads were washed 3 times with 200 µl of TBST. After the last wash, the TBST was removed and replaced with 200 µl of 1.5 – 4 µg of anti-$Ca_v1.2$ diluted in TBST. The beads and antibody mix were incubated for 1 hour at 4 °C with rotation. Beads now bound to antibody were placed on the magnetic

rack and washed twice with 200 µl of TBST. 250 - 400 µg of plasma membrane protein diluted in ~100 - 400 µl of lysis buffer was added to the beads and incubated for 30 mins at 4 °C with rotation. Afterwards, the tube was placed on the magnetic rack and the supernatant removed. The bead-antibody-antigen complex was washed with 100 µl of TBST and the bead suspension was transferred to a new tube, placed on the magnetic rack and the supernatant removed. The captured antigens were then eluted.

Washing and elution of captured antigens

Following formation of the bead-antibody-antigen complex, the tube was placed on the magnetic rack and the supernatant was removed. An aliquot of the supernatant as well as control samples from each wash stage was taken for further analysis. The bead-antibody-antigen complex was washed 3 times using 200 µl of lysis buffer. After the last wash step, the bead-antibody-antigen complex was transferred to a fresh tube to prevent elution of the proteins on the tube walls. Elution of the proteins was carried out using 100 mM glycine (pH 2.4), for non-denaturing elution. The bead-antibody-antigen complex was resuspended in 20 µl of elution buffer and incubated for 10 mins at room temperature with rotation and intermittent agitation of the tube. The tube was then placed on the magnetic rack and the supernatant collected into a fresh tube and stored at -80 °C for SDS-PAGE and western blot analysis. 10 µl of 1M Tris/HCl buffer (pH 7.4) was added to the eluted proteins to neutralize the acidic pH of the elution buffer. The beads were neutralised by washing 3 times with 500 µl of lysis buffer, followed by resuspension in 200 µl of lysis buffer and storage at 4°C.

2.3.4.2 Indirect method

Preparation of the antibody-protein complex

~400 µg of plasma membrane proteins were placed in a 1.5 ml Eppendorf tube and 1.5 µg of Anti $Ca_V1.2$ was added to the tube. The mixture was gently pipetted up and down severally. The was followed by the addition of 200 µl of lysis buffer, after which the tube was placed on the rotation wheel at 4 °C for 2 hours, to allow formation of the antibody-protein complex.

Formation of the bead-antibody-protein complex

Dynabeads™ Protein A (Invitrogen by Thermo Fisher Scientific 10001D) were prepared as described above. The antibody-protein complex in 200 µl of lysis buffer was transferred to the tube containing the Dynabeads protein A and the complex thoroughly resuspended. The bead-antibody-protein complex was incubated for 1 hour at 4°C with rotation, after which the captured antigens were washed and eluted as described above. The immunoprecipitated proteins were then analysed by SDS-PAGE and western blotting as previously described.

2.4. Results

2.4.1 Differentiation of 3T3-L1 Pre-Adipocytes to Adipocytes

3T3-L1 adipocytes were cultured and differentiated as described previously (Zebisch et al., 2012). Day 0 of differentiation was defined as the day by which the 3T3-L1 cells had been confluent for 2 days and induction started.

Exposure of 3T3-L1 pre-adipocytes to the adipogenic mixture that contained 1 µg/ml nM insulin, 0.25 µM dexamethasone, and 0.5 mM 3-isobutyl-1-methylxanthine resulted in a change in the fibroblastic nature of the cells to a more lipid laden, adipocytic phenotype (Figure 2.3). Inclusion of 2 µM rosiglitazone in the differentiation media increased the number of cells that attained the adipocytic phenotype by Day 8. 2 µM rosiglitazone visually enhanced the level of pre-adipocyte differentiation, with ~70 % of the cells accumulating triglycerides by day 9, with expansion of their intracellular lipid droplets and differentiation into adipocytes (Figure 2.3). An additional ~20 % of the cells take up an adipocytic phenotype by day 12 and by day 15, virtually all the cells are differentiated into adipocytes. The differentiated cells were then utilised for further experiments.

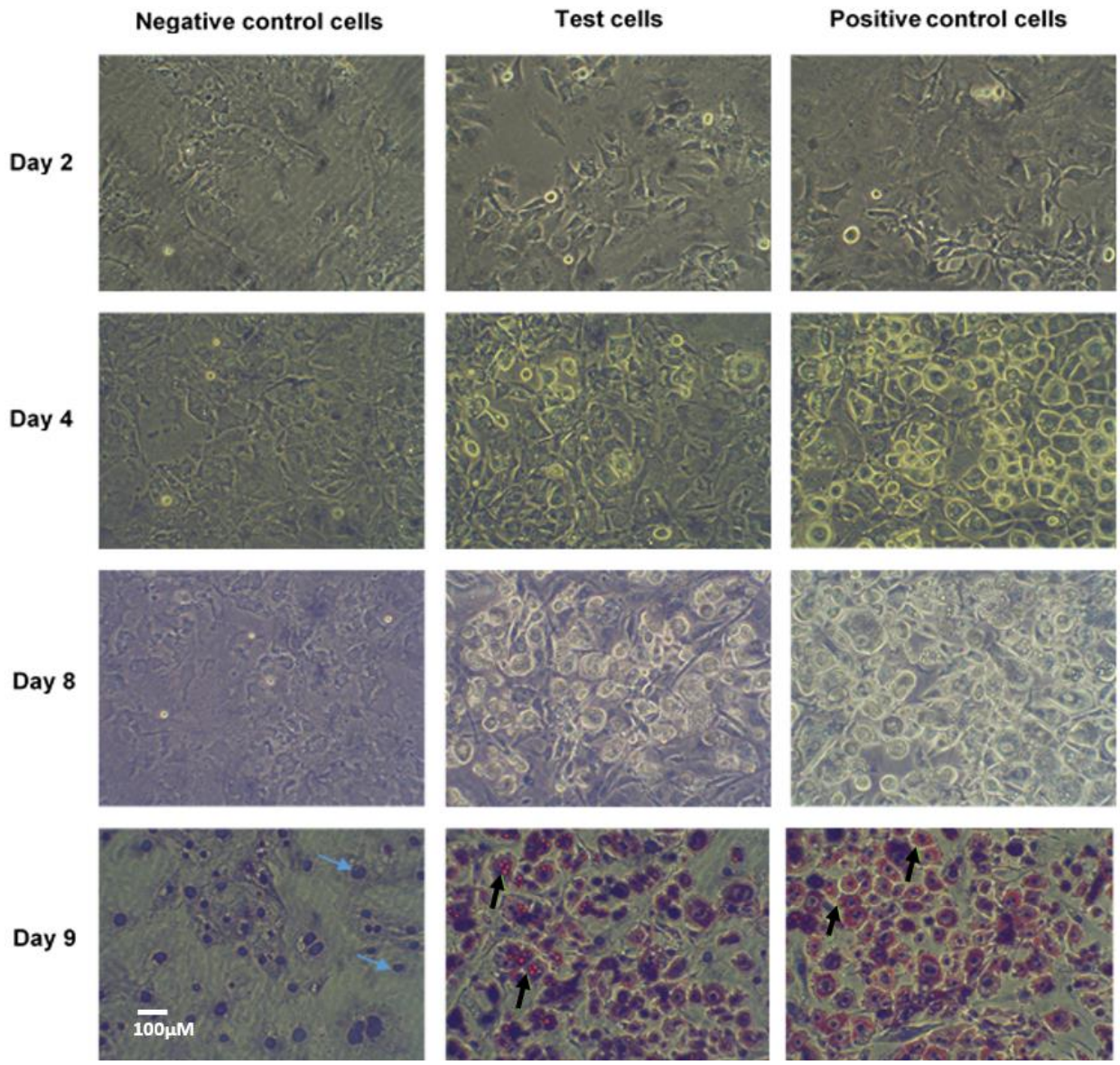

Figure 2.3: Time-course of differentiation of 3T3-L1 pre-adipocytes (passage 11) to adipocytes.

Negative control cells were maintained in BM II, test cells were treated with DFM I (BM II supplemented with 1 ug/ml insulin, 0.5 mM IBMX, 0.25 µM dexamethasone), while positive control cells were treated with DFM I supplemented with 2 µM rosiglitazone. Images were viewed with the x10 objective and captured with a CMEX-18 PRO digital microscope camera (Euromex) attached to a Nikon TMS inverted phase contrast microscope. (Blue arrow indicates purplish-blue staining of the nucleus of undifferentiated 3T3-L1 cells with Harris hematoxylin while black arrow indicates traces of orange-red tints due to Oil red O staining in lipid droplets accumulated by differentiated 3T3-L1 cells, n = 2).

2.4.2 Determination of Protein Expression of Alpha 1 Subunit of Ca_v Channels in 3T3-L1 Adipocytes (Method Development)

Method development including optimisations and validation experiments were performed with proteins isolated from undifferentiated 3T3-L1 pre-adipocytes and differentiated 3T3-L1 adipocytes. Transcriptomics of epididymal fat tissue previously performed in our laboratory showed that the predominantly expressed Ca_V channels in WFAs are the L-type $Ca_V1.2$ and $Ca_V1.3$ channels and the T-type $Ca_V3.1$ channel, hence my focus on these channels for protein expression studies. To confirm the protein expression of $Ca_V1.2$, $Ca_V1.3$ and $Ca_V3.1$ channels in 3T3-L1 adipocytes and murine primary adipocytes, western blotting was carried out using antibodies specific for the α_1 subunit of these channels. Since the channels are known to be expressed in tissues such as the brain and the heart (Catterall, 2011), crude tissue homogenate were prepared from male Wistar rat brain and heart and used as positive control samples. Expression of $Ca_V1.2$, $Ca_V1.3$ and $Ca_V3.1$ proteins in the analysed samples was normalized to that of β-actin, as its expression is thought to be relatively stable across different tissues (Yin et al., 2015).

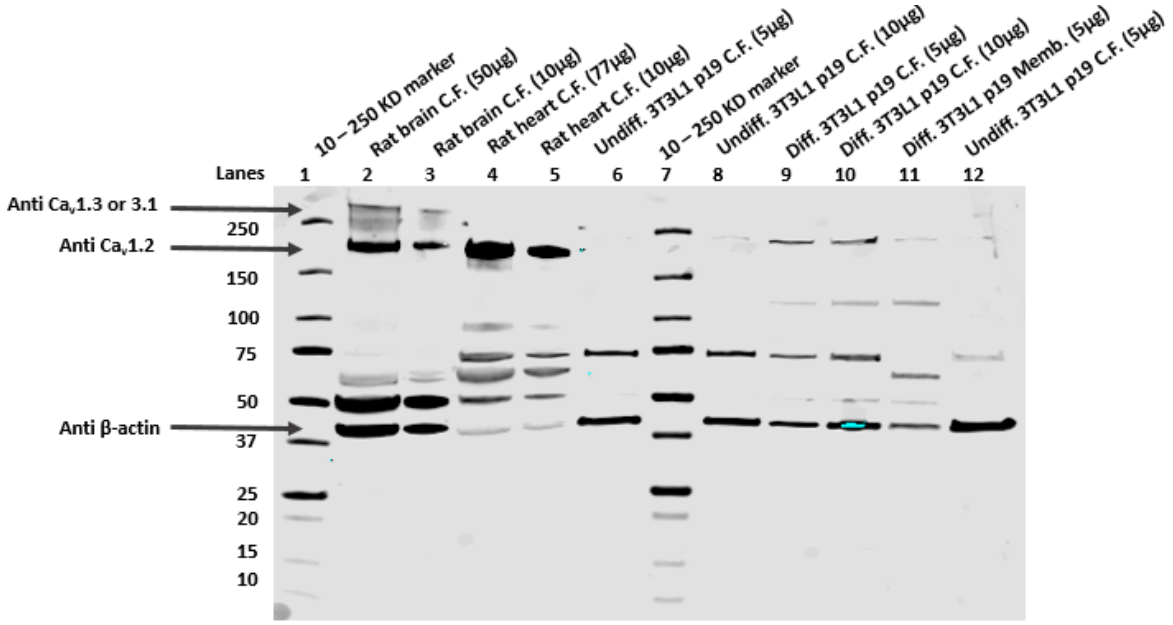

Figure 2.4: Western blot of $Ca_V1.2$, $Ca_V1.3$ and $Ca_V3.1$ and β-actin expression in cytosolic (C.F.) and membrane (memb) fractions of male Wistar rat brain and heart and in undifferentiated (undiff.) and differentiated (diff.) 3T3-L1 cells (p19).

Samples were loaded alongside a 10 kDa – 250 kDa molecular weight protein marker, for band size estimation and the expected band sizes are indicated. Different amounts of proteins were resolved to determine the optimum protein concentration for blotting. (Undiff = undifferentiated, diff = differentiated).

Three major protein bands (lanes 2 and 3) and four major protein bands (lanes 4 and 5) were respectively detected in rat brain and heart tissue lysates and a large band of ~ 250 - 260 kDa (lanes 9 and 10) was detected in the cytosolic fraction of differentiated 3T3-L1 adipocytes (p19) (Figure 2.4). Two low molecular weight bands of ~ 130 kDa and 70 – 75 kDa (lanes 9 - 11) were also detected in the cytosolic and membrane fraction of differentiated 3T3-L1 adipocytes (p19) (Figure 2.4). These data though suggestive of the presence of one or more of the proteins of interest, could not be analysed further as the primary antibodies for $Ca_V1.2$, $Ca_V1.3$ and $Ca_V3.1$ had been probed on the same blot.

The next experiments were conducted to validate the primary antibodies before commencement of further investigations. A distinct band of ~42 kDa, representative of β-actin expression was detected in all the samples analysed, with the exception of the rat heart homogenate, possibly due to the abundance of α-actin over β-actin in the heart (Yin et al., 2015). Consequently, only rat brain homogenate was used as a positive control for further experiments.

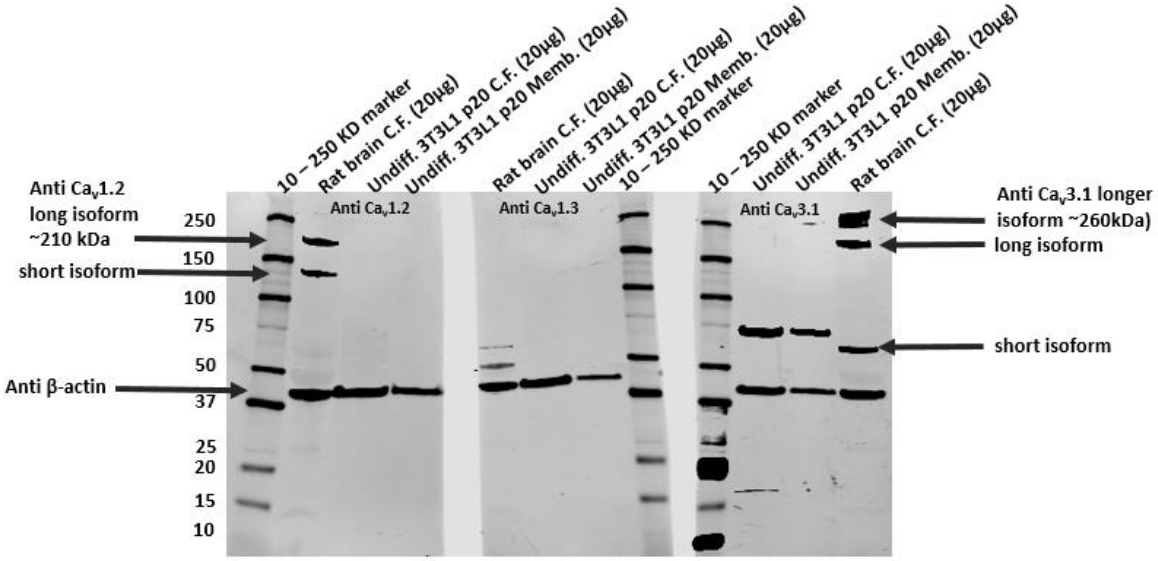

Figure 2.5: Validation of $Ca_V1.2$, $Ca_V1.3$ and $Ca_V3.1$ primary antibodies (Alomone labs, Isreal) in male Wistar rat brain and cytosolic (C.F.) and membrane (memb) fractions of 3T3-L1 pre-adipocytes (p20).

Samples were loaded alongside a 10 kDa – 250 kDa molecular weight protein marker, for band size estimation.

Probing of rat brain tissue lysate and 3T3-L1 pre-adipocytes (p20) with $Ca_V1.2$ specific antibodies on separate blots revealed the presence of two bands, a larger molecular weight protein of ~210 kDa and a smaller molecular weight protein of ~ 130 kDa in rat brain (Figure 2.5; lane 2, Anti-$Ca_V1.2$ blot). No bands were observed in the pre-adipocyte samples. With the $Ca_V3.1$ specific antibody, three bands were detected in rat brain; a large molecular weight protein of ~ 265 kDa, a lower molecular weight protein of ~ 190 kDa and a small protein of < 70 kDa

(Figure 2.5; lane 4, Anti-$Ca_V3.1$ blot). One band of ~ 75 kDa was detected in the cytosolic and membrane fractions of 3T3-L1 pre-adipocytes (p20) using the $Ca_V3.1$ specific antibody (Figure 2.5; lane 2 and 3, Anti-$Ca_V3.1$ blot). No apparent protein bands were detected in any of the samples probed with $Ca_V1.3$ specific antibody.

To further explore the expression of $Ca_V1.2$ and $Ca_V3.1$ channel proteins in 3T3-L1 adipocyte plasma membrane, two different methods were employed to isolate enriched plasma membrane proteins. A method routinely utilised by a different laboratory (denoted method 1 - M1) was compared with a standard method by McKeel and Jarett (1970) (denoted method 2 - M2), to optimize the plasma membrane isolation protocol. Aliquots were taken at each isolation stage and the expression of $Ca_V1.2$ and $Ca_V3.1$ α_1 subunit in different cellular fractions during the isolation of cytosolic and plasma membrane proteins from Day 11 3T3-L1 adipocytes (p20) was determined (Figure 2.6).

The results showed that method 2 was more effective in isolating enriched plasma membrane proteins from the adipocyte preparations (Figure 2.6C and D). With the $Ca_v3.1$ specific antibody, three distinct bands of approximately 130 kDa, 70 – 75 kDa and < 70 kDa were detected in all the fractions resolved, except for the cytosolic (Figure 2.6B; lanes 5 and 9) and nuclear protein fractions (Figure 2.6B; lanes 11), in which the low molecular weight band was absent. With the $Ca_V1.2$ specific antibody, all the protein bands detected were of low molecular weight (<50 kDa) suggesting the protein samples may have been degraded. Hence, the experiment was repeated using only method 2 (Figure 2.7).

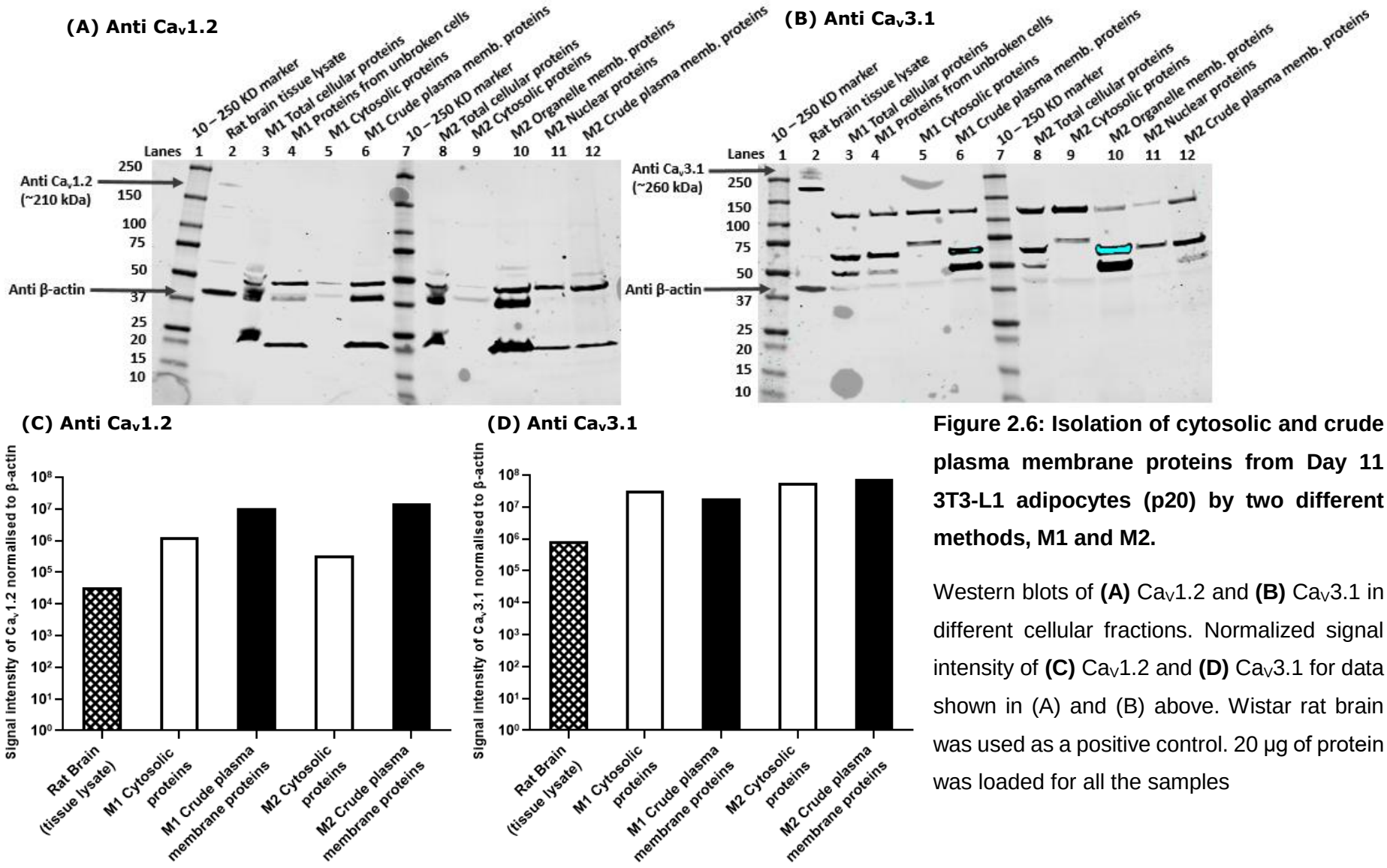

Figure 2.6: Isolation of cytosolic and crude plasma membrane proteins from Day 11 3T3-L1 adipocytes (p20) by two different methods, M1 and M2.

Western blots of **(A)** $Ca_V1.2$ and **(B)** $Ca_V3.1$ in different cellular fractions. Normalized signal intensity of **(C)** $Ca_V1.2$ and **(D)** $Ca_V3.1$ for data shown in (A) and (B) above. Wistar rat brain was used as a positive control. 20 µg of protein was loaded for all the samples

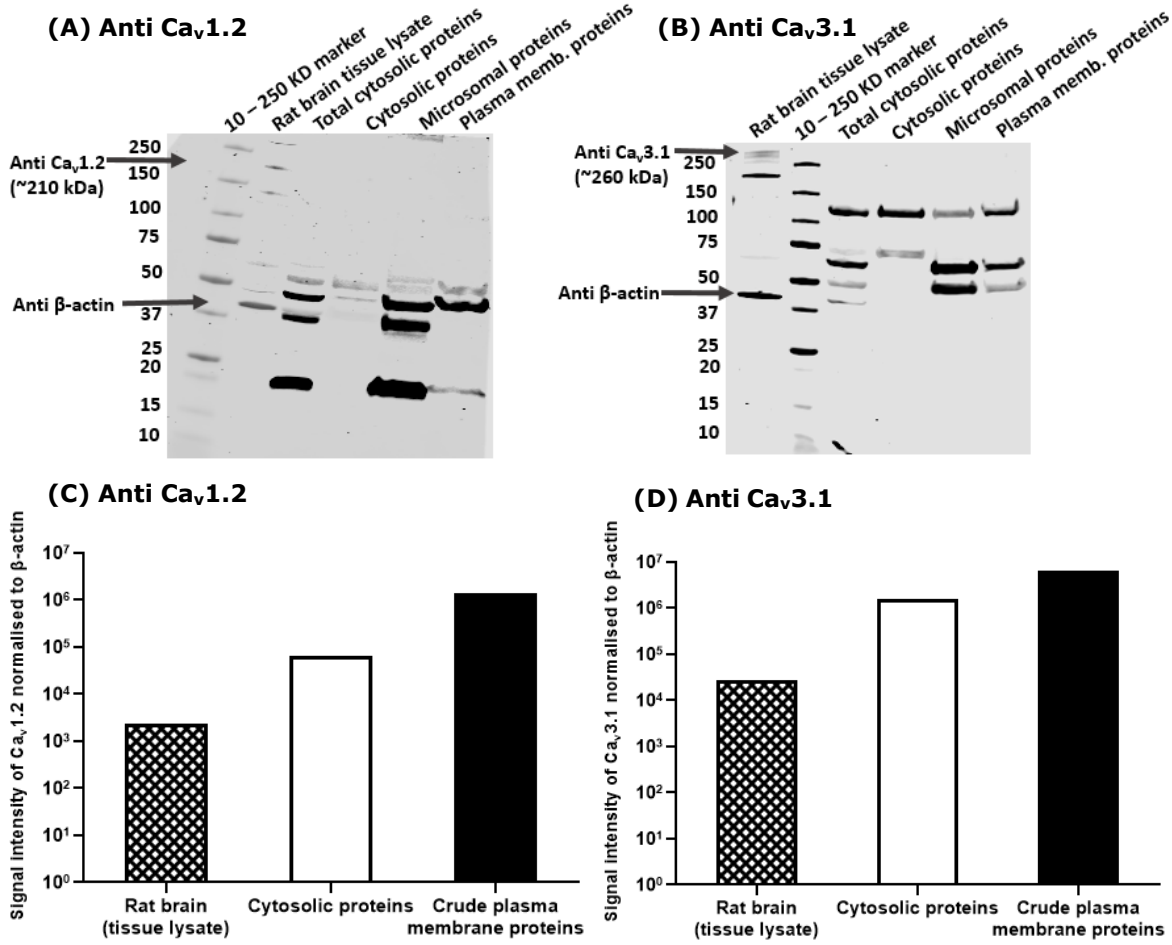

Figure 2.7: Isolation of cytosolic and crude plasma membrane proteins from Day 10 3T3-L1 adipocytes (p19), isolated using the method of McKeel and Jarett (1970).

Western blot of **(A)** $Ca_V1.2$ and **(B)** $Ca_V3.1$ in different cellular fractions. Normalized signal intensity of **(C)** $Ca_V1.2$ and **(D)** $Ca_V3.1$ for data shown in (A) and (B) above. Wistar rat brain was used as a positive control. 20 µg of protein was loaded for all the samples.

The results obtained (Figure 2.7) were very similar to the previous experiment (Figure 2.6) and the degradation observed with the $Ca_V1.2$ specific antibody persisted, warranting reversal to the initial methods which was used for purification of total membrane proteins. Further optimizations were made to the initial method (longer gel electrophoresis time, use of ice-cold transfer buffer, placing the transfer chamber in an ice-tray during the transfer process, incubating with secondary antibodies for a slightly longer duration, some changes to the image studio software settings for image acquisition), and this resulted in better

separation of the larger molecular weight proteins and less degradation of the protein preparations for both cytosolic proteins and crude plasma membrane proteins.

Further optimization experiments were carried out to determine the concentration range over which the signals of the detected proteins were optimum. This was found to be 15 – 20 µg of protein for optimum detection of $Ca_V1.2$ and $Ca_V3.1$ α_1 subunit in cytosolic and crude plasma membrane fractions of male Wistar and Sprague Dawley rat subcutaneous and visceral adipocytes, as well as 3T3-L1 cells. Although the $Ca_V1.3$ specific antibody from Alomone labs had not been successful in detecting the $Ca_V1.3$ channel proteins in previous experiments, its validity was further assessed, as well as a $Ca_V1.3$ specific antibody from Abcam (anti-$Ca_V1.3$ antibody [L48A/9] ab85491), hence its continued use.

A large and a low molecular weight band was detected in the brain tissue lysate, however, no distinct bands were detected in any of the other samples probed with $Ca_V1.3$ specific antibody (Figure 2.8), hence no further experiments were attempted with this antibody.

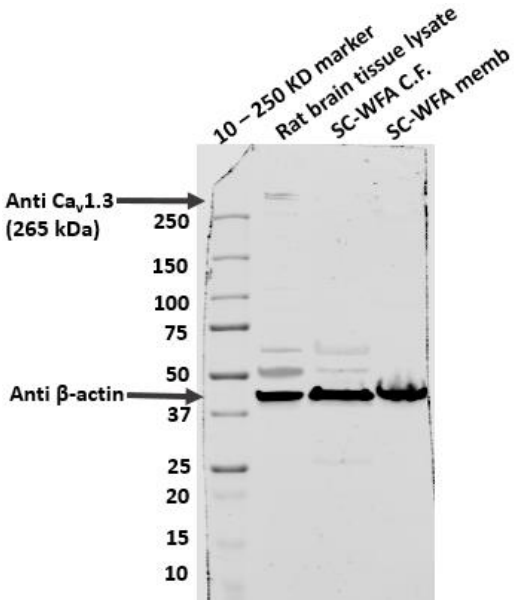

Cav1.3; Alomone (1:500)

Figure 2.8: Representative western blot $Ca_V1.3$ and β-actin expression in cytosolic (C.F.) and membrane (memb) fractions of subcutaneous (SC) male wistar rat adipocytes.

Wistar rat brain was used as a positive control. 20 µg of protein was loaded for all the samples, unless otherwise specified (n ≥ 6 independent experiments).

2.4.3 Molecular Expression of L-Type Calcium Channels in White Fat Adipocytes

Following the above optimizations to the protocol, the protein expression of $Ca_V1.2$ and $Ca_V3.1$ channel proteins in cytosolic and crude plasma membrane fractions of primary white adipocytes and differentiated and undifferentiated 3T3-L1 cells was further explored. Before probing for the presence of our proteins of interest, effective fractionation of the plasma membrane of the adipocytes was confirmed by Western blotting using antibodies (anti β-actin - 1:5,000 (Sigma), anti Na,K-ATPase – 1:20,000 (Abcam)) for markers for the cytosolic fraction, β-actin (~42 kDa), and the plasma membrane fraction, Na,K-ATPase (~98 kDa) (Figure 2.9).

Western blotting of the cytosolic and plasma membrane fractions of both visceral and subcutaneous fat pads with anti Na,K-ATPase showed that the crude plasma membrane preparation protocol initially employed, resulted in successful enrichment of the plasma membrane. This is seen by the higher expression profile of the plasma membrane protein Na,K-ATPase in the plasma membrane fraction compared to the cytosolic fraction in both the visceral (p <0.05, one-way ANOVA and Holm Sidak's test) and subcutaneous AT (p <0.001, one-way ANOVA and Holm Sidak's test) (Figure 2.9B).

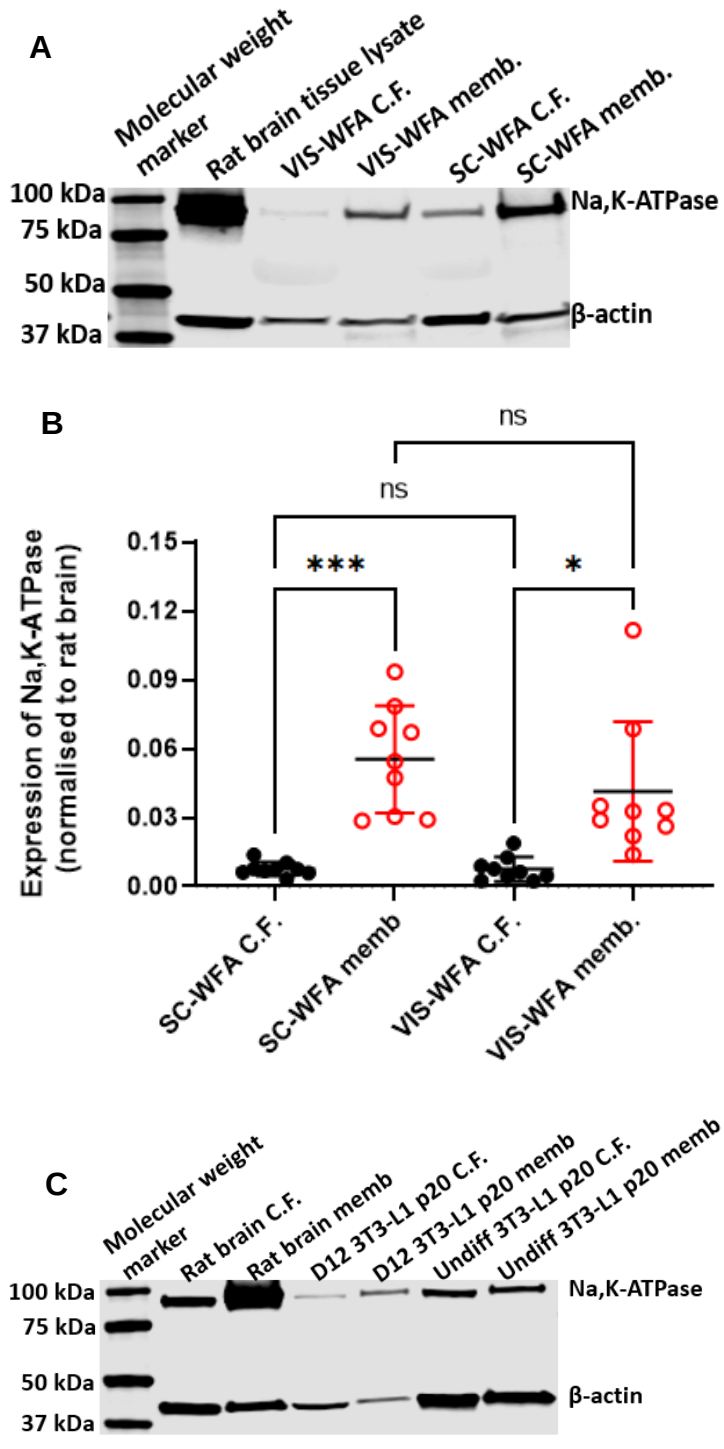

Figure 2.9: Protein expression of Na,K-ATPase and β-actin in cytosolic and plasma membrane fractions of murine adipocytes and 3T3-L1 cells.

(A) Representative western blot of Na,K-ATPase and β-actin in cytosolic (C.F.) and membrane (memb) fractions of primary adipocytes from male Sprague-Dawley and Wistar rats.

(B) Na,K-ATPase expression for data shown in (A) above (n = 9 biological replicates, ***p* ≤ 0.05, ****p* ≤ 0.001, ns = non-significant; Data was analysed using one-way ANOVA and Holm Sidak's post-hoc test, to compare the means of Na,K-ATPase in the cytosolic (C.F.) and plasma membrane (memb.) fractions in each tissue).

(C) Representative western blot of Na,K-ATPase and β-actin in cytosolic (C.F.) and membrane (memb) fractions of day 12 3T3-L1 adipocytes and undifferentiated 3T3-L1 cells.

Going further, the protein expression of $Ca_V1.2$ and $Ca_V3.1$ channel proteins in cytosolic and crude plasma membrane fractions of primary white adipocytes and differentiated and undifferentiated 3T3-L1 cells was explored.

A large molecular weight $Ca_V1.2$ protein was detected in the cytosolic and plasma membrane fractions of SC-WFAs, VIS-WFAs (Figure 2.10A; lanes 3 – 6) and differentiated 3T3-L1 adipocytes, with a determined molecular mass of ~290 kDa (Figure 2.10C; lane 4 and 5). The strong band density of $Ca_V1.2$ in the plasma membrane fraction of the primary adipocytes, was found to be significantly higher than that in the cytosolic fraction of both sub-cutaneous and visceral white adipocytes (p <0.05) (Figure 2.10B). The pre-adipocyte 3T3-L1 cells did not express the large molecular weight protein, but instead showed a similar expression pattern as the control rat brain tissue at ~210 kDa (Figure 2.10A; lane 2; Figure 2.10C; lane 3, 6 and 7). Although the protein expression of $Ca_V1.2$ protein in the differentiated adipocytes was too low for detection using the software data acquisition settings applied for other samples, adjustment of these settings allowed detection of the $Ca_V1.2$ bands in the differentiated 3T3-L1 adipocytes.

With the $Ca_V3.1$ antibody, the full-length Cav3.1 α_1 subunit protein of ~265 kDa, seen in the control rat brain tissue and in the pre-adipocyte 3T3-L1 cells could not be detected in mature adipocytes. Instead, a low molecular weight band of ~130 kDa was detected in the primary adipocytes (Figure 2.11A; lanes 3 – 6) and differentiated 3T3-L1 adipocytes (Figure 2.11C; lane 4 and 5). There was no difference in the expression of this low molecular weight $Ca_v3.1$ in the cytosolic and crude plasma membrane fractions of the different tissues (Figure 2.11B).

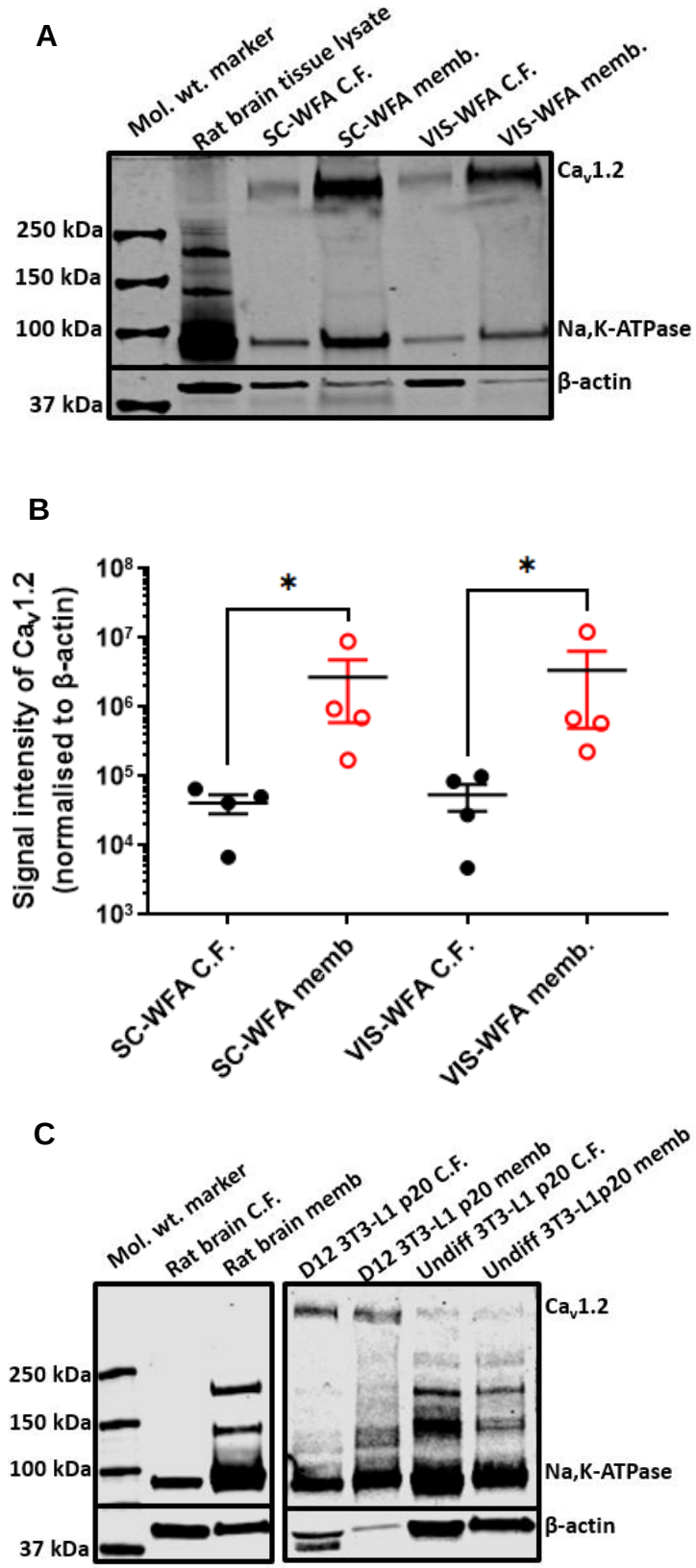

Figure 2.10: Protein expression of Ca$_v$1.2 in cytosolic and plasma membrane fractions of murine adipocytes and 3T3-L1 cells.

(A) Representative western blot of Ca$_v$1.2 in cytosolic (C.F.) and membrane (memb) fractions of sub-cutaneous (SC-WFA) and visceral white fat adipocytes (VIS-WFA) from male Sprague-Dawley and Wistar rats.

(B) Ca$_v$1.2 expression for data shown in (A) above (n = 4 biological replicates, *p ≤ 0.05; Data was analysed using Mann-Whitney test, to compare the means of Ca$_v$1.2 in the cytosolic (C.F.) and plasma membrane (memb.) fractions in each tissue).

(C) Representative western blot of Ca$_v$1.2 in cytosolic (C.F.) and membrane (memb) fractions of day 12 3T3-L1 adipocytes and undifferentiated 3T3-L1 cells (n = 2).

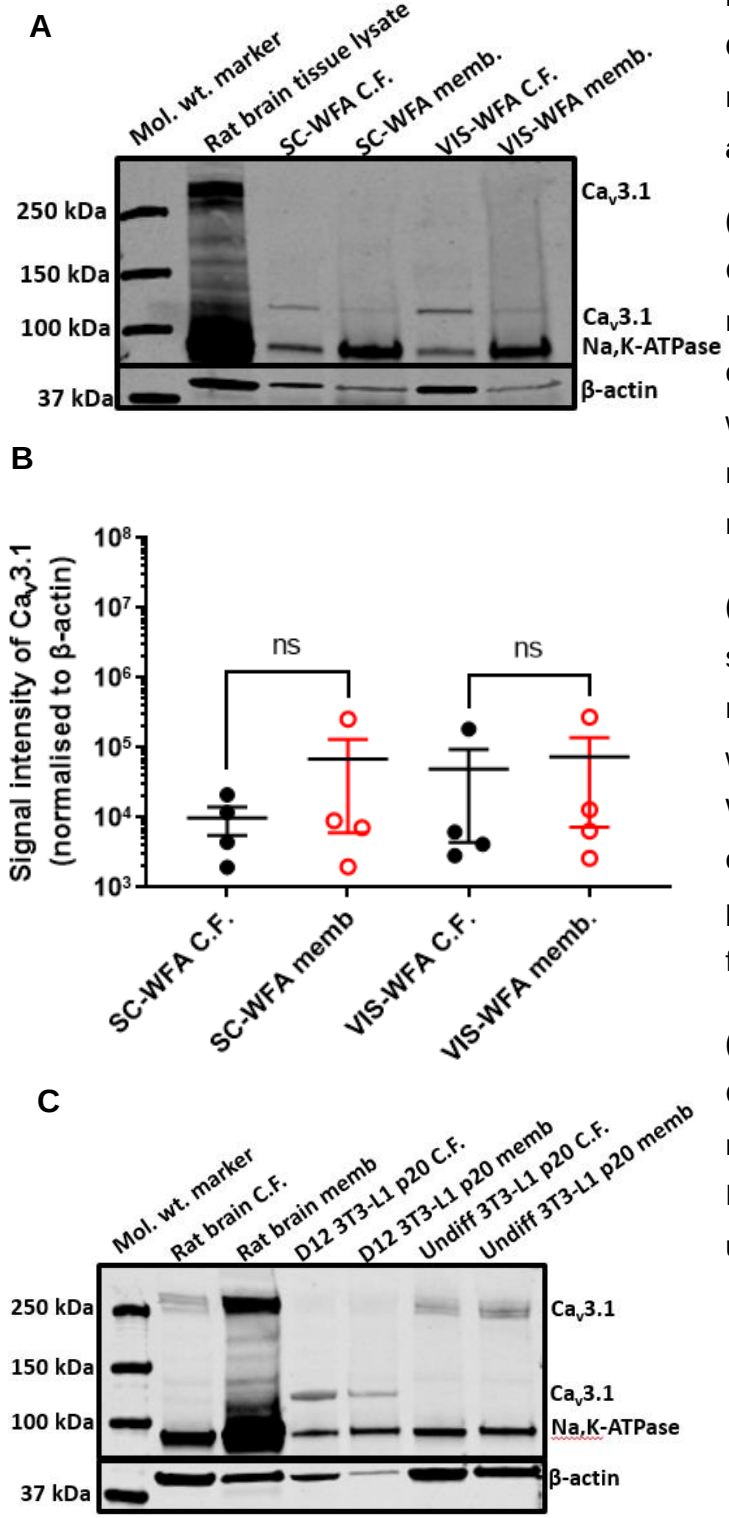

Figure 2.11: Protein expression of Ca$_V$3.1 in cytosolic and plasma membrane fractions of murine adipocytes and 3T3-L1 cells.

(A) Representative western blot of Ca$_V$3.1 in cytosolic (C.F.) and membrane (memb) fractions of sub-cutaneous (SC-WFA) and visceral white fat adipocytes (VIS-WFA) from male Sprague-Dawley and Wistar rats.

(B) Ca$_V$3.1 expression for data shown in (A) above (n = 4 biological replicates, ns = non-significant; Data was analysed using using Mann-Whitney test, to compare the means of Ca$_V$3.1 in the cytosolic (C.F.) and plasma membrane (memb.) fractions in each tissue).

(C) Representative western blot of Ca$_V$3.1 in cytosolic (C.F.) and membrane (memb) fractions of 3T3-L1 adipocytes (day 10) and undifferentiated 3T3-L1 cells (n = 2).

In summary, the observed protein expression pattern of Ca$_V$1.2 and Ca$_V$3.1 channels in the differentiated 3T3-L1 adipocytes was like that in primary adipocytes, with a higher molecular weight Ca$_V$1.2 than that in control tissue, while

the undifferentiated cells showed protein expression patterns similar to the positive control rat brain tissue.

2.4.4 Mass Spectrometry-Based Analysis of WFA Plasma Membrane

To validate the western blot results, plasma membrane fractions of male rat sub-cutaneous and visceral WFAs were subjected to liquid chromatography tandem mass spectrometry (LC-MS/MS) analysis. Prior to mass spectrometric analysis for detection of Ca_V channels in plasma membrane fraction of WFAs, sucrose density gradient approach for plasma membrane enrichment was attempted using 3T3-L1 cells, a more accessible and cost-effective source of plasma membrane proteins compared to fat pads of rats (Figure 2.12).

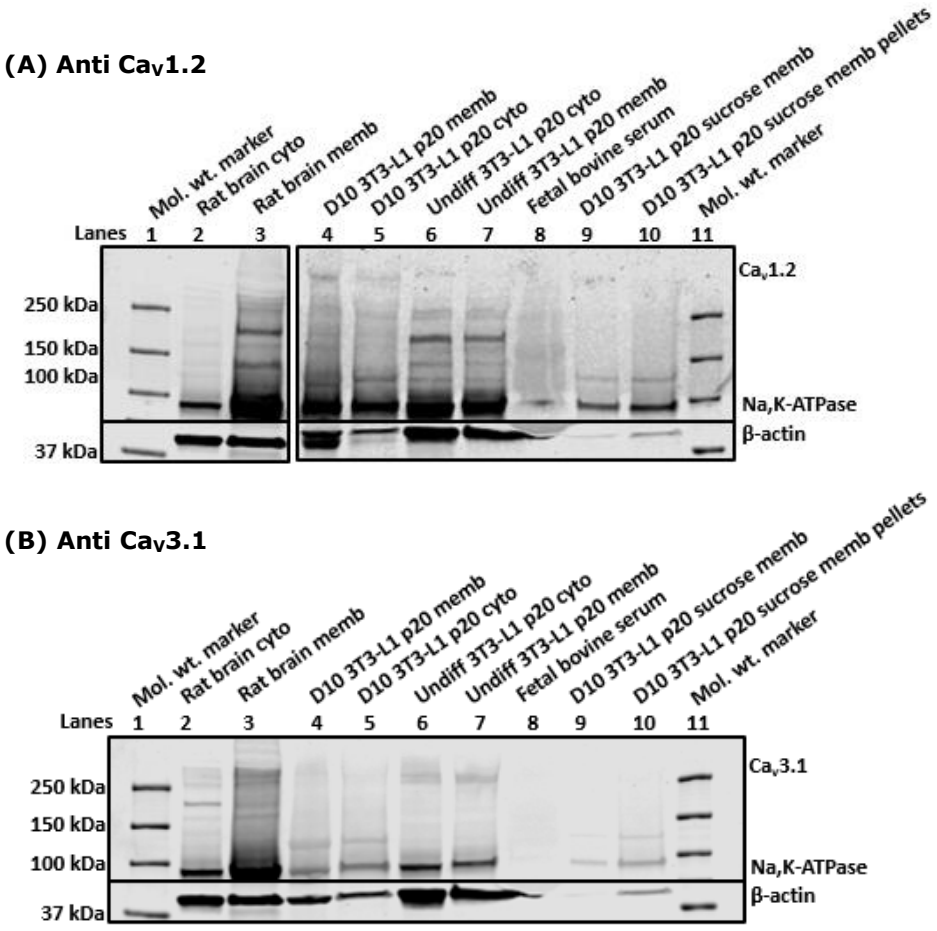

Figure 2.12: Protein expression of $Ca_V1.2$ and $Ca_V3.1$ in plasma membrane of day 10 3T3-L1 (p20) adipocytes, enriched by sucrose density gradient ultracentrifugation.

Western blot of **(A)** $Ca_V1.2$ and **(B)** $Ca_V3.1$ in cytosolic (cyto) and plasma membrane (memb) fractions of day 10 3T3-L1 adipocytes, undifferentiated 3T3-L1 cells and plasma membrane proteins purified from day 10 3T3-L1 using sucrose density gradient ultracentrifugation.

Ca_Vs 1.2 (Figure 2.12A; lanes 4 and 5 for adipocytes at ~290 kDa and lanes 6 and 7 for pre-adipocytes at ~210 kDa) and 3.1 α_1 subunits (Figure 2.12B; lanes 4 and 5 for adipocytes at ~130 kDa and lanes 6 and 7 for pre-adipocytes at ~265 kDa) were successfully detected, with the expected band sizes in the crude plasma membrane fractions prepared using the initially employed optimised plasma membrane isolation procedure. However, neither of the target proteins could be

detected in plasma membrane proteins that were subjected to further purification by sucrose density gradient ultracentrifugation.

2.4.4.1 Detection of Cav channel proteins in SC- and VIS-WFAs

Going further, plasma membrane proteins from male Sprague-Dawley sub-cutaneous (SC) and visceral (VIS) fat pads were purified using the previously optimised and described in-house plasma membrane isolation procedure. Using LC-MS/MS, we detected unique peptide sequences specific for accessory subunits (α2/δ1) of $Ca_V1.2$ protein in both SC and VIS-WFAs plasma membrane. Identification of these accessory subunits in both samples was under a stringent identification criterion of 95% protein threshold, 95 % peptide threshold and minimum of 2 peptides (Figure 2.13B and C). However, at a lower identification criterion of 65% protein threshold, 80% peptide threshold and minimum of 2 peptides, one exclusive unique peptide for the α_1 subunit of $Ca_V1.2$ was detected (Figure 2.13A).

(A) SC-WFA Plasma Membrane (Sample 1)

A0A0G2QC25_RAT (65%), 225,926.6 Da

Voltage-dependent L-type calcium channel subunit alpha OS=Rattus norvegicus OX=10116 GN=Cacna1c PE=1 SV=1

1 exclusive unique peptides, 1 exclusive unique spectra, 1 total spectra, 10/2006 amino acids (0% coverage)

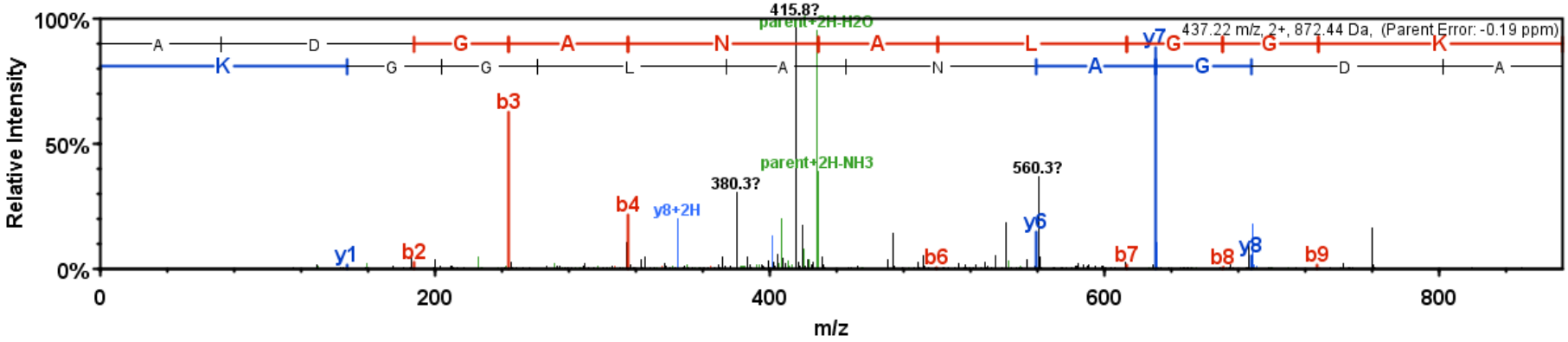

(B) SC-WFA Plasma Membrane (Sample 2 – peptide 1)

A0A0G2K7E5_RAT (100%), 122,731.6 Da

Voltage-dependent calcium channel subunit alpha-2/delta-1 OS=Rattus norvegicus OX=10116 GN=Cacna2d1 PE=1 SV=1

2 exclusive unique peptides, 2 exclusive unique spectra, 2 total spectra, 35/1084 amino acids (3% coverage)

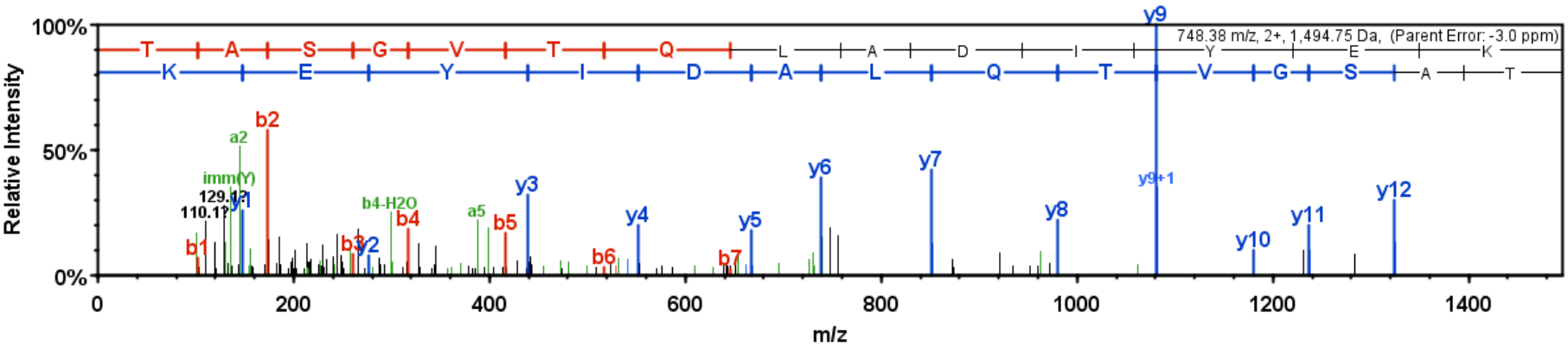

(B) SC-WFA Plasma Membrane (Sample 2 – peptide 2)

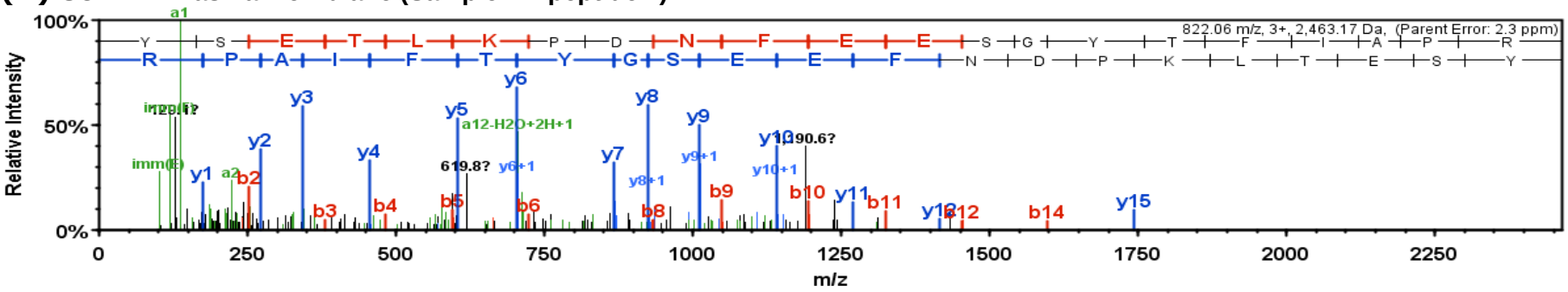

(C) VIS-WFA Plasma Membrane (Sample 2)

A0A0G2K7E5_RAT (95%), 122,731.6 Da

Voltage-dependent calcium channel subunit alpha-2/delta-1 OS=Rattus norvegicus OX=10116 GN=Cacna2d1 PE=1 SV=1

1 exclusive unique peptides, 1 exclusive unique spectra, 1 total spectra, 21/1084 amino acids (2% coverage)

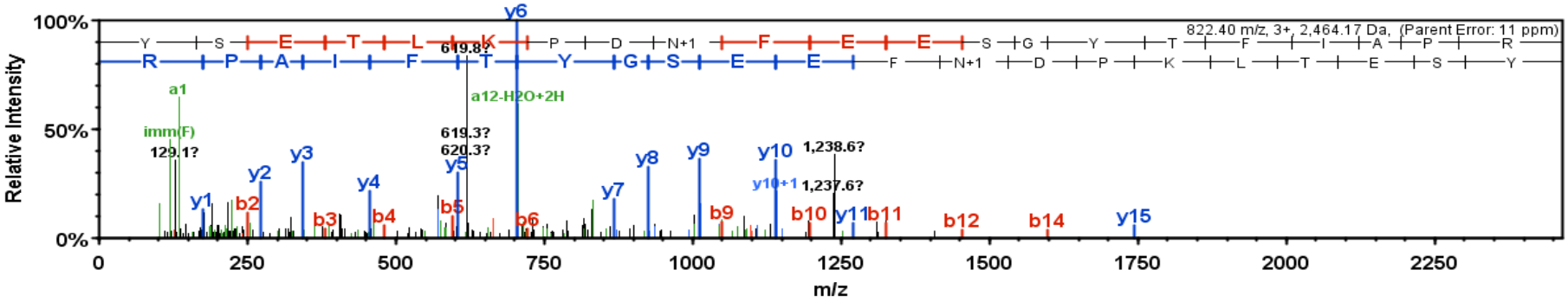

Figure 2.13: Mass spectra of Ca_V channel subunit proteins in rat plasma membrane.

Unique peptide sequences specific to the denoted Ca_V channel subunit for b ions = upper band, and for y ions = lower band. m/z = mass/charge. The b and y ions for a given peptide arise from splitting the original peptide into various amino acids. b ions = peptide fragments that extend from the N-terminus. y ions = peptide fragments that extend from the C-terminus.

2.4.4.2 Immunoprecipitation for enrichment of target proteins

Due to the low abundance and hence difficulty with detection of Ca_V channel proteins in the plasma membrane samples analysed above, immunoprecipitation of the plasma membrane protein preparation using antibodies specific for the target protein (anti $Ca_V1.2$) was carried out to increase the purity of the sample and improve the detection of the proteins of interest by LC-MS/MS. The direct method (pre-immobilized antibody approach) was initially employed, after which the indirect method was also utilised. Rat brain plasma membrane protein was utilised for optimisation of the immunoprecipitation technique due to its abundance and the ease of sourcing the rat brain tissue compared to the difficulties in accumulating equivalent amounts of plasma membrane proteins from fat pads of more animals.

Using both the direct and indirect immunoprecipitation procedures, the attempt to enrich $Ca_V1.2$ proteins was unsuccessful (Figure 2.14). Although $Ca_V1.2$ antibody was able to detect the $Ca_V1.2$ α_1 subunit in the control rat brain tissue lysate as in previous western blot experiments (Figure 2.14, lane 3), the $Ca_V1.2$ α_1 subunit could not be detected in immunoprecipitated proteins from rat brain plasma membrane preparation. Instead, self-association of primary antibodies was detected in samples purified with both the direct and indirect protocols (Figure 2.14; lane 4 and 5).

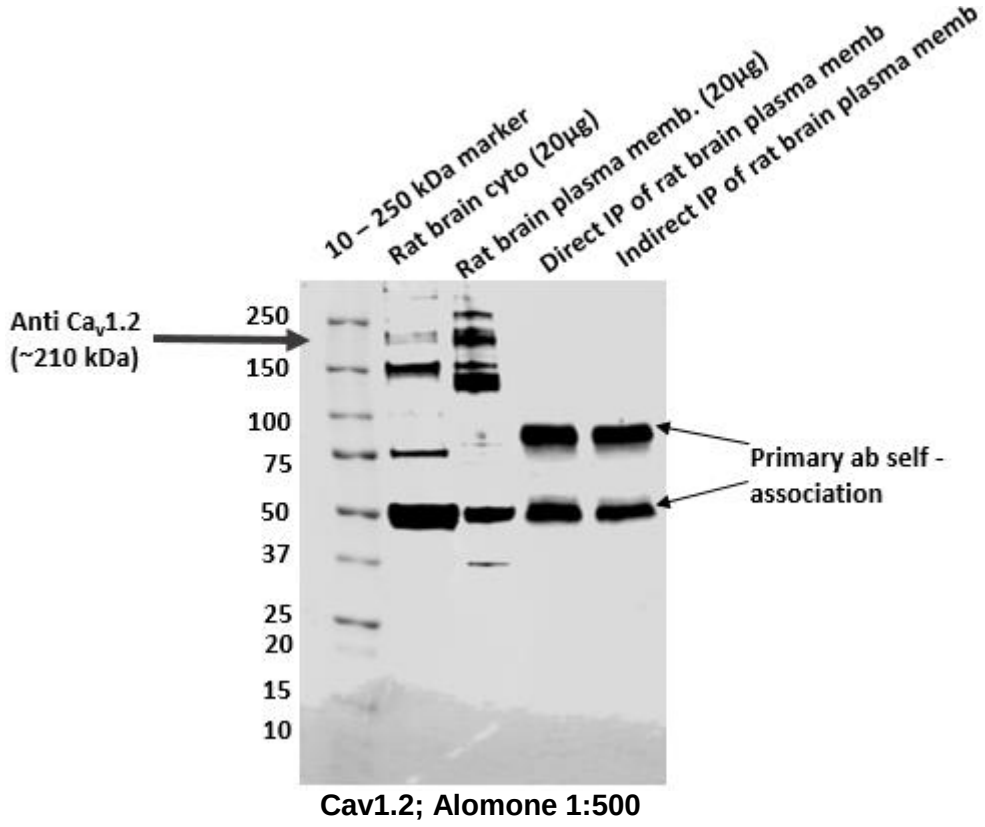

Figure 2.14: Representative western blot of $Ca_V1.2$ from direct and indirect immunoprecipitation of male Sprague-Dawley rat brain plasma membrane proteins.

20 µg of protein was loaded for lanes 2 and 3, while ~400 µg of plasma membrane proteins from rat brain was immunoprecipitated (n = 2 independent experiments). Ab = antibody, IP = immunoprecipitation.

Going further, a pre-clearing step was introduced at the start of the indirect immunoprecipitation technique and the experiment was repeated. Aliquots were collected at each step of the procedure and analysed by western blotting. This was to identify at what purification step my target proteins were probably lost.

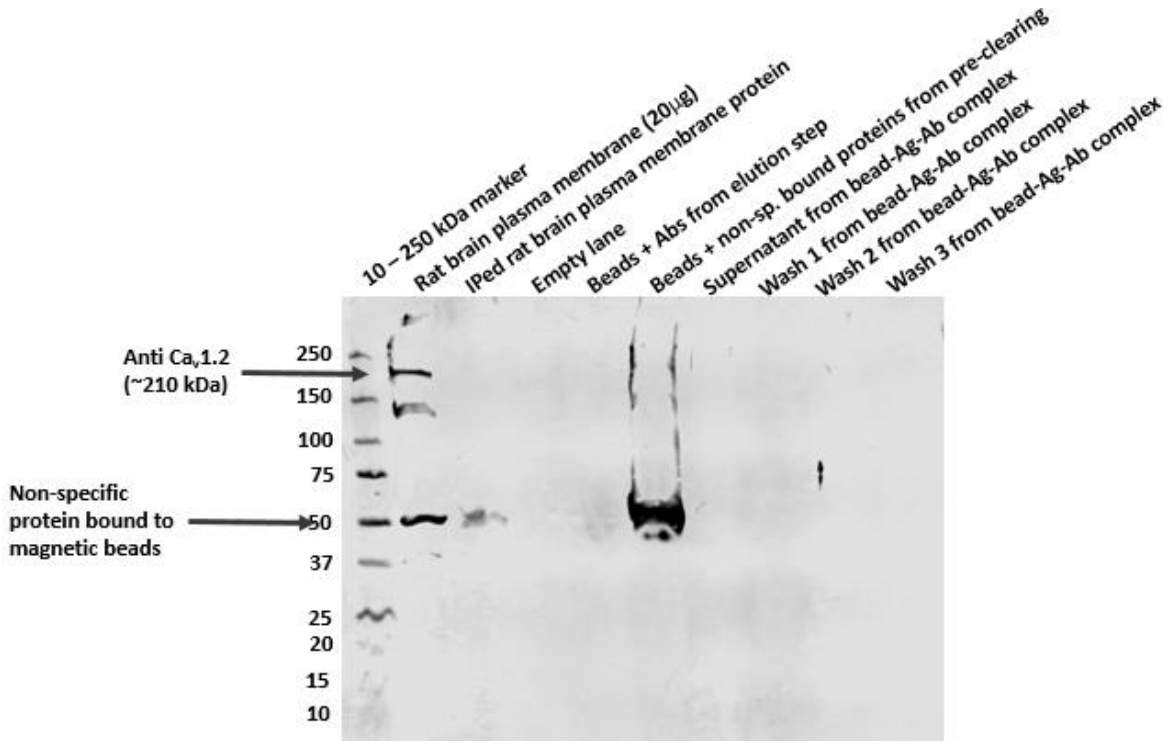

Figure 2.15: Representative western blot of $Ca_V1.2$ from indirect immunoprecipitation of male Sprague-Dawley rat brain plasma membrane proteins.

20μg of protein was loaded for lane 2, while ~400 μg of plasma membrane proteins from rat brain was immunoprecipitated (n = 3 independent experiments). Ab = antibody, IPed = immunoprecipitated, non-sp. = non-specific, bead-Ag-Ab complex = bead-antigen-antibody complex.

$Ca_V1.2$ proteins still could not be detected. Instead, an approximately 50 kDa band was seen in both the immunoprecipitated proteins and the pre-cleared samples (Figure 2.15). No further attempts at plasma membrane protein enrichments were made.

2.5. Discussion

The majority of past research on expression of Ca_V channels in white fat adipocytes suggests the functional expression of these channels, evidenced through calcium imaging data. A recent studies in our laboratory have shown the molecular expression of some $Ca_V1.x$ channels at the gene level through quantitative polymerase chain reaction (Fedorenko, 2019). This study has shown the molecular expression of Ca_V channels in primary and cultured 3T3-L1 adipocytes. Protein expression of $Ca_V1.2$ and $Ca_V3.1$ voltage gated calcium channels in both male Wistar and Sprague-Dawley rat sub-cutaneous and visceral white fat adipocytes and in 3T3-L1 fibroblasts and differentiated adipocytes was detected by western blotting, and the presence of accessory subunits for $Ca_V1.2$ was confirmed in primary WFAs by mass spectrometric analysis. Molecular expression of Ca_V channel proteins in male Wistar and Sprague-Dawley rat sub-cutaneous and visceral WFAs was comparable, hence tissue from either strain of rat was used based on availability.

2.5.1 Rosiglitazone enhances the differentiation of 3T3-L1 pre-adipocytes

Rosiglitazone, a PPARγ agonist, induces differentiation of pre-adipocytes in a dose-dependent manner, with a maximum effect at a concentration of 2 μM. PPARγ typically described as a master regulator of adipocyte differentiation, stimulates perilipin gene expression (Arimura et al., 2004). It sequesters excess lipids in adipocyte lipid droplet by stimulating perilipin expression, resulting in an increase in triglyceride accumulation and lowered circulating non-esterified free fatty acids, thereby inducing the differentiation of pre-adipocytes to adipocytes (Carmen and Víctor, 2006, Zebisch et al., 2012, Ma et al., 2015).

2.5.2 Method optimisation for enriched plasma membrane isolation led to increased protein degradation

An attempt to isolate enriched plasma membrane proteins from 3T3-L1 adipocytes seemed to increase the concentration of isolated proteins (from 5–15 µg in previous experiments to ≥ 20 µg). However, there was obvious degradation of proteins, shown by low molecular weight bands, particularly in the samples probed with $Ca_V1.2$ specific antibody. The excessive protein degradation observed could be attributed to the long duration of time (~ 5 hours) required for processing of the proteins, from the point of cell harvesting to quantification of isolated proteins by Lowry assay. Also, although the normalised signal intensities of $Ca_V1.2$ and $Ca_V3.1$ channel proteins to β-actin in Day 11 3T3-L1 adipocytes (p20) (Figure 2.6), suggest high level expression of these proteins, the signal intensity of β-actin was very weak due to a low dilution of primary antibody (1:30,000 dilution) and may have contributed to the high normalised signal intensities of the channel proteins. This was corrected in subsequent experiments. As neither of the adopted methods (M1 and M2) successfully resulted in isolation of high quality crude plasma membrane proteins, the initially employed plasma membrane isolation technique was subjected to series of adjustments, as detailed in section 2.4.2 above and subsequently utilised. Na,K-ATPase allowed confirmation of fractional enrichment of plasma membrane proteins using my optimized protein isolation technique (Figure 2.9).

2.5.3 $Ca_V1.2$ and $Ca_V3.1$ channel isoforms are expressed in 3T3-L1 adipocytes and murine primary adipocytes

Following differentiation of the *in vitro* adipogenic model, we explored the protein expression of some Ca_V channels in the 3T3-L1 adipocytes and murine primary

adipocytes. The present data suggests the presence of $Ca_V1.2$ and $Ca_V3.1$ channel variants, located both in the cytosolic fraction and in the plasma membrane of 3T3-L1 adipocytes and rat primary adipocytes. The presence of different channel isoforms could arise due to alternative splicing of these channels. In addition to alternative splicing, $Ca_V1.2$ undergoes posttranslational modifications, yielding full-length and proteolytically cleaved C-terminal (CT) channel variants (Raifman et al., 2017). The modulatory function of the CT-auto modulatory domain of $Ca_V1.x$ channels is generally cell-type specific and stabilizes the gating properties of the channel (Scharinger et al., 2015).

2.5.3.1 $Ca_v1.2$ expression

The $Ca_V1.2$ channel has been shown to undergo extensive alternative splicing, which affects its tissue distribution, pharmacology, and electrophysiological properties (Liao and Soong, 2010, Bannister et al., 2011, Liao et al., 2015, Hu et al., 2017). Some researchers have noted the low level occurrence of a higher molecular weight band of $Ca_V1.2$ channels, which is referred to as the longer isoform of this channel and is thought to be expressed in heart and brain (Shistik et al., 1999, Kramer et al., 2012). In this study, we detected the presence of a large molecular weight $Ca_V1.2$ channel isoform (> 250 kDa) in both cytosolic and crude plasma membrane fractions of rat visceral and sub-cutaneous adipocytes, as well as in 3T3-L1 adipocytes, with a significantly higher expression level in the plasma membrane than in the cytosol. This large $Ca_V1.2$ protein band was absent in undifferentiated 3T3-L1 pre-adipocytes, where instead, the expression pattern of $Ca_V1.2$ α_1 subunit seen was like that in the rat brain control tissue. In both rat brain and undifferentiated 3T3-L1 pre-adipocytes, the expression of the two main $Ca_V1.2$ channel isoforms; a short isoform ~140 kDa and a long isoform of ~210

kDa were detected. The long $Ca_V1.2$ channel isoform of ~210 kDa has been detected by our laboratory (Fedorenko, 2019) and others (N'Gouemo et al., 2015), while the detected short $Ca_V1.2$ channel isoform of ~140 kDa may relate to the 130 kDa or 150 kDa non-$Ca_V1.2$ epitope recognised by this antibody in $Ca_V1.2$ knock-out mice (Bavley et al., 2017, Buonarati et al., 2017).

The large molecular weight $Ca_V1.2$ channel isoform in cytosolic and plasma membrane fractions of primary WFAs and differentiated adipocytes of ~290 kDa could be due to glycosylation of this calcium channel in WFAs, particularly in the plasma membrane. N-linked glycosylation of $Ca_V1.2$ channels has been linked to regulation of cell surface expression, as well as gating of the channel (Huang and Zamponi, 2017). It is possible that white fat adipocytes contain numerous N-linked glycosylation sites, leading to increased channel density, as detected by western blotting. Also, PKC promotes plasma membrane expression of $Ca_V1.2$ channels, by increasing trafficking of the channels to the plasma membrane, and perhaps by reduction in the rate of channel internalisation (Raifman et al., 2017).

The cardiac isoform of $Ca_V1.2$, which contains exon 1A of the *Cacna1c* gene, has been referred to as the long isoform of $Ca_V1.2$, while the smooth muscle isoform (Raifman et al., 2017) and the neuronal isoform (Kramer et al., 2012), have both been referred to as the short isoform of the $Ca_V1.2$. Posttranslational modification of cardiac and neuronal α_{1C} gives rise to a full-length isoform of ~ 240 kDa and a CT-truncated form of the channel of ~ 210 kDa (Raifman et al., 2017). The CT-truncated isoform arises due to proteolytic cleavage of the Ca_V α_{1C} subunit around amino acid ~ 1800, though not in heterologous expression systems (Huang and Zamponi, 2017, Raifman et al., 2017). The cleaved C-terminus remains attached to the channel complex and acts as an auto inhibitory domain, as well as a target

site for A kinase anchoring proteins (AKAPs) (Huang and Zamponi, 2017). Liao et al. have detected a $Ca_V1.2$ channel splice variant ($Ca_V1.2_{33L}$) of 160 kDa in neonatal and adult rat hearts, which is impermeable to Ca^{2+} ions. The presence of this splice variant was shown to shift the calcium window current of the reference $Ca_V1.2$ channel to a more negative potential and enhance protein degradation of functional $Ca_V1.2$ channel through the ubiquitin proteasome system (Liao et al., 2015). Kramer et al. (2012) has also detected the expression of the two main $Ca_V1.2$ channel isoforms; a short and a long isoform of ~ 170 kDa and 240 kDa respectively in rat hippocampus. Although majority of literature describes $Ca_v1.2$ to be within the range of 190 – 250 kDa, Heck et al. (2021) has recently described the α_{1C} subunit as a 190 – 270 kDa membrane spanning protein of the Ca_V channel. The upper band size of this protein (Heck et al., 2021) is the closest seen in the literature, to the large molecular weight α_{1C} subunit isoform identified in this study. The functional implication of the large molecular weight $Ca_V1.2$ channel isoform (~290 kDa) detected in this study on the biophysical properties of $Ca_V1.2$ channels in WFAs is yet unknown. The presence of these channels could also have an important contribution to the physiological functions of WFAs regulated by intracellular calcium fluxes through the adipocyte plasma membrane $Ca_V1.2$ channels.

2.5.3.2 $Ca_V3.1$ expression

In this study, we explored the expression of $Ca_V3.1$ α_1 subunit in undifferentiated 3T3-L1 pre-adipocytes, differentiated 3T3-L1 adipocytes as well as visceral and sub-cutaneous WFAs of rat. The detection of the full length $Ca_V3.1$ α_1 subunit of ~265kDa in 3T3-L1 pre-adipocytes in this study is consistent with previous observations (Oguri et al., 2010). Oguri et al. (2010) had shown the presence of

mRNA transcripts for *Cacna1g* as the predominant transcripts amongst the detected Ca_v transcripts (α_{1A}–α_{1I}) in 3T3-L1 pre-adipocytes and cultured primary mouse pre-adipocytes. In addition, the protein expression of this dominantly expressed *Cacna1g* gene was confirmed by both western blotting and immunohistochemical analysis. The expression levels of the $Ca_V3.1$ α_1 subunit was observed to be higher than that in the differentiated adipocytes, as well as in visceral and subcutaneous primary WFAs of male Wistar and Sprague-dawley rats in this study. The observation of higher expression levels of $Ca_V3.1$ in pre-adipocytes than in mature adipocytes, shown by higher band densities of the channel through western blotting has also been noted by Oguri et al. (2010). The expression level of α_{1G} mRNA and $Ca_V3.1$ protein significantly decreased in differentiated adipocytes (Oguri et al., 2010). There is also the possibility that the low molecular weight protein bands detected by the $Ca_V3.1$ antibody are non-$Ca_V3.1$ epitopes recognised by this antibody. The dominant expression profile of $Ca_V3.1$ channels in pre-adipocytes strongly suggests a key role of this channel in pre-adipocyte proliferation and adipose tissue development. This idea is further supported by the observation that the highly selective $Ca_V3.1$ calcium channel antagonist, NNC-55-0396 (a structural analog of mibefradil – T-type calcium channel blocker) (Kim et al., 2015, Huang et al., 2015), but not diltiazem (an L-type calcium channel antagonist) inhibited cell proliferation in pre-adipocytes and effectively blocked progression of the cell cycle (Oguri et al., 2010).

2.5.4 Mass Spectrometry Analysis Revealed Accessory Subunits of $Ca_v1.2$

Mass spectrometric analysis identified the presence of unique peptide sequences, specific to the $Ca_V1.2$ α_1 subunit, and the voltage-gated calcium channel subunit $\alpha2/\delta1$ (an accessory subunit for $Ca_V1.2$ α_1 subunit), although in independent

sample preparations. Although one unique peptide sequence specific to the central, pore-forming $Ca_V1.2$ α_1 subunit was detected, its ions could not be confidently identified due to the low protein and peptide threshold at which it was detected. However, the α_2/δ_1 accessory subunit for $Ca_V1.2$ channel was detected in the plasma membrane fractions of both SC- and VIS-WFAs. Although unique peptide sequences suggesting the expression of $Ca_V1.x$ channels in the plasma membrane of WFAs could be detected, the presence of hundreds of other highly expressed and more abundant proteins could have masked and probably made more difficult identification of the protein of interest.

2.5.5 Immunoprecipitation for enrichment of target proteins was unsuccessful

Immunoprecipitation is a technique for enrichment of target proteins prior to further analysis such as mass spectrometry as was required in this study. Several attempts were made to further enrich Ca_V channel proteins in the samples using antibodies specific to the protein of interest. However, both the direct and indirect methods of protein immunoprecipitation employed were not successful in enriching the target proteins for mass spectrometric analysis.

The direct approach of complexing the primary antibodies with the magnetic beads, before immunoprecipitation of the proteins was initially attempted, as well as the indirect method of forming the antibody-antigen complex first, before binding to magnetic beads. In either case, only the self-associated antibodies could be detected on western blots (Figure 2.14). Although the direct immunoprecipitation method of using pre-immobilised antibody is more widely employed, using free antibodies to form immune complexes is thought to be beneficial if the target protein is present in low concentrations, the antibody has a weak binding affinity

for the antigen or the binding kinetics of the antigen to the antibody are slow. Due to these advantages of the indirect technique over the direct technique, the immunoprecipitation experiments using only the indirect technique was repeated after minor adjustments. The 50 kDa band which was observed (Figure 2.15) was expected in the pre-cleared samples, as this was probably non-specifically antibody bound proteins. It is likely that a more stringent elution buffer was required to successfully elute the protein of interest. However, after several unsuccessful attempts and adjustments to the immunoprecipitation procedure, due to time constraints and limited technical support in molecular techniques, these experiments were halted and other studies continued.

2.5.5 Conclusion

These results show that mature white fat adipocytes express $Ca_V1.2$ α_1 subunit proteins necessary for their function. Expression of $Ca_V1.2$ in the membrane was significantly greater than that in the cytosolic fraction ($p<0.05$; ratio paired T-test). Expression of the detected proteins in the plasma membrane was confirmed by expression of plasma membrane specific Na,K-ATPase. The $Ca_V1.2$ protein detected in white fat adipocytes suggests it is an extended isoform of the canonical $Ca_V1.2$ α_1 neuronal isoform of 210kDa, with a molecular mass of ~290 kDa. The pre-adipocyte 3T3-L1 cells did not express the large molecular weight $Ca_V1.2$ α_1 protein, but instead showed a similar expression pattern as the control rat brain tissue at 210 kDa. With the $Ca_V3.1$ antibody, the full-length $Ca_V3.1$ α_1 subunit protein of ~265 kDa was seen in the control rat brain tissue and in the pre-adipocyte 3T3-L1 cells, however it could not be detected in mature adipocytes. This suggests an involvement of $Ca_V3.1$ in pre-adipocyte development and a lack of functional $Ca_V3.1$ in mature white fat adipocyte. No difference was seen

between the expression profile of $Ca_V1.2$ and $Ca_V3.1$ in primary adipocytes from male Wistar rats and male Sprague-Dawley rats. Mass spectrometric analysis detected the presence of unique peptide sequences specific to the voltage-gated calcium channel subunit α2/δ1 (an accessory subunit for $Ca_V1.2$ α_1 subunit). The physiological relevance of the $Ca_V1.2$ channel protein in white fat adipocytes will be explored in subsequent experiments.

The antibodies employed in this study were unable to detect the presence of $Ca_V1.3$ protein in all the samples tested. However, a previous study from our laboratory has shown the expression of $Ca_V1.3$ protein in the plasma membrane of rat WFAs using an earlier batch of the antibody (Bentley, 2013, Fedorenko, 2019). Other researchers have noted the variability in success of commercial $Ca_V1.3$ antibodies and this is a widely recognised problem (Buonarati et al., 2017).

In addition to adipocytes, adipose tissue contains a wide population of cells, such as macrophages, fibroblasts, pericytes, blood cells, endothelial cells, smooth muscle cells, mesenchymal stem cells, and adipose precursor cells. All of these cells are located in the stromal vascular fraction and are separated from white adipocytes during primary adipocyte isolation. Unlike live cell imaging for intracellular calcium measurement in which the characteristic features of the white adipocyte could be used to confirm effective isolation of white fat adipocytes and the absence of contaminating cells, the purity of primary adipocytes employed in molecular expression studies and proteomic analysis cannot be determined by such means. Hence, there is the possibility of the presence of contaminating cell types in addition to the purified white adipocytes from which proteins were isolated. However, in addition to repeated washing of the cells during the primary adipocyte isolation process and visual inspection to confirm sedimentation of the

stromal vascular fraction, the assurance of the purity of the isolated cells employed in this study as being predominantly white fat cells is based on the absence of genes from other cell types other than white fat adipocyte specific genes from transcriptomic data derived from these cells in our laboratory. Gene expression experiments probing for genes from possible contaminating cells could have been carried out to increase assurance of the purity of the primary adipocyte preparation employed in this study.

CHAPTER THREE

Measurement and modulation of calcium influx in white fat adipocytes

3.1. Introduction

Intracellular calcium concentration is maintained by flux through calcium channels. It is widely acknowledged that calcium channels on plasma and intracellular membrane surfaces show selective permeability to Ca^{2+}, and facilitate calcium entry into the cytoplasm (Zhai et al., 2020), where cytoplasmic calcium serves as an important second messenger in various intracellular signalling pathways, and thus plays a critical role in cellular function and homeostasis. Intracellular Ca^{2+} sources in most cells is through voltage-gated calcium channel (Ca_V channel) Ca^{2+} influx and/or Ca^{2+} release from intracellular endoplasmic reticulum or sarcoplasmic reticulum stores (Komai, 2015). Ca_V channels have been extensively studied in excitable tissues due to their role in membrane depolarization-coupled processes, such as excitation-contraction coupling in cardiac and skeletal muscle cells, neurotransmitter release, and excitation-secretion coupling in endocrine cells. Hence, it is generally accepted that Ca_V channels modulate calcium homeostasis in excitable tissues.

In non-excitable tissues however, intracellular calcium requirements is thought to be controlled mainly through store operated channels, through the molecular interaction of STIM1 on the endoplasmic reticulum and the plasma membrane associated ORA1 protein, as well as other plasma membrane channels such as the non-selective cation transient receptor potential channels (Buchanan and McCloskey, 2016, El Hachmane et al., 2018). Ca_V channels are now known to be

functionally expressed in various non-excitable cells such as immune cells (Badou et al., 2013), red blood cells, epithelial cells and osteocytes (Prideaux et al., 2015). In human T-lymphocytes for instance, the activity of L-type calcium channels is thought to promote activation of transcription factors required for activation of the T-lymphocyte (Stokes et al., 2004, Badou et al., 2013). Adipocytes have been suggested to express Ca_V channels, but functional evidence for the presence of the channels in this cell type is lacking (El Hachmane and Olofsson, 2018).

Unlike excitable cells such as cardiac and skeletal muscle cells with a resting membrane potential (RMP) of < -60 mV, adipocytes possess a less negative RMP (-20 to -40 mV range) (Bentley et al., 2014). Cells with a more negative RMP (< -60 mV) require depolarization to a threshold of -40 to -30 mV for activation of Ca_V channels (Gaur et al., 1998). In contrast, the RMP of adipocytes is within the range of the window with a sustained Ca^{2+} channel activity (Fleischmann et al., 1994), and strongly suggests a key role of $Ca_V1.x$ channels in the maintenance of resting $[Ca^{2+}]_i$ (Smith et al., 1993, Gaur et al., 1998) and regulation of lipolysis in adipocytes (Gaur et al., 1998). In excitable cells, $Ca_V1.x$ channels are regulated mainly by a voltage change across the plasma membrane or through hormonal regulation (Hofmann et al., 2014). Intracellular calcium ion and post-translation modifications also influence gating of $Ca_V1.x$ channels (Satin, 2014).

3.1.1. Voltage regulation of channel activity in adipocytes

Non-excitable cells such as fibroblasts, epithelial cells and endocrine cells that do not exhibit spiking electrical activity have also been established to possess Ca_V channels (Fleischmann et al., 1994). The membrane potential of these non-excitable cells fluctuates, but generally does not depolarise to potentials required to activate the available calcium current to a substantial degree. Instead, these

non-spiking cells display graded changes in their membrane potential, and a small amount of current is available over a voltage range at which steady state current inactivation is incomplete. Measurement of L-type calcium current in a variety of cells including smooth muscle cells (Fleischmann et al., 1994) and arterial myocytes (Navedo et al., 2005), have identified the presence of a "window current" of steady-state calcium fluxes that regulate sustained cellular responses. These steady-state calcium fluxes are detectable at negative potentials in which macroscopic currents are only barely detectable and become inactivated at more positive potentials. The existence of a window-current through $Ca_V1.x$ channels activity has been demonstrated in white fat adipocytes (Fedorenko, 2019). $Ca_V1.x$ channels activity near the resting membrane potential has been identified as an important regulator of cellular function (Fleischmann et al., 1994).

Cl^- has been shown by several studies to be responsible for regulation of WFA resting membrane potential (Bentley et al., 2014, Beigelman and Shu, 1972). Beigelman and Shu (1972) also suggest that K^+, plays a role, in addition to Cl^- in the regulation of WFA resting membrane potential. Changes in these ion concentrations are expected to regulate adipocyte V_m and elicit changes in calcium flux and its intracellular concentration.

3.1.2. Hormonal regulation of channel activity in adipocytes

$Ca_V1.x$ channels are modulated by several hormones, including growth hormone, through activation of G-Protein Coupled Receptors and second messengers such as PKC (see detailed reviews: (Catterall, 2000, Weiss and Dascal, 2015). Hormonal action on WFAs is known to affect both its transmembrane ionic gradients and its transmembrane potential (Ramirez-Ponce et al., 1990).

Regulation of the metabolic functions of AT is mainly through the activity of various cell surface receptors, amongst which include insulin receptors, β-adrenergic receptors and growth hormone receptor (GHR) (Troike et al., 2017). The main actions of growth hormone on the physiological functions of adipose tissue include its direct inhibition of insulin action, reduction of glucose uptake, inhibition of lipogenesis and stimulation of lipolysis (Troike et al., 2017). Growth hormone modulates adipocyte intracellular calcium levels (Gaur et al., 1998), an action which stimulates lipolysis in the adipose tissue (Campbell and Scanes, 1988). Besides it role in lipid and glucose metabolism, growth hormone plays a role in the modulation of the density of L-type calcium channels on the plasma membrane of white adipocytes and consequently, the intracellular free calcium of white fat adipocytes. Its contribution to the maintenance of functional L-type Ca^{2+} channels abundance in adipocyte plasma membrane is further supported by the observation that deprivation of growth hormone to rat primary adipocytes decreased the $Ca_V1.x$ channels in their plasma membrane, determined by $[Ca^{2+}]_i$ imaging, immunoassay and ligand binding studies, resulting in decreased $[Ca^{2+}]_i$ in these cells (Gaur et al., 1998). Consequently, resting $[Ca^{2+}]_i$ in adipocytes has been suggested to be dependent on maintenance of Ca^{2+} influx (Gaur et al., 1998, Fedorenko, 2019).

3.2. Study rationale

Adipocytes have been suggested to express Ca_V channels, but functional evidence for the presence of the channels in this cell type is lacking (El Hachmane and Olofsson, 2018). Epidemiologic evidence suggests an association between elevated serum and/or adipocyte intracellular Ca^{2+} levels and metabolic abnormalities, including type 2 diabetes mellitus and obesity. Experimental insulinemia and/or hyperglycemia both in vivo and in vitro, increases adipocyte

$[Ca^{2+}]_i$ and decreases insulin-stimulated glucose uptake (Reusch et al., 1991). Increased cytosolic Ca^{2+} may induce mitochondrial dysfunction, and the resulting increase in reactive oxygen species could further advance pathological conditions, as seen in the degeneration of dopaminergic neurons in Parkinson's disease (Sun et al., 2014, Sun et al., 2017). Considering the role of L-type calcium channels in lipogenesis and metabolic disease development, understanding how these channels are regulated in white fat adipocytes is pivotal to research efforts in the search for pharmacological targets for the therapeutic management of metabolic disorders.

The emphasis and choice of visceral white fat adipocytes in the studies described herein are based on the knowledge that WAT depots (subcutaneous, intraabdominal, visceral, etc), exhibit marked functional differences despite the presence of common features (Troike et al., 2017). For instance, accumulation of visceral white adipose tissue is associated with higher incidences of metabolic disease states and inflammatory responses, unlike subcutaneous white AT. Also, adipocyte size has been shown to be smaller in subcutaneous fat depots, compared to visceral counterparts (Troike et al., 2017), further supporting the predisposition of visceral white adipocytes to hypertrophy and development of obese phenotypes. The hypertrophic nature of visceral fat adipocytes may explain the observation of preferential storage of toxic environmental pollutants such as polychlorinated biphenyls in this fat tissue type as opposed to storage in subcutaneous white AT (Dirinck et al., 2015), hence our choice of VIS-WFAs for this study. The choice of mice adipocytes, besides our knowledge of mice as the most widely used animal model for human disease research (McKie et al., 2019),

was to see how the observations from mice compare with previous key results in rat adipocytes (Bentley et al., 2014).

3.2.1 Aim of study

The aim of the study is to determine the activity of $Ca_v1.x$ channels under conditions previously shown to depolarise WFAs, by monitoring calcium influx by means of the calcium-sensitive dye, Fluo-4. The specific objectives are as follows:

- To explore the functional existence of L-type voltage-gated Ca^{2+} channels in white fat adipocytes
- To assess the regulation of $Ca_v1.x$ in white fat adipocytes by membrane potential and endogenous compounds such as growth hormone and parathyroid hormone.

3.3. Methodology

3.3.1 Ethical approval and isolation of primary white adipocytes

Animal care and experimental procedures were carried out in accordance with the U.K. Home Office Animals (Scientific Procedures) Act (1986) and were locally approved (ASPA 000187; University of Nottingham).

Primary white adipocytes were isolated from the epididymal fat pads of CD1 male mice (28 – 30g, fed ad libitum, 12 h dark/light cycle; Charles River Laboratory, UK) using a modification of the method of Rodbell (1964). Drugs and chemicals were from Sigma (Poole, United Kingdom). Fat pads were dissected and transferred into 5 ml of Hanks solution [which contained 5.6 mM KCl, 138 mM NaCl, 4.2 mM $NaHCO_3$, 1.2 mM NaH_2PO4, 1.2 mM $MgCl_2$, 2.6 mM $CaCl_2$, 10 mM HEPES, pH 7.4, supplemented with 0.5 % w/v bovine serum albumin fraction V (Sigma A3059) and 5 mM glucose. The fat pad was washed thoroughly to remove residual blood. Any visible arteries as well as the epididymis were carefully dissected out. The fat pad was then cut in ~5mm pieces into a glass scintillation vial which contained 5 ml of 0.2 mg/ml of collagenase type 2 (Sigma C6885). The tissue was minced for 2 minutes and the resulting mixture transferred to a 25 ml Nalgene Erlenmeyer flask. A further 5 ml of Hanks solution was used to rinse the scintillation vial into the flask and the flask was capped and placed in a shaking Grant water bath (Griffin and George 896331) at 37 °C for ~ 25 - 35 minutes (at which time the digest turned milky and turbid, an indication of adipocyte liberation).

Following digestion, the digest was filtered, to remove undigested lumps of tissue, through a 100 µm cell strainer (Sigma CLS431752) into a 20 ml syringe, with an attached Luer lock closed. The suspension was then diluted with additional 10ml

of Hanks buffer and was left for 10 mins to allow the adipocytes rise to the top of the syringe to form a visible white layer, after which time the infranatant was drained off. This characteristic of the adipocytes to float and form a visible white layer due to their high lipid content, aids in the isolation process, as cell debris and other contaminating cell types present within the adipose tissue explants (fibroblasts, macrophages, stromal cells, monocytes and pre-adipocytes (Vázquez-Vela et al., 2008, Bentley, 2013) precipitate out. The adipocytes were re-suspended with another 20 ml of Hanks solution and the above procedure repeated. To obtain the adipocytes, the cells were re-suspended in 20 ml of Hanks solution and after draining off the lower solution, the cells were collected into a 1.5 ml analyser cups (Alpha laboratories QT1500A) at room temperature (~22 °C) for calcium imaging.

3.3.2 Plating and Dye Loading of Cells

For measuring changes in intracellular Ca^{2+}, freshly isolated murine adipocytes were first plated on poly-l-lysine in boric acid (100 µg/ml) coated coverslips (22 mm) for 30 minutes, after which the adipocytes were loaded with 500 µl of 1 µM Fluo 4 AM (acetoxymethyl) in basal solution (Hanks solution supplemented with 0.01 % w/v BSA and 5 mM glucose) for 45-60 minutes at 22 °C in the dark. Loading was performed at room temperature to reduce the likelihood of dye compartmentalisation in accordance with the manufacturer's recommendations. Dye-loaded cells were mounted on the stage of an inverted fluorescence microscope with a charge-coupled device (CCD) camera attached. The cells were continuously perifused at ~28 °C. To perifuse the cells, solutions were gravity-fed through polythene tubing and a peristaltic pump was used to aspirate away the bath solution. Basal solution was first perifused for 5 minutes and drug additions

were made through bath perifusion. Exchange between solutions was performed by manually changing the tube between different solutions, except for the final treatment with triton x-100 which was controlled by switching perfusion of the tube using an electrically controlled two-way valve. The calcium free Hanks buffer was made by substitution of bath $CaCl_2$ with an equivalent concentration of $MgCl_2$. With the exception of rhGH with ddH_2O as its vehicle, all drug dilutions were made with DMSO, unless otherwise specified.

3.3.3 Imaging of Cells

Cells were imaged using an inverted Axiovert 135TV microscope (Carl Zeiss Ltd, Welwyn Garden City, UK) and the light source was provided by a xenon arc lamp. To monitor changes in $[Ca^{2+}]i$, cells loaded with Fluo-4 AM were illuminated continuously throughout the experiment. Fluo-4 AM is an analog of Fluo-3AM with the two chlorine atoms substituted by fluorines, which can be used at lower dye concentrations to generate the same fluorescence signal intensity (Gee et al., 2000). The lower dye loading times and lower loading concentrations of Fluo-4 AM makes its use in cells a less invasive practice (Gee et al., 2000). The dye was excited at 480 nm, with the lowest light intensity that allowed camera detection and visualisation of emitted fluorescence by Fluo 4 loaded-cells, when the observer was dark adapted. To reduce dye loss by photo-bleaching, care was taken not to use a higher light intensity than necessary, i.e. within the lower limits of camera detection (Bentley et al., 2014). For $[Ca^{2+}]_i$ measurements adipocytes were visualised using a x20 FLUO 1.3 NA objective lens. Images were captured at 1 Hz with a CoolSNAP HQ2 camera (Photometrics, UK) with 3x3 pixel binning to increase sensitivity. Live cell recordings were captured and initially processed

using Imaging workbench Ver. 6.0 software (INDEC Biosystems, Santa Clara, CA, USA).

3.3.4 Analysis protocol

Cells or analysis regions of interest (AROI) were selected such that the first AROI (AROI-0) was always designated as the background. Subsequent AROIs were drawn around each adipocyte. The mean fluorescence intensity of each cell with time was then calculated. These values were further analysed using Microcal ORIGIN 6.1 (Microcal Software Inc., Northampton, MA). Lab talk script was created by Dr. Paul A. Smith (see Appendix 2 for the lab talk script) to subtract the background fluorescence (AROI-0) and calibrate $[Ca^{2+}]_i$ for each cell. To calibrate $[Ca^{2+}]_i$, fluorescence changes were measured at the experiment end by a one-point method that involved permeabilization of the cells with 0.05 % Triton X100, with the maximum fluorescence value observed taken as Fmax. To calculate $[Ca^{2+}]_i$ the following equation was used (Equation 1):

$$[Ca^{2+}]_i = Kd \times \frac{F}{Fmax - F}$$

Where F is the background corrected fluorescence, and Kd is the assumed intracellular dissociation constant of Fluo-4: 345 nM (Paredes et al., 2008). The diameter of the adipocytes was determined from the area of the regions of interest drawn around each adipocyte, using a script written by Dr. Paul A. Smith.

3.3.5 Cell selection criteria for data analysis

Cells were screened for inclusion in further analyses by the application of an objective exclusion criteria, defined as follows:

- Cells that did not respond to Triton x100 calibration
- Cells with erratic behaviour

- Cells that apparently leaked dye causing a continuous decrease in $[Ca^{2+}]_i$ throughout the experiment regardless of treatment
- Cells that possessed a continuous increase in $[Ca^{2+}]_i$ throughout the experiment regardless of treatment.

3.3.6 Statistical analysis

Data was analysed using GraphPad Prism Version 7.03 program (GraphPad Software Inc., San Diego, CA). Normality of data was first determined using the D'Agostino-Pearson omnibus normality test. For data sets that were less than n = 10, these were analysed by parametric test (which has more power than non-parametric test). Parametric data sets were analysed by repeated measures One-Way ANOVA for paired data, followed by Dunnett's post-hoc test for multiple comparisons. Data sets which were not normally distributed were analysed by the Friedman's test for repeated measures, followed by Dunn's post-hoc test for multiple comparisons or Mann-Whitney U test for non-paired data. Significance was set at $p < 0.05$, and the values of p for significant differences are indicated in figure legends. Data are mostly shown as box and whisker plots with 2.5–97.5% confidence intervals (CIs). Numerical data are given as mean ± S.E.M. or median with 5% to 95% CIs to two significant figures. The peak $[Ca^{2+}]_i$ for conditions in which the cells responded with transient increases and for the duration of growth hormone perfusion (as different cells responded at different times) was used for analysis, while the steady state $[Ca^{2+}]_i$ values for all other conditions were used. Technical replicates are denoted by n (number of cells), while biological replicates are denoted by f (number of experiments/individual coverslips pooled from different animal preparations) and/or i (number of animal preparations) (Lazic et al., 2018).

3.3.7 Measurement of free Ca^{2+} in the extracellular solution

Free calcium concentration of solutions, $[Ca^{2+}]_{o,}$ were measured with a combination Ca^{2+} electrode (EDT direct ion, Dover, UK) at 20-22◦C. The electrode was calibrated with 25, 2.5 and 0.25 mM $CaCl_2$ solutions made by serial dilution of a 1 M $CaCl_2$ standard with a 150 mM NaCl, 10 mM HEPES (pH 7.4 with NaOH) solution; ionic strengths, I, were calculated as 230, 163 and 156 mM respectively. At these ionic strengths, ideality of behaviour was assumed and ion concentration was used instead of activity. Resultant electrode voltages, E_{Ca}, were fit with the Nernst equation and the $[Ca^{2+}]$ of test solutions obtained by extrapolation. The electrode appeared insensitive to Mg^{2+} since E_{Ca} was unaffected by 4.8 mM $MgCl_2$ added to the calibration solutions.

3.3.8 Estimation of anion affinity for Ca^{2+}

The effect of extracellular chloride reduction on $[Ca^{2+}]_i$ was explored by equimolar substitution of sodium chloride with sodium salts of organic anions (gluconate, glutamate, aspartate and methylsulphonate). At a physiological pH of 7.4, gluconate, glutamate, aspartate and methylsulphonate primarily exist as monovalent anions. The affinity of these anions for free calcium in the extracellular medium was determined by Dr. Paul A. Smith as described below (Akaniro-Ejim and Smith, 2021). In the presence of Ca^{2+}, the anion can exist in three forms: free ligand, L^-; a monomolecular complex, CaL^+ or bimolecular complex, $CaL_{2,}$ as shown in the following reaction scheme:

$$2L^- + Ca^{2+} \underset{k_{-1}}{\overset{k_1}{\rightleftharpoons}} L^- + CaL^+ \underset{k_{-2}}{\overset{k_2}{\rightleftharpoons}} CaL_2$$

Where the association constants ($L\ M^{-1}$) K_{a1} and K_{a2} are given by $K_{a1} = k_1/k_{-1}$ and $K_{a2} = k_2/k_{-2}$ respectively.

Three scenarios exist for binding of the second ligand: a) it is similar but independent of bound ligand such that $K_{a1} \approx K_{a2}$; b) it is impeded by bound ligand such that $K_{a1} > K_{a2}$; c) it is prevented by bound ligand: $K_{a2} \rightarrow 0$.

For scenarios a) and b) at steady state, if $k_{-1} \approx k_{-2}$, then;

$$[CaL^+] = K_{a1} [Ca^{2+}]_f [L^-] \quad (1)$$

$$[CaL_2] = K_{a2} [CaL^+] [L^-] \quad (2)$$

and

$$[Ca^{2+}]_{tot} = [Ca^{2+}]_f + [CaL^+] + [CaL_2] \quad (3)$$

Substitution of equations 1 and 2 into 3 gives

$$[Ca^{2+}]_f = [Ca^{2+}]_{tot} /(1 + K_{a1}[L^-] + K_{a1}K_{a2} [L^-]^2) \quad (4)$$

Where $[Ca^{2+}]_{tot}$ is the total concentration of Ca^{2+}, and $[Ca^{2+}]_f$ the concentration of free Ca^{2+}; it is assumed $[L^-] >> [Ca^{2+}]_{tot}$ such that $[L^-]$ is unaffected by chelation.

Whereas, for scenario c) $K_{a2} = 0$ then simply;

$$[Ca^{2+}]_f = [Ca^{2+}]_{tot} /(1 + K_{a1}[L^-]_{tot}) \quad (5)$$

$$[CaL^+] = [Ca^{2+}]_{tot} - [Ca^{2+}]_f \quad (6)$$

For this scenario only changes in $[L^-]$ due to Ca^{2+} chelation can be accounted for as follows:

$$[CaL^+] = (b - \sqrt{(b^2 - 4[Ca^{2+}]_{tot} [L^-]_{tot})})/2 \quad (7)$$

Where

$$b = [Ca^{2+}]_{tot} + [L^-]_{tot} + 1/K_{a1} \quad (8)$$

$$[Ca^{2+}]_f = [Ca^{2+}]_{tot} - [CaL^+] \quad (9)$$

$$[L^-]_f = [L^-]_{tot} - [CaL^+] \quad (10)$$

Subscripts f and tot refer to free and total concentration, respectively.

3.3.9 Experimental Determination of K_{a1} and K_{a2}

134 mM NaCl in Hanks buffer was substituted with a sodium salt of the test anion. These were mixed with different volumes of standard Hanks containing 152 mM

Cl^-, to form solutions of known anion composition. $[Ca^{2+}]_f$ was measured and plotted as a function of $[L^-]$ (Figure 3.11). To determine K_{a1} and K_{a2} this data was fitted with equations 4 and 5 and the best fit model determined by the F-test. $[Ca^{2+}]_{tot}$ was constrained to that measured in the absence of L^-; median value 2.47 mM (2.36-2.5; 95% C.I., n = 17). Since solutions contained Mg^{2+}, Mg^{2+} binding was expected to decrease $[L^-]_f$. To ascertain if this affected $[Ca^{2+}]_o$, experiments were repeated without $MgCl_2$; the effect on K_{a1} and K_{a2} were undetectable.

3.3.10 Estimation of V_m

The membrane potential (V_m) of adipocytes expected on sequential reduction of bath Cl^- by substitution with organic anions was predicted by Dr. P. A. Smith, using the Goldman Hodgkin Katz (GHK) constant field equation as previously employed (Bentley et al., 2014).

3.4. Results

3.4.1 Primary adipocytes loaded with Fluo 4AM

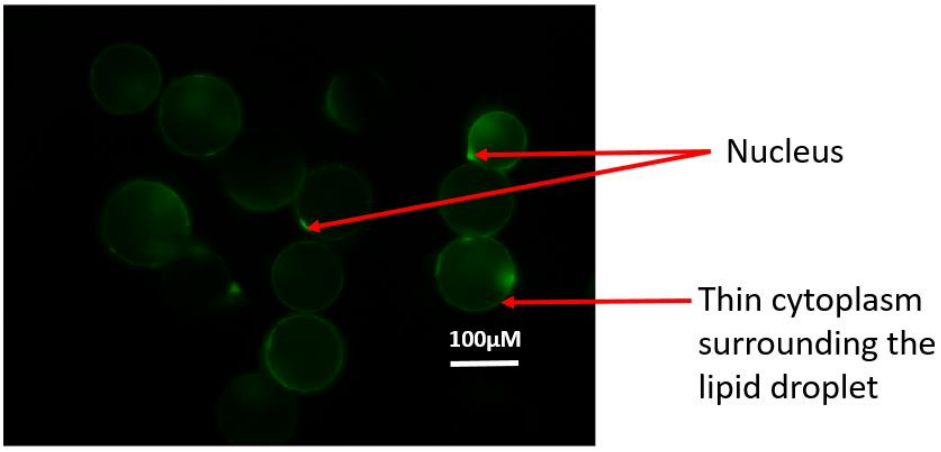

Figure 3.1: Primary adipocytes from CD1 mice loaded with Fluo 4AM.

A representative field of Fluo-4 loaded primary white fat adipocytes, viewed with x20 objective. The images given are pseudo colour image. The green colour is representative of the dye/ Ca^{2+} content of the cell. The black background is indicative of the absence of dye. The primary adipocytes show their characteristic unilocular neutral lipid-rich lipid droplet. This is surrounded by a thin cytoplasm into which the fluo 4 is readily absorbed, with the nucleus being pushed to the periphery of the cell by the intracellular lipid droplet.

Primary white fat adipocytes incubated with fluo 4 am readily absorbed the dye (Figure 3.1). Fluo 4 which is a calcium specific dye, is mainly partitioned into the thin cytoplasm surrounding the adipocyte lipid droplet. The presence of the nuclear knob, a characteristic feature of primary white adipocytes, allowed confirmation of the cells as such.

3.4.2 Functional Expression of L-Type Calcium Channels in WFAs

To determine the existence of Ca^{2+} entry pathways through the plasma membrane of visceral white fat adipocytes, the extracellular $CaCl_2$ (eCa^{2+}) concentration was increased from 2.4 mM to 5 mM. High eCa^{2+} consistently evoked a sustained increase in intracellular calcium concentration ($[Ca^{2+}]_i$) in VIS-WFAs (Figure 3.2A),

with 9.4 % (7 – 13.5 %, 95% C.I.; $P < 0.0001$, Friedman) increase in free calcium concentration from basal levels (Figure 3.2C). This increase in $[Ca^{2+}]_i$ was not restored to basal levels during the washout period and the cells attained a new significantly higher basal $[Ca^{2+}]_i$ than the initial level (10.8 %; 6.3 - 20.3 %, 95% C.I.; $P < 0.0001$, Friedman). On the other hand, addition of an equivalent concentration of $MgCl_2$ to standard Hanks buffer as a divalent cation control for high eCa^{2+} buffer had no effect on intracellular calcium level (Figure 3.2B and C).

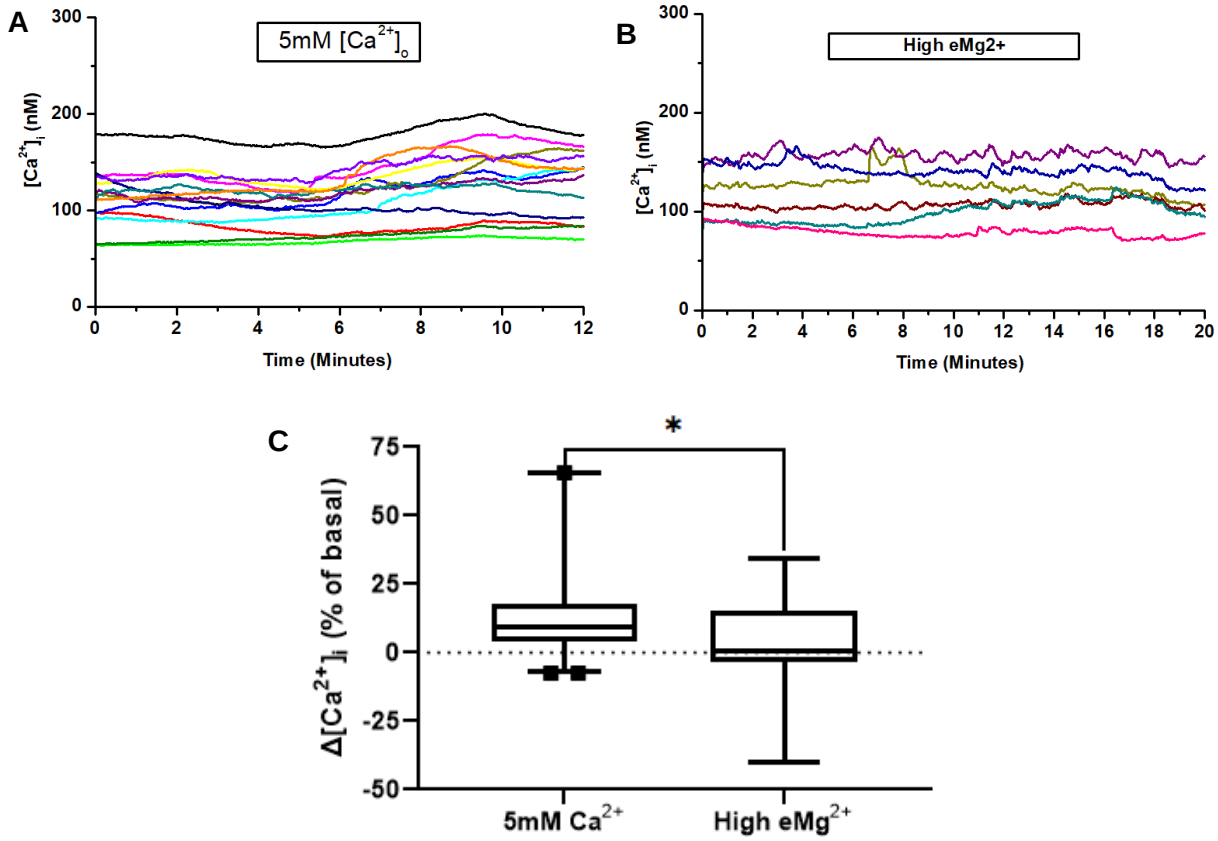

Figure 3.2: 5 mM eCa^{2+} increases $[Ca^{2+}]_i$ in CD1 male mouse VIS-WFAs.

A. Time course measurement of $[Ca^{2+}]_i$ for 10 adipocytes within a single field in response to elevation of eCa^{2+}. All conditions were made for 4-5 minutes. **B.** Time course measurement of $[Ca^{2+}]_i$ for 6 adipocytes within a single field in response to High eMg^{2+}. **C.** Elevation of bath Ca^{2+} to 5 mM increased intracellular calcium from basal (n = 85; f = 18, i = 9), while its divalent control for (High eMg^{2+}) had no effect (n = 17; f = 3, i = 1); $p<0.05$, Mann-Whitney U test.

Closer characterisation of adipocyte size and basal calcium distribution was carried out to help understand if there was any relationship between adipocyte size, basal calcium concentration and high eCa^{2+} induced increase in WFA $[Ca^{2+}]_i$. CD1 male mice visceral adipocytes showed a normal distribution of cell diameter, with a mean diameter of 146.0 μm (138.1-154.0 μm, 95% C.I., n = 85) (Figure 3.3A), while the basal intracellular calcium distribution was left-skewed, with median value 160.0 nM (149.0 – 181.4 nM, 95% C.I., n = 85) (Figure 3.3B). In comparison, subcutaneous adipocytes from CD1 male mice showed a median cell diameter of 96 μm (93.3-99.8 μm, 95% C.I., n = 280), and a left-skewed basal intracellular calcium with median value 122 nM (107-140 nM, 95% C.I., n = 266) (Data from Dr Paul A. Smith).

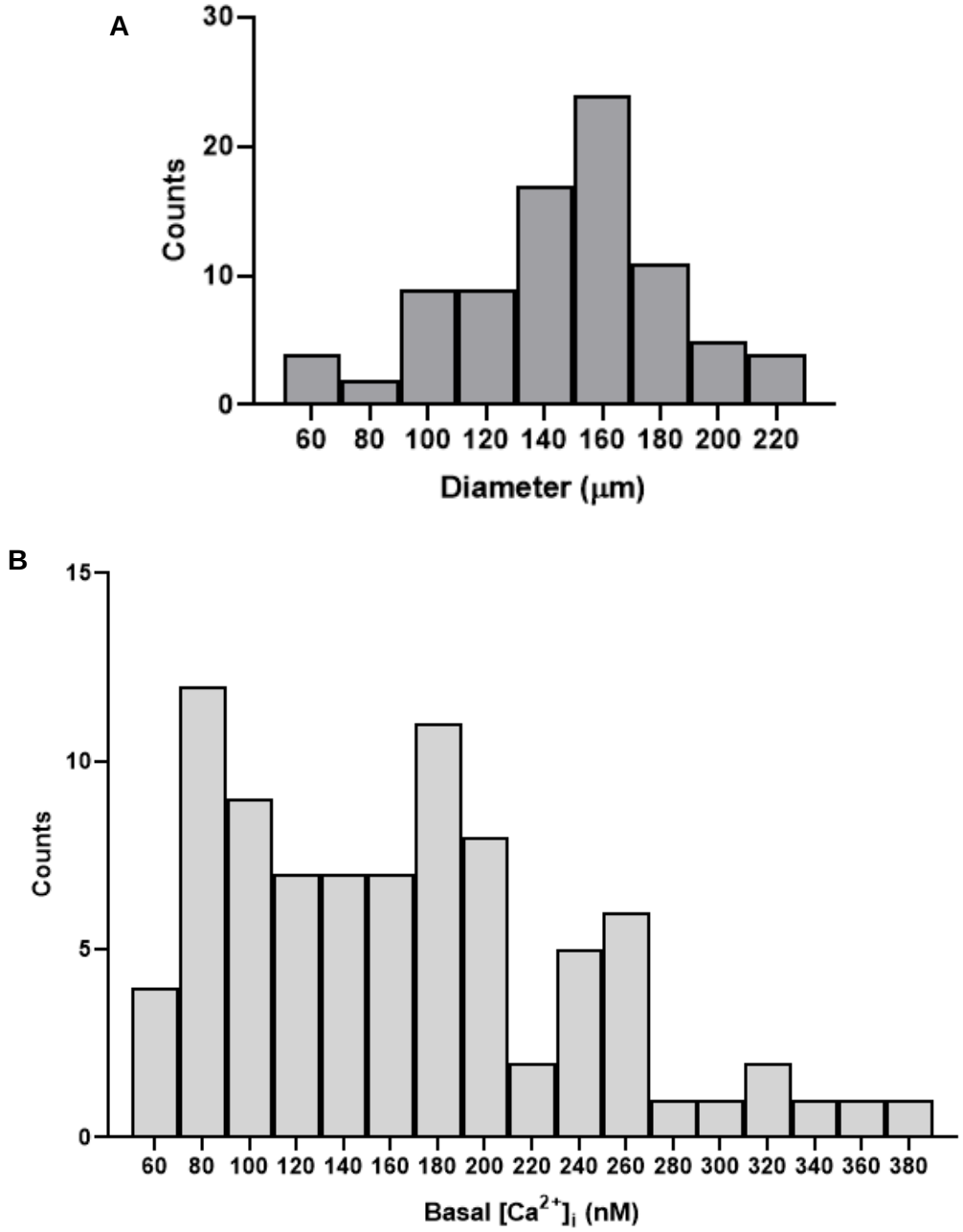

Figure 3.3: Distribution of CD1 male mouse VIS-WFAs diameter and basal $[Ca^{2+}]_i$.

A. Gaussian distribution of adipocyte cell diameter, with mean values of 146.1 µm (138.1-154.0 µm, 95% C.I., n = 85). **B.** Basal $[Ca^{2+}]_i$ of the adipocytes was left-skewed, with median values of 160.0 nM (149.0 – 181.4 nM, 95% C.I., n = 85).

No correlation between visceral adipocyte size and basal intracellular calcium (Spearman rank correlation coefficient, r = 0.13, -0.09 to 0.33, 95% C.I., p = 0.239; Figure 3.4A) or between adipocyte size and the 5 mM Ca^{2+} induced increase in $[Ca^{2+}]_i$ (Spearman r = 0.20, -0.01 to 0.40, 95% C.I., p = 0.060; Figure 3.4B) was observed. However, the increase in basal Ca^{2+} levels due to doubling of extracellular calcium concentration ($[Ca^{2+}]_o$) from 2.5 mM to 5 mM was found to be positively correlated with the basal $[Ca^{2+}]_i$ (Spearman r = 0.35, 0.14 – 0.52, 95% C.I., p = 0.001; Figure 3.4C).

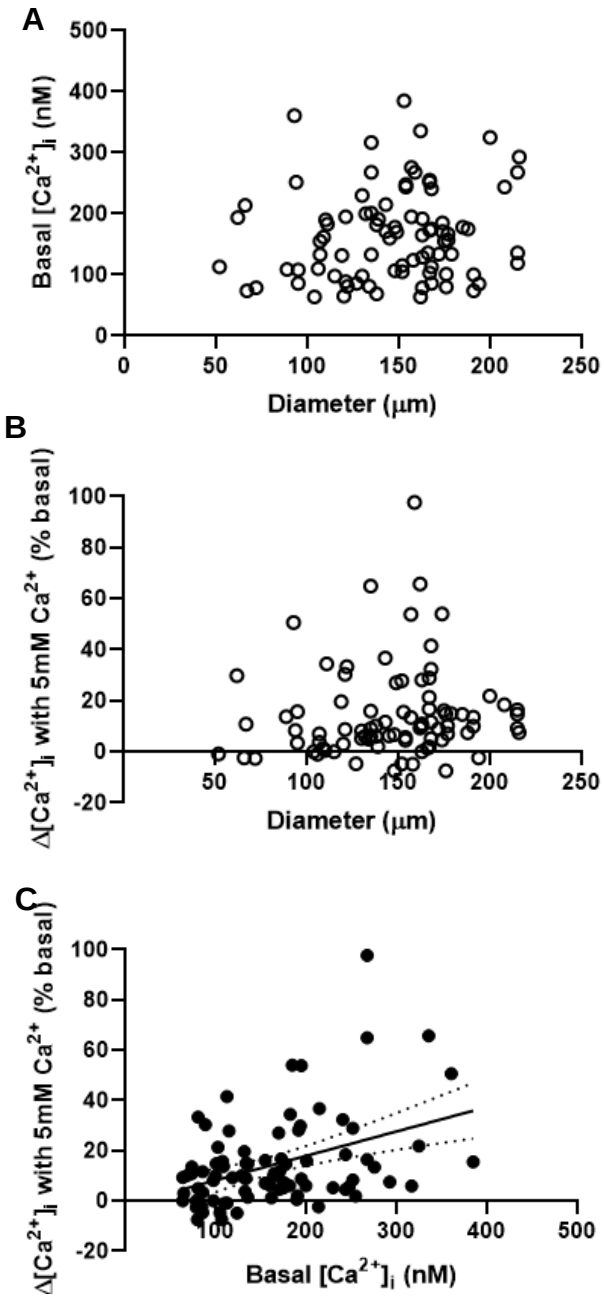

Figure 3.4: Intracellular calcium levels do not correlate with cell diameter but changes with basal measurement in isolated adipocytes.

A. Scatter plot of $[Ca^{2+}]_i$ versus adipocyte diameter, no correlation, n = 85.

B. Scatter plot of % $\Delta[Ca^{2+}]_i$ with 5mM Ca^{2+} versus adipocyte diameter, no correlation.

C. Scatter plot of % $\Delta[Ca^{2+}]_i$ with 5mM Ca^{2+} versus basal intracellular calcium show a positive correlation. Solid lines in (**A**), (**B**) and (**C**) are drawn by linear regression with slopes of 0.311 ± 0.22 nM/μm (P = 0.161), 0.047 ± 0.053 %/ μm (P = 0.378) and 0.097 ± 0.024 %/nM (P < 0.0001) respectively. Dotted lines are 95% C.I. for the fits shown.

Next, the involvement of Ca^{2+} entry through L-type calcium channels in elevated $[Ca^{2+}]_o$ mediated increase in $[Ca^{2+}]_i$ was determined. This was explored by perfusion of 20 μM verapamil, an L-type calcium channel antagonist (Feng et al., 2018).

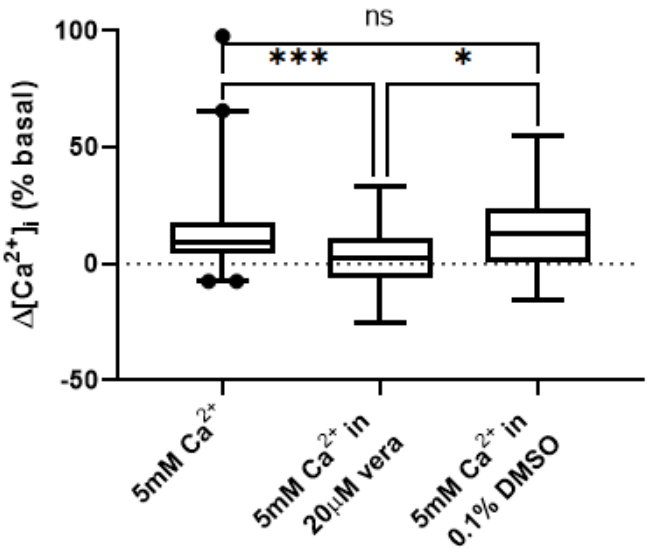

Figure 3.5: 20 μM verapamil inhibits increase in $[Ca^{2+}]_i$ induced by high extracellular Ca^{2+} in CD1 male mouse VIS-WFAs.

Δ$[Ca^{2+}]_i$ elicited by 5 mM calcium applied extracellularly (n = 85; f = 18, i = 9), is inhibited in the presence of 20 μM verapamil; n = 38; f = 5, i = 2. DMSO, the vehicle for 20 μM verapamil, had no effect on intracellular calcium increase due to elevation of $[Ca^{2+}]_o$ in WFAs; n = 21; f = 5, i = 3. (*P < 0.05, ***P < 0.001, ns = non-significant; Kruskal-Wallis with Dunn's multiple comparison test).

20 μM Verapamil blocked the intracellular calcium influx previously elicited by 5 mM eCa^{2+}. In contrast, 0.1 % dimethyl sulfoxide (DMSO), the vehicle for dissolution of verapamil, had no effect on the intracellular calcium influx elicited by 5 mM eCa^{2+} (Figure 3.5). 20 μM Verapamil inhibited basal calcium influx in WFAs by 1.7 %, however this effect was not significant. Interestingly, a negative correlation (Spearman r = -0.339, -0.6012 to -0.0128 % C.I., p = 0.037, n = 38) between adipocyte basal calcium levels and verapamil inhibition of constitutive calcium entry in WFAs (Fedorenko et al., 2019) was observed (Figure 3.6). Adipocytes which showed pronounced inhibition of calcium influx exhibited higher basal calcium levels. No correlation between basal calcium levels and verapamil inhibition of 5 mM eCa^{2+} induced increase in intracellular Ca^{2+} levels was observed.

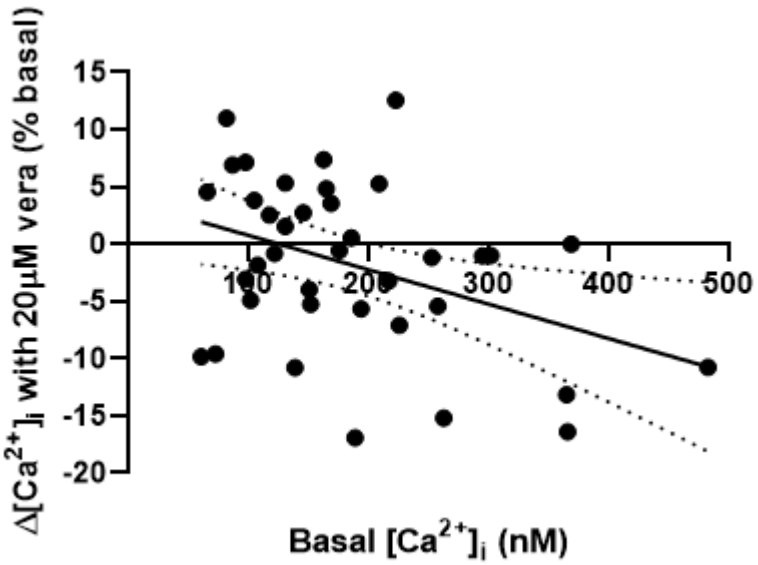

Figure 3.6: 20μM Verapamil inhibits basal $[Ca^{2+}]_i$.

Scatter plot of % $\Delta[Ca^{2+}]_i$ with 20μM verapamil versus basal intracellular calcium shows a negative correlation; n = 38. Solid lines are drawn by linear regression with slope of -0.030 ± 0.011 %/nM ($P < 0.014$). Dotted lines are 95% C.I. for the fit.

Based on the knowledge that L-type calcium channels are sensitive to voltage and hormonal regulation (Hofmann et al., 2014), we sought to determine the effect of membrane depolarization and hormonal regulation on the activity of these channels in white fat adipocytes.

3.4.3 Determination of Voltage Regulation of L-Type Calcium Channels in WFAs

Unlike most other cells in which the resting membrane potential is controlled by potassium ions, the principal ion which regulates the resting membrane potential of WFAs is chloride ion (Perry and Hales, 1969, Beigelman and Shu, 1972, Bentley et al., 2014). In addition, extracellular Cl^- removal has been shown to cause reversible depolarisation of the plasma membrane potential of white adipocytes (Bentley et al., 2014). Based on this knowledge, we aimed to determine if changes in $[Cl^-]_o$ and the associated change in membrane potential can affect the activity

of voltage-gated Ca^{2+} channels and $[Ca^{2+}]_i$. This was done by measuring the $[Ca^{2+}]_i$ in response to varying extracellular chloride containing Hanks buffer in CD1 male mice VIS-WFAs. Extracellular chloride removal was achieved by equimolar substitution of sodium chloride with sodium salts of organic anion in Hanks buffer.

3.4.3.1 Substitution of bath Cl^- with gluconate reversibly decreases intracellular $[Ca^{2+}]$ of white fat adipocytes.

A significant decrease in intracellular calcium concentration from basal levels was observed upon extracellular chloride ion substitution with gluconate ions in VIS-WFAs (Figure 3.7). The magnitude of the observed decrease was negatively correlated with the basal free calcium concentration (Spearman r = -0.64, 113 mM Cl^-, $p<0.01$; r = -0.88, 53 mM Cl^-, $p<0.0001$; r = -0.91, 18 mM Cl^-, $p<0.0001$) (Figure 3.8). Cells with a higher basal free calcium showed a greater-fold decrease in $[Ca^{2+}]_i$ compared to cells with lower basal calcium levels.

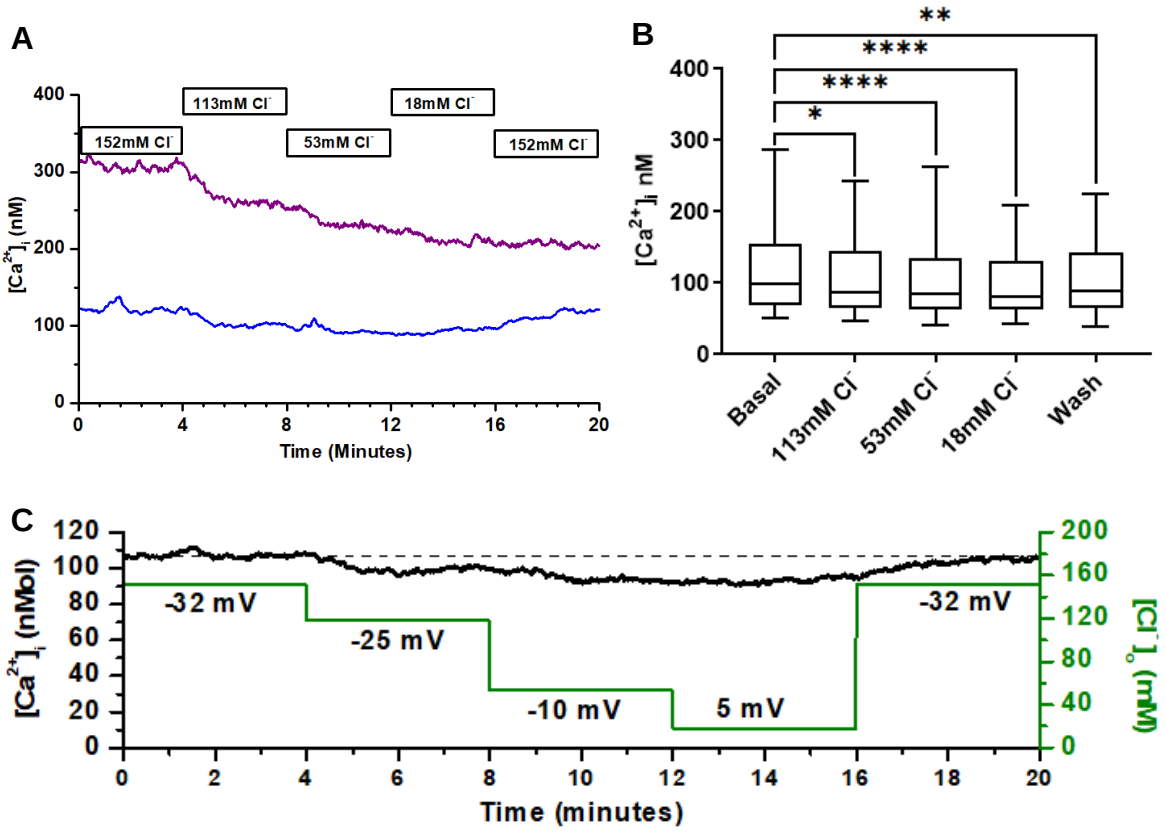

Figure 3.7: Effect of extracellular chloride substitution with gluconate on $[Ca^{2+}]_i$ in CD1 male mouse VIS-WFAs.

A: $[Ca^{2+}]_i$ response of two individual adipocytes to 113, 53 and 18 mM $[Cl^-]_o$ in sodium gluconate Hanks. **B:** $[Ca^{2+}]_i$ response of adipocytes under conditions in A above. Bath $[Cl^-]$ at 152 mM was not substituted for basal and wash (n = 46, f = 11*p < 0.05, **p < 0.01 ****p < 0.0001; Friedman's test, Dunn's post hoc test). **C:** Mean intracellular Ca^{2+} for 5 adipocytes (black line), in response to sequential substitution of 39, 99 and 134 mM bath Cl^- with gluconate as indicated by the green line; and predicted V_m values for the various $[Cl^-]_o$.

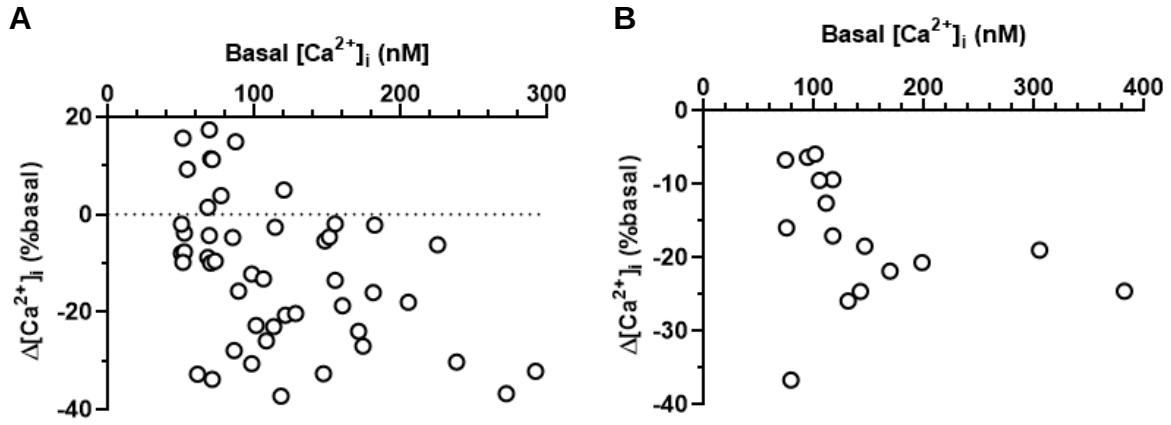

Figure 3.8: Scatter plot of % change in $[Ca^{2+}]_i$ from basal in individual adipocytes in response to extracellular chloride ion substitution with gluconate and glutamate ion.

A: Relationship between basal $[Ca^{2+}]_i$ and the decrease in $[Ca^{2+}]_i$, $\Delta[Ca^{2+}]_i$, in response to 134 mM $gluconate^-$. Adipocytes with higher basal $[Ca^{2+}]_i$ show more response to extracellular chloride removal. **B:** Relationship between basal $[Ca^{2+}]_i$ and $\Delta[Ca^{2+}]_i$, in response to 134 mM $glutamate^-$.

I then assessed a different anion, sodium glutamate for substitution of sodium chloride, to compare its effect with sodium gluconate substitution on $[Ca^{2+}]_i$ in CD1 male mouse VIS-WFAs. Like the observation with sodium gluconate substitution (Figure 3.7), a progressive decrease in intracellular calcium from basal levels was seen in VIS-WFAs in response to 113 mM Cl^- and 53 mM Cl^- monosodium glutamate Hanks, with a negligible recovery at the lowest chloride concentration of 18mM tested (Figure 3.9).

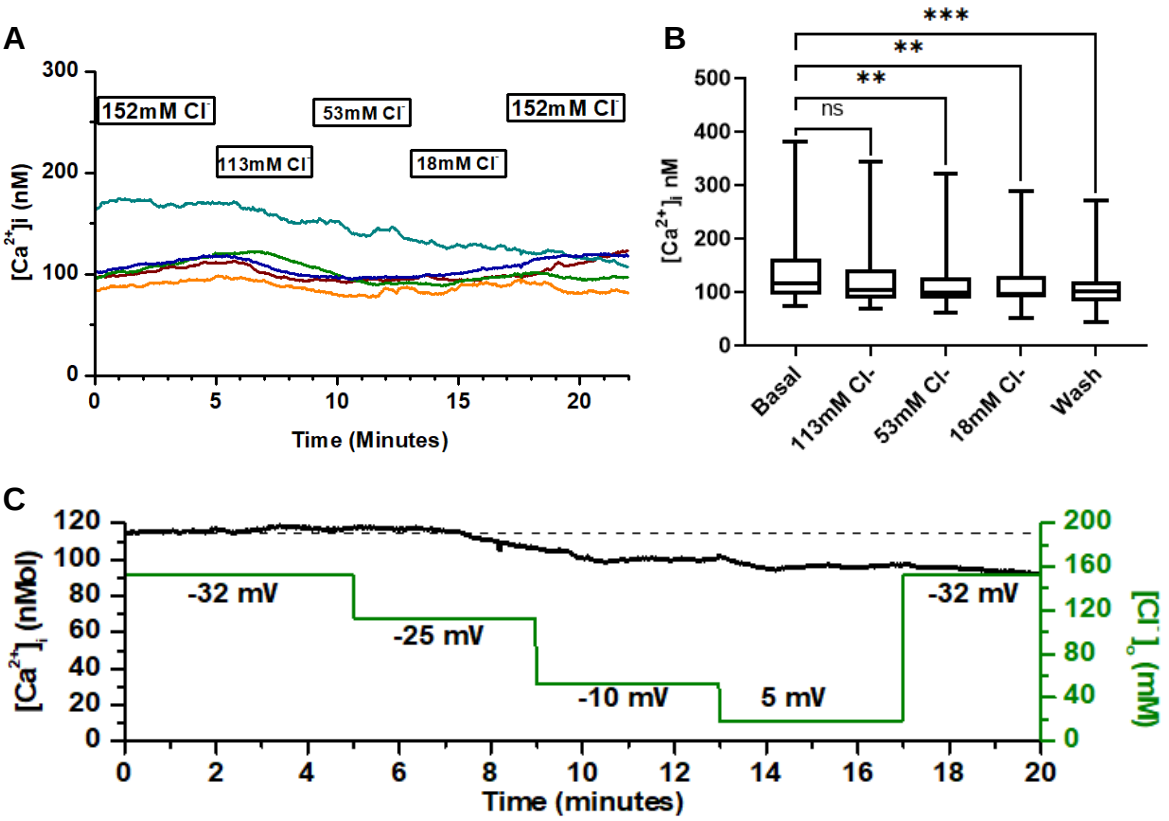

Figure 3.9: Effect of extracellular chloride substitution with glutamate on $[Ca^{2+}]_i$ in CD1 male mouse VIS-WFAs.

A: $[Ca^{2+}]_i$ response of five individual adipocytes to 113, 53 and 18mM $[Cl^-]_o$ in monosodium glutamate Hanks. **B:** $[Ca^{2+}]_i$ response of adipocytes under conditions in A above. Bath $[Cl^-]_o$ (152 mM) was not substituted for basal and wash (n = 16, f = 4 **p < 0.01, ***p < 0.001, ns = non-significant; Friedman's test, Dunn's post hoc test). **C:** Mean intracellular Ca^{2+} for 5 adipocytes (black line), in response to sequential substitution of 39, 99 and 134 mM bath Cl^- with glutamate as indicated by the green line; and predicted V_m values for the various $[Cl^-]_o$.

To assess that the decrease in intracellular calcium in response to extracellular chloride substitution with organic anions was not due to artefacts such as cell movement, dye loss through bleaching or extrusion, and confirm the integrity of these cells, the cells were continuously perifused in bath solution and the effect of high extracellular calcium (5 mM $[Ca^{2+}]_o$) on $[Ca^{2+}]_i$ was tested before and after low chloride medium exposure (Figure 3.10).

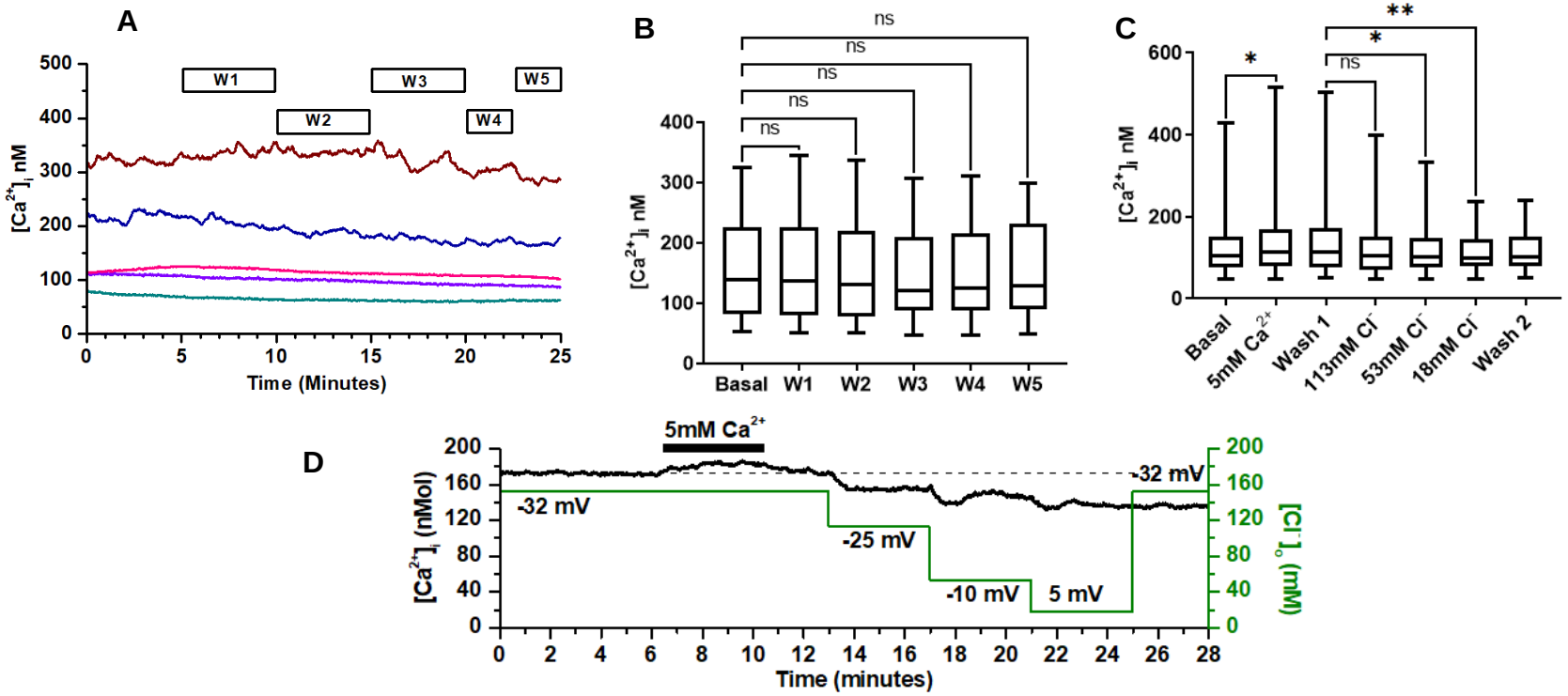

Figure 3.10: Effect of bath exchange, 5 mM $[Ca^{2+}]_o$ and varying $[Cl^-]_o$ on $[Ca^{2+}]_i$ in CD1 male mouse VIS-WFAs.

A: Time course measurement of $[Ca^{2+}]_i$ for 5 individual adipocytes within a single field of view in response to 152 mM $[Cl^-]_o$. No response to alternate changes in bath solution as indicated W1, W2, W3, W4, and W5. **B:** Bath solution was consecutively switched with wash, W1-5, every 3-5 minutes. No change in $[Ca^{2+}]_i$ was observed, (n = 16, f = 4ns = non-significant, RM one-way ANOVA with Dunnett's test). **C:** Pre-exposure of the cells to 5 mM $[Ca^{2+}]_o$ caused an increase in $[Ca^{2+}]_i$ which was followed by a progressive decline on return to the gluconate buffer, (n = 35, f = 7 *p <0.05, **p <0.01; Friedman with Dunn's post-hoc test). **D:** Mean $[Ca^{2+}]_i$ for 6 adipocytes in response to an increase in bath $[Ca^{2+}]$ (black line), followed by sequential substitution of 39, 99 and 134 mM bath Cl^- with gluconate as indicated by the green line (estimated $[Ca^{2+}]_o$ 1.24, 0.47 and 0.3 mM respectively with a k_{a1} of 17 L M^{-1}); and predicted V_m values for the various $[Cl^-]_o$.

The effect of the organic anions was not an artefact of perifusion since multiple solution exchanges had no effect on $[Ca^{2+}]_i$ (Figure 3.10B). Elevation of $[Ca^{2+}]_o$ from 2.5 mM to 5 mM led to an increase of 6.3 % (2.3 – 10.2, 95% CI; Figure 3.10C) in intracellular calcium from basal levels. After the wash period (wash 1), the cells attained a new baseline which was higher than the initial basal $[Ca^{2+}]_i$. The $[Ca^{2+}]_i$ subsequently declined on removal of extracellular chloride, followed by incomplete recovery of the cells on return to standard Hanks with normal chloride concentration (152 mM Cl^-) (wash 2) (Figure 3.10C). Re-exposure of the cells to 5 mM $[Ca^{2+}]_o$ again resulted in an increase in intracellular calcium levels. The increase in $[Ca^{2+}]_i$ on exposure to a high extracellular calcium medium and subsequent decline on gluconate substitution of extracellular chloride as seen in Figure 3.10C, led to the idea of gluconate chelated calcium in the Hanks buffer.

To confirm if the decrease in adipocyte $[Ca^{2+}]_i$ with gluconate was indeed due to chelation of bath Ca^{2+}, the free calcium concentration of varying concentrations of sodium gluconate buffer (0 mM – 134 mM $gluconate^-$) was determined (Figure 3.11). The chelation of calcium by other anionic substitutes for chloride (glutamate, aspartate and methylsulphonate) were also assessed.

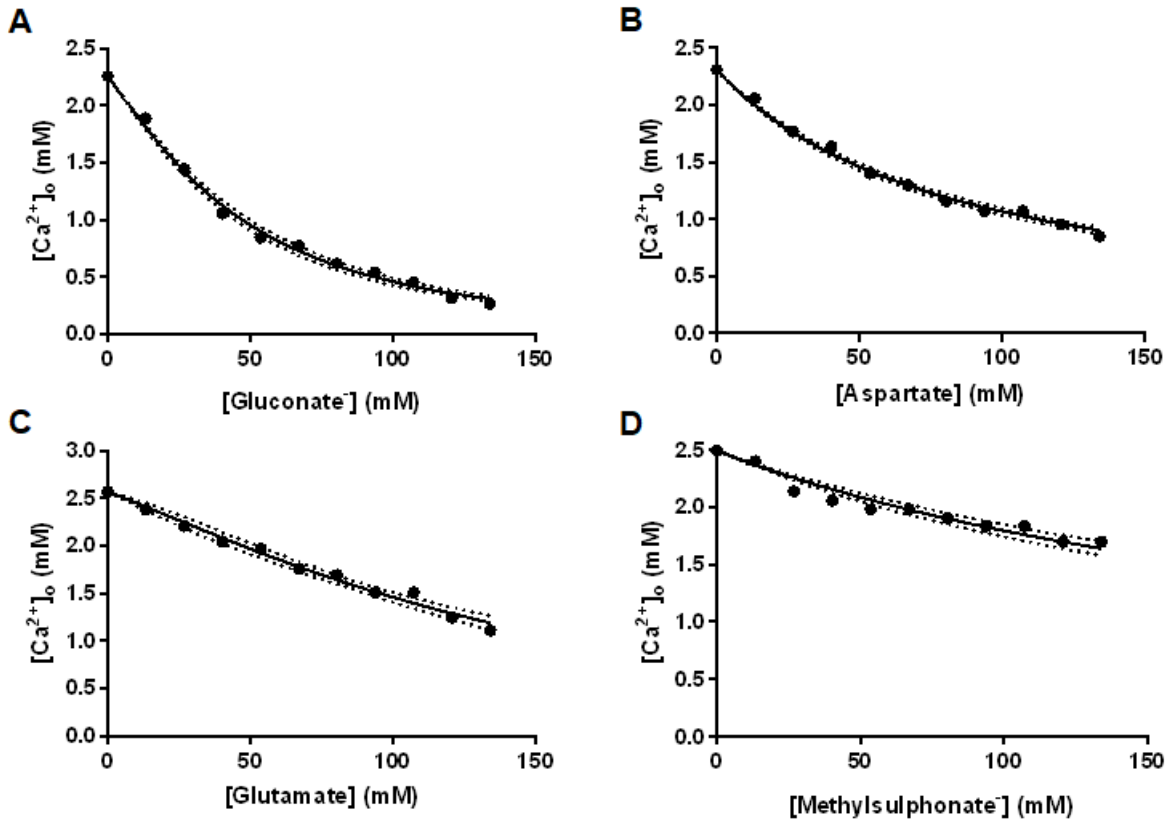

Figure 3.11: Organic anions chelate extracellular Ca^{2+}.

Representative plots of $[Ca^{2+}]_f$ against equimolar substitution of Cl^- with anion indicated. Each point is a single determination. Solid lines are best fits of equation 4 or 5, where for **A)** ka_1 = 15.5 L M^{-1} **B)** Ka_1 = 11.7 L M^{-1}, **C)** ka_1= 7.3 L M^{-1} **D)** ka_1= 3.9 L M^{-1}. Dotted lines are 95% confidence intervals.

There was a progressive reduction in free calcium concentration of the buffer with increasing concentrations of gluconate$^-$. At the highest concentration of gluconate$^-$ tested (134 mM), the free calcium concentration was 200 µM compared to that of standard Hanks buffer at ~2.5 mM. Similarly, a gradual reduction of free calcium concentration of the respective buffers was observed with increasing concentrations of glutamate$^-$ and aspartate$^-$, with methyl sulphonate$^-$ showing the least effect (Figure 3.11).

Going further, we compared the effect of 134 mM gluconate$^-$ buffer (18 mM $[Cl^-]_o$) on the adipocyte $[Ca^{2+}]_i$ with that of an extracellular $[Ca^{2+}]$ of 200 µM. Both the

18 mM $[Cl^-]_o$ sodium gluconate Hanks and the 200 µM extracellular calcium Hanks buffer had comparable effects on $[Ca^{2+}]_i$, decreasing it by -22.15 % (-29.38 to 4.04 %, 95% C.I.) and -29.85 % (-30.71 to -17.56 %, 95% C.I.) respectively, significantly lower than the basal $[Ca^{2+}]_i$ (Figure 3.12A and B).

In an attempt to negate the chelation effect of gluconate, the free calcium concentration of the sodium gluconate low chloride Hanks was titrated to the same level as the basal solution. This was done by addition of increasing volumes of 1 M $CaCl_2$ solution and measurement of the free calcium concentration using a calcium electrode, until the desired free calcium level was attained. The effects of these calcium-supplemented sodium gluconate low chloride Hanks buffer on $[Ca^{2+}]_i$ levels in VIS-WFAs was then assessed.

Maintenance of extracellular Ca^{2+} at 2.6 mM by calcium supplementation prevented the decrease in $[Ca^{2+}]_i$ seen with gluconate (Figure 3.12C and D).

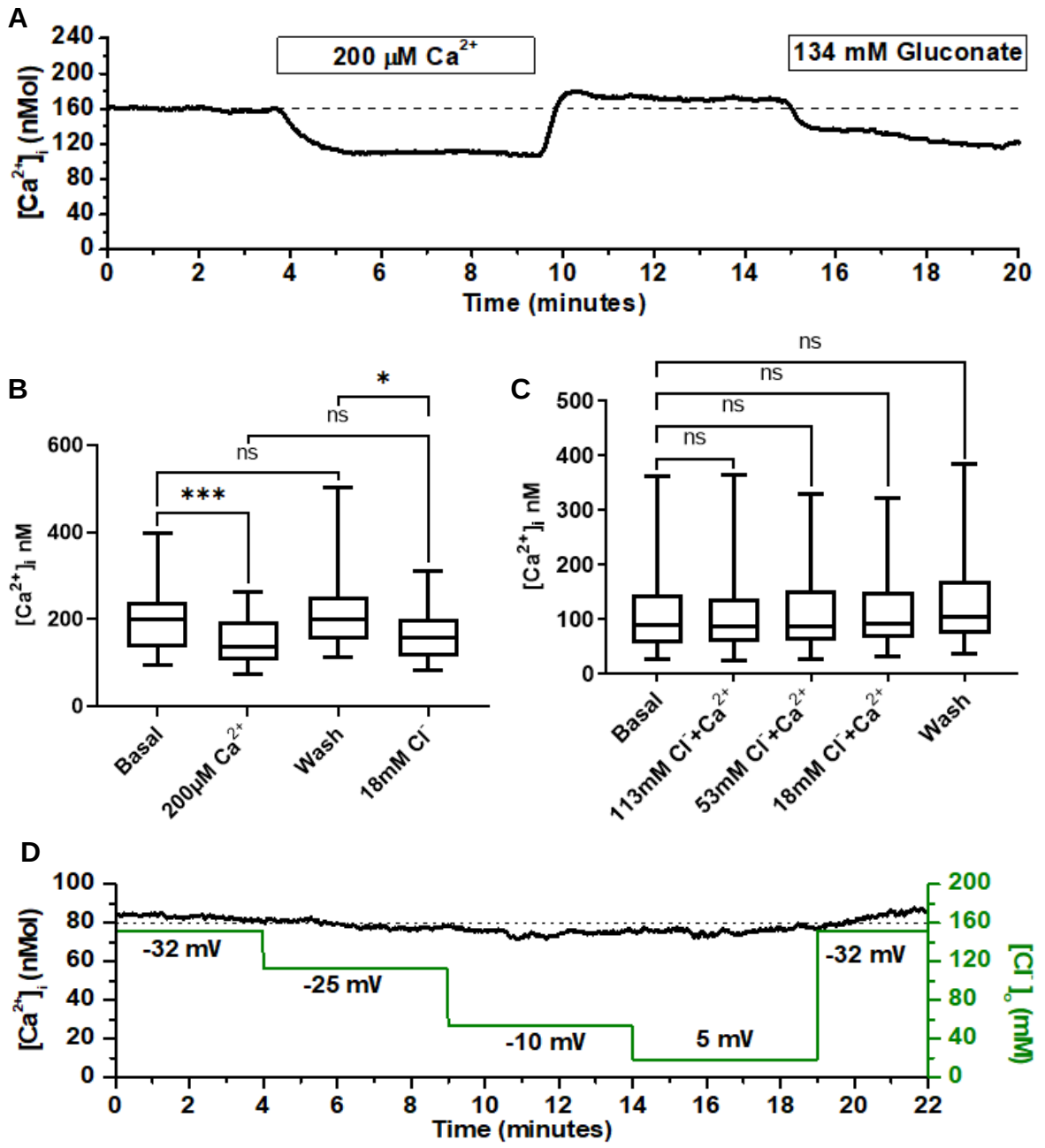

Figure 3.12: Gluconate decreases $[Ca^{2+}]_i$ of adipocytes by chelation, an effect prevented by extracellular Ca^{2+} supplementation.

A: Mean $[Ca^{2+}]$ for 4 adipocytes in response to a reduction in bath Ca^{2+}, followed by substitution of 134 mM bath Cl^- with gluconate. **B:** $[Ca^{2+}]_i$ under the conditions indicated in (A) (n = 15, f = 4 *p <0.05, ***p <0.001; Friedman with Dunn's test) **C:** $[Ca^{2+}]_i$ under conditions indicated in D, where bath Cl^- is sequentially decreased by gluconate substitution but $[Ca^{2+}]_f$ is maintained at 2.5 mM. Basal and wash are 152 mM $[Cl^-]_o$ (n = 16, f = 3; Friedman with Dunn's test). **D:** Mean $[Ca^{2+}]_i$ for 4 adipocytes (black line) in response to equimolar replacement of bath $[Cl^-]_o$ with gluconate (green line), but where free $[Ca^{2+}]$ is maintained at 2.5mM. V_m values (in mV) are predicted.

To determine the best organic anion substitutes for chloride with the least potential for associations with free calcium in extracellular bath solution, we assessed the calcium association constants of other anionic substitutes for chloride: glutamate, aspartate and methylsulphonate (Table 3.1). In addition to the calcium chelating properties of the anions, changes in osmolarity to the buffers due to substitution with these anions was examined. The osmolarity of these chloride substitute buffers was determined by freezing point depression and compared with standard Hanks buffer of 152 mM Cl^-.

Table 3.1: Association constants for the Ca^{2+} ligand salts. Data presented as means ± S.D.

Anion	K_{a1} (L M^{-1}) Using $[L^-]_{tot}$	K_{a2} (L M^{-1})	K_a (L M^{-1}) Using $[L^-]_f$	n
Gluconate	17.2±1.85	= K_{a1}		4
Aspartate	11.8±1	0	12±1	3
Glutamate	8.2±4.1	0	8.4±4.2	5
Methylsulphonate	3.34±0.5	0	3.36±0.5	5

The organic anion with the least affinity for calcium was methyl-sulphonate (Table 3.1). With the exception of methyl-sulphonate, the osmolarity of other anionic buffers examined was lower than that of standard Hanks buffer (Table 3.2).

Table 3.2: Osmolarity of low chloride Hanks buffers determined by freezing point depression method.

	Buffer	Osmolarity (mOsm)
1	Normal Hanks Buffer (152 mM Cl^-)	301.00 ± 1.00
2	Sodium Gluconate Hanks Buffer (18 mM Cl^-)	291.00 ± 3.61
3	Monosodium glutamate Hanks Buffer (18 mM Cl^-)	273.67 ± 1.53
4	L-Aspartic acid sodium Hanks Buffer (18 mM Cl^-)	288.67 ± 1.15
5	Sodium Methyl-sulphonate (18 mM Cl^-)	299.00 ± 2.65

Based on the identification of methyl-sulphonate as the chloride substitute with the least association for extracellular calcium and being isosmotic with standard Hanks chloride at ~300 mOsm, we investigated the effect of changes in $[Cl^-]_o$ by methyl-sulphonate substitution on the activity of voltage-gated Ca^{2+} channels and $[Ca^{2+}]_i$. Reduction of extracellular chloride by substitution with methyl-sulphonate had no effect on $[Ca^{2+}]_i$ in VIS-WFAs (Figure 3.13).

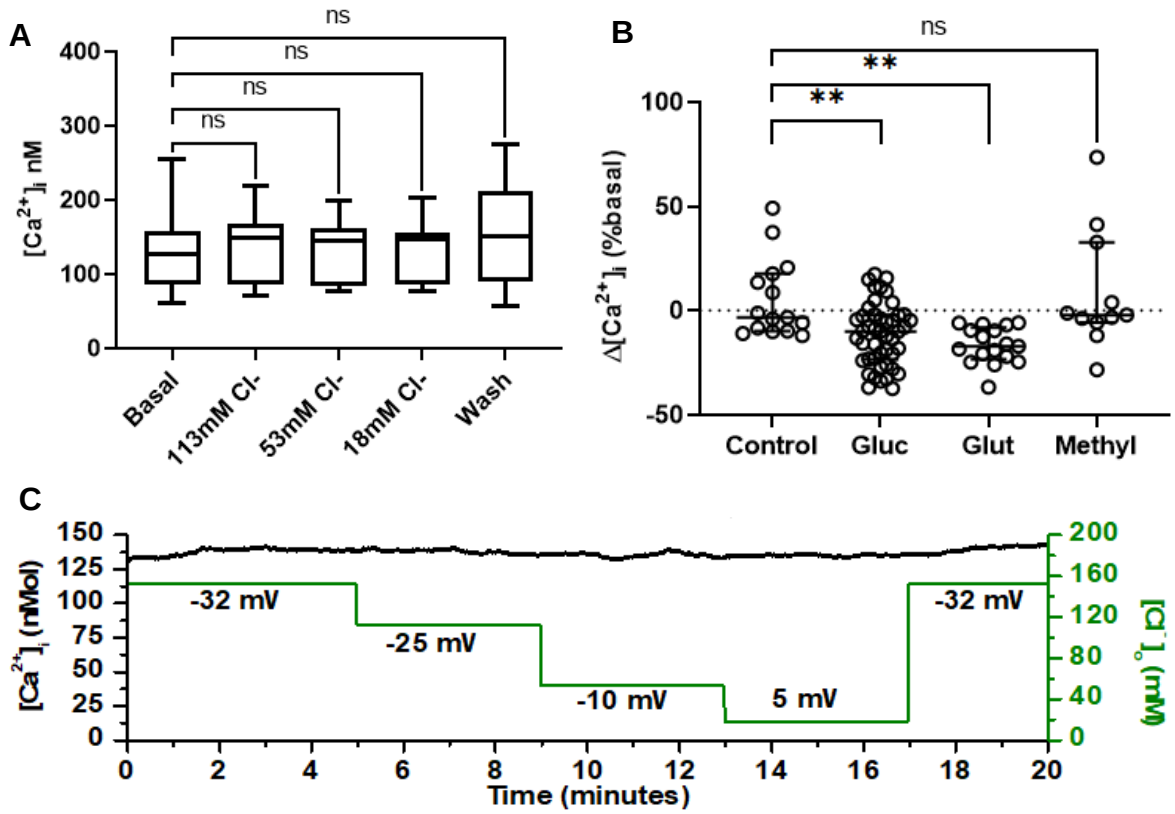

Figure 3.13: Methylsulphonate does not decrease intracellular $[Ca^{2+}]$ of white fat adipocytes.

A: $[Ca^{2+}]_i$ under the conditions shown in C. Basal and wash are 152 mM $[Cl^-]_o$ (n = 16, f = 3, i = 5). Statistical inference by Friedman with Dunn's multiple comparison tests. **B:** Change in $[Ca^{2+}]_i$, $\Delta[Ca^{2+}]_i$, when 134 mM bath Cl^- is substituted with anion indicated. Control, no substitution (n = 15); Gluc, gluconate (n = 46); Glut, glutamate (n = 17); methyl, methylsulphonate (n = 11). Statistical inference One-way ANOVA with Holm-Sidak's multiple comparisons tests. **C:** Mean intracellular Ca^{2+} for 4 adipocytes (black line) in response to equimolar replacement of bath $[Cl^-]_o$, (green line), with methylsulphonate. V_m values (in mV) are predicted.

3.4.3 High extracellular KCl to voltage regulate L-type calcium channels in WFAs

As high KCl applied extracellularly has previously been used to probe for the presence of Ca_V channels in different cell types (Yaguchi and Nishizaki, 2010), including adipocytes (Gaur et al., 1996), we assessed the effect of 50 mM KCl on Ca^{2+} influx in VIS-WFAs. To allow comparison to previous adipocyte work, 50 mM bath KCl was obtained by direct addition of 44.4 mM KCl to standard Hanks buffer without osmotic correction. We also investigated the effect of Bay-K8644, an L-type calcium channel agonist (Hirasawa et al., 1998), on calcium influx. The effects of Bay-K8644 was compared to that of oxytocin, a known GPCR agonist that mobilizes calcium from intracellular endoplasmic reticulum stores in this cell type (Schwartz et al., 1991).

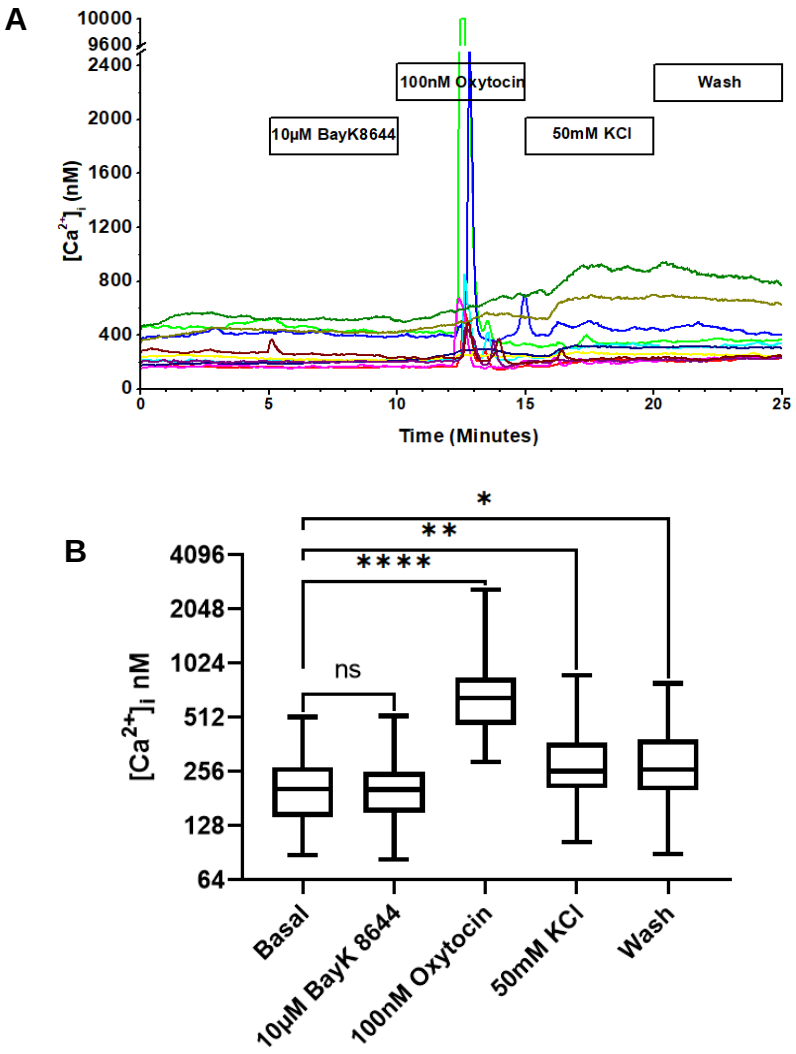

Figure 3.14: Effect of 10µM Bay-K8644, 100nM oxytocin and 50mM KCl on $[Ca^{2+}]_i$ in CD1 male mouse VIS-WFAs.

All $[Ca^{2+}]_i$ measurements were made after 5 minutes for each change in bath composition. **A.** Time course measurement of $[Ca^{2+}]_i$ for 11 adipocytes within a single field of view in response to 10 µM Bay K8644, 100 nM oxytocin and 50 mM KCl. **B.** No effect of 10 µM BayK 8644 on $[Ca^{2+}]_i$ was observed. 50 mM KCl elicited a 37.82 % increase in $[Ca^{2+}]_i$ from basal levels (n = 26, f = 6, i = 4; ***p < 0.001, ns = non-significant; Friedman's test, Dunn's post hoc tes). Peak $[Ca^{2+}]_i$ levels are reported for oxytocin while steady-state $[Ca^{2+}]_i$ levels are reported for all other conditions.

Bay-K8644 had no effect on $[Ca^{2+}]_i$. In contrast, 50 mM KCl caused a sustained increase of 25.40 % (6.954 - 58.54 %, 95% C.I., $p < 0.01$, Friedman's test) in $[Ca^{2+}]_i$ from basal levels (Figure 3.14). The intracellular calcium response of the adipocytes to oxytocin was seen usually within a few minutes in responsive cells.

Most cells showed a rapid transient increase in intracellular calcium, which was several magnitudes higher than basal levels, followed by return to near-basal calcium levels. In a few cells, the initial calcium transient was followed by oscillations which persisted even after oxytocin was removed (Figure 3.14A).

The experimental design was slightly modified to prevent carryover of cell responses to an initial compound on subsequent interventions. The effect of Bay-K8644 on $[Ca^{2+}]_i$ of WFAs was reassessed and compared to that of oxytocin. Additionally, the intracellular calcium response of the adipocytes to FPL 64176, an $Ca_V1.x$ channel agonist with a distinct mechanism of enhancement of macroscopic L-type currents from Bay-K8644 (Tavalin et al., 2004), was also examined.

Unexpectedly, there was no effect of either Bay-K8644 or FPL 64176 on $[Ca^{2+}]_i$ in CD1 mice WFAs (Figure 3.15).

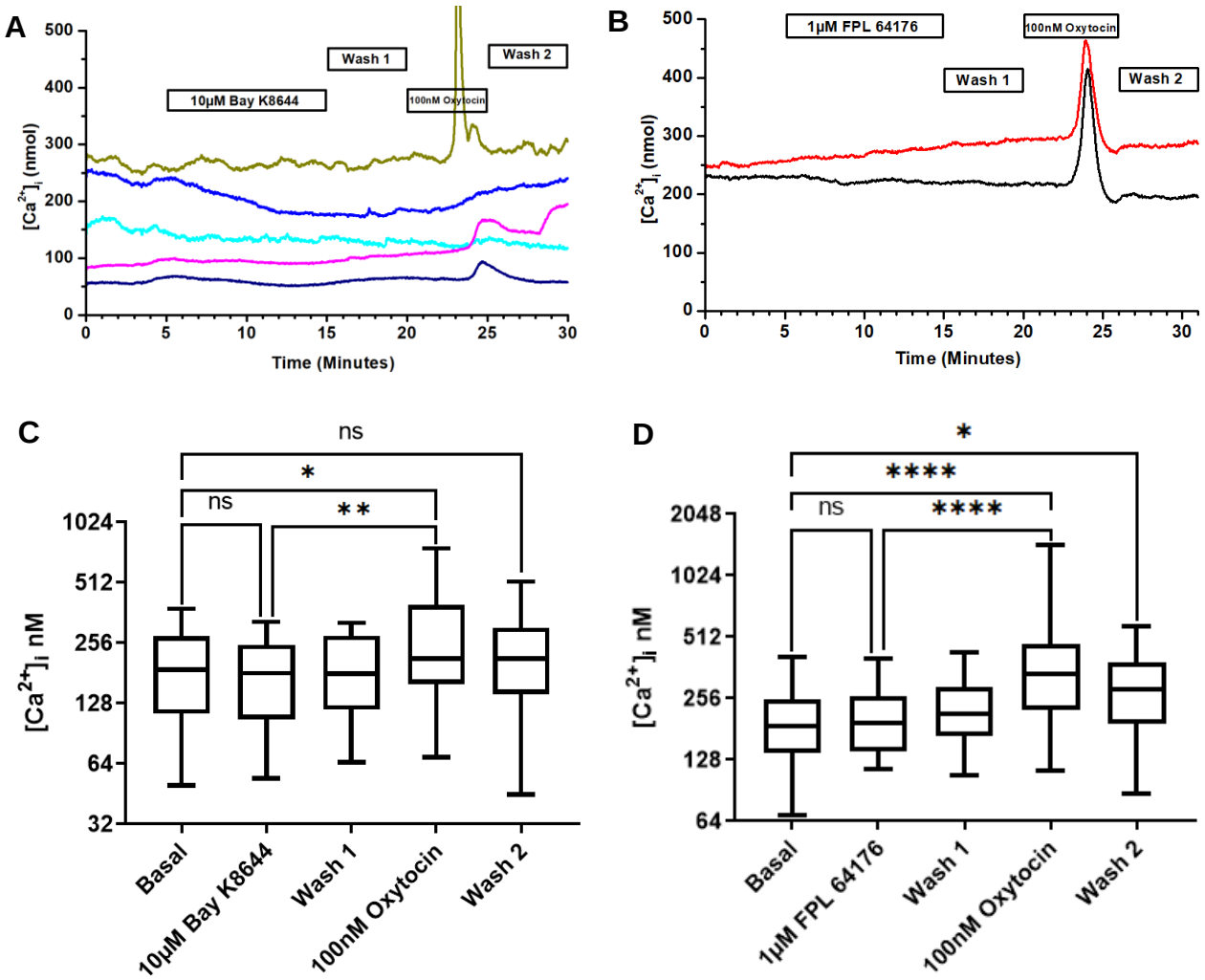

Figure 3.15: Effect of 10 μM Bay K8644 on $[Ca^{2+}]_i$ in CD1 male mouse VIS-WFAs.

Time course measurement of $[Ca^{2+}]_i$ for

(A) 5 adipocytes within a single field of view in response to 10 μM Bay K8644,

(B) 2 adipocytes within a single field of view in response to 1 μM FPL 64176.

(C) Bay K8644 had no effect on $[Ca^{2+}]_i$ compared to basal values, (n = 12, f = 7, i = 4; Data given as 2.5 – 97.5% percentile, line at median; *p < 0.05, **p < 0.01, ns = non-significant; Friedman's test, Dunn's post hoc test).

(D) FPL 64176 had no effect on $[Ca^{2+}]_i$ compared to basal values (n = 17, f = 10, i = 8; *p < 0.05, ****p < 0.0001, ns = non-significant; Friedman's test, Dunn's post hoc test). Peak $[Ca^{2+}]_i$ levels are reported for oxytocin while steady-state $[Ca^{2+}]_i$ levels are reported for all other conditions in both (C) and (D).

Going further, I investigated to what extent the ability of 50 mM KCl to increase $[Ca^{2+}]_i$ was due to the increase in osmolarity by comparison with the effect of addition of equimolar NaCl. On addition of 44.4 mM NaCl (eq. NaCl) to the bath, an increase of 18.02 % (7.07 % - 28.97 %, 95% C.I., $p < 0.05$) in $[Ca^{2+}]_i$ was observed, though not significant from basal (Figure 3.16A and B). Following exposure to 50 mM $[K^+]_o$, the increase in $[Ca^{2+}]_i$ did not return to the previous basal calcium level and attained a new baseline. The magnitude of intracellular calcium increase in cells responsive to 50 mM $[K^+]_o$ (by addition) was negatively correlated (Spearman r = -0.50, p = 0.0207, n=21) with basal calcium levels (Figure 3.16C). Hence, adipocytes with the lower basal calcium levels showed a higher $\Delta[Ca^{2+}]_i$ when exposed to 50 mM $[K^+]_o$ (by addition). The proportion of the assessed adipocyte population which was positively responsive to high $[K^+]_o$ (by addition) was 63 %. Conversely, eq. NaCl was without effect on the mean $[Ca^{2+}]_i$ (Figure 3.16B).

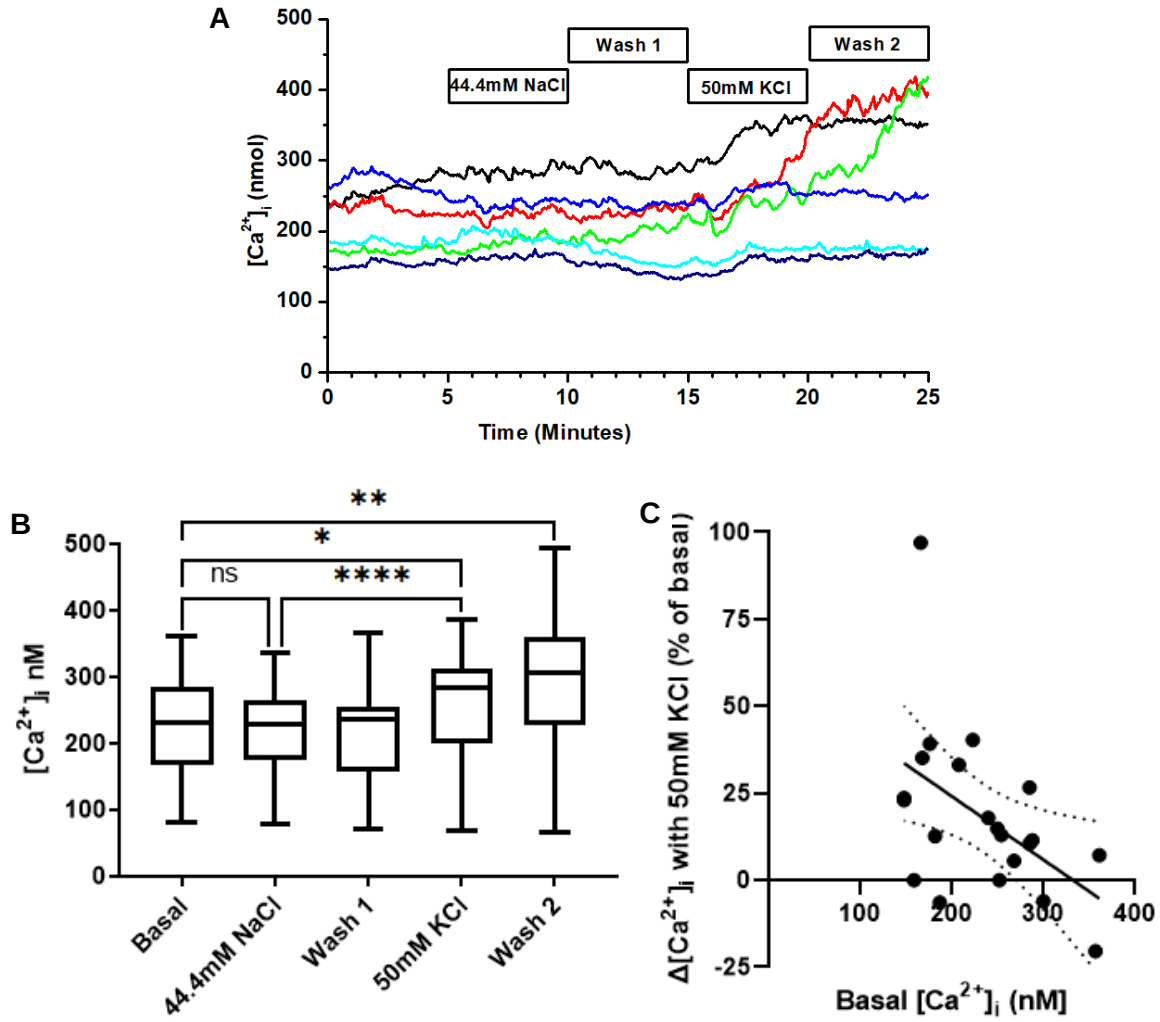

Figure 3.16: Effect of 50 mM $[K^+]_o$ (by addition) and eq. NaCl as ionic control on $[Ca^{2+}]_i$ in CD1 male mouse VIS-WFAs.

A. Time course measurement of $[Ca^{2+}]_i$ for 6 adipocytes within a single field of view in response to 50 mM $[K^+]_o$ (by addition) and equimolar NaCl as osmotic control. **B.** 50 mM $[K^+]_o$ (by addition) increased $[Ca^{2+}]_i$, its osmotic control had no effect, (n = 21, f = 6, i = 3; Data shown as 2.5 – 97.5% percentile, midline at median; *p < 0.05, **p < 0.01, ****p < 0.0001, ns = non-significant; RM one-way ANOVA, Sidak's post hoc test). **C.** Scatter plot of percentage change in $[Ca^{2+}]_i$ (% $\Delta[Ca^{2+}]_i$) from basal due to 50 mM $[K^+]_o$ (by addition) versus basal intracellular calcium for data shown in B, -ve correlation, n = 21. Solid lines are drawn by linear regression with slope of -0.18 ± 0.07%/nM ($P < 0.023$). Dotted lines are 95% C.I. for the fit.

In order to determine the $\Delta[Ca^{2+}]_i$ to high $[K^+]_o$ without the confounding effect of elevated osmolarity, ionic substitution was used. The effect of NaCl removal was first determined by substitution of 44.4 mM NaCl with the non-permeant N-

methyl-D-glucamine chloride (NMDG-Cl). This was then followed by substitution of the NMDG-Cl with K^+ (Figure 3.17).

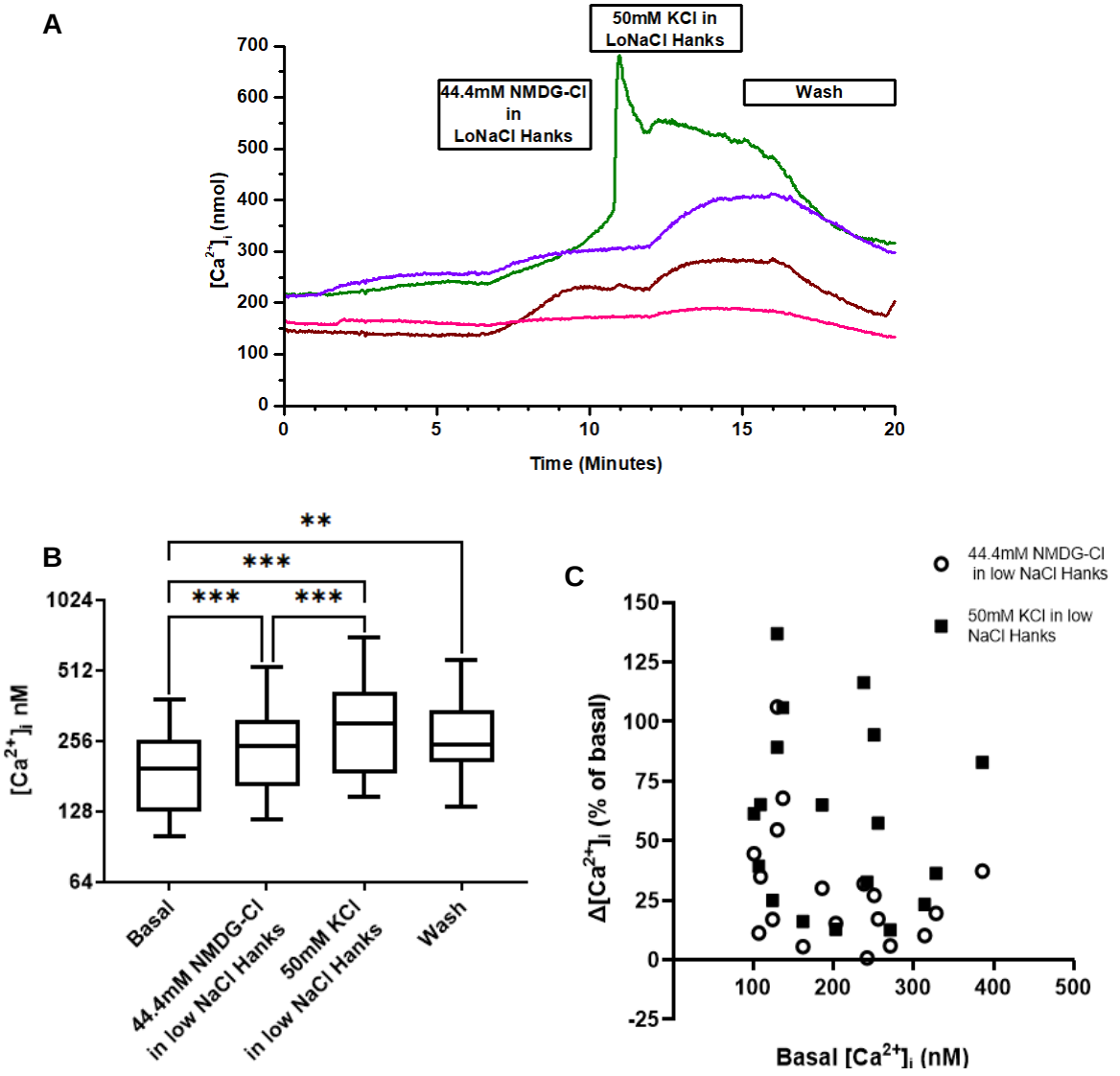

Figure 3.17: NaCl control to determine the effect of 50 mM $[K^+]_o$ (by substitution) on $[Ca^{2+}]_i$ in CD1 male mouse VIS-WFAs.

A. Time course measurement of $[Ca^{2+}]_i$ for 4 adipocytes within a single field of view in response to 50 mM KCl in low NaCl conditions. **B.** Reduction of eNaCl from 138 mM to 94 mM elicited an increase in $[Ca^{2+}]_i$ from basal. 50 mM $[K^+]_o$ (by substitution) induced a further increase in $[Ca^{2+}]_i$ from the low NaCl/NMDG-Cl buffer, (n = 21, f = 7, i = 3; Data shown as 2.5 – 97.5 percentile, midline at median; **p < 0.01, ***p < 0.001; Friedman's test, Dunn's post hoc test). **C.** Scatter plot of % $\Delta[Ca^{2+}]_i$ from basal due to low NaCl/NMDG-Cl (Spearman r = -0.31, p = 0.26, n = 18) and 50 mM $[K^+]_o$ (by substitution) (Spearman r = -0.20, p = 0.41, n = 18) versus basal calcium for data shown in B, no correlation.

Consistent with previous observations (Pepperell et al., 1999), a 44.4 mM reduction in extracellular NaCl from 138 mM to 93.6 mM, by substitution with equimolar NMDG-Cl significantly increased the mean $[Ca^{2+}]_i$ by 23.30% (11.21 % - 37.31 %, 95% C.I., ***p < 0.001; Friedman's test). A further increase of 22.42 % (11.64 % - 31.56 %, 95% C.I., ***p < 0.001; Friedman's test) in $[Ca^{2+}]_i$ was observed on sequential substitution with $[K^+]_o$ (50 mM). There was no correlation (Spearman r = -0.20, p = 0.41, n = 18) between basal $[Ca^{2+}]_i$ and percentage $\Delta[Ca^{2+}]_i$ due to 50mM $[K^+]_o$ (by substitution) (Figures 3.17C). In addition, there was no correlation (Spearman r = -0.31, p = 0.20, n = 18) between basal $[Ca^{2+}]_i$ and low NaCl/NMDG-Cl induced calcium influx in WFAs (Figures 3.17C).

To confirm that the $\Delta[Ca^{2+}]$ observed in response to 50 mM $[K^+]_o$ (by addition) was due to extracellular calcium entry, VIS-WFAs were exposed to 50 mM $[K^+]_o$ (by addition) in the absence of extracellular calcium. The adipocytes were first exposed to calcium free buffer (made by substitution of bath $CaCl_2$ with an equivalent concentration of $MgCl_2$) to establish the intracellular calcium response in the prevailing condition, before the effect of extracellularly applied 50 mM KCl (by addition) in calcium free Hanks was determined.

Removal of extracellular calcium blocked the effect of 50 mM $[K^+]_o$ (by addition) on $\Delta[Ca^{2+}]_i$. Initial exposure of the adipocytes to calcium free conditions caused a 38.78 % (-51.70 to 20.06 %, 95% C.I., *p < 0.05) decline in $[Ca^{2+}]_i$ from basal levels (Figure 3.18A and B). Lowered $[Ca^{2+}]_i$ was maintained when the adipocytes were stimulated by high KCl in calcium free buffer. Reperfusion of standard Hanks resulted in the recovery of the cells from the low $[Ca^{2+}]_i$.

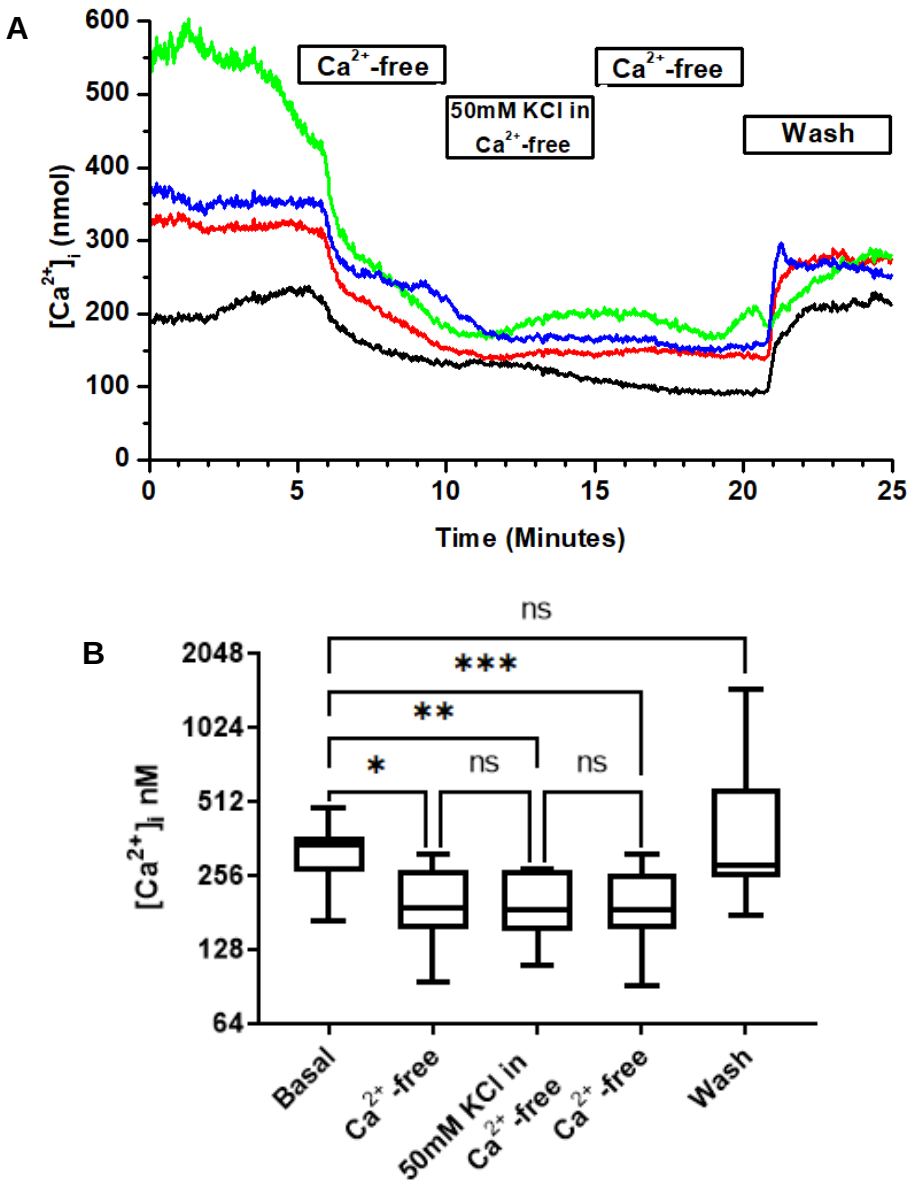

Figure 3.18: Determination of 50 mM KCl addition effect in Ca^{2+}-free Hanks on $[Ca^{2+}]_i$ in CD1 male mouse VIS-WFAs.

A. Time course measurement of $[Ca^{2+}]_i$ for 4 adipocytes within a single field of view in response to 50 mM KCl effect in Ca^{2+}-free Hanks. **B.** Substitution of bath calcium with magnesium blocked the 50 mM KCl (by addition) induced increase in $[Ca^{2+}]_i$, (n = 11, f = 5, i = 3; Data = 2.5 – 97.5 percentile, line at median; ***p < 0.001, **p < 0.01, *p < 0.05, ns = non-significant; Friedman's test, Dunn's post hoc test).

To determine if the $\Delta[Ca^{2+}]_i$ induced by high $[K^+]_o$ (by addition) was sensitive to the L-type calcium-channel antagonist, verapamil was tested (Feng et al., 2018).

Perifusion of 20μM verapamil blocked the $\Delta[Ca^{2+}]_i$ induced by high $[K^+]_o$ (by addition) (Figure 3.19B). Although different adipocytes within the same population showed varying sensitivities to verapamil (by addition) (Figure 3.19A), there was no difference in the $[Ca^{2+}]_i$ between basal conditions and on perfusion of the 50 mM $[K^+]_o$ (by addition) buffer in verapamil. 20μM verapamil also decreased the proportion of cells responsive to 50 mM $[K^+]_o$ (by addition) from 63 % to 25 % (Figure 3.20B).

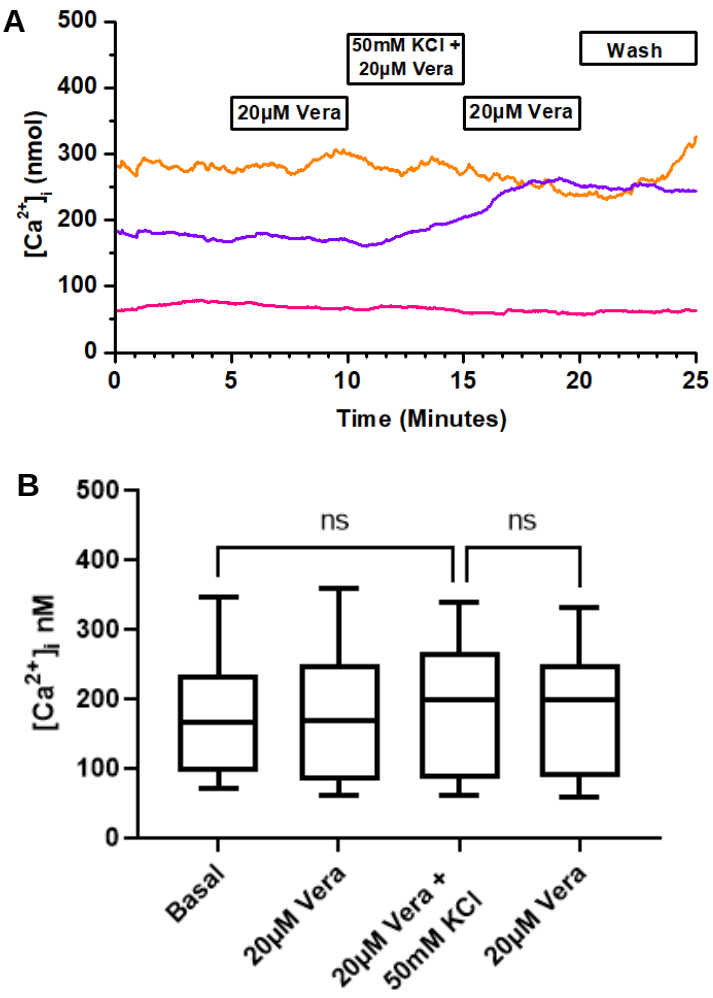

Figure 3.19: Effect of 20μM Verapamil on 50 mM $[K^+]_o$ (by addition) induced increase in $[Ca^{2+}]_i$ in CD1 male mouse VIS-WFAs.

A. Time course measurement of $[Ca^{2+}]_i$ for 3 adipocytes within a single field of view in response to 20 μM verapamil inhibition of 50 mM KCl.

B. Perfusion of 20 μM verapamil blocked the intracellular calcium increase due to 50 mM $[K^+]_o$ (by addition) (n = 20, f = 5, i = 3; Data = 2.5 – 97.5 percentile, mid line at median; ns = non-significant; RM one-way ANOVA, Dunnett's post hoc test).

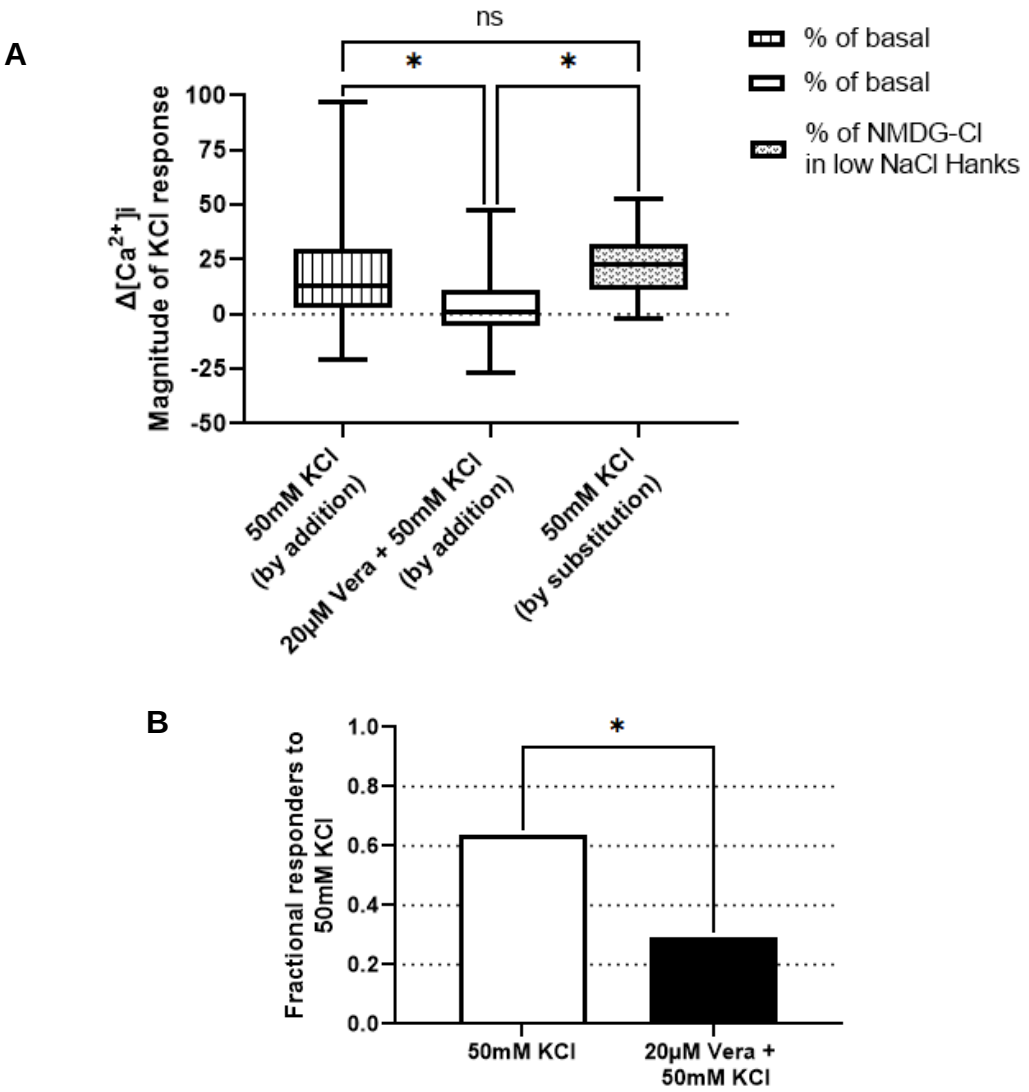

Figure 3.20: Comparison of the magnitude of WFA response and proportion of responders to 50 mM KCl under various conditions.

A. Perfusion of 20 μM verapamil inhibited high KCl induced calcium influx and caused a decline in the $\Delta[Ca^{2+}]$ induced by high $[K^+]$**.** (Data shown = 2.5 – 97.5 percentile, line at median; *$p < 0.05$, ns = non-significant; RM one-way ANOVA, Holm Sidak's post hoc test). **B.** 20 μM verapamil decreased the fractional response of WFAs to 50mM KCl (by addition) by over 50%; (ns = non-significant; Unpaired student T-test).

To determine if sodium calcium exchange (NCX) was involved in the mechanism of the $\Delta[Ca^{2+}]_i$ induced by high $[K^+]$, inhibition to the selective calcium-influx mode NCX exchanger inhibitor, KB-R7943, (Amran et al., 2003) was investigated.

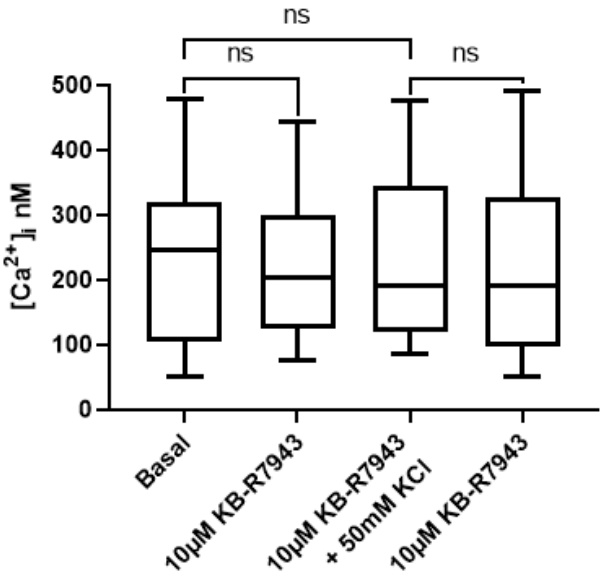

Figure 3.21: Effect of 10 μM KB-R7943 on 50 mM $[K^+]_o$ (by addition) induced increase in $[Ca^{2+}]_i$ in CD1 male mouse VIS-WFAs.

10 μM KB-R7943 blocked the 50 mM KCl (by addition) induced increase in $[Ca^{2+}]_i$ from basal levels (n = 13, f = 6, i = 3; Data shown as 2.5 – 97.5 percentile, mid line at median; ns = non-significant; Friedman's test, Dunn's post hoc test).

Although 10μM KB-R7943 had no effect on basal $[Ca^{2+}]_i$, it blocked the $\Delta[Ca^{2+}]_i$ induced by high $[K^+]$.

To investigate if volume regulatory processes were involved in the mechanisms of $\Delta[Ca^{2+}]_i$ induced by high $[K^+]$, the inhibitory effect of the swelling-activated ion channel blocker, DCPIB was examined. Volume regulatory anion channels (VRACs) are usually activated as a regulatory mechanism to mediate regulatory volume decrease in conditions of cell swelling. 10 μM DCPIB, a blocker for VRACs (Decher et al., 2001, Lv et al., 2019), had no effect on $[Ca^{2+}]_i$ induced by high $[K^+]$. VIS-WFAs showed a 19.49 % (4.25% - 34.74 %, 95% C.I., *$p < 0.05$; Holm-Sidak's test) mean increase in $[Ca^{2+}]_i$ induced by high $[K^+]$ in the presence of the VRAC blocker (Figure 3.22). There was no difference in the magnitude of $\Delta[Ca^{2+}]_i$ elicited

by 50 mM $[K^+]_o$ (by addition) alone or in the presence of DCPIB nor in the proportion of adipocyte responders (Figure 3.23).

In the presence of DCPIB, 50 mM $[K^+]_o$ (by addition) elicited a 19.49 % (4.25% - 34.74%, 95% C.I., *p < 0.05, Unpaired student T-test) in $[Ca^{2+}]_i$ from basal levels.

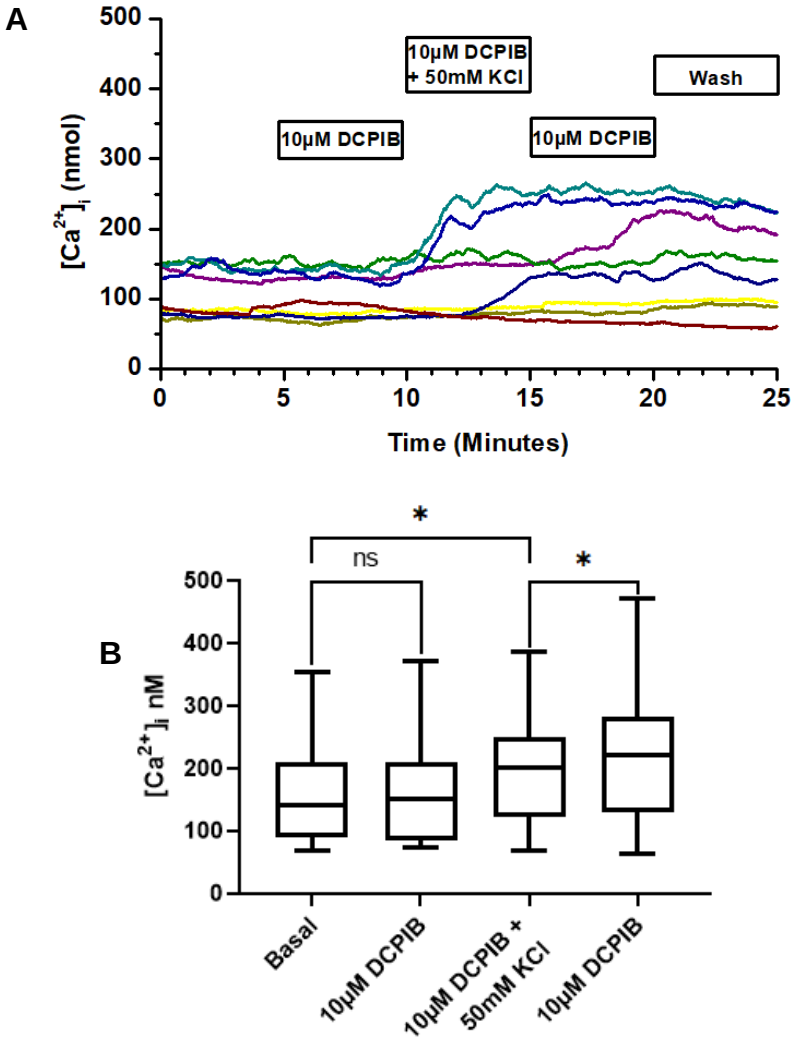

Figure 3.22: Effect of 10 μM DCPIB on 50 mM $[K^+]_o$ (by addition) induced increase in $[Ca^{2+}]_i$ in CD1 male mouse VIS-WFAs.

A. Time course measurement of $[Ca^{2+}]_i$ for 8 adipocytes within a single field of view in response to 10 μM DCPIB inhibition of 50 mM KCl.. **B.** 10 μM DCPIB had no effect on the 50 mM $[K^+]_o$ (by addition) induced increase in $[Ca^{2+}]_i$ from basal levels (n = 15, f = 4, i = 3; Data = 2.5 – 97.5 percentile, line at median; ns = non-significant, *p < 0.05; RM one-way ANOVA, Holm-Sidak's post hoc test).

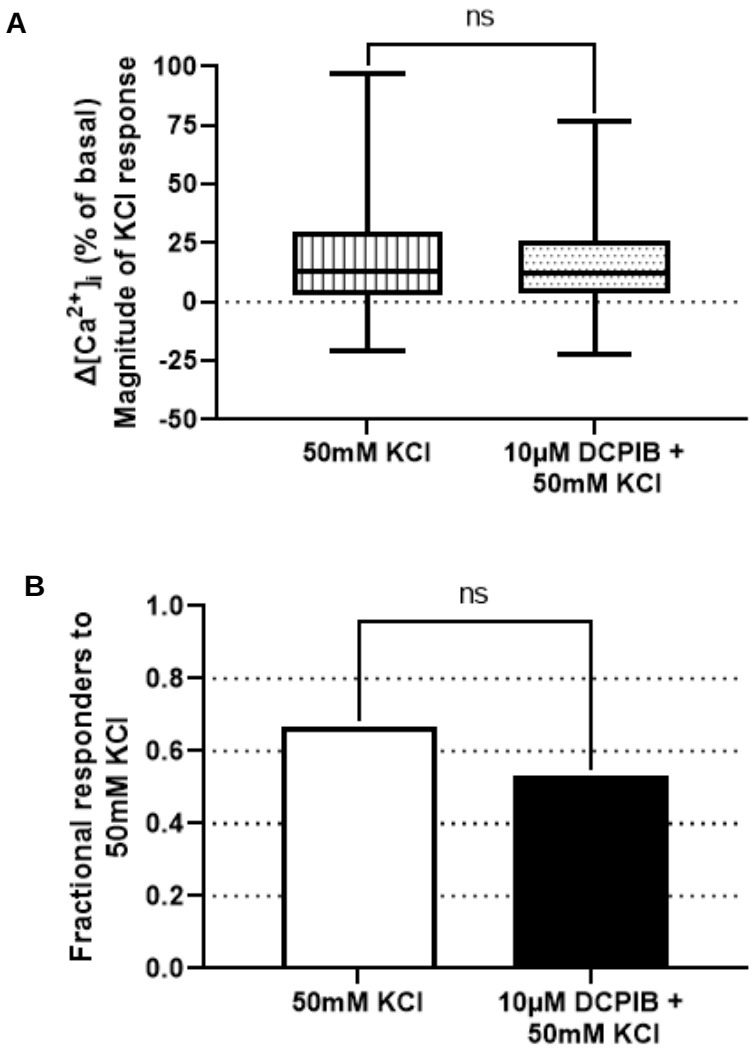

Figure 3.23: Comparison of the magnitude of WFA response and proportion of responders to 50 mM $[K^+]_o$ (by addition) in the presence and absence of 10 μM DCPIB

A. Perfusion of 10 μM DCPIB had no effect on the magnitude of intracellular calcium increase in response to 50 mM $[K^+]_o$ (by addition). In the presence of DCPIB, 50 mM $[K^+]_o$ (by addition) elicited a 19.49 % (4.25% - 34.74 %, 95% C.I., *$p < 0.05$, Unpaired student T-test) in $[Ca^{2+}]_i$ from basal levels. **B.** 10μM DCPIB had no effect on the fractional response of WFAs to 50 mM $[K^+]_o$ (by addition); (ns = non-significant; Unpaired student T-test).

3.4.4 Hormonal Regulation of WFA L-type calcium channels

Previous research have shown the requirement of white adipocytes for growth hormone in maintenance of their resting $[Ca^{2+}]_i$ (Schwartz et al., 1992). In addition, the mechanism of growth hormone stimulated increase of cytoplasmic calcium levels in adipocytes, has been suggested to involve its modulation of L-type Ca^{2+} channel activity (Gaur et al., 1996, Gaur et al., 1998). We assessed the effect of recombinant human growth human (rhGH) on calcium influx in VIS-WFAs, through plasma membrane calcium channels (PMCCs) (Figure 3.24).

Exposure of VIS-WFAs to 20 nM rhGH elicited a 14.17 % (7.166 - 20.51 %, 95% C.I., *$p < 0.05$; Turkey's test) increase in $[Ca^{2+}]_i$, from mean basal levels of 174.5±9.63 nM to 208.6±11.66 nM (Figure 3.24A and 3.24C). The rhGH induced calcium response was observed at different times in individual adipocytes, and was usually after several minutes delay, which was followed by a gradual rise in intracellular calcium which was sustained. Reperfusion of the standard bath solution led to recovery of $[Ca^{2+}]_i$ to basal levels. 0.4 % double distilled water, the solvent for rhGH, was without effect (Figure 3.24B). There was no correlation between basal calcium levels and rhGH induced increase in $[Ca^{2+}]_i$ in the adipocytes (Figure 3.24D).

To explore the source of calcium for the rhGH response, VIS-WFAs were exposed to growth hormone in the presence and absence of extracellular calcium, and its response compared to that of oxytocin, a hormone known to mobilize Ca^{2+} from intracellular stores (Gaur et al., 1996) (Figure 3.25).

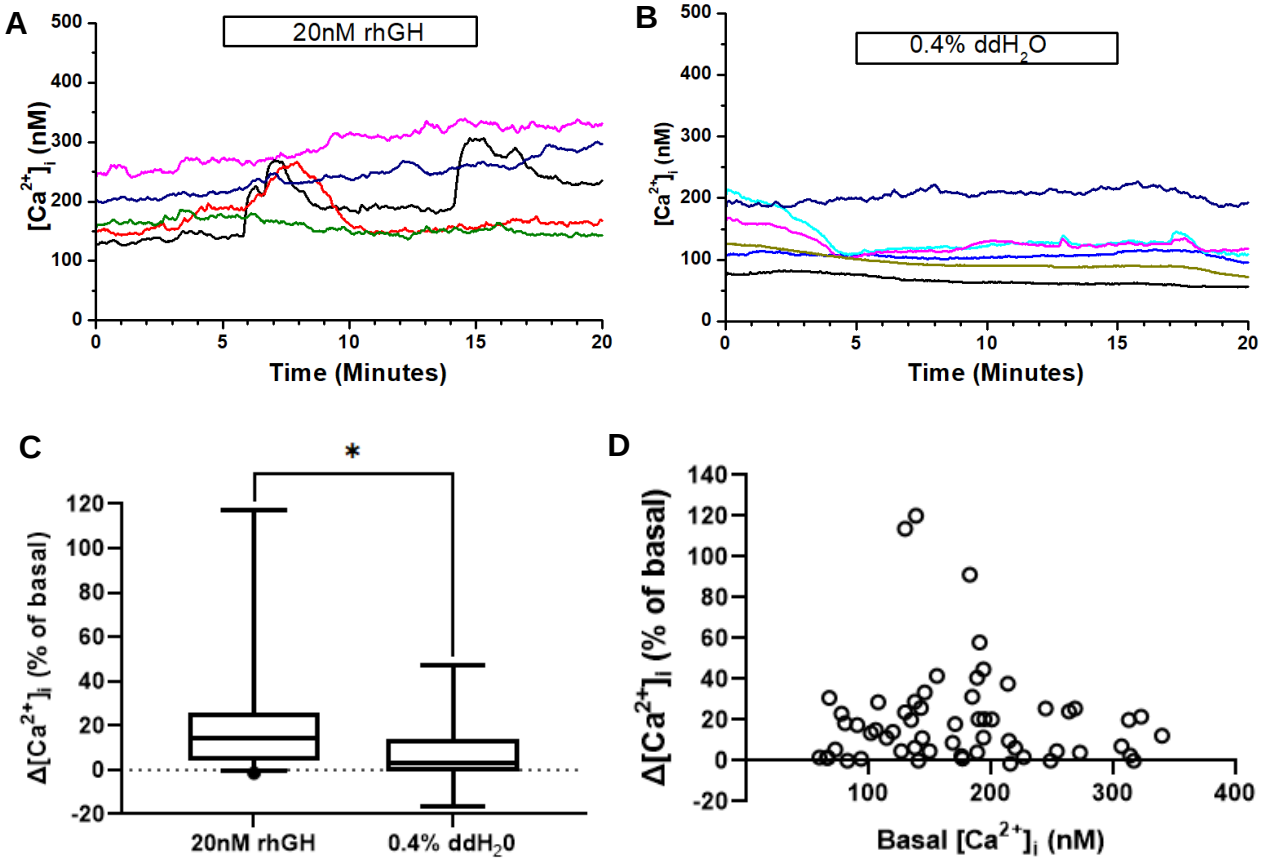

Figure 3.24: $[Ca^{2+}]_i$ response of white fat adipocytes to 20 nM rhGH.

A. Time course measurement of $[Ca^{2+}]_i$ for 5 adipocytes within a single field of view in response to 20 nM rhGH.

B: Time course measurement of $[Ca^{2+}]_i$ for 6 adipocytes within a single field of view in response to 0.4% (vol/vol) ddH_2O (solvent for rhGH).

C: Increase in $[Ca^{2+}]_i$ from basal levels due to rhGH, (n = 59, f = 12, i = 6). 0.4% double distilled water had no effect on basal calcium in white fat adipocytes, (n = 19, f = 8, i = 4); $p<0.05$, Mann-Whitney U test.

D. Scatter plot of % $\Delta[Ca^{2+}]_i$ from basal due to 20 nM rhGH (Spearman r = 0.0085, p = 0.94, n = 59) versus basal calcium, no correlation.

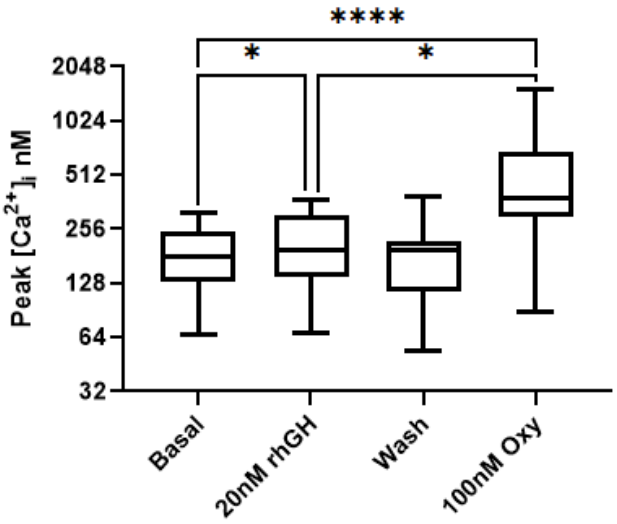

Figure 3.25: $[Ca^{2+}]_i$ response of VIS-WFAs to 20 nM rhGH in the presence of bath calcium, compared to oxytocin.

Comparison of $[Ca^{2+}]_i$ response of VIS-WFAs to 20 nM rhGH and 100 nM oxytocin in the presence of bath calcium. 100 nM oxytocin exerted a higher magnitude of response than did 20 nM rhGH (n = 18, f = 4; n = 3; Data = 2.5 – 97.5 percentile, line at median; *p < 0.05, ****p < 0.0001, Friedman's test, Dunn's post hoc test).

In the presence of bath calcium, the nature of intracellular calcium signalling due to 20nM rhGH was different from that observed with 100 nM oxytocin. Recombinant human growth hormone elicited a 9.32% (4.23 – 23.08 %, 95% C.I.; *p < 0.05, Friedman's test, Dunn's post hoc test) sustained calcium increase whereas, 100 nM oxytocin elicited a more rapid and transient calcium response of 161.9 % (26.12 – 244.2 %, 95% C.I.; ****p < 0.0001, Friedman's test, Dunn's post hoc test) (Figure 3.25).

Removal of extracellular calcium by equimolar substitution with magnesium chloride abolished the effect of rhGH (Figure 3.26A and C), whereas 100μM oxytocin was able to evoke a transient increase in intracellular calcium of 19.95 % (4.878 - 73.21 %, 95% C.I.; ****p < 0.0001, Friedman's test, Dunn's post hoc test) (Figure 3.26B and D) in calcium-free conditions.

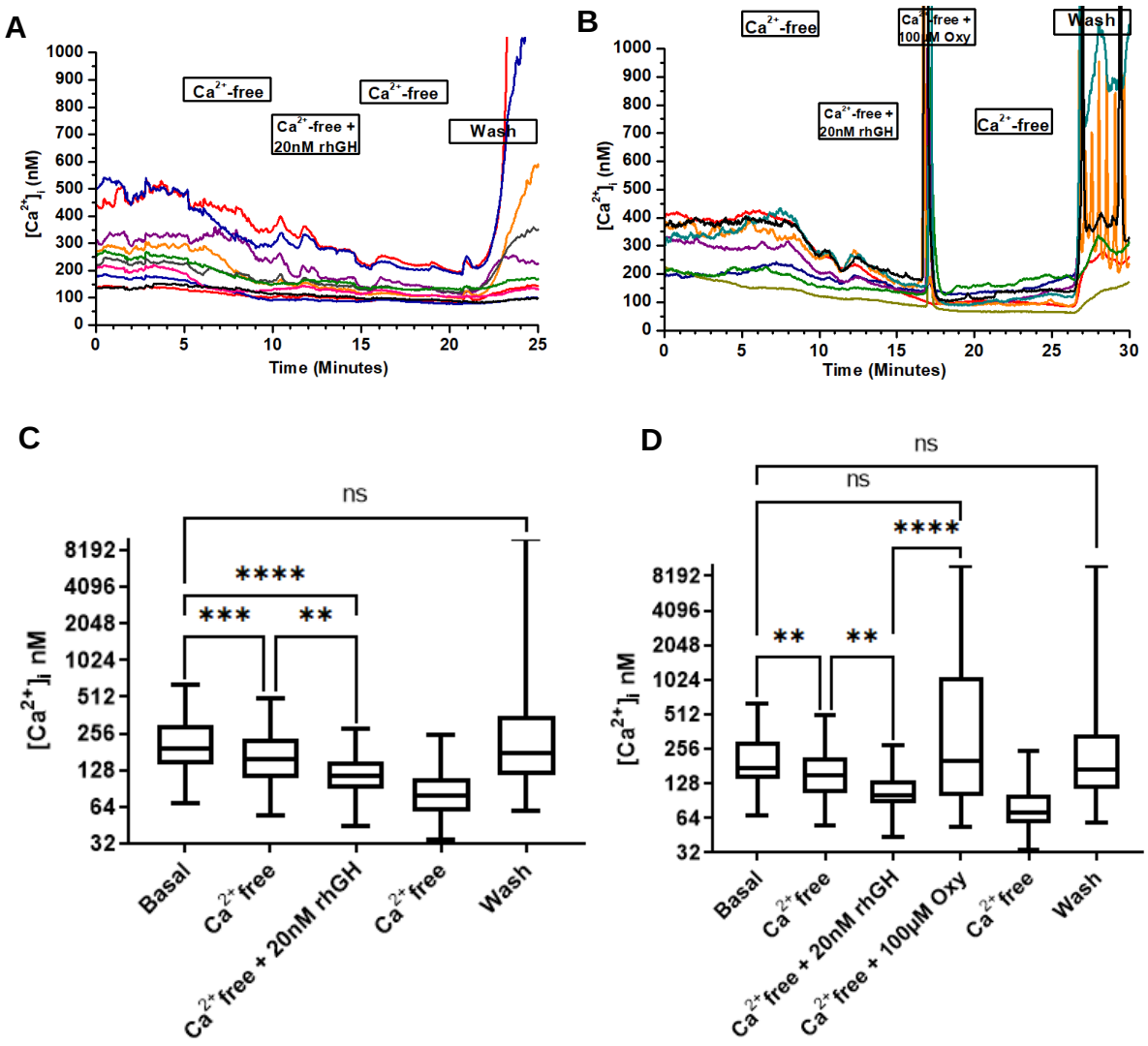

Figure 3.26: $[Ca^{2+}]_i$ response of white fat adipocytes to 20 nM rhGH and 100 μM oxytocin in calcium-free Hanks.

A: Time course measurement of $[Ca^{2+}]_i$ for 10 adipocytes within a single field of view in response to 20 nM rhGH in calcium-free medium.

B: Time course measurement of $[Ca^{2+}]_i$ for 8 adipocytes within a single field of view in response to 20 nM rhGH and then 100nM oxytocin in calcium-free medium.

C: Extracellular Ca^{2+} removal (Ca^{2+}-free) inhibits 20 nM rhGH induced $[Ca^{2+}]_i$ increase in white fat adipocytes (n = 71, f = 10, i = 4; Data shown as 2.5 – 97.5 percentile, midline at median; ns = non-significant; **p <0.01, ***p <0.001, ****p <0.0001, Friedman's test, Dunn's post hoc test).

D: Extracellular Ca^{2+} removal (Ca^{2+} -free) has no effect on intracellular calcium release by oxytocin in white fat adipocytes (n = 57, f = 9, i = 4; Data shown as 2.5 – 97.5 percentile, midline at median; ns = non-significant; **p <0.01, ****p <0.0001, Friedman's test, Dunn's post hoc test).

Next, to determine if L-type calcium channels were involved in the 20 nM rhGH response, the effect of verapamil was investigated (Feng et al., 2018). 20 μM Verapamil blocked the $\Delta[Ca^{2+}]_i$ elicited by 20 nM rhGH (Figure 3.27A and C). There was no difference (Friedman with Dunn's test, $p = 0.167$, $n = 21$) between basal $[Ca^{2+}]_i$ conditions and after perfusion with 20 nM rhGH in verapamil (Figure 3.27C). In contrast to growth hormone, in the presence of 20 μM verapamil, 100nM oxytocin still elicited a 104.6 % (1.76 – 292.3 %, 95% C.I., $p < 0.0001$, Friedman's test) increase in $[Ca^{2+}]_i$, (Figure 3.27D), similar to that seen without verapamil.

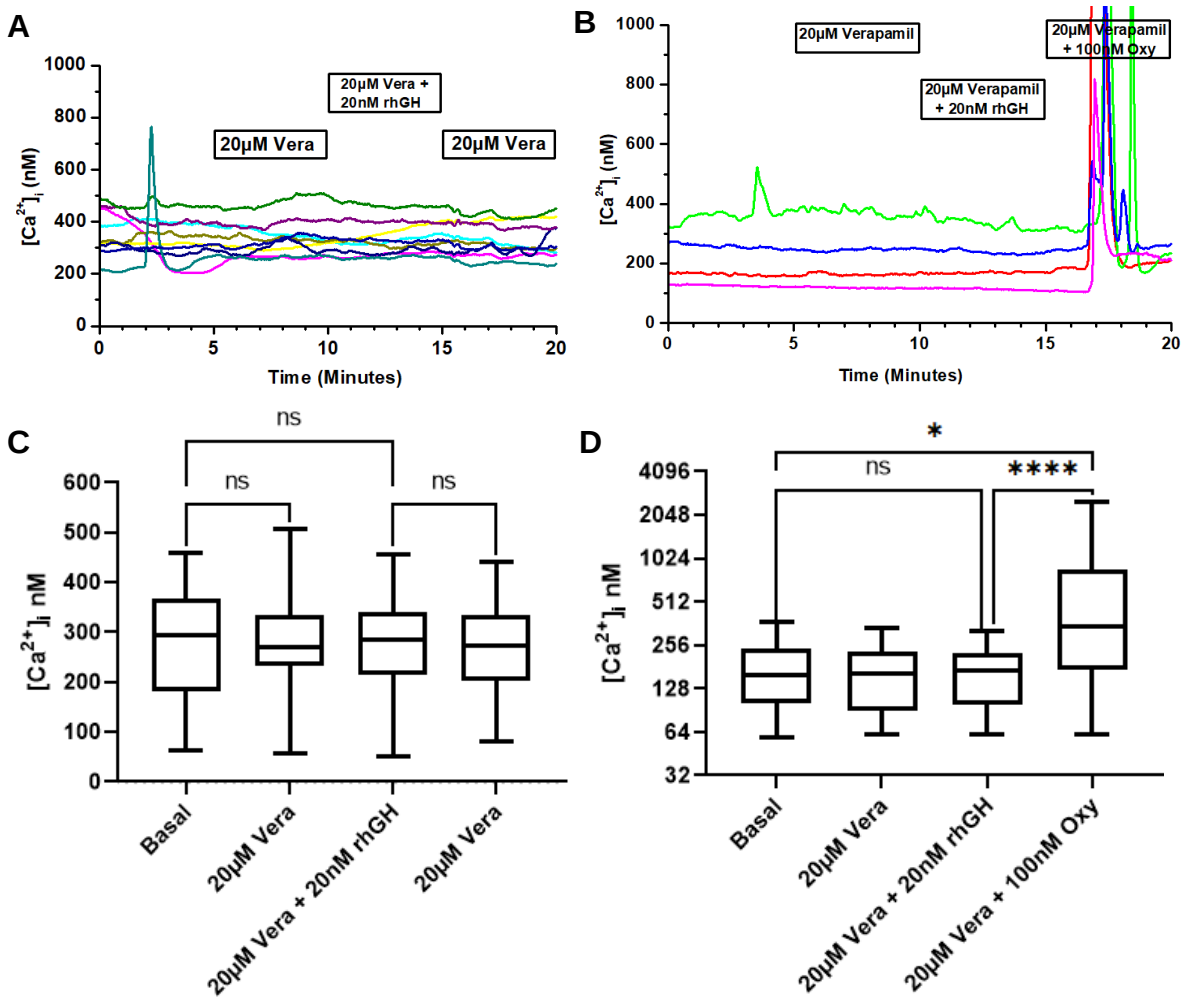

Figure 3.27: $[Ca^{2+}]_i$ response of white fat adipocytes to 20µM verapamil inhibition of 20nM rhGH and 100nM oxytocin.

A: Time course measurement of $[Ca^{2+}]_i$ for 9 adipocytes within a single field of view in response to 20µM verapamil inhibition of 20nM rhGH. **B:** Time course measurement of $[Ca^{2+}]_i$ for 4 adipocytes within a single field of view in response to 20 µM verapamil inhibition of 20 nM rhGH and 100nM oxytocin. **C:** Perfusion of 20 µM verapamil blocked the intracellular calcium increase due to 20 nM rhGH (n = 13, f = 4, i = 2; Data shown as 2.5 – 97.5 percentile, midline at median; ns = non-significant; RM one-way ANOVA, Sidak's post hoc test). **D:** 20 µM verapamil had no effect on intracellular calcium release elicited by 100 nM oxytocin, but effectively blocked 20 nM rhGH induced calcium influx (n = 21, f = 7, i = 4; Data shown as 2.5 – 97.5 percentile, midline at median; ns = non-significant; **p <0.05, ****p <0.0001, Friedman's test, Dunn's post hoc test).

Parathyroid hormone (PTH) has also been reported in the literature to regulate L-type calcium channel activity in rat VIS-WFA, resulting in increased intracellular calcium levels (Ni et al., 1994, Hirasawa et al., 1998, Prideaux et al., 2015). To see if VIS-WFAs from mouse also respond to PTH, 100nM PTH (PTH 1-34) was applied. Response of the adipocytes to the truncated 1-34 isoform of the hormone was compared to the full length peptide (PTH 1-84) (Figure 3.28).

100nM PTH(1-34) had no effect on basal $[Ca^{2+}]_i$ of CD1 mice VIS-WFAs. In contrast, the adipocytes responded to the full length PTH(1-84) by a 12.96 % (9.88 – 21.21 %, 95% C.I., $p < 0.05$, Friedman's test) increase in $[Ca^{2+}]_i$ from basal levels. The $\Delta[Ca^{2+}]_i$ from basal levels due to PTH(1-84) was significantly higher than that elicited by PTH(1-34) (Figure 3.28C), with 67 % of the adipocyte population observed to be sensitive to the full length peptide. Although the majority of the adipocytes showed no response to 100nM PTH(1-34), a small percentage of these cells (32 %) were sensitive to PTH(1-34) induced increase in intracellular calcium concentrations (Figure 3.28D), with both transient and sustained increases observed (Figure 3.28A).

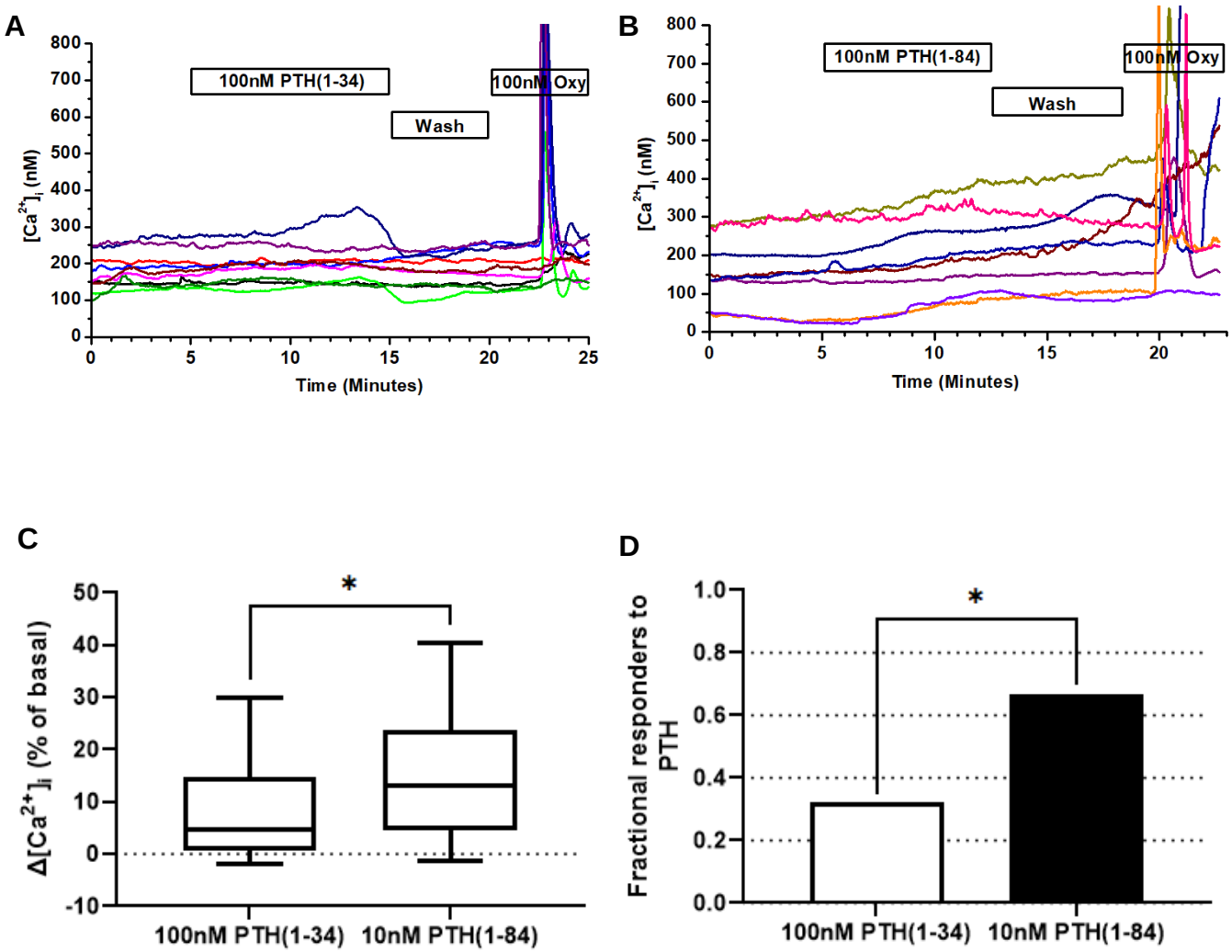

Figure 3.28: Intracellular calcium response of CD1 male mouse to 100nM PTH.

A: Time course measurement of $[Ca^{2+}]_i$ for 9 adipocytes within a single field of view for which majority failed to respond to 100nM PTH(1-34).

B: Time course measurement of $[Ca^{2+}]_i$ for 8 adipocytes within a single field of view in response to 100nM PTH(1-84).

C: Increase in $[Ca^{2+}]_i$ from basal levels due to PTH(1-84), (n = 21, f = 7, i = 4). PTH(1-34) had no effect on basal calcium in white fat adipocytes, (n = 25, f = 4, i = 3); $p<0.05$, Mann-Whitney U test.

D: The fractional response of the adipocyte population to PTH(1-34) was 32 % , while 67 % responded to PTH(1-84); $p<0.05$, Mann-Whitney U test.

3.5. Discussion

3.5.1 Functional L-Type Calcium Channels Exist in WFAs

This study has shown the functional presence of Ca_V channels in VIS-WFAs by the pharmacology of the adipocyte response to antagonists of the channel. The sustained increase in intracellular calcium levels and sensitivity of the calcium influx to inhibition by 20 μM verapamil, an L-type calcium channel antagonist (Feng et al., 2018), both suggest entry of free calcium into the adipocyte through L-type calcium channels. The degree of increase in intracellular calcium due to high extracellular calcium perfusion as observed in this study (9.4 %; 7 – 13.5 %, 95% C.I.; $P < 0.0001$), is similar to previous observations in rats (9 %; 4 – 16 %, 95% C.I.; $P < 0.0001$) (Fedorenko, 2019). However, larger effects of high extracellular calcium on intracellular calcium concentration (up to 132±36% increase in intracellular calcium from basal levels) have been reported (Hardy et al., 1992). Since the dataset in this study (85 cells, 18 replicate experiments from 9 animals) is larger than that of Hardy et al. (1992) which examined only 8 cells from 1 animal, and are comparable to previous reports, it lends more credence to the data presented here as being indicative of the true situation. In addition, increased variability introduced from day-to-day differences in adipocyte preparations, effect of animal health, time of adipocyte preparation and other factors on channel density, could have contributed to the differences in the intracellular calcium response of adipocytes to elevation of extracellular calcium in this study compared to other studies. 20 μM verapamil inhibited the intracellular calcium response of VIS-WFAs from 9.4 % to 2.4 %.

3.5.2 WFA L-type Channels Are Not Sensitive to Voltage Regulation

Experimental modification of extracellular chloride concentration was expected to produce changes in the adipocyte resting membrane potential which would affect

calcium entry through voltage-gated calcium influx pathways in WFAs. Equimolar substitution of sodium chloride with sodium gluconate and sodium glutamate both led to a decrease in $[Ca^{2+}]_i$ levels in CD1 male mouse VIS-WFAs. Initially, with sodium gluconate substitution, the observed decrease in intracellular calcium was due to Ca^{2+} chelation by gluconate, as the ability of gluconate to chelate free calcium has been identified (Phadungath and Metzger, 2011, Vavrusova et al., 2013). Supplementation of the free calcium of the sodium gluconate buffers to a similar level as the basal Hanks solution with normal chloride levels prevented the observed decrease in $[Ca^{2+}]_i$ levels in these cells, but no increases in intracellular calcium was seen. These observations suggest that although functional L-type calcium channels may exist in WFAs, they are not sensitive to membrane potential depolarization by extracellular chloride removal.

As the RMP of WFAs is controlled mainly by chloride ions (Bentley et al., 2014), extracellular chloride removal was expected to cause a shift in the adipocyte membrane potential to a more depolarized state, leading to further opening of Ca_V channels and increased calcium entry in the adipocyte. However, this was not the case. Sequential replacement of the extracellular chloride concentration with methyl-sulphonate had no effect on the intracellular calcium concentration. In fact, it seemed that organic anion substitution of bath chloride directly inhibited $Ca_V1.x$ channel calcium influx in WFAs (Akaniro-Ejim and Smith, 2021), similar to observations in other cell types by previous studies (Garcia et al., 1997, Thoreson et al., 2000, Babai et al., 2010).

The existence of L-type like calcium channels that are not gated by voltage in non-excitable cells have been demonstrated in other cell types. Grafton et al. (2003) has shown the existence of a truncated $Ca_V1.2$ α_1 channel functionally expressed in the plasma membrane of B lymphocytes. In their study, extracellularly applied

50 mM KCl, which was expected to depolarize B-cells from the L3055 BL line had no effect on intracellular calcium entry, result like what I find in mouse WFA. The L3055 B-cell $Ca_v1.2$ channels were also sensitive to verapamil, nifedipine and diltiazem, well established L-type Ca^{2+} channel inhibitors, all of which blocked intracellular calcium entry. The molecular expression of the α_1 and β1 subunits of this channel in the L3055 B-cell was determined by RT-PCR/RNA sequencing and functional protein expression shown by western blotting. The molecular profile of these channels were shown to be closely related to that of L-type $Ca_v1.2$ channels (Grafton et al., 2003).

In another study, non-voltage-gated L-type Ca^{2+} channels, were detected on human T-cell plasma membrane (Stokes et al., 2004), a non-excitable cell similar to the white adipocyte. These non-voltage-gated L-type Ca^{2+} channels, which are important for activation of transcription factors necessary for subsequent human T-cells activation, were also sensitive to inhibition by classical L-type channel antagonists. Moreover, molecular expression of the human T-cell non-voltage-gated L-type Ca^{2+} channels was confirmed by reverse-transcription polymerase chain reaction (Stokes et al., 2004). In this study, molecular expression of the α_1 subunit of $Ca_v1.2$ channel was detected by western blotting in WFAs, with a large molecular weight of >250 kDa (see chapter 2). Although the physiological relevance of this large Ca_v protein in the adipocyte is yet unknown, it could play a role in the lack of effect of voltage manipulations on channel activity and intracellular calcium influx.

With regards to the observed decrease in intracellular calcium levels with glutamate anions, in addition to the observed calcium chelation properties of both gluconate and glutamate (Table 3.1), substitution with both anions could have resulted in an imbalance in osmotic pressure of the perfusion solutions, resulting

in a hypo-osmotic solution, as confirmed by our osmolarity measurement (Table 3.2). This imbalance in osmolarity between the intracellular and extracellular milieu may have created an osmotic pressure gradient on the cells, leading to increased influx of water into the cells (Lang, 2007). Consequently, a decrease in $[Ca^{2+}]_i$ due to dilution of the intracellular solute concentration and dye may have resulted. The osmotic imbalance caused by monosodium glutamate and gluconate could have also activated other coupled membrane transport processes, further contributing to the observed decrease in intracellular calcium levels. For instance, K^+-Cl^- cotransporters are sensitive to activation by cell swelling, which could also arise due to glutamate activation of non-selective cation channels (Lang, 2007). The K^+-Cl^- cotransporter 3 (KCC3) is expressed in adipose tissue (Garneau et al., 2017) and is sensitive to activation by cell swelling. The transport stoichiometry of KCC3 is $1K^+$:$1Cl^-$ and is outwardly directed (Garneau et al., 2017). The resultant decrease in intracellular K^+ concentration with osmotic swelling could increase the driving force for the Na^+,K^+-ATPase (which drives K^+ influx against its concentration gradient), leading to Na^+ efflux and activation of the Na^+/Ca^{2+} exchanger in the forward mode. Consequently, a decrease in intracellular calcium concentration could result by this mechanism.

3.5.3 High extracellular KCl as a means of voltage regulation of WFA L-type calcium channels

In this study, stimulation of VIS-WFAs of CD1 male mice by 50mM extracellular KCl produced an increase in cytoplasmic calcium response through various mechanisms, in an extracellular calcium dependent manner. Removal of extracellular calcium inhibited the ability of 50 mM KCl to mediate calcium influx in white fat adipocytes (Figure 3.18). This is unlike the IP3R agonist, oxytocin, which still increased $[Ca^{2+}]_i$ in calcium free buffer conditions due to calcium release

from endoplasmic reticulum stores; data that supports the extracellular dependence of calcium influx in response to a high KCl buffer.

3.5.3.1 Mechanisms of 50mM KCl induced calcium influx in adipocytes

Osmotic effects (cell swelling/shrinkage), ionic effects (NCKX and NCX activity) and cell membrane depolarisation

Several studies have employed elevation of the extracellular K^+ ion concentration ($[K^+]_o$) to probe for the presence of Ca_V channels in different cell types (Yaguchi and Nishizaki, 2010), including adipocytes (Gaur et al., 1996) and have reported an increase in intracellular calcium in response to high $[K^+]_o$ in these cells. The act of directly adding KCl to the cell without ionic or osmotic correction is a common method to employ this technique (Draznin et al., 1989, Gaur et al., 1996). However, previous research in our laboratory observed that elevation of the $[K^+]_o$ from 5.6 mM to 50 mM by equimolar substitution of bath Na^+ (high $[K^+]_o$ by substitution) had no significant effect on the membrane potential of either primary or 3T3-L1 adipocytes (Bentley et al., 2014). This suggests the absence of K^+ permeable channels and an effect on adipocyte V_m, Ca_V channel activity and consequently on adipocyte intracellular calcium levels. However, the presence of non-selective cation channels, permeable to both K^+ and Na^+ in this cell type (Ringer et al., 2000, Bentley et al., 2014), readily explains why ionic substitution of Na^+ with K^+ does not affect V_m in this cell type.

In this study, we observed that both high $[K^+]_o$ (by addition) and high $[K^+]_o$ (by substitution) caused a significant increase in basal intracellular calcium levels of VIS-WFAs (Figures 3.16 and 3.17). There are several possible mechanisms by which high $[K^+]_o$ (by addition and by substitution) could have promoted calcium influx in these cells; including osmotic and ionic mechanisms, as well as possible depolarisation of the adipocyte membrane potential and opening of Ca_V channels.

Mechanism of 50mM $[K^+]_o$ (by addition)

High extracellular concentrations of KCl has long been reported to depolarise cell membranes, leading to cellular uptake of K^+ and subsequent cell swelling (Lang et al., 1998, Lang, 2007). Regulatory cell volume decrease is a volume regulatory mechanism which cells employ to counteract the effects of cell swelling, by decreasing intracellular osmolarity and cell volume (Lang, 2007). Volume regulatory anion channels (VRACs) which mediate regulatory volume decrease can be activated following hypertonicity induced increase in intracellular osmolality, arising from uptake and accumulation of ions and the accompanied osmotic entry of water (Osei-Owusu et al., 2018). This associated cell swelling promotes VRAC activation, and the influx of calcium from extracellular sources in such condition has been associated with the opening of transmembrane ion channels (Lang, 2007, Hoffmann et al., 2009), including Ca_V channels (Wehner et al., 2003, Hoffmann et al., 2009). The effect of 10μM DCPIB on intracellular calcium influx was assessed to check for the involvement of volume regulatory mechanism in the action of 50mM $[K^+]_o$ (by addition) buffer. DCPIB is a selective inhibitor of VRACs and has been described as the most selective inhibitor of swelling activated chloride current $I_{clswell}$, which is activated during regulatory volume decrease (Sardini et al., 2003).

50mM $[K^+]_o$ (by addition) induced intracellular calcium influx in VIS-WFAs was insensitive to inhibition by the selective VRAC inhibitor, DCPIB (Figure 3.22), and as such had no effect on the adipocyte VRAC activity. In addition, DCPIB neither affected the magnitude of KCl response nor the proportion of adipocyte population that showed a response. This suggests a lack of involvement of swelling-induced VRAC activation and regulatory cell volume decrease in the mechanisms of $[K^+]_o$ (by addition) induced intracellular calcium increase observed in this study.

The mechanism of high $[K^+]_o$ (by addition) induced increase in $[Ca^{2+}]_i$ in VIS-WFAs may involve hyperosmotic induced cell shrinkage and increase in the intracellular solute concentration (Friedrich et al., 2006). The movement of water is mainly determined by the osmotic concentration gradients across the cell membrane. Hence, alterations of intracellular or extracellular osmolarity is followed by the respective movement of water molecules and alterations of cell volume (Lang et al., 1998, Friedrich et al., 2006). When the extracellular osmolarity is higher than the intracellular osmolarity, the cell shrinks due to water loss and this leads to an increase in the concentration of the intracellular solute concentration (Friedrich et al., 2006). With the 50mM $[K^+]_o$ (by addition) buffer being of higher osmotic strength than the standard Hanks buffer, it is likely that the adipocytes when perfused with this solution responded by shrinking, resulting in the increase of their intracellular solute concentration and consequently, an increase in intracellular calcium concentration as was observed. An effect exacerbated by the concentration of the calcium-sensitive fluorophore dye Fluo-4.

Cell shrinkage is known to alkalinize cells, partly due to activation of Na^+/H^+ exchanger, which is a volume regulatory mechanism (Lang et al., 1998, Lang, 2007). This exchange of Na^+ ions for the loss of H^+ ions through the Na^+/H^+ exchanger is expected to contribute to an increase in intracellular Na^+ concentration, leading to a decrease in the chemical gradient for Na^+ across the cell membrane and a decrease in the driving force for Ca^{2+} efflux through the NCX channel. This will lead to activation of the reverse mode of the Na^+/Ca^{2+} exchanger and a consequent increase in $[Ca^{2+}]_i$. The increase in intracellular calcium observed in this experiment was sensitive to inhibition by KBR7943, a blocker for Na^+/Ca^{2+} exchanger, supporting cell shrinkage-induced activation of NCX channel as a possible mechanism of calcium influx in this experiment (Figure 3.16).

On investigating the intracellular calcium response of white fat adipocytes to eq. 50mM $[NaCl]_o$ (by addition) as an osmotic control for elevation of extracellular KCl, we did not observe similar results as with 50mM $[K^+]_o$ (by addition). 50mM NaCl (by addition) had no effect on intracellular calcium levels in the majority of the cells. The electrochemical potential difference for Na^+ across the cell membrane is maintained by the Na^+,K^+-ATPase pump (Friedrich et al., 2006) which pumps three sodium ions out of the cell for every potassium ion pumped into the cell. Coupled with the high extracellular NaCl concentration, both processes should contribute to increasing the magnitude of the Na^+-electrochemical potential difference in the adipocytes. This could block any cell-shrinkage induced activation of the Na^+/H^+-exchanger and prevent the consequent efflux of Na^+ due to activation of the reverse-mode of the Na^+/Ca^+ exchanger. In fact, elevation of extracellular Na^+ would promote normal forward mode NCX to decrease $[Ca^{2+}]_i$, as was observed in some cells (Fig 3.16A).

Cells respond to cell shrinkage by a regulatory volume increase (RVI), leading to cell swelling. Hypertonicity induced cation channels (HICCs) are one of the mechanisms which cells utilise during RVI, in addition to the activity of Na^+-K^+-2Cl- cotransporter and Na^+-H^+ exchanger coupled to the Cl^-/HCO_3^- exchanger (Wehner et al., 2006, Lang, 2007). Due to the higher turn-over rate of channels of ~ 4-5 fold orders of magnitude over transporters, HICCs are thought to play a major role in RVI in most cells (Wehner et al., 2003, Wehner et al., 2006). HICCs do not discriminate much between Na^+ and K^+ ions and so cause Na^+ influx simultaneously with K^+ efflux in cells undergoing RVI (Wehner et al., 2006). Coupled with the activity of the Na^+-H^+ exchanger which alkalinises the cell in response to hyperosmotic-induced cell shrinkage, both processes may have led to increase in intracellular Na^+ concentration causing activation of the reverse-mode

of the Na^+-Ca^{2+}-exchanger. This will lead to an influx of Ca^{2+} ions and an increase in intracellular calcium concentration, as was observed in this experiment. Control experiments which could have been carried out to test this hypothesis was the inhibition of Na^+ conductance by HICCs and Na^+-H^+ antiporter activity using amiloride, to further validate this proposed mechanism of high extracellular KCl induced increase in intracellular calcium in white fat adipocytes.

RVI-induced cell swelling has been reported to cause an increase in intracellular calcium concentration in a variety of cells, due to activation of cell membrane calcium channels which could be activated by membrane depolarization (Wehner et al., 2006), protein kinase C activation, or membrane stretch activated channels; as well as from release of calcium from intracellular calcium stores (Lang et al., 1998). In insulin-secreting beta cells, cell swelling was reported to cause the activation of anion channels and the resulting Cl^- efflux led to depolarisation of the cell membrane, activation of voltage-sensitive calcium channel and influx of calcium resulting in hormone release (Lang et al., 1998). Previous studies (Bentley et al., 2014), as well as results reported here, show that extracellular removal of Cl^- ions does not lead to increase in intracellular calcium levels in this cell type. This suggests that Cl^- efflux led depolarisation and $Ca_V1.x$ channel activation due to osmotic mechanisms may not be involved in the intracellular calcium increase by high $[K^+]_o$ (by addition) in WFAs in this study.

Both cell swelling and cell shrinkage have been observed to activate protein kinase C (Lang et al., 1998). PKC is known to phosphorylate proteins and has been reported to phosphorylate Ca_V channels leading to their activation. In this experiment, the increase in intracellular calcium concentration due to high extracellular potassium was sensitive to partial inhibition by verapamil, a known blocker of the cell membrane L-type calcium channels. This suggests the

possibility that RVI-induced cell swelling in CD1 male mice visceral white fat adipocytes in response to extracellular KCl elevation may have led to the activation of cell membrane L-type calcium channels, contributing to the observed increase in intracellular calcium levels in these cells. On the other hand, in most cells it is expected that as the $[K^+]_o$ increases, the chemical gradient for K^+ decreases and this impedes K^+ efflux, depolarizes the cell and leads to Cl^- entry into the cell (Lang, 2007). However, as the membrane potential of white fat adipocytes is thought to be controlled mainly by Cl^- ions, hypertonicity induced reduction in efflux of K^+ is not expected to depolarise the cell if that were the case. Although verapamil is an L-type calcium channel antagonist, it is also a partial inhibitor of NCX exchangers. Hence the sensitivity of intracellular calcium response of the cells to verapamil in 50 mM extracellular KCl in this study could also be attributed to its partial inhibition of the NCX exchangers and blockade of calcium influx through the reverse mode of the NCX exchanger.

On another hand, there exists the possibility of the contribution of $[K^+]_o$ increases to promote maximal activity of $Ca_V1.x$ channel activity in WFAs based on the observed increase in intracellular calcium. The role of Cl^- as the major ionic determinant of WFA RMP is well established (Bentley et al., 2014, Beigelman and Shu, 1972), however Beigelman and Shu (1972) also suggest that K^+ plays a role, in addition to Cl^- in the regulation of WFA resting membrane potential. Although K^+ may only play a minor role in RMP setting in WFAs, small depolarisations caused by elevating its external concentration may be sufficient to activate $Ca_V1.x$ channels because of the close proximity of the adipocyte RMP to the Ca_V channel activation threshold. This idea is also supported by sensitivity of 50 mM $[K^+]_o$ (by addition) induced intracellular calcium influx in VIS-WFAs to inhibition by verapamil.

Mechanism of 50mM $[K^+]_o$ (by substitution)

The high affinity of potassium dependent sodium-calcium exchanger (NCKX) proteins for extracellular calcium in sodium-free medium (Altimimi and Schnetkamp, 2007), suggests an additional mechanism of calcium influx as seen in Figures 3.17A and B. This idea is supported by the observation of NCKX as the highest expressed NCX form in rat VIS WFA, determined by transcriptomic analysis (Unpublished data - Fedorenko, 2021).

Previous studies in mouse oocytes have shown that removal of extracellular sodium reduces calcium extrusion and promotes intracellular calcium accumulation (Pepperell et al., 1999). KB-R7943 is a highly selective calcium-influx mode NCX exchanger inhibitor (Amran et al., 2003). It is thought to act as a competitive inhibitor for external calcium, with its inhibitory action being relatively fast and reversible after wash. Although the independence of KB-R7943 on exchange direction has been demonstrated, a preference for the reverse mode of NCX has been shown, with an IC_{50} of ≤ 13 μM for $[Na^+]_i$-dependent $^{45}Ca^{2+}$ influx (reverse-mode) and an IC_{50} of ≥ 30 μM for $[Na^+]_o$-dependent $^{45}Ca^{2+}$ efflux (forward mode) (Amran et al., 2003), hence the use of KB-R7943 at a concentration of 10μM in this study. The inhibitory effect of 10 μM KB-R7943 on calcium influx in VIS-WFAs under conditions of high $[K^+]_o$ could also be due to a greater inhibition of basal intracellular calcium, thereby cancelling out the increase mediated by high KCl.

3.5.4 Modulation of L-Type Calcium Channels By Channel Agonists

Bay-K8644 is an L-type calcium channel agonist that binds only to the open state of the channel (Kokubun and Reuter, 1984). Dihydropyridine agonists are known to stabilize $Ca_V1.x$ channels in the open-conducting state for prolonged periods of

time (Feng et al., 2018). Although Bay-K8644 at the concentration employed in this study (10μM) is specific for $Ca_V1.x$ channels (Grafton et al., 2003), and an increase in $[Ca^{2+}]_i$ due to opening of $Ca_V1.x$ channels in response to the channel agonist was expected, Bay-K8644 had no effect on $[Ca^{2+}]_i$ in VIS-WFAs. A few cells however responded to Bay-K exposure with an increase in intracellular calcium levels. These results are similar to a published observation in which Bay-K8644 at the same concentration of 10μM, did not affect basal calcium levels in neuronal cells, but only caused an increase in cytosolic calcium in the presence of other channel regulators such as PTH (Hirasawa et al., 1998). Also, it has been shown that sustained depolarisation of non-excitable cells to potentials that fully activates $Ca_V1.x$ channels does not result in further increases in intracellular calcium concentration (Fleischmann et al., 1994). FPL 64176 is a non-dihydropyridine, L-type specific calcium channel agonist (Tavalin et al., 2004, McDonough et al., 2005), that stabilizes channels in both the closed and open states (Liu et al., 2003, McDonough et al., 2005). Similar to the observation with Bay-K8644, FPL was without effect on the $[Ca^{2+}]_i$ of WFAs.

3.5.5 L-Type Calcium Channels in WFAs Are Hormonally Regulated

During calcium signalling, the source of Ca^{2+} can be reflected by the nature of the Ca^{2+} signal (Hill-Eubanks et al., 2011), with short-lived Ca^{2+} transients being due to release from internal Ca^{2+} stores, while more sustained responses are generally due to gradual influx from plasma membrane L-type Ca^{2+} channels (Cooper, 2000). In this study, rhGH initiated sustained calcium signals, characterized by return of $[Ca^{2+}]_i$ after each peak to the baseline level. The ability of 20 nM recombinant human growth hormone to modulate intracellular calcium levels of VIS-WFAs was sensitive to verapamil, with a requirement for extracellular Ca^{2+}. This suggests growth hormone promotes L-type Ca^{2+} activity without involvement of intracellular

Ca^{2+} stores. Other researchers have also reported an increase in $[Ca^{2+}]_i$ levels in human and rat adipose tissue following exposure to growth hormone (Gaur et al., 1996, Gaur et al., 1998, Chaves et al., 2011). Gaur et al. (1996) have reported a two-fold increase in Ca^{2+} levels following the addition growth hormone to primary rat adipocytes. Like the observations made for white adipocytes of mice in this study, Gaur et al. (1998), found that the calcium influx effect of growth hormone on white fat adipocytes of rat was inhibited by L-type Ca^{2+} channel antagonists and removal of bath Ca^{2+}.

PTH has previously been shown to elevate adipocyte $[Ca^{2+}]_i$ both in vitro and in vivo (Reusch et al., 1991). In the present study, adipocytes were exposed to 100 nM PTH(1-34) or 100 nM PTH(1-84) to determine the effect of PTH on Ca_V channel activity in white adipocytes. Transient and sustained increases in intracellular calcium were seen in a small number of VIS-WFAs in response to 100nM PTH(1-34). PTH has previously been reported to mediate intracellular calcium signalling by modulating calcium release via Gq signalling pathway and inositol triphosphate receptor-mediated release of stored calcium, as well as modulation of plasma membrane L-type calcium channel and influx of calcium from the extracellular environment (Ni et al., 1994). The calcium signals due to PTH, suggests the ability of PTH(1-84) to modulate the activity of L-type Ca^{2+} channels on CD1 male mouse VIS-WFAs, leading to sustained increases in intracellular calcium levels (Figure 3.28C). Calcium transients due to Gq protein mediated release of intracellular calcium from ER stores as seen with oxytocin occurs rapidly. However, the calcium signals observed from PTH(1-84) action in these cells developed gradually and was sustained, suggesting the build-up of intracellular calcium due to calcium influx from Ca_V channels. Previous studies have reported an increase in cytosolic calcium in rat adipocytes due to exposure to PTH(1-84), and the lack of effect of

PTH(1-34) on intracellular calcium concentration in these cells (Ni et al., 1994). Other studies have however reported an increase in cytosolic calcium following exposure to PTH(1-34), but also noted a significantly higher effect of PTH(1-84) over the active amino terminal fragment on modulation of cytosolic calcium levels in rat hippocampal cells (Hirasawa et al., 1998). In this study, we observed an increase in intracellular calcium only in response to the full length peptide PTH(1-84). Due to time constraints, the sensitivity of PTH(1-84) induced calcium signals to inhibition by $Ca_V1.x$ channel antagonists was not explored.

3.5 Conclusion

This study has shown the functional expression of $Ca_V1.x$ channels in mice primary WFAs, similar to the observations by previous studies of the existence of $Ca_V1.x$ channels in non-excitable cells; including osteoclasts (Miyauchi et al., 1990) and human T-lymphocytes (Kotturi and Jefferies, 2005). The general lack of response of the adipocytes to extracellular ionic manipulation to alter cell membrane potential and promote calcium influx suggests a lack of dependence of $Ca_V1.x$ channels in this cell type on voltage regulations. This is similar to the observation by others of the nature of $Ca_V1.x$ channels in other non-excitable cells (Kotturi and Jefferies, 2005). There also exists a possibility for a minor sensitivity of these channels in WFAs to voltage regulation based on 50mM $[K^+]_o$ (by addition) induced intracellular calcium influx in VIS-WFAs and its inhibition by verapamil. The results from this study also shows that $Ca_V1.x$ channels in WFAs are hormonally regulated. Identification of the calcium signals elicited by both growth hormone and PTH(1-84) as being mediated by $Ca_V1.x$ channels was based on the nature of the calcium signal. Seminal studies in calcium signalling have differentiated the calcium oscillators by identifying the source of the calcium transient. $Ca_V1.x$ channel-mediated calcium signals build up gradually and are sustained within the cells.

This is similar to observations of rhGH and PTH(1-84) mediated calcium signals in WFAs in this study. Furthermore, absence of calcium transients after prolonged incubation in calcium-free media support the dependence on extracellular calcium and functional activity of PMCCs in WFAs. Identification of the channels as $Ca_V1.x$ channels was further confirmed by their sensitivity to dihydropyridine antagonists and inhibition of rhGH-mediated calcium signals.

CHAPTER FOUR

Role of calcium in adipocyte lipolysis and lipophile release

4.1 Introduction

Lipolysis refers to the breakdown of triacylglycerides (TAG) into non-esterified fatty acids and glycerol in the adipose tissue (Bolsoni-Lopes and Alonso-Vale, 2015, Grabner et al., 2021). The cyclic adenosine monophosphate (cAMP)-dependent protein kinase A (PKA) is responsible for the phosphorylation of key lipases in lipolysis, including ATGL and HSL (Grabner et al., 2021). The effect of intracellular calcium on PKA activity is thought to involve activity of the Ca^{2+}-sensitive, isoform III of adenylyl cyclase found in WFAs (Wang et al., 2009). Beta-adrenergic activation of stimulatory G-protein coupled receptors lead to the activation of adenylyl cyclase, which promotes cAMP production and consequently, PKA activation leading to lipolysis. Calcitrophic hormones such as PTH promote an increase in intracellular calcium levels and are also lipolytic, with augumented lipolytic actions under increasing calcium levels. The activity of adenylyl cyclase and hence cAMP levels can be stimulated by the calcium-dependent protein kinase, PKC (Carmen and Víctor, 2006). However, no effect of increasing calcium levels on cAMP levels have been reported in basal conditions (Ziegler et al., 1980).

Adipocyte lipolysis is under tight positive and negative hormonal control. For instance, insulin is thought to be the most anti-lipolytic hormone through the protein kinase B (PKB/Akt)-dependent activation of PDE3B and subsequent inhibition of cAMP-dependent lipolysis. However, the dose–response of lipolysis to insulin is bell-shaped, with insulin being anti-lipolytic at low concentrations, while

at higher concentrations of insulin, lipolysis is increasingly restored due to inhibition of PDE3B (Jönsson et al., 2019). Similar to the action of insulin, different studies suggest that intracellular calcium may exhibit both lipolytic and anti-lipolytic effects in the adipose tissue. The idea of the bell-shaped response of adipocyte lipolysis to extracellular calcium is supported by the work of Ziegler et al. (1980), in which low (0 mM) and high (2.77 mM) concentrations of extracellular calcium inhibited both basal and stimulated (isoproterenol and PTH) lipolysis. Optimal lipolysis was seen at a calcium concentration of 0.92 mM (Ziegler et al., 1980).

4.1.1 Relationship between lipolysis and mechanisms of lipophile release

The release of fat-stored lipophilic compounds during the lipolytic process has been shown by recent studies. Particularly, Louis et al. (2014) developed a functional *in-vitro* model of adipocyte lipolysis in which differentiated rat adipocytes which had been loaded with the POP, PCB-153, was shown to release the compound when lipolysis was stimulated. The exact mechanism by which fat stored compounds are released during the lipolytic process is as yet unknown, however, it is plausible that the reduction of the triglyceride laden core of the adipocyte lipid droplet will cause a decline in the available storage capacity of the adipocyte for these highly lipophilic compounds.

4.2 Background literature on role of calcium in regulation of lipolysis

4.2.1 Promotion of lipolysis and inhibition of obesity by intracellular calcium

Adipocyte lipolysis is promoted by intracellular calcium, as both stimulated and basal lipolysis are inhibited in calcium-free conditions (Fedorenko, 2019). The role of intracellular calcium in the promotion of lipolysis is supported by the observation

of Izawa et al. (1983), in which incubation of calcium-deficient tissue in calcium-free buffer decreased adrenaline, nor-adrenaline and adrenocorticotropin-stimulated lipolysis. In addition, the dose-dependent inhibition of rat VIS-WFA lipolysis by verapamil and diltiazem lends support for the involvement of calcium influx through $Ca_V1.x$ channels in the promotion of adipocyte lipolysis (Song et al., 2019). In isoproterenol stimulated lipolysis, isoproterenol acts through stimulatory G protein to activate adenylate cyclase, while forskolin directly activates the catalytic subunits of adenylate cyclase; both leading to cyclic AMP production, activation of cAMP-dependent PKA and induction of lipolysis. In the absence of calcium, cAMP production due to isoproterenol and forskolin activity is unaffected, however, their lipolytic activity is diminished. This suggests that the requirement of calcium in the lipolytic response to both isoproterenol and forskolin is distal to the production of cAMP (Allen and Beck, 1986).

High intracellular calcium has been demonstrated to relieve high-fat diet (HFD) induced obesity in mice (Sun et al., 2012b). Intracellular calcium is thought to mediate its anti-obesity effects by modulating fat metabolism, through an increase in lipolysis and decrease in lipogenesis (Sun et al., 2012b, Zhang et al., 2019), an effect reversible by the L-type calcium channel antagonist, nifedipine (Sun et al., 2012b).

4.2.2 Lipolytic action of intracellular calcium promoting hormones

Growth hormone has been recognized as a potent regulator of adipose tissue fat mass and adiposity, through its direct effect on cAMP and PKA pathways (Frühbeck et al., 2014). Growth hormone equally activates MAPK/ERK 1/2 pathway, leading to phosphorylation of β3 adrenergic receptor and HSL by ERK 1/2 and induction of adipocyte lipolysis (Grabner et al., 2021). The role of growth hormone in the

regulation of adipocyte lipolysis is supported by the observation of ~40% decrease in lipolysis and non-esterified fatty acids in growth hormone-deficient individuals, with a return to normal values upon commencement of growth hormone replacement therapy. Studies have shown that growth hormone exerts a delayed lipolytic action (2-3 hours after exogenous administration) compared to the near immediate lipolytic action of catecholamines (Frühbeck et al., 2014). The mechanism of growth hormone action on lipolysis is thought to involve JAK2 signalling pathway, as adipocyte specific disruption of JAK2 in mice has been shown to result in a decrease in lipolysis and increased body fat mass (Nordstrom et al., 2013), Jurkat-Rott and Lehmann-Horn (2004). According to Hansen et al. (2002), growth hormone potently and dose dependently stimulates lipolysis in humans by an as yet undetermined molecular pathway. In animal studies however, the process is thought to involve cAMP-dependent signalling mechanisms which increase responsiveness of β-adrenoceptor signalling. The lipolytic action of growth hormone is also thought to be depot specific, with the visceral adipose tissue being more sensitive to growth hormone action (Nielsen et al., 2014, Berryman et al., 2016, Kopchick et al., 2020).

PTH is a calcitrophic hormone which has been demonstrated to stimulate lipolysis in human adipose tissue (Ziegler et al., 1980). However, at high concentrations, PTH also inhibits adipose tissue lipolysis and promotes lipogenesis by inhibition of catecholamine induced lipolysis (Frühbeck et al., 2014). The anti-lipolytic action of PTH is further amplified by its stimulation of calcitriol production, leading to intracellular calcium increases and further inhibition of lipolysis.

4.2.3 Inhibition of lipolysis by intracellular calcium

The anti-lipolytic effect of increased intracellular calcium concentrations has been reported (Xue et al., 1998, Xue et al., 2001), and is thought to be due to the activity of an adipocyte phosphodiesterase (PDE) (Xue et al., 2001). This adipocyte phosphodiesterase possibly acts at a step proximal to PKA activation, with its activity similar to the anti-lipolytic activity of insulin through PDE3B activity. The increased intracellular calcium activated adipocyte phosphodiesterase is thought to inhibit lipolysis induced by phosphodiesterase inhibitors such as isobutyl methyl-xanthine (IBMX), as well as inhibition of isoproterenol induced lipolysis, leading to decreased cAMP activity and decreased HSL phosphorylation (Xue et al., 2001, Frühbeck et al., 2014). Intracellular calcium increases in adipocytes, due to calcium influx through Ca_V channels and receptor-mediated calcium release, respectively stimulated by KCl and arginine vasopressin, led to inhibition of forskolin (an adenylate cyclase activator) induced lipolysis (Xue et al., 1998). In addition, the anti-lipolytic effects of the recombinant agouti protein in human adipocytes was shown to be sensitive to inhibition by the L-type calcium channel antagonist, nitrendipine (Xue et al., 1998). This data further supports the idea that intracellular calcium influx through Ca_V channels on the adipocyte plasma membrane can exhibit anti-lipolytic effects.

4.2.4 Evidence of extracellular calcium and lipophile release

Obesogens are a subset of endocrine disrupting chemicals which can be found in food and beverage packaging, flame retardants, cleaning products, pesticides, etc., and are capable of causing alterations to metabolism, leading to increased adiposity and a predisposition to obesity (Lee et al., 2017, Griffin et al., 2020). Environmentally persistent pollutants or persistent organic pollutants (POPs) such as polychlorinated biphenyls which principally target the lipid droplet of adipocytes

are also obesogenic (Lee et al., 2017, Aaseth et al., 2022). The lipophilicity of obesogens means they are readily sequestered in the adipose tissue, thereby creating a sink for these harmful chemicals in the body (La Merrill et al., 2013, Louis et al., 2014). Some of the characteristics of POPs which perpetuates their sequestration in the adipose tissue and persistence in the body include their high octanol/water partition coefficient (K_{OW}), their long half-lives and the low molecular weight of these chemicals and their metabolites, making them readily diffusible into adipocytes (Griffin et al., 2020). Due to the biphasic half-life of such compounds, their elimination from the body is dependent on their release from the adipose tissue into the blood. Hence, the amount the POPs released from the adipose tissue into the general circulation and the amount of POPs eliminated from the circulation, determine the serum concentration of POPs and their exposure of target organs (Lee et al., 2018).

4.3 Study rationale

Obesogenic and diabetogenic lipophilic compounds can accumulate in large amounts in adipose tissue where they may become sequestered (Lee, 2021). Persistent organic pollutants (POPs) are strong lipophilic chemicals with long half-lives which are readily accumulated by WFAs (Lee et al., 2017, Lee et al., 2020, Lee, 2021), and in addition to their neurotoxic effects are both obesogenic and diabetogenic (Lee, 2021). The adipose tissue accumulation of persistent organic pollutants and other highly lipophilic obesogenic and diabetogenic chemicals means that overtime, lipolysis can lead to the release of these compounds into the body's circulation (Lee et al., 2020).

Recent research shows that during adipocyte lipolysis, in addition to release of non-esterified fatty acids, POPs can be gradually released from their storage sites

in the lipid droplet (Lee et al., 2020, Lee et al., 2017). As adipocyte lipolysis is controlled by intracellular calcium concentration, the latter may invariably play a role in the release of lipophiles from WFAs during lipolysis and consequently on lipophilic compound induced obesity. A better understanding of the effect of high intracellular calcium conditions on adipocyte lipolysis and lipophile release will contribute to the development of effective treatment strategies for management of lipophilic chemical-induced obesity and type 2 diabetes.

4.4 Aim of study

The aim of the study is to determine the role of intracellular calcium in the mobilisation of lipophilic compounds, using the lipophile, Nile red, as a surrogate marker. The specific objectives are as follows:

- To investigate the effect of high intracellular calcium conditions on:
  - ✓ Nile red release from white fat adipocytes
  - ✓ free fatty acid release from adipocytes
- To determine the correlation between adipocyte lipolysis and lipophile release from white fat adipocytes.

4.3. Methodology

4.3.1 Measurement of Nile red loading and release

4.3.1.1 Primary Adipocyte Isolation

Visceral adipocytes were prepared from epididymal fat pads excised from male Sprague-dawley rats (body weight 350 - 450 g), fed ad libitum (Charles River Laboratory, Kent, UK). Animals were killed by stunning, followed by cervical dislocation in accordance with UK Home Office guidelines. Primary white adipocytes were isolated from the fat pads using a modification of the method of Rodbell (1964), as described in Chapter 2 above. To obtain the adipocytes, the cells were re-suspended in 20 ml of Hanks solution and after draining off the supranatent, the cells were collected into a 2 ml tube, at room temperature (~22 °C) for Nile red fluorescence imaging.

4.3.1.2 Nile red as a marker for measurement of stored lipophiles released from white fat adipocytes

Nile red (9-diethylamino-5H-benzo[α]phenoxa-phenoxazine-5-one) is a lipid-soluble fluorescent probe which allows the in situ staining of lipids, and has been used to quantify neutral lipids and hydrophobic proteins in many biological systems (Greenspan and Fowler, 1985, Bertozzini et al., 2011, Rumin et al., 2015). Nile red is photostable and strongly fluorescent in organic solvents and hydrophobic environments. However, its excitation and emission spectra are shifted to shorter wavelengths as the polarity of the surrounding environment decreases. Hence, by proper selection of excitation and emission wavelengths, neutral and polar lipids in a biological system being examined can be accurately differentiated (Greenspan and Fowler, 1985, Bertozzini et al., 2011). Nile red is characterized by two specific spectra of fluorescence: yellow-gold fluorescence (excitation 450 - 500 nm, emission > 528 nm) and red fluorescence (excitation

515 - 560 nm, emission > 590 nm). For measurement of dye release from the neutral lipid store of the adipocyte lipid droplet, Nile red fluorescence was examined for yellow-gold fluorescence (528 nm), as Greenspan and Fowler (1985) have shown this wavelength as being optimum for the selective staining of cytoplasmic lipid droplet by Nile red. The stock solution of Nile red (10 mg/ml) was prepared in dimethyl sulfoxide and stored at 4 ^{o}C, protected from light. The working solutions of Nile red, used for the staining of the intracellular lipids, was prepared *ex tempore* by diluting a stock solution of dye in Hanks buffer.

4.3.1.3 Nile red loading of isolated adipocytes and measurement of Nile red release from Sprague-Dawley rat VIS-WFAS

Freshly isolated visceral white fat adipocytes were suspended in Hanks buffer. 12.5 µg/ml Nile red working solution in Hanks buffer (0.5 % BSA and 5 mM glucose) was prepared from a 10 mg/ml Nile red stock in DMSO. 200 µl of packed cell volume of the adipocytes were re-suspended in 1000 µl of Nile red, to give a final dye concentration of 10 µg/ml and incubated in the dark for 1 hour. The Nile red fluorescence of the loaded cells was measured either before or after the loaded cells were washed with Hanks buffer. For the latter, a 19 gauge needle and syringe was used to remove the infranatant solution, after which the cells were washed twice in Hanks solution before resuspension in 1ml of the appropriate treatment solution. For the latter experiments following optimization of the protocol, the cells were re-suspended in 2 ml of the appropriate treatment solution. The cells were then incubated in the dark at 22 °C or on a heating block at 32 °C for up to 1 hour as indicated. Following this, an aliquot of infranatant solution (50 - 95 µl) was collected for later assessment of free fatty acid release, while for Nile red fluorescence measurement and determination of Nile red release, 5 µl of cells was

suspended in 95 µl of Hanks buffer (0.5 % BSA and 5 mM glucose) and snap shots of the cells taken with the microscope.

4.3.1.4 Measurement of Nile red release from 3T3-L1 adipocytes and CD1 mice VIS-WFAs

Visceral WFAs were prepared from epididymal fat of CD1 male mouse using standard methods as previously described in chapter 3. The adipocyte cell suspension was transferred into 1.5 ml analyser cups (Alpha laboratories Cat. no. QT1500A) and the adipocytes were allowed to float to the top of the tube. The cells were then attached to coverslips by placing poly l-lysine coated coverslips over the cells for ~25 mins. The primary adipocytes were then placed in contact with poly l-lysine coated coverslips to allow attachment of the cells to the coverslip. Afterwards, primary adipocytes attached to the coverslip or 3T3-L1 adipocytes grown on coverslips were placed in the sample chamber, followed by addition of 1ml of Hanks buffer. The temperature of the microscope stage and perfusion system was maintained at 32 - 37°C and the light intensity was chosen based on the minimum intensity that allowed visualisation of the fluorescent cells in the dark. After 60 secs (1 minute) of recording, 1 ml of Nile red at 20 µg/ml was added to the dish, to bring the Nile red concentration to 10 µg/ml. Following 30 mins of static Nile red loading, the cells were washed by perifusion of Hanks buffer for 10 minutes. This was followed by perfusion of the appropriate treatment solution into the cells for 10 minutes. Static incubation of the cells (continuous perifusion for CD1 mice adipocytes) in the treatment solution continued for a further 80 minutes (50 minutes for CD1 mice adipocytes), after which the cells were washed by perifusion of Hanks for 10 mins and the experiment was stopped.

4.3.1.5 Imaging of Cells

Images were collected on an inverted Axiovert 135TV microscope (Carl Zeiss Ltd, Welwyn Garden City, UK) equipped with X20 objective lens Plan-Fluar/0.5, and the light source was provided by a xenon arc lamp. To measure fluorescence emission from Sprague-Dawley rat VIS-WFAS under static incubation, cells were illuminated and snap shots taken in representative cells during different time points. For continuous monitoring of fluorescence emission from 3T3-L1 adipocytes and CD1 mice VIS-WFAs, the sequence interval of the acquisition protocol was set to capture images every 60 secs, with a 4 x 4 camera binning. Images were captured with a CoolSNAP HQ2 camera (Photometrics, UK). The dye was excited at 480 nm, with the lowest light intensity that allowed camera detection and visualisation of emitted fluorescence by Nile red loaded-cells, when the observer was dark adapted. The cells were then brought into focus and the imaging system started. Live cell recordings were captured and initially processed using Imaging workbench Ver. 6.0 software (INDEC Biosystems, Santa Clara, CA, USA). Image analysis was done by placing regions of interest over cells in the field of view captured and data collected. The files were processed further using Microcal ORIGIN 6.1 (Microcal Software Inc., Northampton, MA). The diameter of the adipocytes was determined from the area of the regions of interest drawn around each adipocyte, using a script written by Dr. Paul A. Smith.

4.3.2 Free fatty acid assay

Free fatty acid (FFA) release was used to measure lipolysis. 150 µl of cell media was removed at different time points during Nile red release experiments, labelled appropriately and stored at −80 °C prior to assay. FFA was assayed with a non-esterified FFA assay kit (WAKO chemicals). After subtraction of blank, data were normalized to the absorbance of the FFA standards, corrected for dilution and

expressed as micromoles of FFA per millilitre packed cell volume (PCV) of adipocytes.

4.3.3 Analysis of Nile red spatial distribution in 3T3-L1 adipocytes by confocal microscopy

Cell medium was removed from Day 11 3T3-L1 adipocytes grown on No. 1.5 glass coverslips and the cells were washed twice with Hanks buffer containing 5 mM glucose and 0.5 % BSA. The coverslip was securely placed in the sample chamber and cells were successively loaded with 1 µg/ml of Cell Brite Red (Biotium cat. 30023) for 30 mins (to visualise the cell membrane), 2 µg/ml of Hoechst 33342 for 10 mins (to visualise the nucleus) and 10 µg/ml Nile red (Sigma N3013, Lot #SLBP9326V) for 2 mins in the dark. Each dye incubation was followed by a wash step before incubation with the next dye. Following dye loading, the adipocytes were washed twice for the final time and 1 ml of Hanks buffer added to the cells in the sample chamber prior to fluorescence detection. The sample chamber was placed on the microscope stage and images were captured on a Zeiss LSM880 confocal microscope equipped with X63 oil immersion objective lens Plan-Apo/1.4. The instrument was controlled through the Carl Zeiss Zen software, version 2. Excitation and emission wavelengths were 647/681 nm for cell brite, 440/480 nm for Hoechst 33342 and 561/598 nm for Nile red. Collected data was analysed using FIJI software.

4.3.4 Statistical analysis

Data was analysed using GraphPad Prism Version 7.03 program (GraphPad Software Inc., San Diego, CA). Normality of data was first determined using the D'Agostino-Pearson omnibus normality test as recommended by Prism, to test if the data followed a Gaussian distribution. Parametric data sets were analysed by

repeated measures One-Way ANOVA for paired data, followed by Dunnett's post-hoc test for multiple comparisons. Data sets that were not normally distributed were analysed by the Friedman's test for repeated measures, followed by Dunn's post-hoc test for multiple comparisons or Mann-Whitney U test for non-paired data. Significance was set at $p < 0.05$, and the values of p for significant differences are indicated in figure legends. Data are mostly shown as box and whisker plots with 2.5 – 97.5 % confidence intervals (CIs). Numerical data are given as mean ± S.D. or median with 5% to 95% CIs to two significant figures. Technical replicates are denoted by n (number of cells), while biological replicates are denoted by f (number of experiments/individual coverslips pooled from different animal preparations) and/or i (number of animal preparations) (Lazic et al., 2018).

4.4. Results

4.4.1 Determination of Nile red loading in primary rat adipocytes

Before examining the effect of calcitropic hormones on the release of the lipophilic marker, Nile red, from WFAs, the kinetics of Nile red in these cell types was first determined. The absorption of the fluorescence dye was initially assessed, after which the optimum concentration for dye loading was determined, followed by determination of Nile red release under different conditions.

Initially, the adipocytes were loaded with 1 µg/ml of Nile red and the absorption of the dye was monitored and fluorescence intensity measurements obtained at specific time points. WFAs readily absorbed the lipophilic Nile red dye and the fluorescence intensity of Nile red was time-dependent (Figure 4.1). There was no difference in the fluorescence signal intensity of the adipocytes loaded with Nile red for 60 mins compared with 120 mins. However, at 10 mins of dye loading, the recorded signal intensity was significantly lower (****$p < 0.0001$; Friedman's test, Dunn's post hoc test) than other time points measured. The adipocytes did not become saturated with Nile red over the 2 hours of incubation at a 1 µg/ml. Only 2 of the 61 cells examined became saturated with the dye at the 60 mins time point.

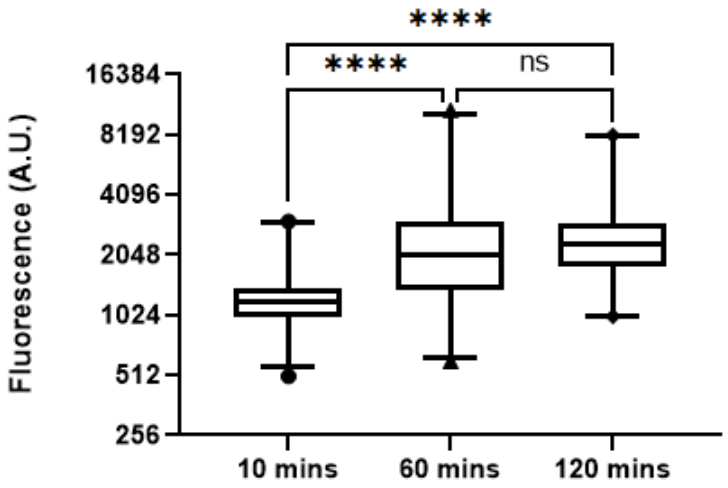

Figure 4.1 Effect of incubation length on Nile red fluorescence of male Sprague-Dawley rat VIS-WFAs.

WFAs were loaded in the dark, at room temperature with 1 µg/ml on nile red and fluorescence intensity was measured at 528nm with a green bandpass filter. 10 mins: n = 54, f = 3; 60 mins: n = 61, f = 4; 120 mins: n = 41, f = 4; Data are expressed as mean ± S.D. (****p < 0.0001; Friedman's test, ns = non-significant, Dunn's post hoc test).

By visual inspection, some cells within the same field of view seemed to be more fluorescent than others (Figure 4.2). To determine if this observation was a function of cell size, the diameter of the adipocytes was measured and compared with the fluorescence intensity of the corresponding adipocyte. At the different time points of Nile red fluorescence measurement, there was no correlation between adipocyte diameter and fluorescence intensity signal observed in the cells (10 mins: Spearman rank correlation coefficient, r = -0.006717, -0.2815 to 0.2691 95% C.I., p = 0.961; 60 mins: r = 0.1149, -0.1484 to 0.3631 95% C.I., p = 0.377; 120 mins: r = 0.1994, -0.1246 to 0.4850 95% C.I., p = 0.211 (Figure 4.3). In addition, no change was observed in the diameter of the cells over the time course of the experiment (Figure 4.4).

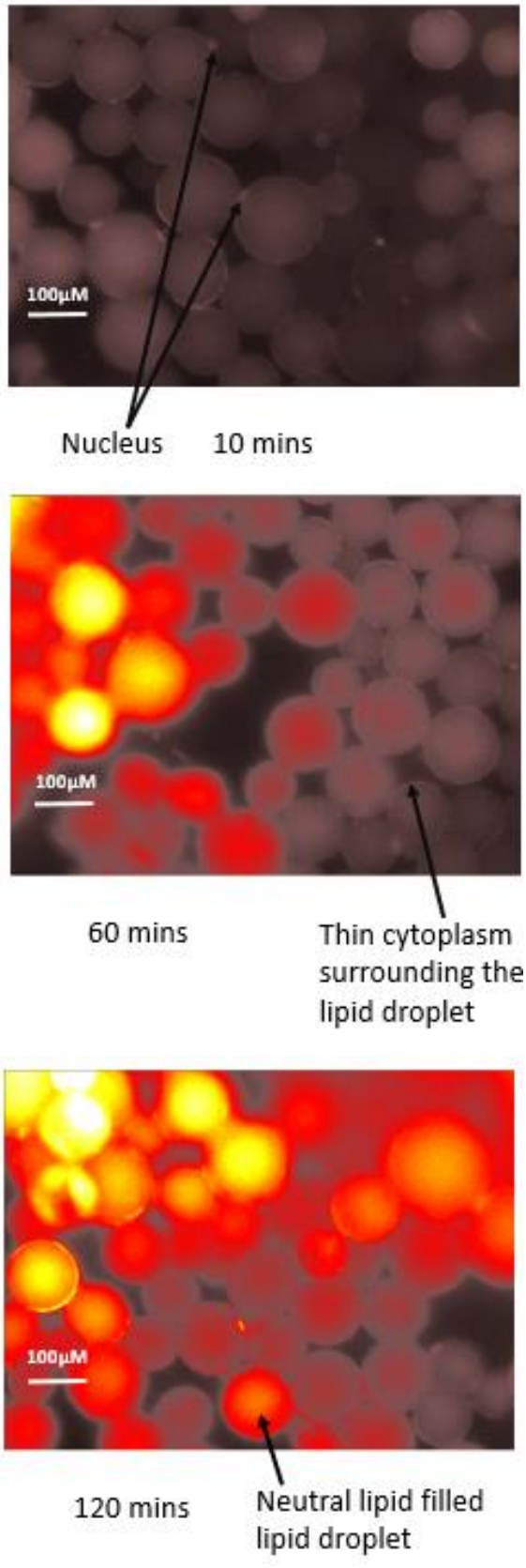

Figure 4.2: Time-course of Nile red loading of male Sprague-Dawley rat VIS-WFAs.

Three different field of views taken at the time points indicated for Nile red loaded adipocytes, viewed with x20 objective. The images given are pseudo colour image. The pale pink/red colour is representative of the dye content of the cell. The grey background is indicative of the absence of dye. The primary adipocytes show their characteristic unilocular neutral lipid-rich lipid droplet, into which the Nile red is readily absorbed. This is surrounded by a thin cytoplasm, with the nucleus being pushed to the periphery of the cell by the intracellular lipid droplet.

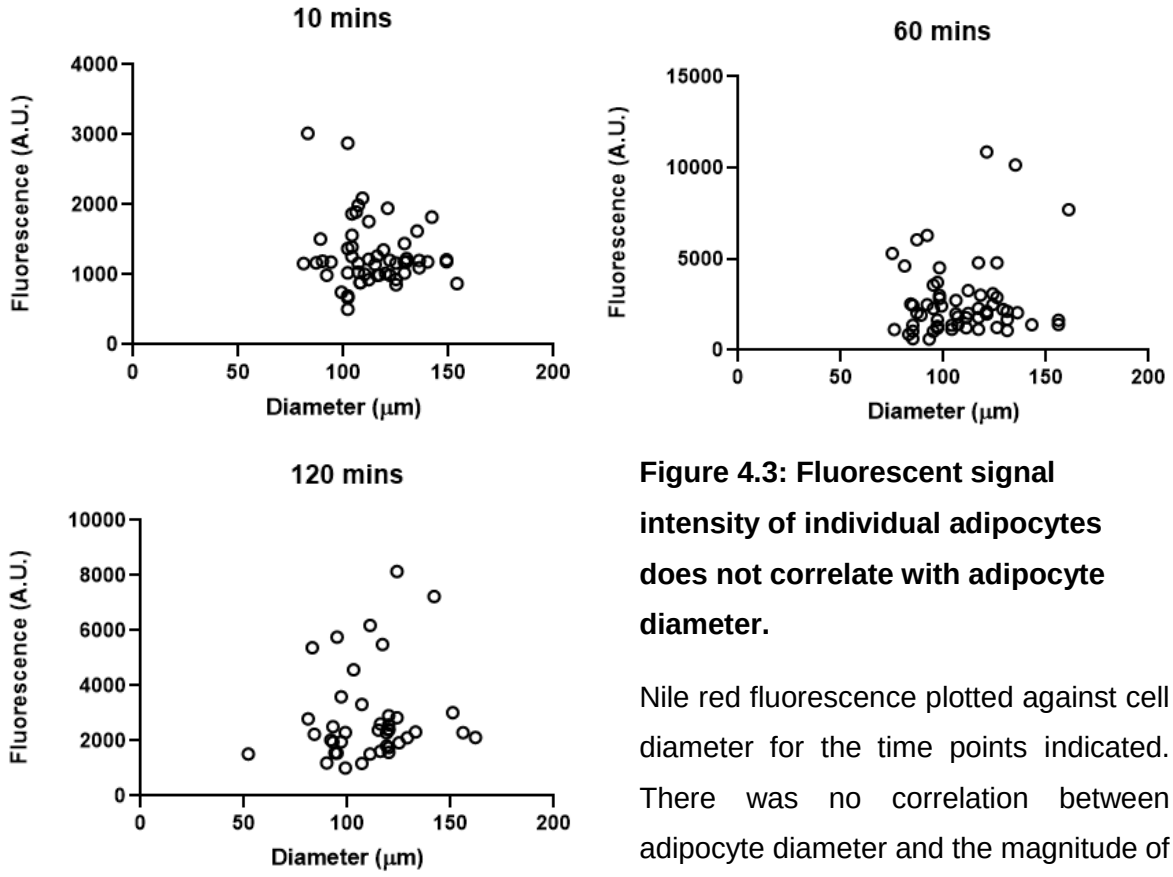

Figure 4.3: Fluorescent signal intensity of individual adipocytes does not correlate with adipocyte diameter.

Nile red fluorescence plotted against cell diameter for the time points indicated. There was no correlation between adipocyte diameter and the magnitude of fluorescent signal recorded for individual adipocytes within the same field of view.

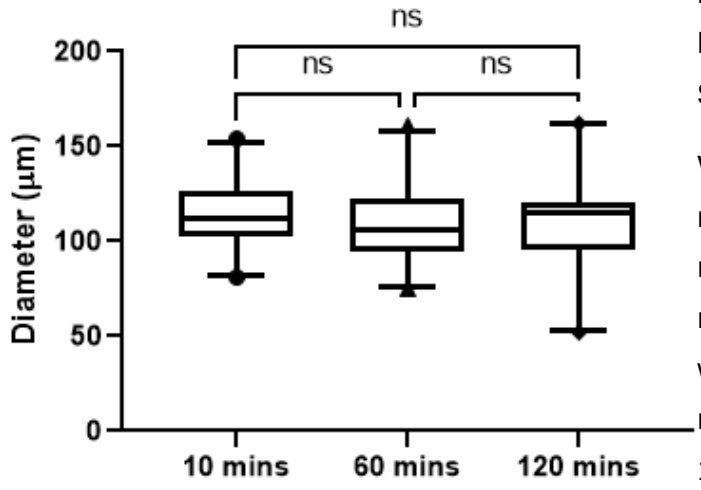

Figure 4.4: Length of dye loading had no effect on diameter of Sprague-Dawley rat VIS-WFAs.

WFAs were loaded in the dark, at room temperature with 1 μg/ml on Nile red and fluorescence intensity was measured at wavelengths of 528nm with a green bandpass filter. 10 mins: n = 54, f = 3; 60 mins: n = 61, f = 4; 120 mins: n = 41, f = 4; Data are expressed as mean ± S.D. (ns = non-significant, one-way ANOVA, Holm-Sidak's multiple comparisons test.

4.4.2 Determination of optimum Nile red concentration for measurement of Nile red release.

To determine the optimum Nile red concentration for measurement of Nile red release, adipocytes were separately incubated with Nile red at concentrations of 1 µg/ml, 5 µg/ml or 10 µg/ml and the effect of the dye concentration on the emitted fluorescence light was measured. To investigate the kinetics of Nile red absorption, the emitted fluorescence light of rat VIS-WFAs was separately evaluated at 10, 60 and 120 minutes for the different dye concentrations.

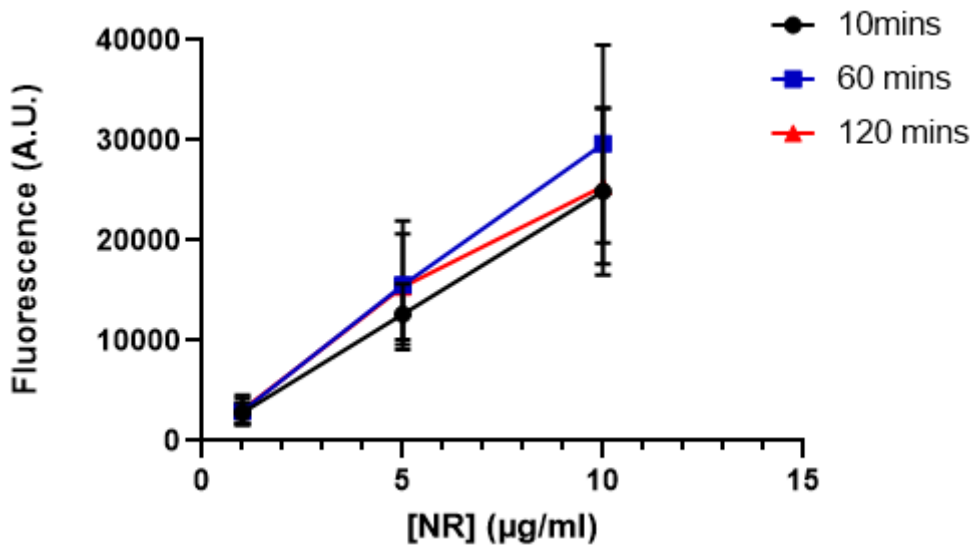

Figure 4.5: Concentration dependence of nile red fluorescence signal intensity of male Sprague-Dawley rat VIS-WFAs at different time points.

WFAs were loaded in the dark, at room temperature with 1 µg/ml, 5 µg/ml or 10 µg/ml nile red and fluorescence intensity was measured at 528nm with a green bandpass filter. (Data are expressed as mean ± S.D.,1 µg/ml: 10 mins: n = 33, f = 2; 60 mins: n = 33, f = 2; 120 mins: n = 33, f = 3; 5 µg/ml: 10 mins: n = 33, f = 2; 60 mins: n = 33, f = 2; 120 mins: n = 33, f = 3; 10 µg/ml: 10 mins: n = 33, f = 3; 60 mins: n = 33, f = 3; 120 mins: n = 33, f = 3; ns = non-significant, two-way ANOVA, Turkey's multiple comparisons test).

The fluorescence emission of rat VIS-WFAs was found to be positively correlated with increasing Nile red concentrations (10 mins: Spearman rank correlation coefficient, r = 0.89, 0.84 to 0.92 95% C.I., $p < 0.0001$; 60 mins: r = 0.8779,

0.8213 to 0.9174 95% C.I., $p < 0.0001$; 120 mins: r = 0.8784, 0.8219 to 0.9177 95% C.I., $p < 0.0001$).

As the fluorescence emission intensity of the adipocytes was linear over the concentration range of Nile red examined and did not saturate, all further experiments were carried out using the dye at a working concentration of 10 µg/ml. Nile red fluorescence stabilisation at lower concentrations took a longer time, and the chosen concentration was within the range previously employed by others (Genicot et al., 2005).

4.4.3 Determination of Nile red release and free fatty acid release from WFAs under various conditions

Following optimisation of dye loading conditions, the release of the absorbed dye under various treatment conditions, including conditions which had been previously shown to increase intracellular calcium in this study (Chapter 3) and other studies, was determined. The release of Nile red from adipocyte was measured as a decline in fluorescence signal intensity and the data expressed as Nile red (NR) loss (in arbitrary units) relative to the zero time point for all treatment conditions.

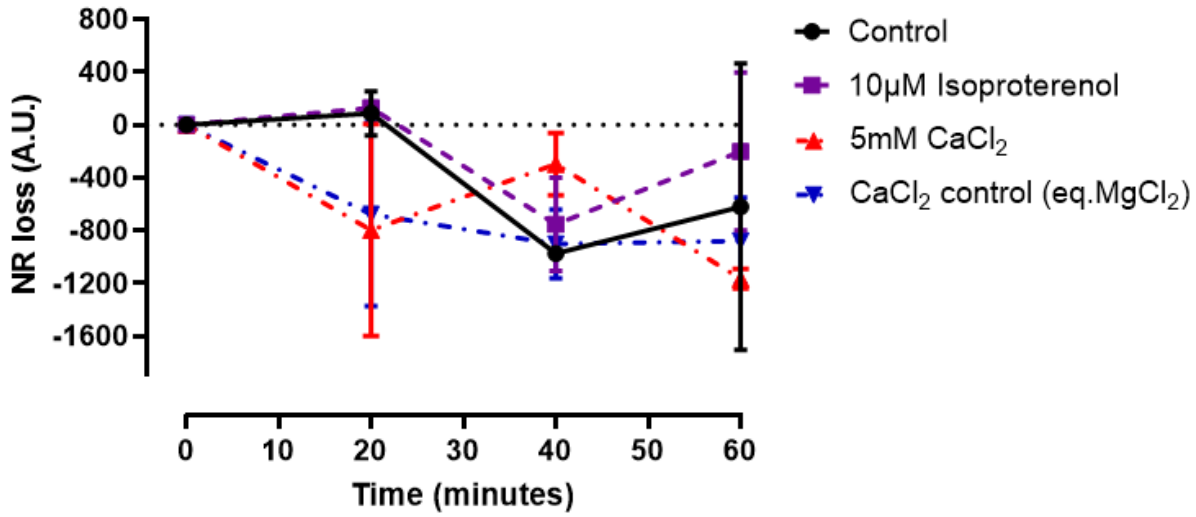

Figure 4.6: Effect of extracellular calcium and isoproterenol on Nile red release from Sprague Dawley VIS-WFAs following a 60 minutes incubation.

Primary VIS-WFAs were loaded with Nile red for 20 minutes in the dark, at room temperature, then washed and separately stimulated with the conditions indicated. The release of Nile red from adipocytes, measured as a decline in fluorescence signal intensity under static incubation conditions for a duration of 60 minutes was monitored. The data are expressed as Nile red (NR) loss (in arbitrary units) relative to the zero-time point for all treatment conditions. Results are mean ± S.D. of two separate experiments (n = 2, f = 59, i = 2).

There was no effect of high extracellular calcium or isoproterenol on Nile red release from rat VIS-WFAs compared to unstimulated control conditions (Figure 4.6). Stimulation of the adipocytes with isoproterenol for 20 minutes did not promote any loss of Nile red and was like control conditions. Dye release from the adipocytes following 40 minutes and 60 minutes of treatment was similar in both isoproterenol treated cells and control cells. Incubation with 5 mM $CaCl_2$ after 40 minutes seemed to inhibit the loss or release of Nile red from the cells compared to other treatment conditions, however this effect of high calcium was not significant. Like the lack of effect of high extracellular calcium conditions on Nile red release, free fatty acid analysis showed comparable effects of 5 mM $CaCl_2$ and control conditions on the release of non-esterified fatty acids from rat adipocytes

(Figure 4.7). In contrast, isoproterenol caused a progressive increase in free fatty acid release from the cells at all time points examined.

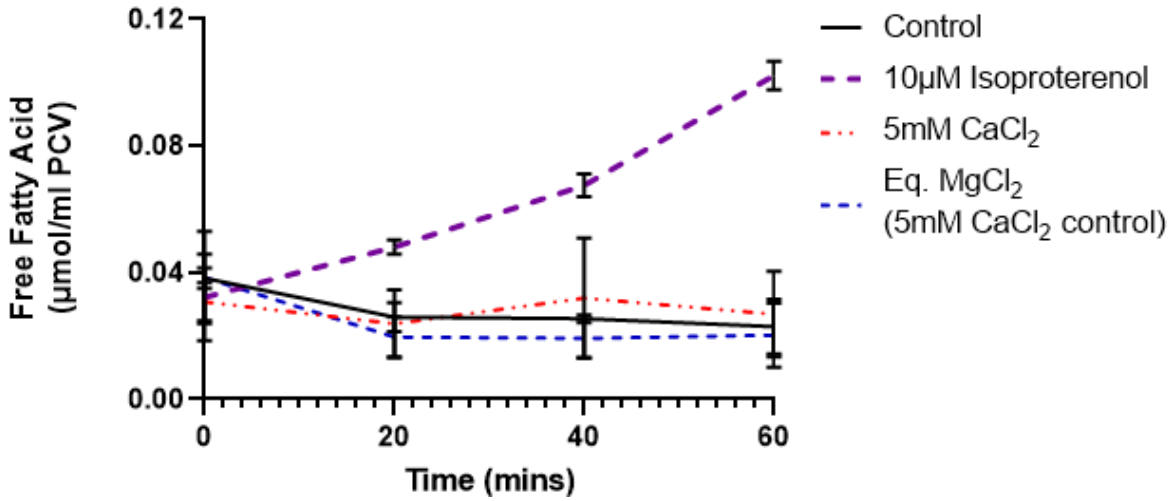

Figure 4.7: Free fatty acid release by Sprague-Dawley rat VIS-WFAs under various conditions and at different time points.

Primary VIS-WFAs were loaded with 10 µg/ml Nile red for 20 mins in the dark at room temperature, then washed and separately stimulated with 10 µM isoproterenol or 5mM $CaCl_2$. Dye release was monitored by fluorescence microscopy and aliquots of the incubation media were collected at the specified times and free fatty acid analysis was performed. Data are expressed as micromoles of FFA per millilitre packed cell volume (PCV) of adipocytes. Results are mean ± S.D. of two experiments; n = 2 biological replicates.

Due to the lack of effect of extracellular calcium on free fatty acid release following one hour of adipocyte stimulation (Figure 4.7), the duration of incubation was extended and the experiment was repeated (Figures 4.8 and 4.9).

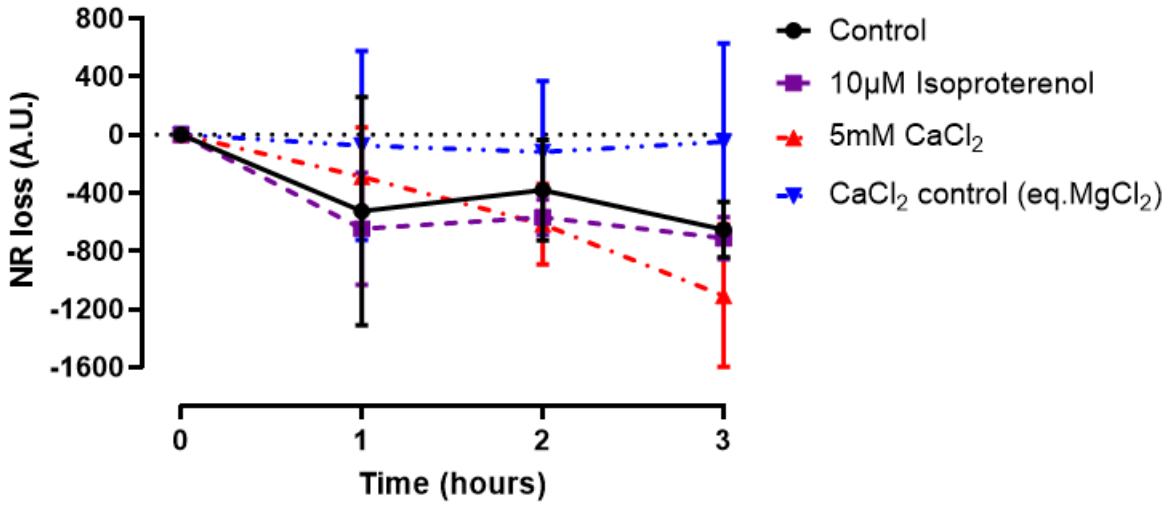

Figure 4.8: Effect of extracellular calcium and isoproterenol on Nile red release from Sprague Dawley rat VIS-WFAs following a 3 hour incubation.

Primary VIS-WFAs were separately loaded with Nile red for 20 minutes in the dark, at room temperature, then washed and separately stimulated with 10µM isoproterenol or 5mM $CaCl_2$. The release of Nile red from adipocytes, measured as a decline in fluorescence signal intensity under static incubation conditions for a duration of 3 hours was monitored. The data are expressed as Nile red (NR) loss (in arbitrary units) relative to the zero time point for all treatment conditions. Results are mean ± S.D. of three separate experiments; (n = 3, f = 69, i = 3).

There was no effect of intracellular calcium promoting conditions or isoproterenol on Nile red release from rat VIS-WFAs compared to unstimulated control conditions (Figure 4.8). Similar to the observation in the shorter experiments, isoproterenol stimulation of dye release from the adipocytes mirrored that seen under control conditions at all-time points examined. Although a progressive increase in Nile red loss was observed in $CaCl_2$ treated cells, this effect was not significant compared to other treatment conditions.

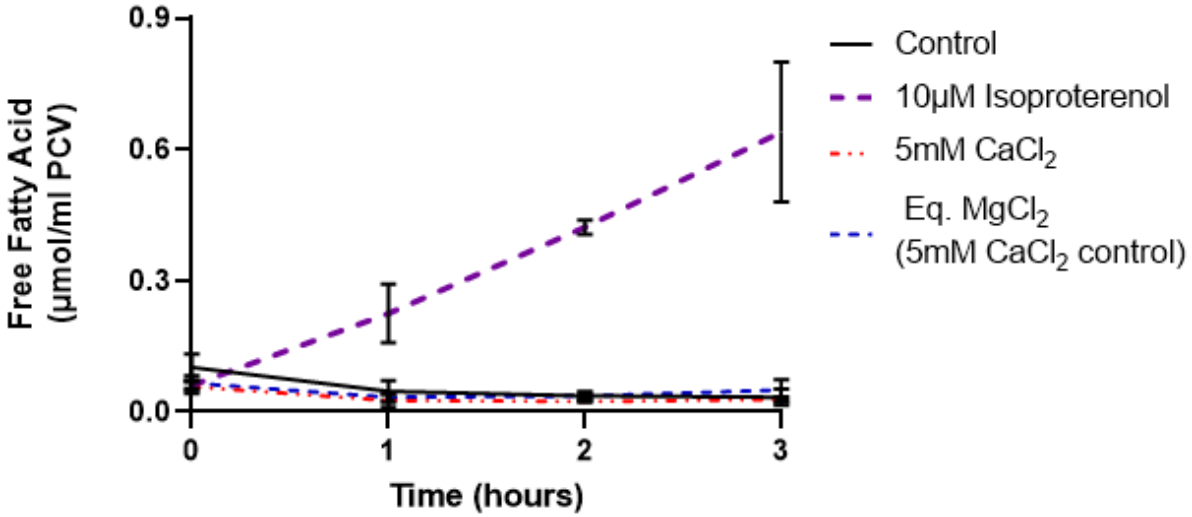

Figure 4.9: Free fatty acid release by rat VIS-WFAs following stimulation by extracellular calcium and isoproterenol for a 3 hour duration.

WFAs were loaded with 10 µg/ml Nile red for 20 mins in the dark at room temperature, then washed and separately stimulated with 10 µM isoproterenol or 5 mM $CaCl_2$. Dye release was monitored by fluorescence microscopy and aliquots of the incubation media were collected at the specified times and free fatty acid analysis was performed. Data are expressed as micromoles of FFA per millilitre packed cell volume (PCV) of adipocytes. Results are mean ± S.D. of three separate experiments; n = 3 biological replicates.

Determination of free fatty acid concentration in the incubation media showed that under static incubation conditions, 5mM extracellular calcium failed to stimulate the release of non-esterifed fatty acids from VIS-WFAs for the 3 hour duration of the incubation (Figure 4.9). Similarly, under basal lipolytic conditions, shown by control experiment with no treatment, there was negligible release of FFAs. In contrast, isoproterenol caused a progressive release of non-esterified free fatty acids from the adipocytes, which was linearly correlated with time (Pearson's r = 0.94, 0.82 to 0.98, 95% C.I., $p < 0.0001$).

4.4.4 Effect of calcitropic hormones on Nile red release and adipocyte lipolysis in Sprague Dawley rat VIS-WFAs

Pilot experiment to study of calcitropic hormones affected the rate of decline in fluorescence signal intensity of Nile red loaded cells. Following Nile red loading of the adipocytes and subsequent incubation with 10 μM isoproterenol, 20 nM rhGH, 100 nM PTH (1-84) or 100 nM oxytocin, with the exception of rhGH, inhibited Nile red loss at the 1 hour post incubation time (Figure 4.10). From 2 hours onwards, rhGH inhibited dye efflux from the adipocytes. Isoproterenol was employed as a positive regulator of adipocyte lipolysis. Both oxytocin and isoproterenol arrested the loss of Nile red from the adipocytes over the 3 hours incubation period. In comparison with the control condition, which is reflective of basal lipolytic conditions, there was a progressive loss of Nile red. Despite the decreased rate of Nile red loss seen with all other treatment conditions other than control, the effect of these hormones on adipocyte release of Nile red was however not significantly different from control conditions. Hence, calcitrophic hormones overall, had no effect on Nile red release from these cells.

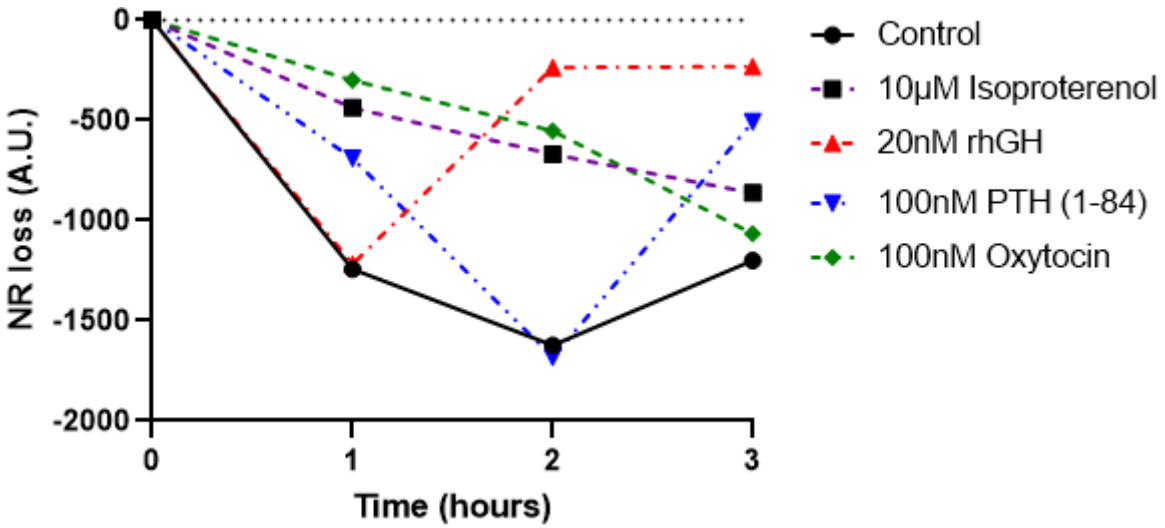

Figure 4.10: Effect of calcitropic hormones on Nile red loss from VIS-WFAs at different time points.

Primary VIS-WFAs were loaded with 10 μg/ml Nile red for 20 mins in the dark at room temperature, then washed and separately stimulated with 10 μM isoproterenol, 20 nM rhGH, 100 nM PTH (1-84) or 100 nM oxytocin. The release of Nile red from adipocytes, measured as a decline in fluorescence signal intensity under static incubation conditions for a duration of 3 hours was monitored. The data are expressed as Nile red (nr) loss (in arbitrary units) relative to the zero time point for all treatment conditions, n = 1, f = 23, i = 1.

Hormones which promote intracellular calcium increases showed no effect on adipocyte lipolysis. Consistent with previous results (Figure 4.9), isoproterenol stimulated a time-dependent release of non-esterified free fatty acids from VIS-WFAs (Figure 4.11). In contrast, 20 nM rhGH, 100 nM PTH (1-84) and 100 nM oxytocin had no lipolytic effect on the adipocytes at all time points examined.

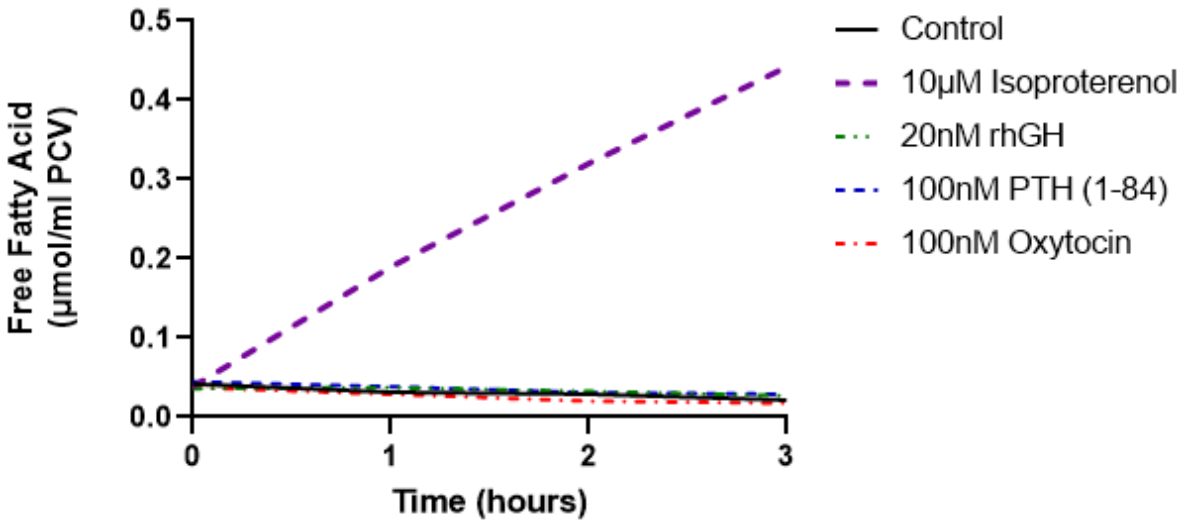

Figure 4.11: Effect of different hormones on free fatty acid release from VIS-WFAs at different time points.

Primary VIS-WFAs were loaded with 10 µg/ml Nile red for 20 mins in the dark at room temperature, then washed and separately stimulated with 10µM isoproterenol, 20nM rhGH, 100nM PTH (1-84) or 100nM oxytocin. Dye release was monitored by fluorescence microscopy and aliquots of the incubation media were collected at the specified times and free fatty acid analysis was performed. Data are expressed as micromoles of FFA per millilitre packed cell volume (PCV) of adipocytes, n = 1.

Although an increase in free fatty acids was observed following adipocyte stimulation with isoproterenol, the experimental conditions were modified. The experimental set-up was changed from a static incubation system with periodic monitoring of adipocyte fluorescence signal intensity to continuous perfusion with continuous monitoring, to prevent re-esterification processes and possibly dye reabsorption by the adipocytes. Due to the challenge of the primary adipocytes being washed away following continuous perifusion for prolonged periods of time differentiated 3T3 cells were used instead since these were well adhered to the coverslips. The even distribution of Nile red loading across the adipocyte lipid droplet was first determined using confocal microscopy, before determination of Nile red release under various conditions.

4.4.5 Nile red was absorbed into the core of the adipocyte lipid droplet

Confocal microscopy showed the distribution of Nile red loading across the lipid droplet of 3T3-L1 adipocytes. Sub-cellular partitioning of Nile red, Hoechst stain and Cell Brite into the adipocyte lipid droplet, nucleus and cell membrane respectively was confirmed by image analysis (Figure 4.12). Examination of Nile red spatial distribution within the adipocyte lipid droplet showed that the lipophilic marker was evenly absorbed to the core of the adipocyte lipid droplet (Figure 4.13). Also, fluorescence intensity of the adipocyte was independent of the size of the lipid droplet within the adipocyte, inferred by visual inspection of the cells.

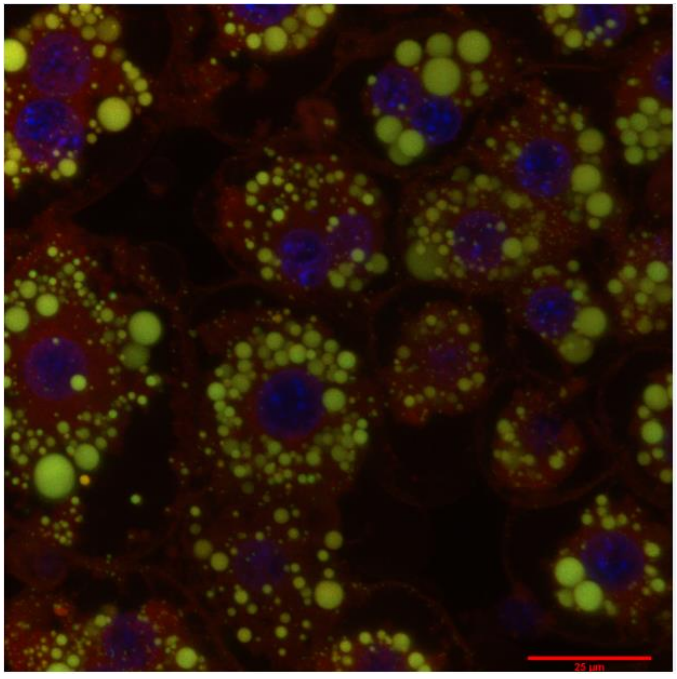

Figure 4.12: Sub-cellular fractionation of Nile red into the lipid droplet of 3T3-L1 adipocytes

Confocal imaging of 3T3-L1 adipocytes showed the sub-cellular fractionation of Nile red within the cell. Yellow-gold - lipid droplet stained with Nile red, blue – nucleus stained with Hoechst stain, red – cell membrane stained with Cell brite. Scale bar = 25 µM.

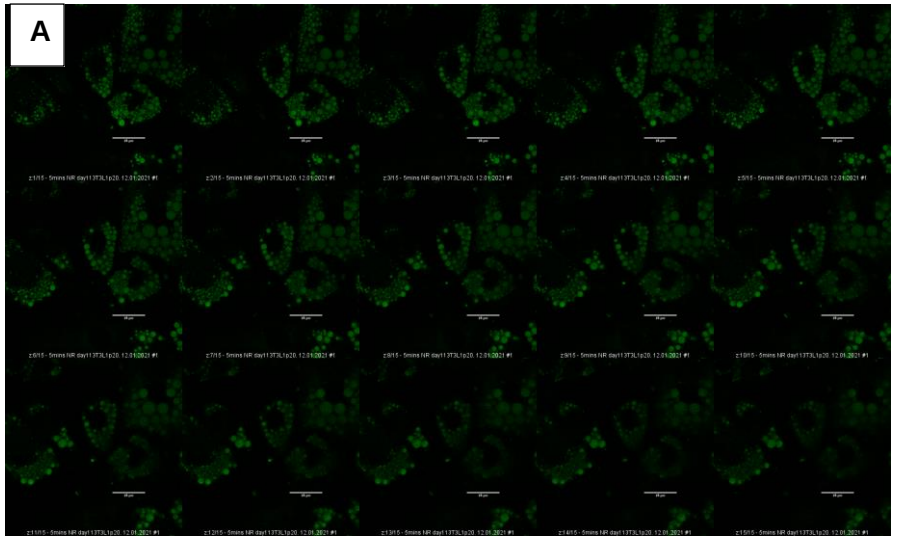

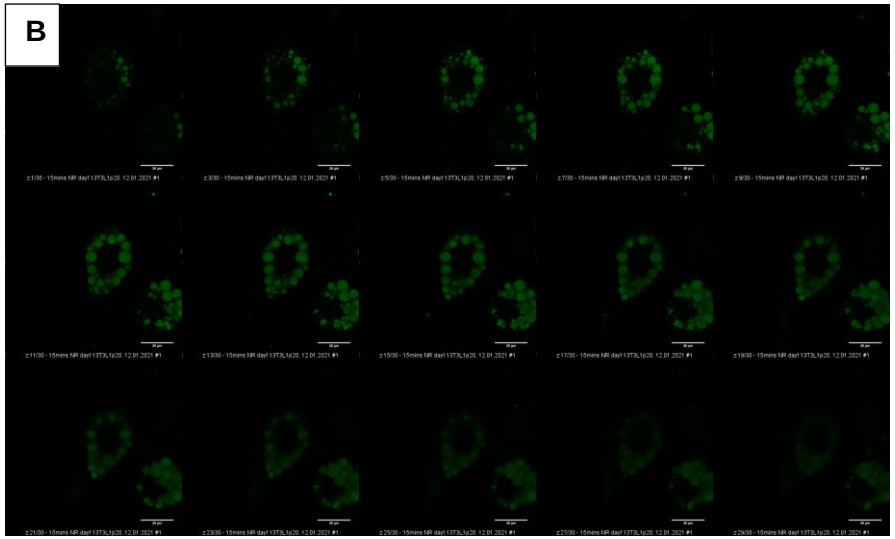

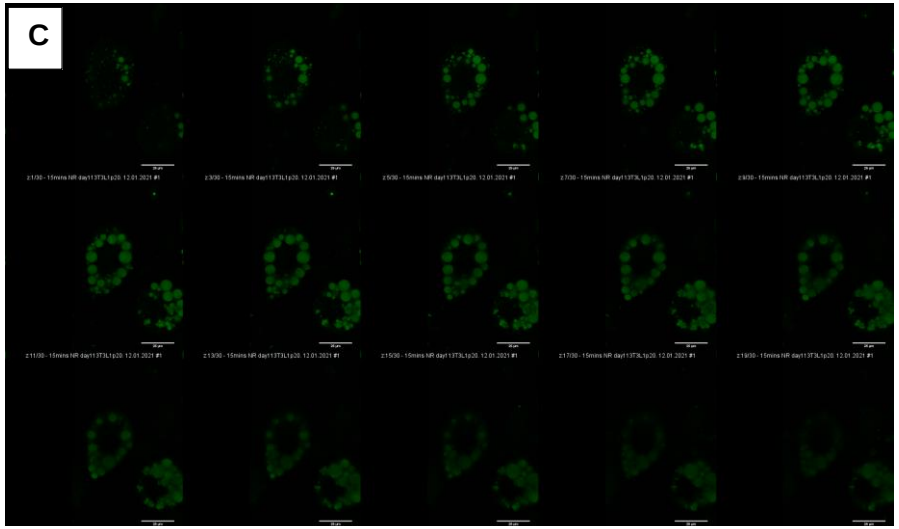

Figure 4.13: Spatial distribution of Nile red in 3T3-L1 adipocytes

Z-stacks of 3T3-L1 adipocytes loaded with Nile red for **(A)** 5 minutes (15 slices) **(B)** 15 minutes (30 slices) and **(C)** 30 minutes (17 slices), to show distribution of the lipophilic marker into the core of the adipocyte lipid droplet. Scale bar = 25 µM.

4.4.6 Effect of lipolytic and calcitropic hormones on Nile red release from 3T3-L1 adipocytes

Following confirmation of Nile red absorption into the core of the adipocyte lipid droplet and its homogeneous spatial distribution, the effect of isoproterenol, rhGH and oxytocin on Nile red release from 3T3-L1 adipocytes was monitored. This was under conditions of incubation by continuous perfusion and continuous monitoring of fluorescence emission for 90 minutes at 37°C. Nile red loss, expressed as percentage change in Nile red fluorescence from the zero time point (basal), with negative values signifying fluorescence quenching due loss of dye molecules from the adipocyte and positive values signifying fluorescence enhancement.

A progressive decline in Nile red fluorescence, signifying Nile red release from the adipocytes, was observed under all experimental conditions, including control cells incubated with Hanks buffer only (Figure 4.14). There was no difference of the different stimulatory conditions on Nile red release from the differentiated 3T3-L1 adipocytes, with exception of the 90 minute time point at which isoproterenol was more effective at stimulation Nile red release than unstimulated control conditions (Figure 4.15).

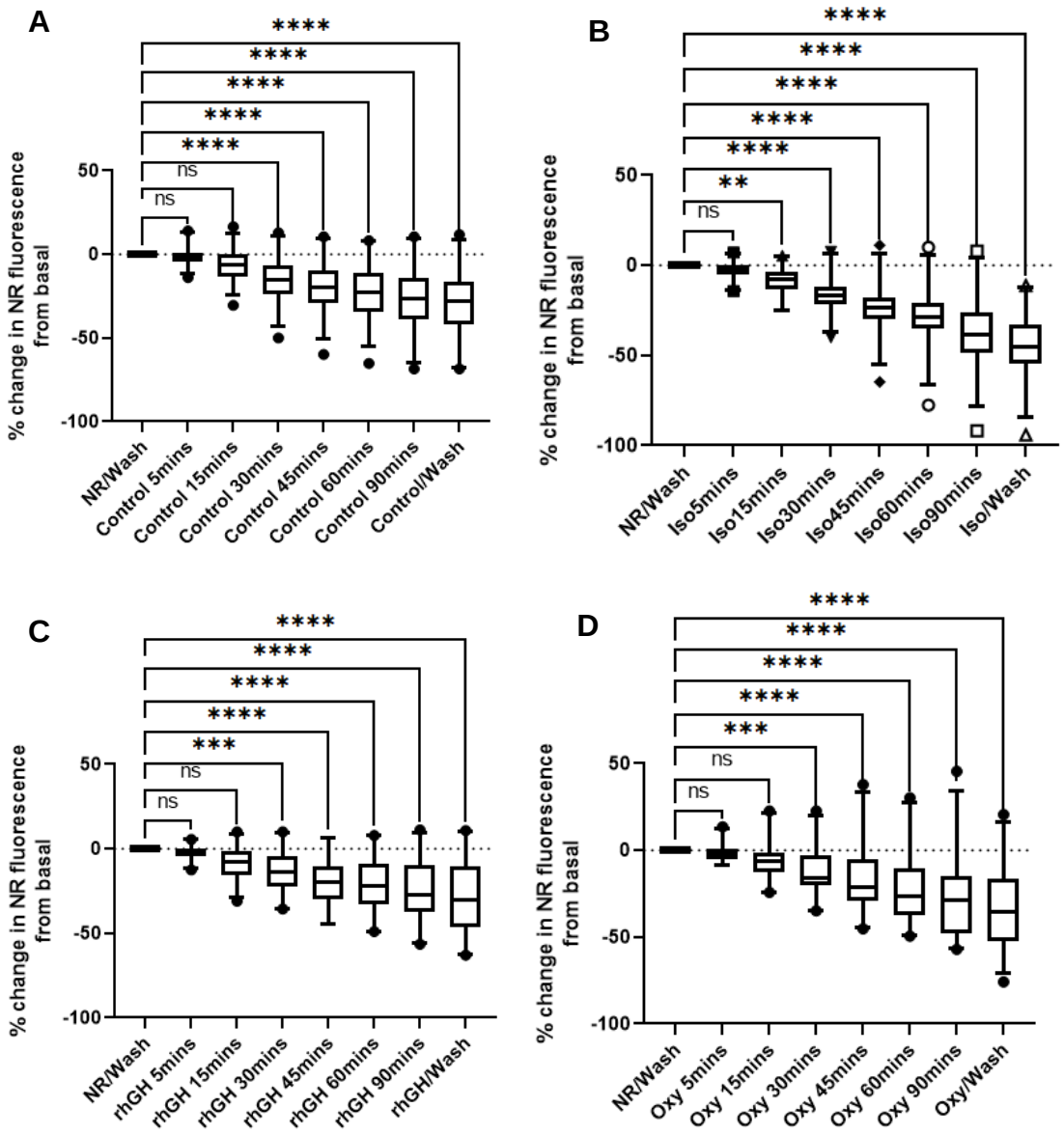

Figure 4.14: Time course effect of lipolytic and calcitropic hormones on Nile red release from differentiated 3T3-L1 adipocytes.

(A) The basal decline in Nile red fluorescence from 3T3-L1 adipocytes occurred from 30 mins onwards (n = 58; f = 4; i = 4). **(B)** 10 µM isoproterenol elicited a progressive decline in Nile red fluorescence from 3T3-L1 adipocytes from 15 mins onwards; n = 53; f = 3; i = 3. **(C)** 20 nM recombinant human growth hormone (rhGH) (n = 42; f = 4; i = 3) and **(D)** 100 nM oxytocin (n = 42; f = 4; i = 3) elicited a progressive decline in Nile red fluorescence from 3T3-L1 adipocytes from 30 mins onwards; Data are expressed as box and whisker plots showing median, interquartile range, 2.5 and 97.5% confidence intervals (***P < 0.001, ****P < 0.0001, ns = non-significant; Friedman's test).

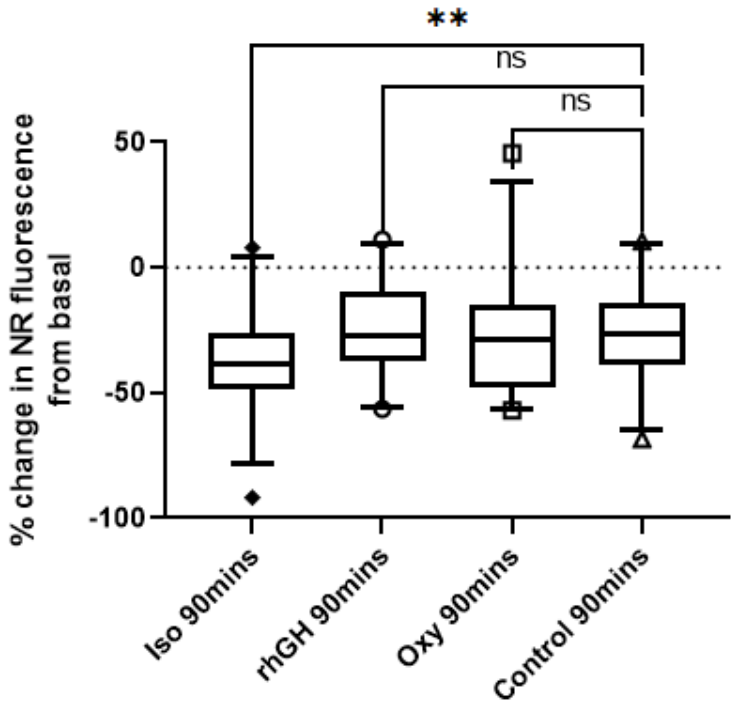

Figure 4.15: Nile red release from 3T3-L1 adipocytes was promoted by isoproterenol

The decline in Nile red fluorescence from 3T3-L1 adipocytes under control conditions by 90 minutes of incubation was significantly lower than that observed under stimulated conditions by 10 μM isoproterenol. Data are expressed as box and whisker plots showing median, interquartile range, 2.5 and 97.5% confidence intervals (**P < 0.01, ns = non-significant; Kruskal-Wallis's test).

Following the observation of Nile red release from 3T3-L1 adipocytes in 10μM isoproterenol and the calcitropic hormones, the ability of primary adipocytes from mice to release stored lipophiles from primary adipocytes under similar experimental conditions was investigated. Neither 10 μM isoproterenol nor 20 nM rhGH promoted Nile red release from primary mouse adipocytes (Figure 4.16), instead, a progressive increase in Nile red fluorescence signal intensity was observed. Under control conditions, representative of basal lipolytic conditions, an increase in Nile red fluorescence from 45 – 60 minutes of adipocyte monitoring was observed.

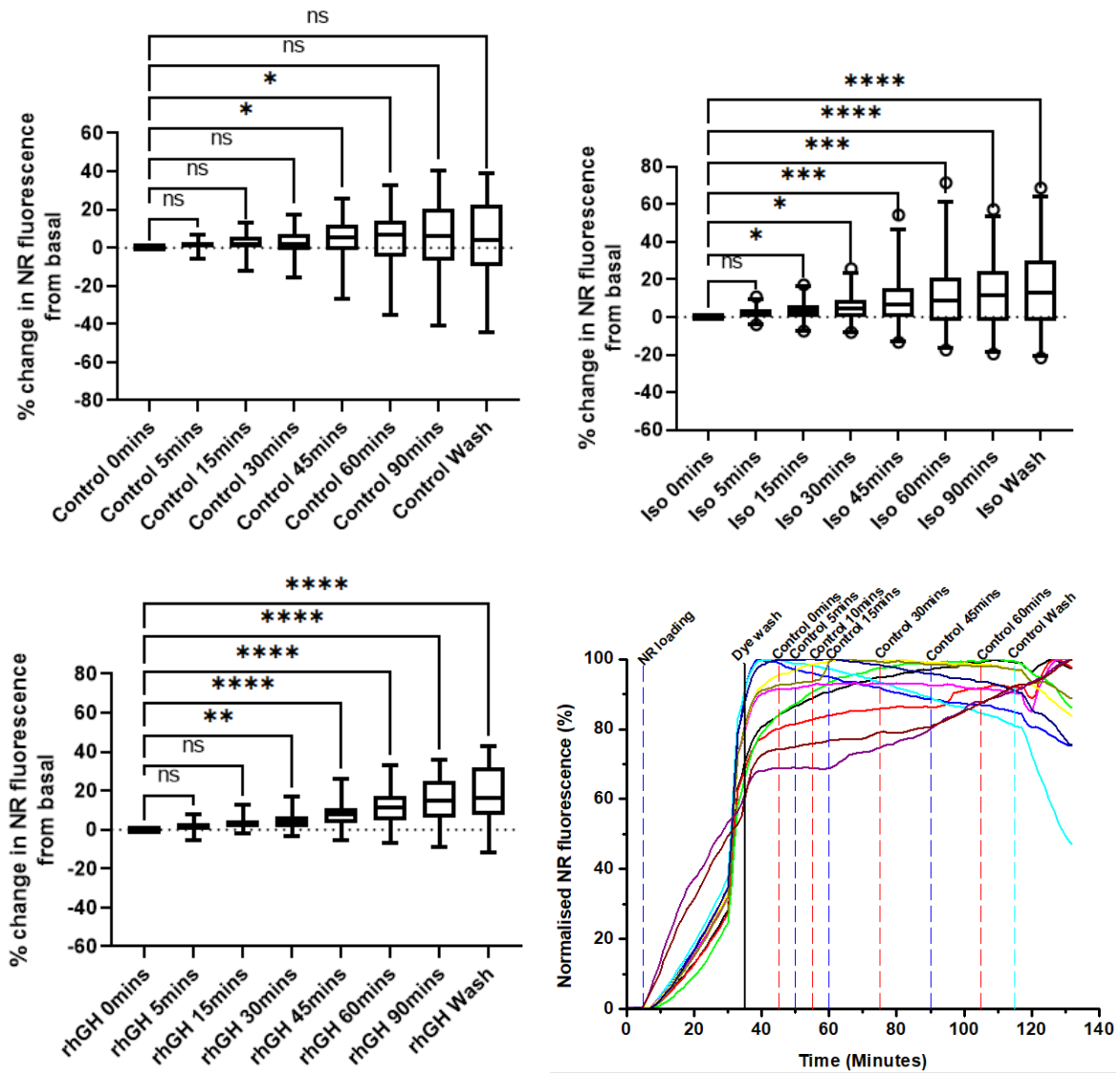

Figure 4.16: Time course effect of lipolytic and calcitropic hormones on Nile red release from CD1 mice VIS-WFAs.

(A) Under control conditions, Nile red loss, expressed as percentage change in Nile red fluorescence from the zero time point (basal) was not observed (n = 36; f = 4; i = 4). **(B)** 10μM isoproterenol; n = 50; f = 4; i = 3 and **(C)** 20nM recombinant human growth hormone (rhGH) (n = 33; f = 3; i = 3) failed to elicit the release of Nile red from CD1 mice VIS-WFAs.; Data are expressed as box and whisker plots showing median, interquartile range, 2.5 and 97.5% confidence intervals (*P < 0.05, **P < 0.01, ***P < 0.001, ****P < 0.0001, ns = non-significant; Friedman's test). **(D)** A representative trace of 13 cells within the same field of view showing nile red loading and release by CD1 male VIS-WFAs, under control conditions.

Although a decline in Nile red fluorescence signifying Nile red release was observed in some CD1 mouse adipocytes (Figure 4.16D), the cumulative effect in all treatment conditions was an increase in Nile red fluorescence signal intensity. There was no difference in the magnitude of Nile red fluorescence enhancement under various treatment conditions from the CD1 mice adipocytes, with exception of the 60 minute time point at which rhGH effectively inhibited dye release compared to unstimulated control conditions (Figure 4.17).

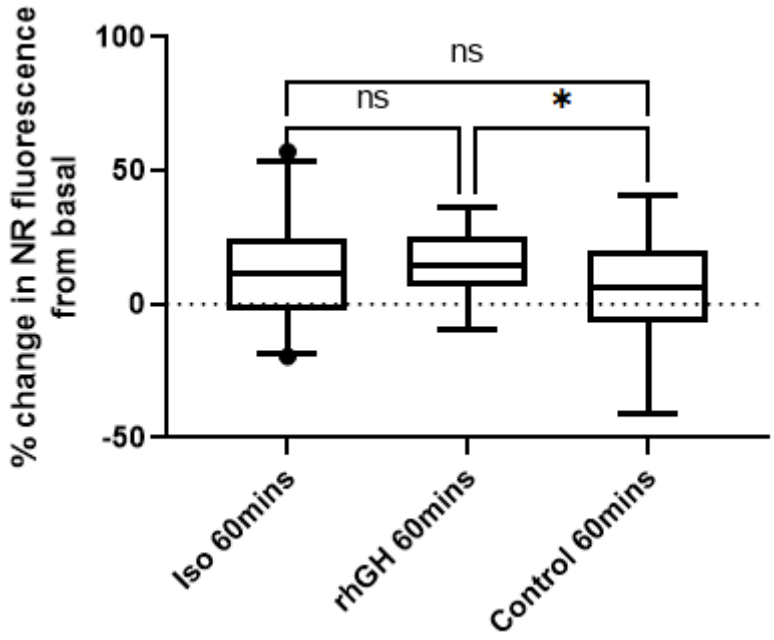

Figure 4.17: Nile red release was inhibited in CD1 mice VIS-WFAs

Recombinant human growth hormone elicited a higher magnitude of effect than control conditions on inhibition of Nile red release from CD1 mice adipocytes by 60 minutes. Data are expressed as box and whisker plots showing median, interquartile range, 2.5 and 97.5% confidence intervals (*P < 0.05, ns = non-significant; Holm Sidak's test).

4.5. Discussion

4.5.1 Nile red fluorescence signal intensity is both time and concentration dependent

The optimal time window and dye concentration for monitoring white adipocyte release of stored lipophiles by Nile red fluorescence was determined to be 20 minutes loading time at 10 µg/ml of Nile red (Figure 4.5). The fluorescence signal intensity of Nile red loaded adipocytes was seen to be dependent on both dye concentration and length of dye loading. An increase in dye concentration led to a progressive increase in the emitted fluorescence, which was linearly correlated. The choice of Nile red at a concentration of 10µg/ml was due to the need for up to 20 minutes of loading time for the primary adipocytes to reach maximal fluorescence. Also, Nile red at this concentration, is within the range previously employed by other studies (Genicot et al., 2005). Additionally, it is recommended that Nile red be used at the highest concentration that gives a linear and stable signal (Pick and Rachutin-Zalogin, 2012). At lower dye concentrations, the stabilisation of Nile red fluorescence took a longer time.

Yet, the kinetics of Nile red fluorescence has not been studied in primary white adipocytes. In algae, Nile red fluorescence quenching, resulting from self-interactions of lipid droplet associated dye molecules, has been reported to occur within 5 minutes to 1 hour depending on the species (Pick and Rachutin-Zalogin, 2012). Nile red fluorescence quenching is also dependent on dye concentration and is eliminated at low dye concentrations. The decline in Nile red fluorescence seen at 120 mins post dye addition to the cells could be due to quenching of the dye fluorescence at that concentration. It was observed that the adipocytes exhibit a heterogenous response both in their absorption and release of Nile red. This is

agrees with an earlier observation of the heterogenous nature of intracellular calcium response of WFAs to calcitropic conditions.

4.5.2 Nile red was evenly distributed across the adipocyte lipid droplet

The cellular uptake of Nile red is thought to occur by passive diffusion of dye molecules (Snipstad et al., 2014), initially past the cell membrane and then into the core of the lipid droplet (Pick and Rachutin-Zalogin, 2012, Ramírez-Castrillón et al., 2021). The distribution of Nile red loading across the adipocyte lipid droplet was determined with confocal microscopy to confirm the absorption of the dye within the core of the adipocyte lipid droplet and even distribution of the dye across the cell. As previous Nile red release experiments carried out on primary rat adipocytes showed an increase in Nile red fluorescence signal intensity later after an initial decline, suggesting dye reabsorption, there was need to confirm that the lipophilic marker was absorbed into the core of the adipocyte lipid droplet during the dye loading period. Z-stacks of the dye loaded 3T3-L1 adipocytes showed that the cells absorbed the Nile red dye in as soon as 5 minutes following incubation, and that this was homogeneous in topological distribution with no obvious radial gradients.

Although fluorescent dyes such as Nile red have been stated to have limitations in their specificity for the lipid droplet, such as the localisation to cellular lysosomal phospholipid inclusions (Brown et al., 1992, Daemen et al., 2016), confocal microscopy revealed that Nile red was well absorbed into the core of the adipocyte lipid droplet. In addition, the emitted fluorescence from Nile red loaded adipocytes was band-pass filtered at a wavelength below the optimum emission peak of 600 nm, although this has previously been confirmed to still be within the range for detection of Nile red from the neutral lipid laden core of white adipocytes

(Greenspan and Fowler, 1985, Genicot et al., 2005, Daemen et al., 2016). Fluorescence detection of Nile red absorption by membrane phospholipids is at a wavelength above 600nm (Pick and Rachutin-Zalogin, 2012, Daemen et al., 2016).

4.5.3 High extracellular calcium and isoproterenol had no effect on the release of Nile red from primary adipocytes compared to basal conditions

The comparable effects and similar pattern of Nile red release from primary adipocytes subjected to 3 hours of isoproterenol stimulation and basal conditions suggests that non-physiological processes may have contributed to the observed dye efflux. The lack of effect of both isoproterenol and intracellular calcium promoting conditions on the release of Nile red from rat VIS-WFAs could be due to the reabsorption of released dye molecules by the adipocyte lipid droplet. It is likely that self-associated dye molecules become dissociated with the release of Nile red, resulting in a steady-state or even increased fluorescence signal intensities following stimulation of the fat cell by treatment agents. Possibly, the experimental setup employed in this study was not suitable for continuous and error-free monitoring of Nile red release from the lipid laden core of the adipocyte lipid droplet. Application of the recently developed transgenic lipid droplet reporter method by Lumaquin et al. (2021), for live imaging of lipid droplet dynamics over time could allow a more efficient monitoring of lipophilic compound release during lipolytic conditions from the adipocyte lipid droplet, than was employed in this study. In addition, tracking the levels of lipid-droplet associated proteins by immunofluorescent methods, using antibodies conjugated to fluorophores such as green fluorescent protein, could allow a more reliable assessment of the effect of

calcitropic conditions on lipolysis, and its the correlation with adipocyte release of stored lipophiles.

4.5.4 High intracellular calcium promoting conditions had no effect on FFA release from primary adipocytes

In this study, it was observed that conditions which had unequivocally been shown to increase WFA intracellular calcium levels had no effect on free fatty acid release from WFAs. The concentration of free fatty acids released within one hour of incubation under control conditions, representative of basal lipolysis, was negligible and comparable to that released by the adipocytes following stimulation with 5 mM $CaCl_2$ or its control (eq. $MgCl_2$) (Figure 4.7 and 4.9). Despite the increase in the length of adipocyte stimulation from one hour (Figure 4.7) to 3 hours (Figure 4.9), 5 mM extracellular calcium failed to elicit a measurable release of free fatty acids from the adipocytes.

Perilipin (PLIN) is the most abundant protein expressed on the surface of adipocyte lipid droplets and is the major substrate of cAMP-dependent protein kinase (PKA) during stimulated lipolysis. With PKA stimulation, the activity of ATGL is increased by 20-fold, through its coactivator, comparative gene identification-58 (CGI-58). Perilipin acts as a sink for CGI-58 and is reported to sequester CGI-58 from ATGL under basal conditions (Miyoshi et al., 2008). Of the three main lipolysis-associated proteins (ATGL, HSL and PLINA), PLIN A expression has the most effect on basal (constitutive lipolysis) (Miyoshi et al., 2008). Over-expression of PLIN A in MEF adipocytes caused a dramatic decrease in glycerol and fatty acid release. The absence of FFA release under basal lipolytic conditions from rat VIS-WFAs, may thus be explained by an inhibitory effect of PLIN on ATGL activity on the surface of the adipocyte lipid droplet.

With regards to high extracellular calcium and calcitropic hormones, the result from this study suggests the anti-lipolytic effects of high intracellular calcium conditions in primary rat adipocytes. Similar observations of the lack of effect of high intracellular calcium promoting conditions on free fatty acid release were made in primary mouse adipocytes and in 3T3-L1 adipocytes. Isoproterenol which is a known lipolytic agent was employed as a positive regulator of adipocyte lipolysis, and its lipolytic potential after addition to the cells was confirmed at all the time points examined. A recent study has shown maximal stimulation of cAMP by isoproterenol in as soon as 5 minutes of isoproterenol addition to the adipocytes. Also, lipolysis, determined by glycerol release, proceeded at a maximal rate and was sustained at this rate for at least 15 minutes (Jönsson et al., 2019). In this study, 10 μM isoproterenol stimulated WFA lipolysis within 20 minutes of addition to the cells. The magnitude of isoproterenol stimulated lipolysis was seen to be linearly correlated with time.

4.5.5 Correlation between adipocyte lipolysis and Nile red release in rat VIS-WFAs

The observations in this study did not show any correlation between adipocyte lipolysis and Nile red release from rat VIS-WFAs. Although isoproterenol efficiently stimulated adipocyte lipolysis in a time-dependent manner, the resulting increase in free fatty acids was not mirrored by a simultaneous increase in Nile red release from the same cells. With both 10 μM isoproterenol and 5 mM $CaCl_2$, Nile red was still lost at a similar rate to control from primary rat adipocytes. However, the non-linear pattern of Nile red fluorescence decrease in isoproterenol treated cells and the time of dye loss, measured as Nile red fluorescence decrease with time in both isoproterenol and $CaCl_2$ treated cells, suggests that both processes may not

have occurred simultaneously. Also, the lack of effect of 5 mM $CaCl_2$ on free fatty acid release supports a discordance in the simultaneous occurrence of Nile red release and lipolysis in the same cells.

4.5.6 Calcium promoting hormones and isoproterenol caused the release of Nile red from 3T3-L1 adipocytes, but not CD1 mouse adipocytes

The change in the experimental set-up from a static incubation system with periodic measurement of the adipocytes' dye content through Nile red fluorescence measurement, to incubation by continuous perfusion and continuous fluorescence emission monitoring system, resulted in the increase in dye loss from the 3T3-L1 adipocytes. Nile red loss was expressed as percentage change in Nile red fluorescence from the zero time point (basal) for all treatment conditions, with negative values signifying fluorescence quenching due loss of dye molecules from the adipocyte and positive values signifying fluorescence enhancement. The choice of time intervals for measurement of fluorescence signal intensity levels was based on the knowledge that some hormones stimulate calcium release and/or exert their effect in as little as 5 minutes following stimulation of the adipocytes. For instance, oxytocin causes transient release of stored intracellular calcium from endoplasmic reticulum stores in as soon as 5 minutes, while hormones such as growth hormone cause sustained calcium influx through plasma membrane calcium channels into the adipocyte. As a result, the chosen time intervals allowed examination of the effect of both modes of calcium entry on Nile red release from these cells.

The absence of perilipin in 3T3-L1 adipocytes (Brasaemle et al., 2000, Miyoshi et al., 2008, Bézaire and Langin, 2009), may explain the observed effect of the time course and rate of Nile red release under control conditions being like that under

stimulated conditions, possibly due to similar rates of lipolysis in both conditions. As free fatty acid assay could not be performed on collected media from this experiment, the correlation between Nile red release and lipolysis in CD1 VIS-WFAs and 3T3-L1 adipocytes could not be inferred. Although a decline in Nile red fluorescence was observed in some CD1 mouse adipocytes, the cumulative effect in all treatment conditions was an increase in Nile red fluorescence signal intensity.

4.6 Conclusion

High intracellular calcium promoting conditions appeared to impair lipolysis in primary rat adipocytes and possibly rate of mobilisation of fat stored lipophiles in primary rat and mouse adipocytes. In addition to a lack of effect of intracellular calcium promoting conditions on Nile red release from primary adipocytes, fluorescence enhancements in the primary adipocytes could have resulted due to dequenching of interacting dye molecules. Nile red loss from 3T3-L1 adipocytes, even in control conditions, could be attributed to the absence of perilipin coating on the adipocyte lipid droplet. Non-regulated lipolysis occurring in these cells could have significantly contributed to the release of fat stored lipophiles, irrespective of stimulatory conditions. Free fatty acid analysis would have allowed determination whether the decrease in Nile red seen in 3T3-L1 cells was physiologically stimulated. The Nile red results should however be interpreted with caution due to the question of suitability of Nile red as a surrogate for fat-stored POP and sensitivity of the experimental technique employed for determination of Nile red release.

CHAPTER FIVE

General Discussion

5.1 Discussion

The aetiology of metabolic disorders such as type 2 diabetes and obesity has been shown to include derangements in physiological processes of WFAs such as lipolysis, as well as exposure to highly lipophilic persistent organic pollutants. These lipophilic fat stored compounds capable of causing metabolic derangements are said to be obesogenic and diabetogenic and are gradually released from the adipose tissue during the lipolytic process. This study set out to characterise the expression of Ca_V channels in WFAs at the protein level and determine the functional expression and regulation of the identified channels by measurement of intracellular calcium. As intracellular calcium signalling plays a role in lipolysis, the effect of intracellular calcium on WFA lipolysis was explored by measurement of FFA release under conditions known to unequivocally increase intracellular calcium. In addition, the correlation between lipolysis and release of fat stored obesogenic and diabetogenic compounds was explored using Nile red as a marker for lipophilic fat stored compounds.

Western blotting showed the molecular expression of the α_1 subunit of $Ca_V1.2$ channels, which was differentially expressed in the plasma membrane of primary WFAs and 3T3-L1 adipocytes. The detected protein of ~290 kDa is thought to be an extended splice isoform or a post-translationally modified form of the canonical neuronal $Ca_V1.2$ α_1 subunit protein at 250 kDa. This large protein, detected only in adipocytes (primary cells and cell lines), was absent in 3T3-L1 pre-adipocytes. The undifferentiated adipocytes instead expressed a $Ca_V1.2$ α_1 subunit protein at

210 kDa, similar to the control tissue – rat brain. A $Ca_V3.1$ α_1 subunit protein at 265 kDa was detected in 3T3-L1 pre-adipocytes, similar to rat brain tissue. The absence of the $Ca_V3.1$ α_1 subunit protein in mature adipocytes, suggests a key role of the channel in adipocyte development and maturation. Proteomic analysis detected the unique peptide sequences specific to $Ca_V1.2$ α_2/δ_1 subunit in rat visceral and subcutaneous fat cells, an accessory subunit necessary for $Ca_V1.2$ α_1 subunit functioning.

Calcium imaging showed that the molecularly expressed Cav channels in white fat cells are functional, and are indeed L-type in nature. This was determined by sensitivity of the growth hormone and high extracellular calcium mediated calcium signals to inhibition by L-type calcium channel antagonists. Intracellular calcium signalling in male CD1 visceral adipocytes were seen to be unaffected by manipulation to extracellular chloride, an ion shown by previous research to be majorly involved in the regulation of adipocyte membrane potential. Although increases in intracellular calcium was seen with elevation of extracellular potassium, it is likely that other mechanisms such as reverse mode of sodium calcium exchange and potassium dependent calcium exchange could have contributed to the observed increase in intracellular calcium. The detected Ca_V channels in the study were sensitive to hormonal regulation, as both recombinant human growth hormone and the full length parathyroid hormone (1-84), but not parathryroid hormone (1-34), modulated channel activity as seen with increase in intracellular calcium.

Measurement of changes in fluorescent intensity of adipocytes loaded with nile red, a highly lipophilic fluorescent dye, showed that conditions which unequivocally increase intracellular calcium, such as elevation of extracellular calcium and

stimulation by rhGH, as well as the lipolytic hormone, isoproterenol, had no effect on the release of fat stored compounds in primary white fat cells. In contrast to the observations with nile red release, free fatty acid analysis confirmed the lipolytic effect of isoproterenol, but not elevation of intracellular calcium on the adipocytes. It seems that the experimental design employed in this study may not have been sensitive enough to detect the loss of nile red against the backdrop of the lipid laden core of the adipocyte. These results however validate previous research which have shown the expression of Ca_V channels in white adipocytes at the gene level and have extended our understanding of the functioning and regulation of these channels in fat cells.

This study has shown functional expression of $Ca_V1.2$ channels, and also the anti-lipolytic effects of high intracellular calcium conditions in primary rat adipocytes. It seems that on one hand, the activity of these channels being antilipolytic, confers a protective effect on the body, with regards to holding in accumulated obesogenic and diabetogenic compounds. The slowed release of these fat-stored lipophilies protects other vital organs of body from the toxic effects resulting from exposure to these compounds. On the other hand, antilipolytic effects of Ca_V channel activity in WFAs could exacerbate the obesity phenotype, by promoting accumulation of neutral lipids and hypertrophy of the fat cell.

5.2 Limitations of study

Some of the challenges encountered with the use of nile red fluorescence to monitor lipophile release from the adipocyte lipid droplet could be attributed to the limitations of nile red dye as a neutral lipid specific dye. For instance, the nonspecific binding of nile red to lipophilic sites other than the adipocyte lipid droplet results in a high fluorescence background (Tatenaka et al., 2019). Also,

concerns relating to variations in nile red fluorescence signal intensities have been pointed out (Pick and Rachutin-Zalogin, 2012) and are due to photobleaching or instability of the molecule (Ramírez-Castrillón et al., 2021). These limitations can confound long-term monitoring of lipid droplet dynamics with nile red as was intended in this study. It is also possible that with the white adipocyte acting like a sink for lipophilic compounds, the amount of nile red being released by the primary adipocytes may be too little to detect and/or measure against the backdrop of the magnitude of the nile red dye within the core of the fat cell.

5.3 Recommendations for further studies

Additional experiments may need to be carried out to validate some of the findings in this study. For instance, the $Ca_V1.x$ agonists, Bay-K8644 and FPL 64176, were without effect on intracellular calcium in male CD1 mice VIS-WFAs. The effect of these agonists on calcium influx in high extracellular potassium conditions or in the presence of other conditions shown here to promote intracellular calcium increase such as rhGH or PTH(1-84), could be explored. Also, determination of the sensitivity of PTH(1-84) mediated calcium influx to $Ca_V1.x$ antagonists and in calcium-free buffer conditions could be carried out, to unequivocally confirm the involvement of Ca_V channels and dependence on extracellular calcium in PTH(1-84) action in this cell type. The involvement of potassium dependent sodium calcium exchanger in intracellular calcium increases due to elevation of extracellular potassium by sodium substitution, could be further explored using specific blockers for the for NCKX, as NCX blockers such as KB-R7943 have no effect on this exchanger.

There is also need for more repeats as well as additional experiments for nile red release and free fatty analysis respectively. Although the results in this study

suggest a lack of effect of intracellular calcium promoting conditions on nile red and free fatty acid release in rat primary adipocytes, additional experiments employing calcium channel antagonists such as verapamil, to block calcium entry and measurements under calcium-free conditions need to be performed. This will help validate the observations in this study and also help establish the actual contribution of intracellular calcium on adipocyte lipolysis and in the aetiology of metabolic disease development.

5.4 Conclusion

This study has shown the molecular expression of the α_1 subunit of $Ca_V1.2$, as well as its accessory α_2/δ_1 subunit in visceral and subcutaneous primary WFAs. The detected channels were seen to be functional in mediating calcium transients and seem to be predominantly sensitive to hormonal regulation. The role of these channels in the physiological functioning of the fat cell was explored. However, further experiments are needed to advance our knowledge and understanding of the role of these channels in white fat adipocyte lipolysis and release of fat stored lipophiles. Additionally, considering the role of intracellular calcium in adipogenesis and development of the obesity phenotype, Ca_V channels in WFAs may be potential therapeutic targets for the management of uncontrolled lipolysis in hypertrophic dysfunctional adipocytes.

REFERENCES

AASETH, J., JAVORAC, D., DJORDJEVIC, A. B., BULAT, Z., SKALNY, A. V., ZAITSEVA, I. P., ASCHNER, M. & TINKOV, A. A. 2022. The Role of Persistent Organic Pollutants in Obesity: A Review of Laboratory and Epidemiological Studies. *Toxics,* 10, 65.

AHIMA, R. S. 2006. Adipose tissue as an endocrine organ. *Obesity,* 14.

AHIMA, R. S. & FLIER, J. S. 2000. Adipose tissue as an endocrine organ. *Trends in Endocrinology & Metabolism,* 11, 327-332.

AHMADIAN, M., WANG, Y. & SUL, H. S. 2010. Lipolysis in adipocytes. *The international journal of biochemistry & cell biology,* 42, 555-559.

AKANIRO-EJIM, N. E. & SMITH, P. A. 2021. Intracellular Ca2+ in Mouse White Fat Adipocytes: Effects of Extracellular Anions, Growth Hormone, and Their Interaction with Ca2+ Influx. *Bioelectricity,* 3, 282-291.

ALLEN, D. O. & BECK, R. R. 1986. Role of calcium ion in hormone-stimulated lipolysis. *Biochemical pharmacology,* 35, 767-772.

ALTIMIMI, H. F. & SCHNETKAMP, P. P. 2007. Na+/Ca2+-K+ exchangers (NCKX): functional properties and physiological roles. *Channels,* 1, 62-69.

AMRAN, M. S., HOMMA, N. & HASHIMOTO, K. 2003. Pharmacology of KB - R7943: A Na+ – Ca2+ exchange inhibitor. *Cardiovascular drug reviews,* 21, 255-276.

ARIMURA, N., HORIBA, T., IMAGAWA, M., SHIMIZU, M. & SATO, R. 2004. The peroxisome proliferator-activated receptor γ regulates expression of the perilipin gene in adipocytes. *Journal of Biological Chemistry,* 279, 10070-10076.

ARNER, P. 1992. Adrenergic receptor function in fat cells. *The American journal of clinical nutrition,* 55, 228S-236S.

ARSENESCU, V., ARSENESCU, R. I., KING, V., SWANSON, H. & CASSIS, L. A. 2008. Polychlorinated biphenyl-77 induces adipocyte differentiation and proinflammatory adipokines and promotes obesity and atherosclerosis. *Environmental health perspectives,* 116, 761.

AVASTHY, N., JEREMY, J. & DANDONA, P. 1988. The role of calcium in mediating phorbol ester-and insulin-stimulated adipocyte lipogenesis. *Diabetes research (Edinburgh, Scotland),* 9, 91-95.

BABAI, N., KANEVSKY, N., DASCAL, N., ROZANSKI, G. J., SINGH, D. P., FATMA, N. & THORESON, W. B. 2010. Anion-sensitive regions of L-type CaV1. 2 calcium channels expressed in HEK293 cells. *PLoS One,* 5, e8602.

BADOU, A., JHA, M. K., MATZA, D. & FLAVELL, R. A. 2013. Emerging roles of L-type voltage-gated and other calcium channels in T lymphocytes. *Frontiers in immunology,* 4, 243.

BAE, Y. K., KWON, J. H., KIM, M., KIM, G.-H., CHOI, S. J., OH, W., YANG, Y. S., JIN, H. J. & JEON, H. B. 2018. Intracellular calcium determines the adipogenic differentiation potential of human umbilical cord blood-derived Mesenchymal stem cells via the Wnt5a/β-Catenin signaling pathway. *Stem Cells International,* 2018.

BAKER, N. A., ENGLISH, V., SUNKARA, M., MORRIS, A. J., PEARSON, K. J. & CASSIS, L. A. 2013a. Resveratrol protects against polychlorinated biphenyl-mediated impairment of glucose homeostasis in adipocytes. *The Journal of nutritional biochemistry,* 24, 2168-2174.

BAKER, N. A., KAROUNOS, M., ENGLISH, V., FANG, J., WEI, Y., STROMBERG, A., SUNKARA, M., MORRIS, A. J., SWANSON, H. I. & CASSIS, L. A. 2013b. Coplanar polychlorinated biphenyls impair glucose homeostasis in lean C57BL/6 mice and mitigate beneficial effects of weight loss on glucose homeostasis in obese mice. *Environmental health perspectives,* 121, 105.

BANNISTER, J. P., BULLEY, S., NARAYANAN, D., THOMAS-GATEWOOD, C., LUZNY, P., PACHUAU, J. & JAGGAR, J. H. 2012. Transcriptional upregulation of α2δ-1 elevates arterial smooth muscle cell voltage-dependent Ca2+ channel surface expression and cerebrovascular constriction in genetic hypertension. *Hypertension,* 60, 1006-1015.

BANNISTER, J. P., THOMAS-GATEWOOD, C. M., NEEB, Z. P., ADEBIYI, A., CHENG, X. & JAGGAR, J. H. 2011. CaV1. 2 channel N-terminal splice variants modulate functional surface expression in resistance size artery smooth muscle cells. *Journal of Biological Chemistry,* 286, 15058-15066.
BAVLEY, C. C., FISCHER, D. K., RIZZO, B. K. & RAJADHYAKSHA, A. M. 2017. Cav1. 2 channels mediate persistent chronic stress-induced behavioral deficits that are associated with prefrontal cortex activation of the p25/Cdk5-glucocorticoid receptor pathway. *Neurobiology of Stress,* 7, 27-37.
BEIGELMAN, P. M. & HOLLANDER, P. B. 1963. Effect of insulin and rat weight upon rat adipose tissue membrane resting electrical potential (REP). *Diabetes,* 12, 262-267.
BEIGELMAN, P. M. & SHU, M. J. 1972. Adipose Resting Membrane Potential: In Vitro Responses to Cl-and K+. *Proceedings of the Society for Experimental Biology and Medicine,* 141, 618-621.
BENTLEY, D. C. 2013. *Investigation into the ion channels and plasma membrane properties of white adipocytes.* University of Nottingham.
BENTLEY, D. C., PULBUTR, P., CHAN, S. & SMITH, P. A. 2014. Etiology of the membrane potential of rat white fat adipocytes. *Am J Physiol Endocrinol Metab,* 307, E161-75.
BERRIDGE, M., BOOTMAN, M. & RODERICK, H. 2003. Calcium signaling: dynamics, homeostasis, and remodeling. *Nature,* 4, 517-529.
BERRIDGE, M. J. 1997. Elementary and global aspects of calcium signalling. *The Journal of physiology,* 499, 291-306.
BERRIDGE, M. J. 2014. Module 3: Ion Channels. *Cell Signalling Biology,* 6.
BERRIDGE, M. J. & DUPONT, G. 1994. Spatial and temporal signalling by calcium. *Current opinion in cell biology,* 6, 267-274.
BERRIDGE, M. J., LIPP, P. & BOOTMAN, M. D. 2000. The versatility and universality of calcium signalling. *Nature reviews Molecular cell biology,* 1, 11.
BERRYMAN, D. E., HENRY, B., HJORTEBJERG, R., LIST, E. O. & KOPCHICK, J. J. 2016. Developments in our understanding of the effects of growth hormone on white adipose tissue from mice: implications to the clinic. *Expert review of endocrinology & metabolism,* 11, 197-207.
BERTOZZINI, E., GALLUZZI, L., PENNA, A. & MAGNANI, M. 2011. Application of the standard addition method for the absolute quantification of neutral lipids in microalgae using Nile red. *Journal of microbiological methods,* 87, 17-23.
BÉZAIRE, V. & LANGIN, D. 2009. Regulation of adipose tissue lipolysis revisited: Symposium on 'Frontiers in adipose tissue biology'. *Proceedings of the Nutrition Society,* 68, 350-360.
BEZANILLA, F. 2000. The voltage sensor in voltage-dependent ion channels. *Physiological reviews,* 80, 555-592.
BLEICHER, S. J., FARBER, L., LEWIS, A. & GOLDNER, M. G. 1966. Electrolyte-activated lipolysis in vitro: modifying effect of calcium. *Metabolism,* 15, 742-748.
BOLSONI-LOPES, A. & ALONSO-VALE, M. I. C. 2015. Lipolysis and lipases in white adipose tissue–An update. *Archives of endocrinology and metabolism,* 59, 335-342.
BOOTMAN, M. D., BERRIDGE, M. J. & RODERICK, H. L. 2002. Calcium signalling: more messengers, more channels, more complexity. *Current Biology,* 12, R563-R565.
BOUREZ, S., LE LAY, S., VAN DEN DAELEN, C., LOUIS, C., LARONDELLE, Y., THOMÉ, J.-P., SCHNEIDER, Y.-J., DUGAIL, I. & DEBIER, C. 2012. Accumulation of polychlorinated biphenyls in adipocytes: selective targeting to lipid droplets and role of caveolin-1. *PLoS One,* 7, e31834.
BRASAEMLE, D. L., RUBIN, B., HARTEN, I. A., GRUIA-GRAY, J., KIMMEL, A. R. & LONDOS, C. 2000. Perilipin A increases triacylglycerol storage by decreasing the rate of triacylglycerol hydrolysis. *Journal of Biological Chemistry,* 275, 38486-38493.
BROWN, W., SULLIVAN, T. & GREENSPAN, P. 1992. Nile red staining of lysosomal phospholipid inclusions. *Histochemistry,* 97, 349-354.
BUCHANAN, P. J. & MCCLOSKEY, K. D. 2016. Ca V channels and cancer: canonical functions indicate benefits of repurposed drugs as cancer therapeutics. *European Biophysics Journal,* 45, 621-633.

BUONARATI, O. R., HENDERSON, P. B., MURPHY, G. G., HORNE, M. C. & HELL, J. W. 2017. Proteolytic processing of the L-type Ca 2+ channel alpha 11.2 subunit in neurons. *F1000Research,* 6.
BURAEI, Z. & YANG, J. 2010. The β subunit of voltage-gated Ca2+ channels. *Physiological reviews,* 90, 1461-1506.
BURLESON, E. & DOUGHERTY, S. D. 2012. Arctic justice: Addressing persistent organic pollutants. *Law & Ineq.,* 30, 57.
CAMPBELL, R. M. & SCANES, C. G. 1988. Pharmacological investigations on the lipolytic and antilipolytic effects of growth hormone (GH) in chicken adipose tissue in vitro: evidence for involvement of calcium and polyamines. *Proceedings of the Society for Experimental Biology and Medicine,* 188, 177-184.
CARMEN, G.-Y. & VÍCTOR, S.-M. 2006. Signalling mechanisms regulating lipolysis. *Cellular signalling,* 18, 401-408.
CASTEILLA, L., PÉNICAUD, L., COUSIN, B. & CALISE, D. 2008. Choosing an adipose tissue depot for sampling. *Adipose tissue protocols.* Springer.
CATTERALL, W. A. 2000. Structure and regulation of voltage-gated Ca2+ channels. *Annual review of cell and developmental biology,* 16, 521-555.
CATTERALL, W. A. 2011. Voltage-gated calcium channels. *Cold Spring Harb Perspect Biol,* 3, a003947.
CHAVES, V. E., FRASSON, D. & KAWASHITA, N. H. 2011. Several agents and pathways regulate lipolysis in adipocytes. *Biochimie,* 93, 1631-1640.
CHUSYD, D. E., WANG, D., HUFFMAN, D. M. & NAGY, T. R. 2016. Relationships between rodent white adipose fat pads and human white adipose fat depots. *Frontiers in nutrition,* 3, 10.
CLAPHAM, D. E. 2007. Calcium signaling. *Cell,* 131, 1047-1058.
DAEMEN, S., VAN ZANDVOORT, M. A., PAREKH, S. H. & HESSELINK, M. K. 2016. Microscopy tools for the investigation of intracellular lipid storage and dynamics. *Molecular metabolism,* 5, 153-163.
DAROFF, R. B. & AMINOFF, M. J. 2014. *Encyclopedia of the neurological sciences*, Academic press.
DECHER, N., LANG, H. J., NILIUS, B., BRÜGGEMANN, A., BUSCH, A. E. & STEINMEYER, K. 2001. DCPIB is a novel selective blocker of ICl, swell and prevents swelling - induced shortening of guinea - pig atrial action potential duration. *British journal of pharmacology,* 134, 1467-1479.
DIRINCK, E., DIRTU, A., JORENS, P., MALARVANNAN, G., COVACI, A. & VAN GAAL, L. 2015. Pivotal role for the visceral fat compartment in the release of persistent organic pollutants during weight loss. *The Journal of Clinical Endocrinology & Metabolism,* 100, 4463-4471.
DOLPHIN, A. C. 2009. Calcium channel diversity: multiple roles of calcium channel subunits. *Current opinion in neurobiology,* 19, 237-244.
DOLPHIN, A. C. 2016. Voltage - gated calcium channels and their auxiliary subunits: physiology and pathophysiology and pharmacology. *The Journal of physiology,* 594, 5369-5390.
DOLPHIN, A. C. 2018. Voltage-gated calcium channels: Their discovery, function and importance as drug targets. *Brain and neuroscience advances,* 2, 2398212818794805.
DRAZNIN, B. 1993. Cytosolic calcium and insulin resistance. *American journal of kidney diseases,* 21, S32-S38.
DRAZNIN, B., LEWIS, D., HOULDER, N., SHERMAN, N., ADAMO, M., GARVEY, W. T., LEROITH, D. & SUSSMAN, K. 1989. Mechanism of insulin resistance induced by sustained levels of cytosolic free calcium in rat adipocytes. *Endocrinology,* 125, 2341-2349.
DRAZNIN, B., SUSSMAN, K., ECKEL, R., KAO, M., YOST, T. & SHERMAN, N. 1988. Possible role of cytosolic free calcium concentrations in mediating insulin resistance of obesity and hyperinsulinemia. *The Journal of clinical investigation,* 82, 1848-1852.

DRAZNIN, B., SUSSMAN, K., KAO, M., LEWIS, D. & SHERMAN, N. 1987. The existence of an optimal range of cytosolic free calcium for insulin-stimulated glucose transport in rat adipocytes. *Journal of Biological Chemistry,* 262, 14385-14388.

EL HACHMANE, M. F., ERMUND, A., BRÄNNMARK, C. & OLOFSSON, C. S. 2018. Extracellular ATP activates store-operated Ca2+ entry in white adipocytes: functional evidence for STIM1 and ORAI1. *Biochemical Journal*, BCJ20170484.

EL HACHMANE, M. F. & OLOFSSON, C. S. 2018. A mechanically activated TRPC1-like current in white adipocytes. *Biochemical and biophysical research communications,* 498, 736-742.

ENAN, E. & MATSUMURA, F. 1994. 2, 3, 7, 8 - Tetrachlorodibenzo - p - dioxin (TCDD) - induced changes in glucose transporting activity in guinea pigs, mice, and rats in vivo and in vitro. *Journal of Biochemical and Molecular Toxicology,* 9, 97-106.

ERTEL, E. A., CAMPBELL, K. P., HARPOLD, M. M., HOFMANN, F., MORI, Y., PEREZ-REYES, E., SCHWARTZ, A., SNUTCH, T. P., TANABE, T. & BIRNBAUMER, L. 2000. Nomenclature of voltage-gated calcium channels. *Neuron,* 25, 533-535.

FALOIA, E., CAMILLONI, M. A., GIACCHETTI, G. & MANTERO, F. 2000. Adipose tissue as an endocrine organ? A review of some recent data. *Eating and Weight Disorders - Studies on Anorexia, Bulimia and Obesity,* 5, 116-123.

FEDORENKO, O. P., PAWITRA; BANKE, ELIN; AKANIRO-EJIM, NNEOMA E; BENTLEY, DONNA C; OLOFSSON, CHARLOTTA S; CHAN, SUE AND SMITH, PAUL A. 2019. Identification and role of CaV1.2 and CaV1.3 L-type Ca2+ channels in white fat adipocytes. *Submitted manuscript.*

FEIJÓO-BANDÍN, S., RODRÍGUEZ-PENAS, D., GARCÍA-RÚA, V., MOSQUERA-LEAL, A., GONZÁLEZ-JUANATEY, J. & LAGO, F. 2016. Adipokines at the Cardiovascular System: Role in Health and Disease. *SM J Endocrinol Metab,* 2, 1009.

FENG, T., KALYAANAMOORTHY, S. & BARAKAT, K. 2018. L-Type Calcium Channels: Structure and Functions. *Ion Channels in Health and Sickness.* IntechOpen.

FLECHTNER-MORS, M., JENKINSON, C., ALT, A., ADLER, G. & DITSCHUNEIT, H. 2002. In vivo α1-adrenergic lipolytic activity in subcutaneous adipose tissue of obese subjects. *Journal of Pharmacology and Experimental Therapeutics,* 301, 229-233.

FLEISCHMANN, B. K., MURRAY, R. K. & KOTLIKOFF, M. I. 1994. Voltage window for sustained elevation of cytosolic calcium in smooth muscle cells. *Proceedings of the National Academy of Sciences,* 91, 11914-11918.

FOROSTYAK, O., FOROSTYAK, S., KORTUS, S., SYKOVA, E., VERKHRATSKY, A. & DAYANITHI, G. 2016. Physiology of Ca2+ signalling in stem cells of different origins and differentiation stages. *Cell calcium,* 59, 57-66.

FRIEDMAN, J. M. & HALAAS, J. L. 1998. Leptin and the regulation of body weight in mammals. *Nature,* 395, 763.

FRIEDRICH, B., MATSKEVICH, I. & LANG, F. 2006. Cell volume regulatory mechanisms. *Mechanisms and Significance of Cell Volume Regulation,* 152, 1-8.

FRUHBECK, G., GÓMEZ-AMBROSI, J., MURUZÁBAL, F. J. & BURRELL, M. A. 2001. The adipocyte: a model for integration of endocrine and metabolic signaling in energy metabolism regulation. *American Journal of Physiology-Endocrinology And Metabolism,* 280, E827-E847.

FRÜHBECK, G., MÉNDEZ-GIMÉNEZ, L., FERNÁNDEZ-FORMOSO, J.-A., FERNÁNDEZ, S. & RODRIGUEZ, A. 2014. Regulation of adipocyte lipolysis. *Nutrition research reviews,* 27, 63-93.

GARCIA, L., FAHMI, M., PREVARSKAYA, N., DUFY, B. & SARTOR, P. 1997. Modulation of voltage-dependent Ca2+ conductance by changing Cl-concentration in rat lactotrophs. *American Journal of Physiology-Cell Physiology,* 272, C1178-C1185.

GARNEAU, A. P., MARCOUX, A.-A., FRENETTE-COTTON, R., MAC-WAY, F., LAVOIE, J. L. & ISENRING, P. 2017. Molecular insights into the normal operation, regulation and multisystemic roles of K+-Cl− cotransporter 3 (KCC3). *American Journal of Physiology-Cell Physiology*.

GAUR, S., MORTON, M. E., FRICK, G. P. & GOODMAN, H. M. 1998. Growth hormone regulates the distribution of L-type calcium channels in rat adipocyte membranes. *American Journal of Physiology-Cell Physiology,* 275, C505-C514.
GAUR, S., YAMAGUCHI, H. & GOODMAN, H. M. 1996. Growth hormone increases calcium uptake in rat fat cells by a mechanism dependent on protein kinase C. *American Journal of Physiology-Cell Physiology,* 270, C1485-C1492.
GEE, K. R., BROWN, K., CHEN, W. U., BISHOP-STEWART, J., GRAY, D. & JOHNSON, I. 2000. Chemical and physiological characterization of fluo-4 Ca2+-indicator dyes. *Cell calcium,* 27, 97-106.
GENICOT, G., LEROY, J., VAN SOOM, A. & DONNAY, I. 2005. The use of a fluorescent dye, Nile red, to evaluate the lipid content of single mammalian oocytes. *Theriogenology,* 63, 1181-1194.
GERHARDT, C., GROS, J., STROSBERG, A. & ISSAD, T. 1999. Stimulation of the extracellular signal-regulated kinase 1/2 pathway by human beta-3 adrenergic receptor: new pharmacological profile and mechanism of activation. *Molecular pharmacology,* 55, 255-262.
GOUDARZI, F., MOHAMMADALIPOUR, A., KHODADADI, I., KARIMI, S., MOSTOLI, R., BAHABADI, M. & GOODARZI, M. T. 2018. The role of calcium in differentiation of human adipose-derived stem cells to adipocytes. *Molecular biotechnology,* 60, 279-289.
GRABNER, G. F., XIE, H., SCHWEIGER, M. & ZECHNER, R. 2021. Lipolysis: cellular mechanisms for lipid mobilization from fat stores. *Nature Metabolism,* 3, 1445-1465.
GRAFTON, G., STOKES, L., TOELLNER, K.-M. & GORDON, J. 2003. A non-voltage-gated calcium channel with L-type characteristics activated by B cell receptor ligation. *Biochemical pharmacology,* 66, 2001-2009.
GREENSPAN, P. & FOWLER, S. D. 1985. Spectrofluorometric studies of the lipid probe, nile red. *Journal of lipid research,* 26, 781-789.
GRIFFIN, M. D., PEREIRA, S. R., DEBARI, M. K. & ABBOTT, R. D. 2020. Mechanisms of action, chemical characteristics, and model systems of obesogens. *BMC Biomedical Engineering,* 2, 1-13.
HAFFNER, D. & SCHECTER, A. 2014. Persistent organic pollutants (POPs): a primer for practicing clinicians. *Current Environmental Health Reports,* 1, 123-131.
HANSEN, T. K., GRAVHOLT, C. H., ØRSKOV, H., RASMUSSEN, M. H., CHRISTIANSEN, J. S. & JØRGENSEN, J. O. L. 2002. Dose dependency of the pharmacokinetics and acute lipolytic actions of growth hormone. *The Journal of Clinical Endocrinology & Metabolism,* 87, 4691-4698.
HARDY, R. W., LADENSON, J. H., HRUSKA, K. A., JIWA, A. H. & MCDONALD, J. 1992. The effects of extracellular calcium and epinephrine on cytosolic-free calcium in single rat adipocytes. *Endocrinology,* 130, 3694-3702.
HECK, J., PALMEIRA DO AMARAL, A. C., WEIßBACH, S., EL KHALLOUQI, A., BIKBAEV, A. & HEINE, M. 2021. More than a pore: How voltage-gated calcium channels act on different levels of neuronal communication regulation. *Channels,* 15, 322-338.
HIRASAWA, T., NAKAMURA, T., MORITA, M., EZAWA, I., MIYAKAWA, H. & KUDO, Y. 1998. Activation of dihydropyridine sensitive Ca2+ channels in rat hippocampal neurons in culture by parathyroid hormone. *Neuroscience letters,* 256, 139-142.
HOFFMANN, E. K., LAMBERT, I. H. & PEDERSEN, S. F. 2009. Physiology of cell volume regulation in vertebrates. *Physiological reviews,* 89, 193-277.
HOFMANN, F., FLOCKERZI, V., KAHL, S. & WEGENER, J. W. 2014. L-type CaV1. 2 calcium channels: from in vitro findings to in vivo function. *Physiological reviews,* 94, 303-326.
HU, Z., LIANG, M. C. & SOONG, T. W. 2017. Alternative Splicing of L-type CaV1. 2 Calcium Channels: Implications in Cardiovascular Diseases. *Genes,* 8, 344.
HUANG, J. & ZAMPONI, G. W. 2017. Regulation of voltage gated calcium channels by GPCRs and post-translational modification. *Current opinion in pharmacology,* 32, 1-8.

HUANG, W., LU, C., WU, Y., OUYANG, S. & CHEN, Y. 2015. T-type calcium channel antagonists, mibefradil and NNC-55-0396 inhibit cell proliferation and induce cell apoptosis in leukemia cell lines. *Journal of Experimental & Clinical Cancer Research,* 34, 1-15.

IZAWA, T., KOSHIMIZU, E., KOMABAYASHI, T. & TSUBOI, M. 1983. Effects of Ca2+ and calmodulin inhibitors on lipolysis induced by epinephrine, norepinephrine, caffeine and ACTH in rat epididymal adipose tissue. *Nihon Seirigaku zasshi. Journal of the Physiological Society of Japan,* 45, 36-44.

JONES, B. H., KIM, J. H., ZEMEL, M. B., WOYCHIK, R. P., MICHAUD, E. J., WILKISON, W. O. & MOUSTAID, N. 1996. Upregulation of adipocyte metabolism by agouti protein: possible paracrine actions in yellow mouse obesity. *American journal of physiology-endocrinology and metabolism,* 270, E192-E196.

JÖNSSON, C., CASTOR BATISTA, A. P., KJØLHEDE, P. & STRÅLFORS, P. 2019. Insulin and β-adrenergic receptors mediate lipolytic and anti-lipolytic signalling that is not altered by type 2 diabetes in human adipocytes. *Biochemical Journal,* 476, 2883-2908.

JURKAT - ROTT, K. & LEHMANN - HORN, F. 2004. The impact of splice isoforms on voltage - gated calcium channel α 1 subunits. *The Journal of physiology,* 554, 609-619.

KELLER, A., NESVIZHSKII, A. I., KOLKER, E. & AEBERSOLD, R. 2002. Empirical statistical model to estimate the accuracy of peptide identifications made by MS/MS and database search. *Analytical chemistry,* 74, 5383-5392.

KERSHAW, E. E. & FLIER, J. S. 2004. Adipose tissue as an endocrine organ. *J Clin Endocrinol Metab,* 89, 2548-56.

KIM, J. T. & LEE, H. K. 2014. Metabolic syndrome and the environmental pollutants from mitochondrial perspectives. *Reviews in Endocrine and Metabolic Disorders,* 15, 253-262.

KIM, K. H., KIM, D., PARK, J. Y., JUNG, H. J., CHO, Y.-H., KIM, H. K., HAN, J., CHOI, K.-Y. & KWON, H. J. 2015. NNC 55-0396, a T-type Ca2+ channel inhibitor, inhibits angiogenesis via suppression of hypoxia-inducible factor-1α signal transduction. *Journal of Molecular Medicine,* 93, 499-509.

KIM, M.-J., MARCHAND, P., HENEGAR, C., ANTIGNAC, J.-P., ALILI, R., POITOU, C., BOUILLOT, J.-L., BASDEVANT, A., LE BIZEC, B. & BAROUKI, R. 2011. Fate and complex pathogenic effects of dioxins and polychlorinated biphenyls in obese subjects before and after drastic weight loss. *Environmental health perspectives,* 119, 377.

KIM, M. J., PELLOUX, V., GUYOT, E., TORDJMAN, J., BUI, L.-C., CHEVALLIER, A., FOREST, C., BENELLI, C., CLÉMENT, K. & BAROUKI, R. 2012. Inflammatory pathway genes belong to major targets of persistent organic pollutants in adipose cells. *Environmental health perspectives,* 120, 508.

KOIVISTO, A., DOTZLER, E., RUß, U., NEDERGAARD, J. & SIEMEN, D. 1993. Nonselective cation channels in brown and white fat cells. *Nonselective Cation Channels.* Springer.

KOKUBUN, S. & REUTER, H. 1984. Dihydropyridine derivatives prolong the open state of Ca channels in cultured cardiac cells. *Proceedings of the National Academy of Sciences,* 81, 4824-4827.

KOMAI, A. 2015. *Molecular and physiological regulation of adiponectin exocytosis in white adipocytes*.

KOPCHICK, J. J., BERRYMAN, D. E., PURI, V., LEE, K. Y. & JORGENSEN, J. O. 2020. The effects of growth hormone on adipose tissue: old observations, new mechanisms. *Nature Reviews Endocrinology,* 16, 135-146.

KOTTURI, M. F. & JEFFERIES, W. A. 2005. Molecular characterization of L-type calcium channel splice variants expressed in human T lymphocytes. *Molecular immunology,* 42, 1461-1474.

KRAMER, A. A., INGRAHAM, N. E., SHARPE, E. J. & MYNLIEFF, M. 2012. Levels of Cav1.2 L-Type Ca2+ Channels Peak in the First Two Weeks in Rat Hippocampus Whereas Cav1.3 Channels Steadily Increase. *Journal of signal transduction,* 2012.

LA MERRILL, M., EMOND, C., KIM, M. J., ANTIGNAC, J.-P., LE BIZEC, B., CLÉMENT, K., BIRNBAUM, L. S. & BAROUKI, R. 2013. Toxicological function of adipose tissue: focus on persistent organic pollutants. *Environmental health perspectives,* 121, 162.

LACINOVÁ, L. & HOFMANN, F. 2001. Voltage-dependent calcium channels. *Heart physiology and pathophysiology,* 4.

LAFONTAN, M. 2011. Historical perspectives in fat cell biology: the fat cell as a model for the investigation of hormonal and metabolic pathways. *American Journal of Physiology-Cell Physiology,* 302, C327-C359.

LAFONTAN, M., MORO, C., SENGENES, C., GALITZKY, J., CRAMPES, F. & BERLAN, M. 2005. An unsuspected metabolic role for atrial natriuretic peptides: the control of lipolysis, lipid mobilization, and systemic nonesterified fatty acids levels in humans. *Arteriosclerosis, thrombosis, and vascular biology,* 25, 2032-2042.

LANG, F. 2007. Mechanisms and significance of cell volume regulation. *Journal of the American college of nutrition,* 26, 613S-623S.

LANG, F., BUSCH, G. L., RITTER, M., VOLKL, H., WALDEGGER, S., GULBINS, E. & HAUSSINGER, D. 1998. Functional significance of cell volume regulatory mechanisms. *Physiological reviews,* 78, 247-306.

LANNER, J. T., KATZ, A., TAVI, P., SANDSTROM, M. E., ZHANG, S.-J., WRETMAN, C., JAMES, S., FAUCONNIER, J., LÄNNERGREN, J. & BRUTON, J. D. 2006. The role of Ca2+ influx for insulin-mediated glucose uptake in skeletal muscle. *Diabetes,* 55, 2077-2083.

LAZIC, S. E., CLARKE-WILLIAMS, C. J. & MUNAFÒ, M. R. 2018. What exactly is 'N'in cell culture and animal experiments? *PLoS biology,* 16, e2005282.

LEE, D.-H. 2021. Can Environmental Pollutants Be a Factor Linking Obesity and COVID-19? *Journal of Korean Medical Science,* 36.

LEE, D.-H., JACOBS, D. R. & PORTA, M. 2006a. Could low-level background exposure to persistent organic pollutants contribute to the social burden of type 2 diabetes? : BMJ Publishing Group Ltd.

LEE, D.-H., LEE, I.-K., JIN, S.-H., STEFFES, M. & JACOBS, D. R. 2007. Association between serum concentrations of persistent organic pollutants and insulin resistance among nondiabetic adults: results from the National Health and Nutrition Examination Survey 1999–2002. *Diabetes care,* 30, 622-628.

LEE, D.-H., LEE, I.-K., SONG, K., STEFFES, M., TOSCANO, W., BAKER, B. A. & JACOBS, D. R. 2006b. A strong dose-response relation between serum concentrations of persistent organic pollutants and diabetes: results from the National Health and Examination Survey 1999–2002. *Diabetes care,* 29, 1638-1644.

LEE, D.-H., PORTA, M., JACOBS JR, D. R. & VANDENBERG, L. N. 2014. Chlorinated persistent organic pollutants, obesity, and type 2 diabetes. *Endocrine reviews,* 35, 557-601.

LEE, Y.-M., JACOBS JR, D. R. & LEE, D.-H. 2018. Persistent organic pollutants and type 2 diabetes: a critical review of review articles. *Frontiers in endocrinology,* 9, 712.

LEE, Y. M., KIM, K. S., JACOBS, D. & LEE, D. H. 2017. Persistent organic pollutants in adipose tissue should be considered in obesity research. *Obesity Reviews,* 18, 129-139.

LEE, Y. M., PARK, S. H. & LEE, D. H. 2020. Intensive weight loss and cognition: The dynamics of persistent organic pollutants in adipose tissue can explain the unexpected results from the Action for Health in Diabetes (Look AHEAD) study. *Alzheimer's & Dementia,* 16, 696-703.

LI, G., WANG, J., LIAO, P., BARTELS, P., ZHANG, H., YU, D., LIANG, M. C., POH, K. K., YU, C. Y. & JIANG, F. 2017. Exclusion of alternative exon 33 of CaV1. 2 calcium channels in heart is proarrhythmogenic. *Proceedings of the National Academy of Sciences,* 114, E4288-E4295.

LIAO, P. & SOONG, T. W. 2010. Understanding alternative splicing of Cav 1.2 calcium channels for a new approach towards individualized medicine. *Journal of biomedical research,* 24, 181-186.
LIAO, P., YU, D., HU, Z., LIANG, M. C., WANG, J. J., YU, C. Y., NG, G., YONG, T. F., SOON, J. L. & CHUA, Y. L. 2015. Alternative splicing generates a novel truncated Cav1. 2 channel in neonatal rat heart. *Journal of Biological Chemistry,* 290, 9262-9272.
LIM, S., AHN, S. Y., SONG, I. C., CHUNG, M. H., JANG, H. C., PARK, K. S., LEE, K.-U., PAK, Y. K. & LEE, H. K. 2009. Chronic exposure to the herbicide, atrazine, causes mitochondrial dysfunction and insulin resistance. *PloS one,* 4, e5186.
LIPSCOMBE, D., HELTON, T. D. & XU, W. 2004. L-type calcium channels: the low down. *Journal of neurophysiology,* 92, 2633-2641.
LIU, L., GONZALEZ, P. K., BARRETT, C. F. & RITTENHOUSE, A. R. 2003. The calcium channel ligand FPL 64176 enhances L-type but inhibits N-type neuronal calcium currents. *Neuropharmacology,* 45, 281-292.
LORD, G. M., MATARESE, G., HOWARD, J. K., BAKER, R. J., BLOOM, S. R. & LECHLER, R. I. 1998. Leptin modulates the T-cell immune response and reverses starvation-induced immunosuppression. *Nature,* 394, 897.
LOUIS, C., VAN DEN DAELEN, C., TINANT, G., BOUREZ, S., THOMÉ, J.-P., DONNAY, I., LARONDELLE, Y. & DEBIER, C. 2014. Efficient in vitro adipocyte model of long-term lipolysis: A tool to study the behavior of lipophilic compounds. *In Vitro Cellular & Developmental Biology-Animal,* 50, 507-518.
LUMAQUIN, D., JOHNS, E., MONTAL, E., WEISS, J. M., OLA, D., ABUHASHEM, A. & WHITE, R. M. 2021. An in vivo reporter for tracking lipid droplet dynamics in transparent zebrafish. *Elife,* 10, e64744.
LUNZ, V., ROMANIN, C. & FRISCHAUF, I. 2019. STIM1 activation of Orai1. *Cell calcium,* 77, 29-38.
LV, J., LIANG, Y., ZHANG, S., LAN, Q., XU, Z., WU, X., KANG, L., REN, J., CAO, Y. & WU, T. 2019. DCPIB, an inhibitor of volume-regulated anion channels, distinctly modulates K2P channels. *ACS Chemical Neuroscience,* 10, 2786-2793.
MA, X., LEE, P., CHISHOLM, D. J. & JAMES, D. E. 2015. Control of adipocyte differentiation in different fat depots; implications for pathophysiology or therapy. *Frontiers in endocrinology,* 6, 1.
MARTINEZ-SANTIBAÑEZ, G., CHO, K. W. & LUMENG, C. N. 2014. Imaging white adipose tissue with confocal microscopy. *Methods in enzymology.* Elsevier.
MCDONOUGH, S. I., MORI, Y. & BEAN, B. P. 2005. FPL 64176 modification of CaV1. 2 L-type calcium channels: dissociation of effects on ionic current and gating current. *Biophysical journal,* 88, 211-223.
MCKEEL, D. W. & JARETT, L. 1970. Preparation and characterization of a plasma membrane fraction from isolated fat cells. *The Journal of cell biology,* 44, 417-432.
MCKIE, G. L., MEDAK, K. D., KNUTH, C. M., SHAMSHOUM, H., TOWNSEND, L. K., PEPPLER, W. T. & WRIGHT, D. C. 2019. Housing temperature affects the acute and chronic metabolic adaptations to exercise in mice. *The Journal of Physiology,* 597, 4581-4600.
MIYAUCHI, A., HRUSKA, K. A., GREENFIELD, E. M., DUNCAN, R., ALVAREZ, J., BARATTOLO, R., COLUCCI, S., ZAMBONIN-ZALLONE, A., TEITELBAUM, S. L. & TETI, A. 1990. Osteoclast cytosolic calcium, regulated by voltage-gated calcium channels and extracellular calcium, controls podosome assembly and bone resorption. *The Journal of cell biology,* 111, 2543-2552.
MIYOSHI, H., PERFIELD, J. W., OBIN, M. S. & GREENBERG, A. S. 2008. Adipose triglyceride lipase regulates basal lipolysis and lipid droplet size in adipocytes. *Journal of cellular biochemistry,* 105, 1430-1436.
MORRISON, S. & MCGEE, S. L. 2015. 3T3-L1 adipocytes display phenotypic characteristics of multiple adipocyte lineages. *Adipocyte,* 4, 295-302.
N'GOUEMO, P., AKINFIRESOYE, L. R., ALLARD, J. S. & LOVINGER, D. M. 2015. Alcohol withdrawal-induced seizure susceptibility is associated with an upregulation of

CaV1. 3 channels in the rat inferior colliculus. *International Journal of Neuropsychopharmacology,* 18.
NAVEDO, M. F., AMBERG, G. C., VOTAW, V. S. & SANTANA, L. F. 2005. Constitutively active L-type Ca2+ channels. *Proceedings of the National Academy of Sciences,* 102, 11112-11117.
NESVIZHSKII, A. I., KELLER, A., KOLKER, E. & AEBERSOLD, R. 2003. A statistical model for identifying proteins by tandem mass spectrometry. *Analytical chemistry,* 75, 4646-4658.
NI, Z., SMOGORZEWSKI, M. & MASSRY, S. G. 1994. Effects of parathyroid hormone on cytosolic calcium of rat adipocytes. *Endocrinology,* 135, 1837-1844.
NIELSEN, T. S., JESSEN, N., JØRGENSEN, J. O. L., MØLLER, N. & LUND, S. 2014. Dissecting adipose tissue lipolysis: molecular regulation and implications for metabolic disease. *Journal of molecular endocrinology,* 52, R199-R222.
NORDSTROM, S. M., TRAN, J. L., SOS, B. C., WAGNER, K.-U. & WEISS, E. J. 2013. Disruption of JAK2 in adipocytes impairs lipolysis and improves fatty liver in mice with elevated GH. *Molecular Endocrinology,* 27, 1333-1342.
OGURI, A., TANAKA, T., IIDA, H., MEGURO, K., TAKANO, H., OONUMA, H., NISHIMURA, S., MORITA, T., YAMASOBA, T. & NAGAI, R. 2010. Involvement of CaV3. 1 T-type calcium channels in cell proliferation in mouse preadipocytes. *American Journal of Physiology-Cell Physiology,* 298, C1414-C1423.
OSEI-OWUSU, J., YANG, J., DEL CARMEN VITERY, M. & QIU, Z. 2018. Molecular biology and physiology of volume-regulated anion channel (VRAC). *Current topics in membranes,* 81, 177-203.
PAREDES, R. M., ETZLER, J. C., WATTS, L. T., ZHENG, W. & LECHLEITER, J. D. 2008. Chemical calcium indicators. *Methods,* 46, 143-151.
PARK, H.-J., MIN, S.-H., WON, Y.-J. & LEE, J.-H. 2015. Asn-Linked Glycosylation Contributes to Surface Expression and Voltage-Dependent Gating of Ca v 1.2 Ca 2+ Channel. *Journal of Microbiology and Biotechnology,* 25, 1371-1379.
PATEL, S. 2018. Ins and outs of Ca2+ transport by acidic organelles and cell migration. *Communicative & Integrative Biology,* 11, 803-13.
PATEL, S. & KILPATRICK, B. S. 2018. Two-pore channels and disease. *Biochimica Et Biophysica Acta (BBA)-Molecular Cell Research,* 1865, 1678-1686.
PEPPERELL, J., KOMMINENI, K., BURADAGUNTA, S., SMITH, P. & KEEFE, D. 1999. Transmembrane regulation of intracellular calcium by a plasma membrane sodium/calcium exchanger in mouse ova. *Biology of reproduction,* 60, 1137-1143.
PERRY, M. & HALES, C. 1969. Rates of efflux and intracellular concentrations of potassium, sodium and chloride ions in isolated fat-cells from the rat. *Biochemical Journal,* 115, 865-871.
PERSHADSINGH, H. A., LEE, L.-Y. & SNOWDOWNE, K. W. 1989. Evidence for a sodium/calcium exchanger and voltage - dependent calcium channels in adipocytes. *FEBS letters,* 244, 89-92.
PESTANA, D., FARIA, G., SÁ, C., FERNANDES, V. C., TEIXEIRA, D., NORBERTO, S., FARIA, A., MEIRELES, M., MARQUES, C. & CORREIA-SÁ, L. 2014. Persistent organic pollutant levels in human visceral and subcutaneous adipose tissue in obese individuals—Depot differences and dysmetabolism implications. *Environmental research,* 133, 170-177.
PHADUNGATH, C. & METZGER, L. 2011. Effect of sodium gluconate on the solubility of calcium lactate. *Journal of dairy science,* 94, 4843-4849.
PICK, U. & RACHUTIN-ZALOGIN, T. 2012. Kinetic anomalies in the interactions of Nile red with microalgae. *Journal of microbiological methods,* 88, 189-196.
PITT, G. S. & MARX, S. O. 2014. Calmodulin and CaMKII as Ca2+ Switches for Cardiac Ion Channels. *Cardiac Electrophysiology: From Cell to Bedside.* Elsevier.
POWELL, K. L., CAIN, S. M., SNUTCH, T. P. & O'BRIEN, T. J. 2014. Low threshold T-type calcium channels as targets for novel epilepsy treatments. *Br J Clin Pharmacol,* 77, 729-39.

PRIDEAUX, M., DALLAS, S. L., ZHAO, N., JOHNSRUD, E. D., VENO, P. A., GUO, D., MISHINA, Y., HARRIS, S. E. & BONEWALD, L. F. 2015. Parathyroid hormone induces bone cell motility and loss of mature osteocyte phenotype through L-calcium channel dependent and independent mechanisms. *PloS one,* 10, e0125731.
PROENÇA, A., SERTIÉ, R., OLIVEIRA, A., CAMPAAA, A., CAMINHOTTO, R., CHIMIN, P. & LIMA, F. 2014. New concepts in white adipose tissue physiology. *Brazilian Journal of Medical and Biological Research,* 47, 192-205.
RAIFMAN, T. K., KUMAR, P., HAASE, H., KLUSSMANN, E., DASCAL, N. & WEISS, S. 2017. Protein kinase C enhances plasma membrane expression of cardiac L-type calcium channel, CaV1. 2. *Channels,* 11, 604-615.
RAMÍREZ-CASTRILLÓN, M., JARAMILLO-GARCIA, V. P., LOPES BARROS, H., PEGAS HENRIQUES, J. A., STEFANI, V. & VALENTE, P. 2021. Nile red incubation time before reading fluorescence greatly influences the yeast neutral lipids quantification. *Frontiers in microbiology,* 12, 619313.
RAMIREZ-PONCE, M., ACOSTA, J. & BELLIDO, J. 1990. Electrical activity in white adipose tissue of rat. *Rev Esp Fisiol,* 46, 133-8.
REUSCH, J. E.-B., BEGUM, N., SUSSMAN, K. E. & DRAZNIN, B. 1991. Regulation of GLUT-4 phosphorylation by intracellular calcium in adipocytes. *Endocrinology,* 129, 3269-3273.
RICHARD, A. J., WHITE, U., ELKS, C. M. & STEPHENS, J. M. 2020. Adipose tissue: physiology to metabolic dysfunction. *Endotext [Internet]*.
RINGER, E., RUSS, U. & SIEMEN, D. 2000. β3-Adrenergic stimulation and insulin inhibition of non-selective cation channels in white adipocytes of the rat. *Biochimica et Biophysica Acta (BBA)-Biomembranes,* 1463, 241-253.
RODBELL, M. 1964. The metabolism of isolated fat cells. *Comprehensive Physiology*.
RODRÍGUEZ, A., EZQUERRO, S., MÉNDEZ-GIMÉNEZ, L., BECERRIL, S. & FRÜHBECK, G. 2015. Revisiting the adipocyte: a model for integration of cytokine signaling in the regulation of energy metabolism. *American Journal of Physiology-Endocrinology and Metabolism,* 309, E691-E714.
RUIZ-OJEDA, F. J., RUPEREZ, A. I., GOMEZ-LLORENTE, C., GIL, A. & AGUILERA, C. M. 2016. Cell Models and Their Application for Studying Adipogenic Differentiation in Relation to Obesity: A Review. *Int J Mol Sci,* 17.
RUMIN, J., BONNEFOND, H., SAINT-JEAN, B., ROUXEL, C., SCIANDRA, A., BERNARD, O., CADORET, J.-P. & BOUGARAN, G. 2015. The use of fluorescent Nile red and BODIPY for lipid measurement in microalgae. *Biotechnology for biofuels,* 8, 1-16.
RUZZIN, J., PETERSEN, R., MEUGNIER, E., MADSEN, L., LOCK, E.-J., LILLEFOSSE, H., MA, T., PESENTI, S., SONNE, S. B. & MARSTRAND, T. T. 2010. Persistent organic pollutant exposure leads to insulin resistance syndrome. *Environmental health perspectives,* 118, 465.
SARDINI, A., AMEY, J. S., WEYLANDT, K.-H., NOBLES, M., VALVERDE, M. A. & HIGGINS, C. F. 2003. Cell volume regulation and swelling-activated chloride channels. *Biochimica et Biophysica Acta (BBA)-Biomembranes,* 1618, 153-162.
SATIN, J. 2014. Regulation of cardiac calcium channels. *Cardiac Electrophysiology: From Cell to Bedside.* Elsevier.
SCHARINGER, A., ECKRICH, S., VANDAEL, D. H., SCHÖNIG, K., KOSCHAK, A., HECKER, D., KAUR, G., LEE, A., SAH, A. & BARTSCH, D. 2015. Cell-type-specific tuning of Cav1. 3 Ca2+-channels by a C-terminal automodulatory domain. *Frontiers in cellular neuroscience,* 9, 309.
SCHWARTZ, Y., GOODMAN, H. M. & YAMAGUCHI, H. 1991. Refractoriness to growth hormone is associated with increased intracellular calcium in rat adipocytes. *Proceedings of the National Academy of Sciences,* 88, 6790-6794.
SCHWARTZ, Y., YAMAGUCHI, H. & GOODMAN, H. M. 1992. Growth hormone increases intracellular free calcium in rat adipocytes: correlation with actions on carbohydrate metabolism. *Endocrinology,* 131, 772-778.
SETHI, J. K. & HOTAMISLIGIL, G. S. The role of TNFα in adipocyte metabolism. Seminars in cell & developmental biology, 1999. Elsevier, 19-29.

SHI, H., DIRIENZO, D. & ZEMEL, M. B. 2001. Effects of dietary calcium on adipocyte lipid metabolism and body weight regulation in energy - restricted aP2 - agouti transgenic mice. *The FASEB journal,* 15, 291-293.
SHISTIK, E., KEREN-RAIFMAN, T., IDELSON, G. H., BLUMENSTEIN, Y., DASCAL, N. & IVANINA, T. 1999. The N terminus of the Cardiac L-type Ca2+ Channel α1C Subunit THE INITIAL SEGMENT IS UBIQUITOUS AND CRUCIAL FOR PROTEIN KINASE C MODULATION, BUT IS NOT DIRECTLY PHOSPHORYLATED. *Journal of Biological Chemistry,* 274, 31145-31149.
SMITH, P., ASCHROFT, F. & FEWTRELL, C. 1993. Permeation and gating properties of the L-type calcium channel in mouse pancreatic beta cells. *The Journal of general physiology,* 101, 767-797.
SMITH, P. A., CHAN, S., PULBUTR, P. & BENTLEY, D. 2014. Basal calcium influx in rat white fat adipocytes is mediated via CaV1. 3 voltage gated calcium channels. *In Proceedings of The Physiological Society,* 32, PC014
SNIPSTAD, S., WESTRØM, S., MØRCH, Y., AFADZI, M., ÅSLUND, A. K. & DE LANGE DAVIES, C. 2014. Contact-mediated intracellular delivery of hydrophobic drugs from polymeric nanoparticles. *Cancer nanotechnology,* 5, 1-18.
SONG, Z., WANG, Y., ZHANG, F., YAO, F. & SUN, C. 2019. Calcium signaling pathways: key pathways in the regulation of obesity. *International Journal of Molecular Sciences,* 20, 2768.
SQUIRE, L. R., DRONKERS, N. & BALDO, J. 2009. *Encyclopedia of neuroscience*, Elsevier.
STOKES, L., GORDON, J. & GRAFTON, G. 2004. Non-voltage-gated L-type Ca2+ Channels in Human T Cells PHARMACOLOGY AND MOLECULAR CHARACTERIZATION OF THE MAJOR α PORE-FORMING AND AUXILIARY β-SUBUNITS. *Journal of Biological Chemistry,* 279, 19566-19573.
SUKUMAR, P., SEDO, A., LI, J., WILSON, L. A., O'REGAN, D., LIPPIAT, J. D., PORTER, K. E., KEARNEY, M. T., AINSCOUGH, J. F. & BEECH, D. J. 2012. Constitutively active TRPC channels of adipocytes confer a mechanism for sensing dietary fatty acids and regulating adiponectin. *Circulation research*, CIRCRESAHA. 112.270751.
SUN, C., QI, R., WANG, L., YAN, J. & WANG, Y. 2012a. p38 MAPK regulates calcium signal-mediated lipid accumulation through changing VDR expression in primary preadipocytes of mice. *Molecular biology reports,* 39, 3179-3184.
SUN, C., WANG, L., YAN, J. & LIU, S. 2012b. Calcium ameliorates obesity induced by high-fat diet and its potential correlation with p38 MAPK pathway. *Molecular biology reports,* 39, 1755-1763.
SUN, Y., SUKUMARAN, P., BANDYOPADHYAY, B. C. & SINGH, B. B. 2014. Physiological function and characterization of TRPCs in neurons. *Cells,* 3, 455-475.
SUN, Y., ZHANG, H., SELVARAJ, S., SUKUMARAN, P., LEI, S., BIRNBAUMER, L. & SINGH, B. B. 2017. Inhibition of L-type Ca2+ channels by TRPC1-STIM1 complex is essential for the protection of dopaminergic neurons. *Journal of Neuroscience*, 3010-16.
TANG, Z. Z., LIANG, M. C., LU, S., YU, D., YU, C. Y., YUE, D. T. & SOONG, T. W. 2004. Transcript scanning reveals novel and extensive splice variations in human L-type voltage-gated calcium channel, Cav1. 2 α1 subunit. *Journal of Biological Chemistry,* 279, 44335-44343.
TATENAKA, Y., KATO, H., ISHIYAMA, M., SASAMOTO, K., SHIGA, M., NISHITOH, H. & UENO, Y. 2019. Monitoring lipid droplet dynamics in living cells by using fluorescent probes. *Biochemistry,* 58, 499-503.
TAVALIN, S. J., SHEPHERD, D., CLOUES, R. K., BOWDEN, S. E. & MARRION, N. V. 2004. Modulation of single channels underlying hippocampal L-type current enhancement by agonists depends on the permeant ion. *Journal of neurophysiology,* 92, 824-837.
THORESON, W. B., NITZAN, R. & MILLER, R. F. 2000. Chloride efflux inhibits single calcium channel open probability in vertebrate photoreceptors: chloride imaging and cell-attached patch-clamp recordings. *Visual neuroscience,* 17, 197-206.

TRAYHURN, P. & BEATTIE, J. H. 2001. Physiological role of adipose tissue: white adipose tissue as an endocrine and secretory organ. *Proceedings of the Nutrition Society,* 60, 329-339.
TROIKE, K. M., HENRY, B. E., JENSEN, E. A., YOUNG, J. A., LIST, E. O., KOPCHICK, J. J. & BERRYMAN, D. E. 2017. Impact of growth hormone on regulation of adipose tissue. *Comprehensive Physiology,* 7, 819-840.
TRUJILLO, M. E. & SCHERER, P. E. 2006. Adipose tissue-derived factors: impact on health and disease. *Endocrine reviews,* 27, 762-778.
TUROVSKY, E., KAIMACHNIKOV, N., TUROVSKAYA, M., BEREZHNOV, A., DYNNIK, V. & ZINCHENKO, V. 2012. Two mechanisms of calcium oscillations in adipocytes. *Biochemistry (Moscow) Supplement Series A: Membrane and Cell Biology,* 6, 26-34.
UEBELE, V. N., GOTTER, A. L., NUSS, C. E., KRAUS, R. L., DORAN, S. M., GARSON, S. L., REISS, D. R., LI, Y., BARROW, J. C. & REGER, T. S. 2009. Antagonism of T-type calcium channels inhibits high-fat diet–induced weight gain in mice. *The Journal of clinical investigation,* 119, 1659-1667.
VACLAVIK, E., TJONNELAND, A., STRIPP, C., OVERVAD, K., WEBER, J. P. & RAASCHOU-NIELSEN, O. 2006. Organochlorines in Danish women: predictors of adipose tissue concentrations. *Environmental research,* 100, 362-370.
VASCONCELOS, L. H., SOUZA, I. L., PINHEIRO, L. S. & SILVA, B. A. 2016. Ion Channels in Obesity: Pathophysiology and Potential Therapeutic Targets. *Frontiers in pharmacology,* 7, 58.
VAVRUSOVA, M., MUNK, M. B. & SKIBSTED, L. H. 2013. Aqueous solubility of calcium L-lactate, calcium D-gluconate, and calcium D-lactobionate: importance of complex formation for solubility increase by hydroxycarboxylate mixtures. *Journal of agricultural and food chemistry,* 61, 8207-8214.
VÁZQUEZ-VELA, M. E. F., TORRES, N. & TOVAR, A. R. 2008. White adipose tissue as endocrine organ and its role in obesity. *Archives of medical research,* 39, 715-728.
WANG, P., MARIMAN, E., RENES, J. & KEIJER, J. 2008. The secretory function of adipocytes in the physiology of white adipose tissue. *Journal of cellular physiology,* 216, 3-13.
WANG, Y., DENG, X. & GILL, D. L. 2010. Calcium signaling by STIM and Orai: intimate coupling details revealed. *Science signaling,* 3, pe42-pe42.
WANG, Z., LI, V., CHAN, G. C., PHAN, T., NUDELMAN, A. S., XIA, Z. & STORM, D. R. 2009. Adult type 3 adenylyl cyclase–deficient mice are obese. *PloS one,* 4, e6979.
WEHNER, F., BONDARAVA, M., TER VELD, F., ENDL, E., NÜRNBERGER, H. R. & LI, T. 2006. Hypertonicity - induced cation channels. *Acta Physiologica,* 187, 21-25.
WEHNER, F., OLSEN, H., TINEL, H., KINNE-SAFFRAN, E. & KINNE, R. K. 2003. Cell volume regulation: osmolytes, osmolyte transport, and signal transduction. *Reviews of physiology, biochemistry and pharmacology*, 1-80.
WEISS, S. & DASCAL, N. 2015. Molecular aspects of modulation of L-type calcium channels by protein kinase C. *Current molecular pharmacology,* 8, 43-53.
WESTERINK, R. H. 2014. Modulation of cell viability, oxidative stress, calcium homeostasis, and voltage-and ligand-gated ion channels as common mechanisms of action of (mixtures of) non-dioxin-like polychlorinated biphenyls and polybrominated diphenyl ethers. *Environmental Science and Pollution Research,* 21, 6373-6383.
WHITEHEAD, J. P., MOLERO, J. C., CLARK, S., MARTIN, S., MENEILLY, G. & JAMES, D. E. 2001. The role of Ca2+ in insulin-stimulated glucose transport in 3T3-L1 cells. *Journal of Biological Chemistry,* 276, 27816-27824.
WORRALL, D. S. & OLEFSKY, J. M. 2002. The effects of intracellular calcium depletion on insulin signaling in 3T3-L1 adipocytes. *Molecular Endocrinology,* 16, 378-389.
WU, J., YAN, Z., LI, Z., QIAN, X., LU, S., DONG, M., ZHOU, Q. & YAN, N. 2016. Structure of the voltage-gated calcium channel Cav1. 1 at 3.6 Å resolution. *Nature,* 537, 191-196.

XUE, B., GREENBERG, A. G., KRAEMER, F. B. & ZEMEL, M. B. 2001. Mechanism of intracellular calcium ([Ca2+] i) inhibition of lipolysis in human adipocytes. *The FASEB Journal,* 15, 2527-2529.
XUE, B., MOUSTAID-MOUSSA, N., WILKISON, W. O. & ZEMEL, M. B. 1998. The agouti gene product inhibits lipolysis in human adipocytes via a Ca2+-dependent mechanism. *The FASEB Journal,* 12, 1391-1396.
YAGUCHI, T. & NISHIZAKI, T. 2010. Extracellular high K+ stimulates vesicular glutamate release from astrocytes by activating voltage - dependent calcium channels. *Journal of cellular physiology,* 225, 512-518.
YANEV, S. & CHALDAKOV, G. N. 2012. Adipose tissue: a master in toxicology. *Adipobiology,* 4, 59-66.
YANG, J. 2016. Calcium channel structures come of age. *Cell Research,* 26, 1271-1272.
YIN, Z., REN, J. & GUO, W. 2015. Sarcomeric protein isoform transitions in cardiac muscle: a journey to heart failure. *Biochimica et Biophysica Acta (BBA)-Molecular Basis of Disease,* 1852, 47-52.
ZEBISCH, K., VOIGT, V., WABITSCH, M. & BRANDSCH, M. 2012. Protocol for effective differentiation of 3T3-L1 cells to adipocytes. *Anal Biochem,* 425, 88-90.
ZEMEL, M. B. 1998. Nutritional and endocrine modulation of intracellular calcium: implications in obesity, insulin resistance and hypertension. *Molecular and Cellular Effects of Nutrition on Disease Processes.* Springer.
ZEMEL, M. B. 2002. Regulation of adiposity and obesity risk by dietary calcium: mechanisms and implications. *Journal of the American College of Nutrition,* 21, 146S-151S.
ZEMEL, M. B. & SUN, X. 2008. Calcitriol and energy metabolism. *Nutrition reviews,* 66, S139-S146.
ZHAI, M., YANG, D., YI, W. & SUN, W. 2020. Involvement of calcium channels in the regulation of adipogenesis. *Adipocyte,* 9, 132-141.
ZHANG, F., YE, J., MENG, Y., AI, W., SU, H., ZHENG, J., LIU, F., ZHU, X., WANG, L. & GAO, P. 2018. Calcium supplementation enhanced Adipogenesis and improved glucose homeostasis through activation of Camkii and PI3K/Akt signaling pathway in porcine bone marrow mesenchymal stem cells (pBMSCs) and mice fed high fat diet (HFD). *Cellular physiology and biochemistry,* 51, 154-172.
ZHANG, F., YE, J., ZHU, X., WANG, L., GAO, P., SHU, G., JIANG, Q. & WANG, S. 2019. Anti-obesity effects of dietary calcium: The evidence and possible mechanisms. *International journal of molecular sciences,* 20, 3072.
ZHANG, H. Y., LIAO, P., WANG, J. J., YU, D. J. & SOONG, T. W. 2010. Alternative splicing modulates diltiazem sensitivity of cardiac and vascular smooth muscle Cav1. 2 calcium channels. *British journal of pharmacology,* 160, 1631-1640.
ZIEGLER, R., JOBST, W., MINNE, H. & FAULHABER, J. 1980. Calciotropic hormones and lipolysis of human adipose tissue: role of extracellular calcium as conditioning but not regulating factor. *Endokrinologie,* 75, 77-88.

APPENDIX

Appendix 1: Composition of Some Buffers and Solutions

Lysis buffer

- 50mM Tris-HCl (pH 7.4)
- 2mM EDTA
- 320mM Sucrose
- 1:100 Protease inhibitor cocktail (Sigma 8340)

Lowry A solution, 500ml contains:

- 2g NaOH
- 1g SDS
- 10g $NaCO_3$

Lowry B solution contains:

- 1% CuSO4
- 2% NaK Tartate

6X Solubilisation Buffer, 100 ml with ddH_20 contains:

- 2.4g Sodium dodecyl sulphate (SDS)
- 3ml Glycerol
- 9.3g Dithiothreitol (DTT)
- 4ml β-mercaptoethanol
- 8.33ml 1.5M Tris-HCl

SDS-PAGE / Electrophoresis Buffer (10 x), 1000ml with dH_20 (pH 8.3) contains:

- 10g Sodium dodecyl sulphate (SDS)
- 144g Glycine

- 30.3g Tris-base

Transfer Buffer, TB (x1) contains:

- 14.4g Glycine
- 3.03g Tris-base
- 200ml Methanol
- 800ml dH_20

TBS, pH 7.6 (x10), 1000ml with dH_20 (pH 7.6) contains:

- 30.3g Tris-base
- 73.0g NaCl
- 800ml dH_20

TBS/0.1 % Tween (TBST), 1000ml contains:

- 100ml 1x TBS
- 900ml dH_20
- 1ml Tween-20

Coomassie blue stain

- Methanol (50% v/v) – 100ml
- Glacial acetic acid (20%) – 40ml
- Coomassie brilliant blue (0.12%) – 0.24g

Make up to 200ml with ddH_20

Destain for coomassie blue

- Methanol (10% v/v) – 20ml
- Glacial acetic acid (10%) – 20ml

Make up to 200ml with ddH_20

Appendix 2: Lab Talk Script

```
//Adipo_9_Calib 5 Nov 2018//
//layer -d;//

worksheet -d B%[%h,>'A'];
%n=C%h;
%A=%h;
ncs=wks.ncols;
nrs=wks.nrows;
xen=nrs-1;
ks=xen-10;
d=0;K=0;
xen=nrs;

//check cells//
 for(i=ncs;i>1;i--){
  window -t plot calibrate1 %n;
  layer -w %A i 1 i nrs 200;
  getyesno (Use record) Y;
  layer -d;
   if (y==0){
    d=d+1;
    del wcol(i);
   }
   else{
    k=k+1;
   };
 };

//now smooth raw data and form average//
ncs=wks.ncols;
nct=ncs+1;
tot=ncs-1;
worksheet -c average;
col(average)[nrs]=0;
wcol(nct)=0;
for(i=2;i<=ncs;i++){
   curve.data$=%(%h,i);
   curve.SmoothPts=3;
   curve.result$=%(%h,nct);
   curve.adjave();
   wcol(i)=wcol(nct);
};
wcol(nct)=0;
for(i=2;i<=ncs;i++){
  wcol(nct)=wcol(nct)+wcol(i);
};
//calculate average and plot//
wcol(nct)=wcol(nct)/(ncs-1);
wks.col$(nct).label$=$(ncs-1);

%n=%h;
window -t plot calibrate2 G%nAverage;
layer -w %n nct 1 nct nrs 200;
```

```
//get calibration timings//
k=0;kd=350;
getnumber
(Kd Fluo4 in nm) kd
(Calib Start) xmid
(Calib End) xen
(Linear regression) k:2s
(Regress start) xst
(Regress end) xed
(Calibration times);
//type $(xre) $(xst) $(xen);//
layer-d;

//find min fluo and correct//;
 loop (n,2,ncs){
  limit %(%h,n) -b xmid -e xen;
  ymin=limit.ymin;
  wcol(n)=wcol(n)-ymin;
 };

//linear regression and normalization//
 if (k==1){
   loop (n,2,ncs){
    lr %(%h,n) -b xst -e xed;
    wcol(nct)=lr.b*wcol(1)+lr.a;
    wcol(n)=wcol(n)*100/wcol(nct);
   };
 loop (n,2,ncs){
  limit %(%h,n) -b xmid -e xen;
  wcol(n)=wcol(n)-limit.ymin;
 };
};


//find max and calculate cal//;
 loop (n,2,ncs){
  limit %(%h,n) -b xmid -e xen;
  ymax=limit.ymax;
  wcol(nct)=wcol(n)/(ymax-wcol(n));
  limit %(%h,n) -b xmst -e xmid;
  wcol(n)=kd*wcol(nct);

 };
loop (n,2,ncs) {
%(%H,n)=%(%H,n)<=0?10000:%(%H,n);
%(%H,n)=%(%H,n)>=10000?10000:%(%H,n);
}


 ncs=wks.ncols-1;
 nrs=wks.nrows;
 d=0; k=0;
 for(i=ncs;i>1;i--){
  worksheet -s i 1 i xmid;
  worksheet -p 200 calcium1;
```

```
  getyesno KEEP Y;
  layer -d;
   if (y==0){
    del wcol(i);
    d=d+1;
   }
   else{
    k=k+1;
   };
  };

//now form average//
ncs=wks.ncols-1;
nct=ncs+1;
col(average)[nrs]=0;
wcol(nct)=0;
for(i=2;i<=ncs;i++){
wcol(nct)=wcol(nct)+wcol(i);
};

//calculate average and plot//
wcol(nct)=wcol(nct)/(ncs-1);
wks.col$(nct).label$=$(ncs-1);
worksheet -c int;

%n=%h;
worksheet -s 2 1 ncs xmid;
worksheet -p 200 calcium1;
window -r %h G%n;

//get timings//
getnumber
(Treat A start) TAs
(Treat B Start) TBs
(Treat C start) TCs
(Treat D start) TDs
(Measurement times A-D);

getnumber
(Treat E start) TEs
(Treat F start) TFs
(Treat G start) TGs
(Treat H start) THs
(Treat end) ks
(Measurement times E-H);

layer -d;

%n=%h;
worksheet -s 2 1 ncs xmid;
worksheet -p 200 calcium1;
window -r %h G%n;

//draw limits and reset if necessary//
draw -n TAs -d 1 -w 1 -l -v TAs;
draw -n TBs -d 1 -w 1 -l -v TBs;
```

```
draw -n TCs -d 1 -w 1 -l -v TCs;
draw -n TDs -d 1 -w 1 -l -v TDs;
draw -n TEs -d 1 -w 1 -l -v TEs;
draw -n TFs -d 1 -w 1 -l -v TFs;
draw -n TGs -d 1 -w 1 -l -v TGs;
draw -n THs -d 1 -w 1 -l -v THs;
draw -n ks -c 2 -d 1 -w 1 -l -v ks;

TAs.color=color(blue);
TBs.color=color(red);
TCs.color=color(blue);
TDs.color=color(red);
TEs.color=color(blue);
TFs.color=color(red);
TGs.color=color(blue);
THs.color=color(red);
Ks.color=color(cyan);

TAs.hmove=1;
TBs.hmove=1;
TCs.hmove=1;
TDs.hmove=1;
TEs.hmove=1;
TFs.hmove=1;
TGs.hmove=1;
THs.hmove=1;
ks.hmove=1;


//get timings//
getnumber
(Treat A start) TAs
(Treat B Start) TBs
(Treat C start) TCs
(Treat D start) TDs
(Measurement times A-D);

getnumber
(Treat E start) TEs
(Treat F start) TFs
(Treat G start) TGs
(Treat H start) THs
(Treat end) ks
(Measurement times E-H);


draw -n TAs -d 1 -w 1 -l -v TAs;
draw -n TBs -d 1 -w 1 -l -v TBs;
draw -n TCs -d 1 -w 1 -l -v TCs;
draw -n TDs -d 1 -w 1 -l -v TDs;
draw -n TEs -d 1 -w 1 -l -v TEs;
draw -n TFs -d 1 -w 1 -l -v TFs;
draw -n TGs -d 1 -w 1 -l -v TGs;
draw -n THs -d 1 -w 1 -l -v THs;
draw -n ks -c 2 -d 1 -w 1 -l -v ks;
```

```
//output//

window -n n results;
type.notes$=results;
type.redirection=2;
type \n;
type Worksheet %n;

type $(ncs-1)\t\t$(TAs)\t$(TBs)\t$(TCs)\t$(TDs)\t$(TEs)\t$(TFs)\t$(TGs)\t$(THs);
type Cell\tbasal\tSSA\tSSB\tSSC\tSSD\tSSE\tSSF\tSSG\tSSH;

loop (n,2,ncs){

Abasal=0;ctreatA=0;ctreatB=0;ctreatC=0;ctreatD=0;ctreatE=0;ctreatF=0;ctreatG=0;ct
reatH=0;
  loop (m,1,30){
    Abasal=Abasal+%(%n,n,TAs-m);
    ctreatA=ctreatA+%(%n,n,TBs-m);
    ctreatB=ctreatB+%(%n,n,TCs-m);
    ctreatC=ctreatC+%(%n,n,TDs-m);
    ctreatD=ctreatD+%(%n,n,TEs-m);
    ctreatE=ctreatE+%(%n,n,TFs-m);
    ctreatF=ctreatF+%(%n,n,TGs-m);
    ctreatG=ctreatG+%(%n,n,THs-m);
    ctreatH=ctreatH+%(%n,n,ks-m);
  };

  Abasal=Abasal/30;
  ctreatA=ctreatA/30;
  ctreatB=ctreatB/30;
  ctreatC=ctreatC/30;
  ctreatD=ctreatD/30;
  ctreatE=ctreatE/30;
  ctreatF=ctreatF/30;
  ctreatG=ctreatG/30;
  ctreatH=ctreatH/30;

  type                                                                                $(n-
1)\t$(int(Abasal))\t$(int(ctreatA))\t$(int(ctreatB))\t$(int(ctreatC))\t$(int(ctreatD))\t$(in
t(ctreatE))\t$(int(ctreatF))\t$(int(ctreatG))\t$(int(ctreatH));

};

type Maximum;
type Cell\tbasal\tSSA\tSSB\tSSC\tSSD\tSSE\tSSF\tSSG\tSSH;
loop (n,2,ncs){
limit %(%n,n) -b TAs -e TBs; MaxA=limit.ymax;
limit %(%n,n) -b TBs -e TCs; MaxB=limit.ymax;
limit %(%n,n) -b TCs -e TDs; MaxC=limit.ymax;
limit %(%n,n) -b TDs -e TEs; MaxD=limit.ymax;
limit %(%n,n) -b TEs -e TFs; MaxE=limit.ymax;
limit %(%n,n) -b TFs -e TGs; MaxF=limit.ymax;
limit %(%n,n) -b TGs -e THs; MaxG=limit.ymax;
limit %(%n,n) -b THs -e ks; MaxH=limit.ymax;
```

```
type $(n-1)\t\t$(int(MaxA))\t$(int(MaxB))\t$(int(MaxC))\t$(int(MaxD))\t$(int(MaxE))\t$(int(MaxF))\t$(int(MaxG))\t$(int(MaxH));
};

type Minimum;
type Cell\tbasal\tSSA\tSSB\tSSC\tSSD\tSSE\tSSF\tSSG\tSSH;
loop (n,2,ncs){
limit %(%n,n) -b TAs -e TBs; MinA=limit.ymin;
limit %(%n,n) -b TBs -e TCs; MinB=limit.ymin;
limit %(%n,n) -b TCs -e TDs; MinC=limit.ymin;
limit %(%n,n) -b TDs -e TEs; MinD=limit.ymin;
limit %(%n,n) -b TEs -e TFs; MinE=limit.ymin;
limit %(%n,n) -b TFs -e TGs; MinF=limit.ymin;
limit %(%n,n) -b TGs -e THs; MinG=limit.ymin;
limit %(%n,n) -b THs -e ks; MinH=limit.ymin;

type $(n-1)\t\t$(int(MinA))\t$(int(MinB))\t$(int(MinC))\t$(int(MinD))\t$(int(MinE))\t$(int(MinF))\t$(int(MinG))\t$(int(MinH));

};
```